Physik-Department

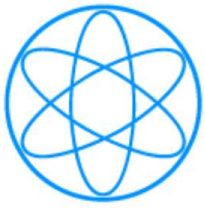

Many-particle physics with ultracold gases

Dissertation

von

Matthias Punk

Technische Universität München

Technische Universität München

Physik-Department

Lehrstuhl T34, Univ.-Prof. Dr. Wilhelm Zwerger

Many-particle physics with ultracold gases

Matthias Punk

Vollständiger Abdruck der von der Fakultät für Physik der Technischen Universität München zur Erlangung des akademischen Grades eines

Doktors der Naturwissenschaften

gehnehmigten Dissertation.

Vorsitzender:	Univ.-Prof. Christian Pfleiderer, Ph.D.
Prüfer der Dissertation:	
	1. Univ.-Prof. Dr. Wilhelm Zwerger
	2. Univ.-Prof. Dr. Ulrich Schollwöck Ludwig-Maximilians-Universität München

Die Dissertation wurde am 12.01.2010 bei der Technischen Universität München eingereicht und durch die Fakultät für Physik am 08.02.2010 angenommen.

Zusammenfassung

Die vorliegende Dissertation befasst sich mit verschiedenen Aspekten der Vielteilchenphysik von ultrakalten Quantengasen. Der erste Teil behandelt die theoretische Basis der Radio-Frequenz-Spektroskopie von ultrakalten Fermigasen in der Nähe von Feshbach-Resonanzen. Konkret werden Spektralfunktionen und die daraus folgenden RF-Spektren von stark wechselwirkenden Fermigasen am Unitaritätspunkt berechnet. Weiters wird der Polaron-Molekül-Übergang mit Hilfe von Variationsmethoden untersucht. Der kritische Wert der Wechselwirkungsstärke des Übergangs wird berechnet und mit experimentellen Ergebnissen verglichen. Der letzte Abschnitt beschäftigt sich mit der Nichtgleichgewichtsdynamik von Heisenberg-Spinketten. Hier wird die unitäre Zeitentwicklung eines Néel-Zustands analysiert. Der antiferromagnetische Ordnungsparameter relaxiert im Allgemeinen exponentiell, wobei die zugehörige Relaxationszeit am isotropen Heisenbergpunkt minimal ist.

Abstract

This thesis is concerned with different aspects of many-particle-physics in the context of ultracold quantum gases. The first part deals with the theoretical basis of radio-frequency-spectroscopy of ultracold Fermi gases near Feshbach-resonances. In particular, we calculate spectral functions and the corresponding rf-spectra of strongly interacting Fermi gases at unitarity. Furthermore, we study the polaron-to-molecule transition using variational methods. We calculate the critical value of the interaction strength and compare it to experimental results. The last part deals with non-equilibrium dynamics of Heisenberg-spin-chains, where the unitary time evolution of a Néel-state is analyzed. Quite generally, the antiferromagnetic order parameter relaxes exponentially and the corresponding relaxation time exhibits a minimum at the isotropic Heisenberg point.

Contents

Chapter 1

Introduction

Starting with the first experimental realization of Bose-Einstein condensates (BEC) with lasercooled atomic vapors in 1995 [1, 2] and the subsequent generation of degenerate Fermi gases in 1999 [3], the physics of ultracold atomic quantum gases evolved rapidly in the last decade, triggering lots of experimental and theoretical work in this field[1]. In particular, two developments have had a tremendous impact. First of all, the use of Feshbach resonances gave experimentalists a unique tool, making it possible to tune the interaction strength between atoms in cold gases. Using this method, the BCS-BEC crossover from weakly bound Cooper pairs to a Bose-Einstein condensate of tightly bound bosonic molecules was realized for the first time with ultracold atomic Fermi gases. Due to the importance of the BCS-BEC crossover problem for a large part of this thesis, we will briefly review it below.

The second major achievement was the implementation of optical lattices, which allows experimentalists to study atomic gases in periodic potentials that are ubiquitous in usual solid state systems. Indeed, cold gases in optical lattices almost perfectly realize Hubbard Hamiltonians, thereby enabling physicists to study strongly correlated quantum systems using the tools of atomic physics. As a bonus, the parameters of the Hubbard model can be tuned easily by adjusting the optical lattice. From this point of view, cold gases can be considered as quantum simulators for basic many-body Hamiltonians in condensed matter physics, which have no direct realization in nature and are hard to tackle theoretically.

Ultracold atomic gases are particularly interesting, because they are very clean systems, allow for a high degree of experimental control and offer the ability to study relatively simple quantum mechanical systems, where a direct comparison between experimental results and theoretical ab initio calculations is feasible. All these nice features and advantages come at some cost, however. In particular, the arsenal of experimental tools to probe the properties of ultracold atomic gases is much smaller than in usual solid state physics and many measurement methods require to release the atomic cloud from the trap, thereby destroying the system. Nevertheless, many striking experiments have already shown the versatility and the vast range of potential applications of ultracold atomic gases, and there is much more to be expected in the upcoming years.

In this theoretical thesis we consider problems that are closely connected to exper-

[1] For a review see e.g. [4] and [5].

iments which have been performed recently, or are about to be carried out in the near future. Thus, many of the facets of ultracold gases that have been mentioned above will play a role in the subsequent chapters. In particular, Feshbach resonances are a necessary ingredient in the first two chapters, where some aspects of the BCS-BEC crossover in ultracold Fermi gases are discussed. The first chapter also deals with theoretical aspects of a particular method to measure pairing correlations in cold gases, which has been applied with much success in recent years. Finally, optical lattices play an important role in the last chapter of this thesis, where quench problems in Heisenberg spin-chains are studied.

BCS-BEC crossover in ultracold atomic gases

It is known since the seminal work of Bardeen, Cooper and Shrieffer (BCS) in 1957 [6], that a Fermi gas with weak attractive interactions has an instability towards pair formation and exhibits a phase transition to a superfluid state below a critical temperature T_c. In a simple picture, this phase transition can be understood as Bose-Einstein condensation (BEC) of bosonic Cooper pairs, although one has to keep in mind that Cooper pairs are far from being local molecules. Now one can ask what happens, if the interactions are cranked up in such a way, that two Fermions form a tightly bound molecule instead of a weakly bound Cooper pair. The first theoretical investigations of this BCS-BEC crossover scenario were conducted by Eagles [7] and Leggett [8], using the BCS ground state as a variational ansatz for the whole crossover regime. Although the BCS-BEC crossover problem was of purely theoretical interest at that time, it regained lots of theoretical attention due to the possibility of its experimental realization in ultracold atomic gases with the help of Feshbach resonances.

In experiments with cold Fermi gases usually the isotopes ^6Li or ^{40}K are used. These neutral alkaline atoms typically interact via a Lennard-Jones potential, i.e. at large distances the attractive interaction is governed by van der Waals forces, and the potential well supports on the order of ~ 100 bound states. In the ultracold limit, however, the scattering properties are determined solely by the position of the energetically highest bound state. In particular, the scattering amplitude of two atoms in the ultracold limit, i.e. at small relative momenta, takes the form[2]

$$f(k \to 0) = \frac{1}{-a^{-1} - ik + \mathcal{O}(k^2)}\,, \tag{1.1}$$

where the only parameter that enters the problem is the s-wave scattering length a, which is only sensitive to the position of the bound state that is closest to the continuum threshold. In the ultracold limit the complicated Lennard-Jones potential can thus be replaced with a pseudopotential (we set $\hbar = 1$ throughout)

$$V(\mathbf{x}) = \frac{4\pi a}{m}\,\delta(\mathbf{x})\,, \tag{1.2}$$

[2]The validity of the low momentum expansion of the scattering amplitude actually defines the ultracold limit.

which captures the physics of the uppermost bound state in the van der Waals potential and gives rise to a scattering amplitude of the form (1.1) after regularization[3]. For negative scattering lengths $a < 0$ the interaction is attractive, whereas positive scattering lengths $a > 0$ lead to a repulsive interaction. One has to keep in mind however, that a two-particle bound state exists only for repulsive interactions $a > 0$. Indeed, the poles of the scattering amplitude in the upper half complex plane determine the energy of two-body bound states [10]. For our low energy scattering amplitude (1.1) we get a pole in the UHP for positive scattering lengths $a > 0$, corresponding to a bound state energy $E_b = -(ma^2)^{-1}$. Due to the s-wave nature of the contact potential (1.2) it is clear that only Fermions in two different internal pseudo-spin states can interact, because of the Pauli principle. In the context of cold atomic gases these pseudo spin states correspond to two different hyperfine states of the atoms.

Feshbach resonances are scattering resonances, where a two-body bound state exists in a closed scattering channel that corresponds to a different hyperfine state configuration of the two scattering atoms. Due to the hyperfine interaction of the atoms at short distances, the open channel couples to the closed channel. If the energy of a true bound state in the closed channel coincides with the incident energy of the two atoms in the open channel, a scattering resonance appears and the scattering length diverges. Because of the different magnetic moments of the hyperfine states in the open and closed channels, the relative position of the bound state in the closed channel can be tuned with respect to the open channel by applying a magnetic field. This gives rise to a magnetic field dependence of the scattering length of the form

$$a(B) = a_{bg}\left(1 - \frac{\Delta B}{B - B_0}\right), \tag{1.3}$$

where B_0 and ΔB parameterize the position and the width of the resonance. a_{bg} is the background scattering length, which is determined by the position of the uppermost bound state in the open channel.

The BCS-BEC crossover problem can now be understood as follows. For weak attractive interactions $a \to 0^-$ (the BCS-limit) two Fermions in different pseudo-spin states form a Cooper pair and the Fermi gas becomes unstable below a critical temperature T_c. The typical pair radius ξ is determined by the BCS energy-gap via $\xi \sim \Delta^{-1} \sim \exp((k_F|a|)^{-1})$ and is much larger than the typical interparticle spacing $\xi \gg k_F^{-1}$, which is set by the Fermi momentum k_F. Note that the Cooper pair is not a true two-particle bound state, but a many-body effect. Indeed, Cooper pairing is only possible in the presence of a Fermi sea, which is obvious from the fact that the gap vanishes as $k_F \to 0$. Now, if the attractive interaction is increased, the pair radius ξ gets smaller. At resonance $a \to \pm\infty$ it is on the order of the interparticle spacing $\xi \sim k_F^{-1}$. After crossing the resonance, a true two-body bound state appears in the problem at positive scattering lengths $a > 0$, with a bound state energy $E_b = -(ma^2)^{-1}$. Going further away from the resonance torwards the BEC-limit $k_F a \ll 1$, where $|E_b| \gg \varepsilon_F$, two Fermions in different pseudo-spin states will form a tightly bound molecule with a typical pair radius $\xi \sim a$ that is much smaller

[3]In the literature the regularized contact potential is known as 'Fermi pseudo-potential', see e.g. [9].

than the interparticle spacing $\xi \ll k_F^{-1}$. In this limit the bosonic molecules will form a Bose-Einstein condensate below a critical temperature.

The so called unitary point, where the scattering length diverges $a \to \pm\infty$ and a two particle bound state is just about to form, is particularly interesting from a theoretical point of view. Here, the only remaining length and energy scale is given by the Fermi momentum and the Fermi energy, because the divergent scattering length has to drop out of all observables. All thermodynamic properties of the unitary gas are thus determined by universal numbers times the dimensionful quantities built from the Fermi energy and the Fermi momentum. Furthermore, the theoretical description of the unitary Fermi gas is a highly non-trivial problem, because there is no small parameter that can be used for a controlled expansion. Much effort has been put into the determination of the universal parameters at unitarity in recent years, both from the theoretical as well as the experimental side (see e.g. [4]).

The BCS-BEC crossover for the case of an equal number of Fermions in both pseudo-spin states ($n_\uparrow = n_\downarrow$) is by now a rather well understood problem. In particular, the topology of the phase diagram is simple: there are only two phases – normal and superfluid – and the phase transition between these two happens at a critical temperature that evolves smoothly from the BCS- to the BEC-limit. The situation changes drastically, however, if a population imbalance ($n_\uparrow > n_\downarrow$) is imposed on the system. In this case not even the topology of the phase diagram at zero temperature is known, let alone the precise positions of the critical points. For the imbalanced gas reliable results are only available for the two weakly interacting BCS- and BEC-limits. A detailed discussion of some aspects of the phase diagram for the BCS-BEC crossover with a population imbalance can be found in Sec. 2.1.

Outline

The outline of this thesis is as follows. The first chapter deals with rf-spectroscopy in ultracold Fermi gases. This measurement method is used widely in order to study pairing correlations in these systems. After giving an overview on the theoretical basis of rf-spectroscopy in ultracold gases, we calculate the rf-response of imbalanced Fermi gases using a non-selfconsistent T-matrix approach. In particular we focus on Fermions in the normal state at unitarity, where recent measurements observed unexpected line-shifts.

In the second chapter we discuss the BCS-BEC crossover in the limit of an extreme population imbalance. In particular we study the $(N+1)$-particle system of a single minority atom immersed in a Fermi sea of majority atoms, interacting via a s-wave contact potential. This problem has some interesting features, such as a quantum phase transition from a state with polaronic binding to a state where the minority Fermion forms a molecular two-body bound state with one of the majority atoms. Building on previous work by Chevy [11] who studied the polaronic part of the $(N+1)$-body problem using a variational ansatz, we construct a complementary variational wave function that describes the molecular side of the transition and determine the position of the critical point of the polaron to molecule transition.

The third chapter deals with quantum quench problems in one dimensional Heisenberg

spin chains. Here we study the unitary time evolution of a Néel ordered initial state and determine the relaxation timescales by calculating the time evolution of the staggered magnetization using different techniques. These include time dependent mean fields, numerical simulations, exactly solvable models and effective low energy theories.

Chapter 2

RF-spectroscopy of ultracold atomic Fermi gases

The method of rf-spectroscopy was introduced in 2004 by the group of R. Grimm in Innsbruck as an experimental tool to observe effects of pairing in attractively interacting, ultracold, two-component Fermi gases [12]. In ultracold gases, the different pseudo-spin species are usually represented by different hyperfine states of the atoms. The idea of rf-spectroscopy is to use an external rf-field to drive the Rabi-transition between two hyperfine states in order to transfer atoms from one of the two occupied states of the interacting Fermi gas to an initially empty hyperfine state. If the Fermions in the initial state form molecules, it is clear that the external rf-field has to provide the binding energy in order to break the molecule and transfer one of the atoms to a different hyperfine state. Thus, the rf-spectrum is shifted to positive frequencies compared to the bare Rabi-transition frequency.

At the time when the first rf-measurements of balanced Fermi gases[1] came up, the observation of a shifted line in the rf-spectrum was thought to be an unambiguous signature of Cooper-pairing and thus of superfluidity in ultracold Fermi gases. The situation changed in 2007, however, when the first rf-measurements of imbalanced Fermi gases were performed in the group of W. Ketterle at MIT [13]. Indeed, for a sufficiently large mismatch of the Fermi energies of the two fermionic species, it is known that superfluidity is lost and the Fermi gas enters a normal state. This is sometimes called the Pauli pair-breaking mechanism or the Clogston-Chandrasekhar limit [14, 15]. The experiments of the Ketterle group have shown that the rf-spectra of the interacting, imbalanced Fermi gas in the normal state are shifted by almost the same amount as in the paired superfluid state[2]. Thus, the presence of a shifted rf-spectrum is not a direct indication of superfluidity in ultracold atomic gases.

The interpretation of the early rf-experiments in Innsbruck was further complicated by

[1]The term "balanced" refers to the fact, that the number of atoms in the two pseudo-spin states is equal, i.e. $n_\uparrow = n_\downarrow$. For imbalanced Fermi gases we use the convention that $n_\uparrow > n_\downarrow$.

[2]In this experiment, superfluidity was unambiguously verified by the creation of vortices.

the presence of final state interactions[3]. Indeed, the third, initially empty hyperfine state also interacts with the other two and thus the rf-spectra are not a probe of the interacting two-component Fermi system alone. Early theoretical interpretations of the experimental data neglected the strong final state interactions completely [16, 17].

The motivation for the work presented in this chapter is two-fold. First of all, our aim is to get a better understanding of the influence of final state interactions on the rf-spectra. This is particularly important in order to obtain quantitative information from the rf-measurements about the system of interest. The second motivation is to provide a theoretical basis for the rf-measurements in the normal phase of the imbalanced Fermi gas from the Ketterle group.

The outline of this chapter is as follows. In Sec. 2.1 we briefly discuss the BCS-BEC crossover in imbalanced Fermi gases. In particular, we focus on qualitative aspects of the phase diagram. The theory of rf-spectroscopy in ultracold quantum gases will be examined in Sec. 2.2. In the last section 2.3 we present a many-body theory for the normal state of the imbalanced Fermi gas and use it to calculate the rf-spectra at unitarity and zero temperature.

2.1 BCS-BEC crossover in imbalanced Fermi gases

The BCS-BEC crossover in balanced Fermi gases, i.e. with an equal number of up- and down-spins, is by now a rather well understood problem. The situation is different however, if a population imbalance between the two Fermion species is introduced. For strong interactions close to the unitarity limit a plethora of new possible phases have been predicted (see [18] and references therein).

In the following we discuss qualitative aspects of the phase diagram, which are essentially based on extrapolations from the weakly interacting limits. We start from a single channel channel model for the Feshbach resonance [4], describing a two-component Fermi gas with a contact interaction $V(x) = 4\pi a/m\,\delta(x)$. The dimensionless inverse interaction parameter is $v = (k_F a)^{-1}$, where a is the s-wave scattering length and we define k_F as the Fermi momentum of the fully polarized gas at the total density, i.e. $k_F^3 = 6\pi^2 n$. The corresponding Fermi energy is given by $\varepsilon_F = k_F^2/(2m)$. The interaction potential is attractive for negative scattering lengths and supports a two-particle bound state with binding energy $E_b = -(ma^2)^{-1}$ for positive scattering lengths.

For the discussion of the phase diagram of the imbalanced Fermi gas at zero temperature, we choose an ensemble with fixed total particle number $N = N_\uparrow + N_\downarrow$ but with a fluctuating relative particle number $\delta N = N_\uparrow - N_\downarrow$. This can be achieved by introducing an effective magnetic field h that couples to the two-different spin-states $\sigma = \uparrow, \downarrow$ in the standard form

$$\hat{H}' = -h\left(\hat{N}_\uparrow - \hat{N}_\downarrow\right), \tag{2.1}$$

i.e. h can be thought of as a 'Zeeman' field that couples to the 'spin' of the atoms and favors a finite population imbalance. At a fixed total density $n = n_\uparrow + n_\downarrow$, the

[3] In recent rf-experiments the hyperfine states are chosen in such a way, that the final state interactions are small and can be neglected.

ground state energy $u(n,h)$ per volume is then a function of n and h. It determines the chemical potentials of the majority and minority species from $\mu_{\uparrow,\downarrow} = \mu \pm h$ where $\mu = \partial u(n,h)/\partial n$ is the average chemical potential. In addition, it also fixes the imbalance from $\delta n = n_\uparrow - n_\downarrow = -\partial u(n,h)/\partial h$.

At zero temperature, there are two critical fields $h_c(v)$ and $h_s(v)$ that separate two simple limiting phases from a regime, in which nontrivial ground states are expected: the lower critical field h_c is defined by a vanishing population imbalance $n_\uparrow = n_\downarrow$ for $h < h_c$ and determines the boundary of the balanced superfluid phase. The upper critical field h_s, which will be called 'saturation field' in the following, is defined by the condition of complete polarization for $h > h_s$, i.e. $n_\downarrow = 0$ and $n_\uparrow = n$. Since a single component Fermi system does not interact due to the s-wave nature of the interaction potential in the ultracold limit, the regime $h > h_s$ corresponds to an ideal gas of majority Fermions, i.e. it is a fully polarized, normal state.

The asymptotic form of the two critical fields h_c and h_s in the limit of vanishing interactions (i.e. the BCS-limit for $v \to -\infty$ and the BEC-limit for $v \to +\infty$) can be inferred from a simple mean field analysis. We start by considering the two critical fields in the BCS-limit. In this regime the attractively interacting Fermi gas can be described very well within BCS-theory and the critical field h_c has been calculated already by Clogston [14] and Chandrasekhar [15]

$$h_c(v \to -\infty) = \frac{\Delta}{\sqrt{2}} \tag{2.2}$$

where Δ is the BCS gap parameter. It is important to note that the phase transition from the superfluid to the normal state at h_c is a first order transition in the BCS regime, because the polarization $\delta n/n$ jumps from zero to a non-zero value[4]. The leading order behavior of the saturation field h_s in the BCS-limit can be obtained by calculating the Zeeman field above which a non-interacting Fermi gas is fully polarized. This occurs right at $\mu_\downarrow = 0$, i.e. at $h = \mu = \mu_\uparrow/2$. The next-to-leading order correction can be obtained from mean-field theory. Indeed, at h_s the change in the chemical potential of the minority Fermions due to the interaction with the majority Fermi sea is given by the mean field value $\delta\mu_\downarrow = gn$. The asymptotics of the saturation field in the BCS-limit is thus given by

$$h_s(v \to -\infty) = \varepsilon_F \left(\frac{1}{2} + \frac{2}{3\pi|v|} \right) + \mathcal{O}(v^{-2}) \tag{2.3}$$

where ε_F is the Fermi energy of the fully polarized majority gas, as defined above.

In order to obtain the asymptotics of the two critical fields in the BEC-limit $v \to +\infty$, we formulate a simple mean field theory of bosonic molecules interacting with each other and with the excess Fermions. In a Landau expansion, the Landau free-energy u per volume for the bosonic molecules and the excess Fermions up to leading order in the interaction, as a function of the total density $n = n_\uparrow + n_\downarrow$, the density imbalance $\delta n = n_\uparrow + n_\downarrow$ and the magnetic field h is given by

$$u(n,\delta n,h) = \frac{3}{5}\,\varepsilon_{F\delta}\,\delta n + E_b \frac{n-\delta n}{2} + g_{ad}\frac{n-\delta n}{2}\,\delta n + \frac{g_{dd}}{2}\frac{(n-\delta n)^2}{4} - h\,\delta n \tag{2.4}$$

[4]We note that within a grand canonical description the total particle density n also jumps at the critical field h_c, c.f. [19].

as the sum of the Fermi energy of the excess Fermions, the binding energy of the molecules and the interaction energies. The atom-dimer interaction strength $g_{ad} = 3\pi a_{ad}/m$ and the dimer-dimer interaction strength $g_{dd} = 2\pi a_{dd}/m$ can be expressed in terms of the corresponding scattering lengths, the exact values of which are given by $a_{ad} = 1.18a$ and $a_{dd} = 0.6a$ [20]. The last term describes the coupling to the magnetic field h. The true ground state energy density $u(n, h)$ is determined by the minimum of the Landau free-energy $u(n, \delta n, h)$ with respect to the density imbalance δn. Before proceeding it is convenient to rewrite Eq. (2.4) in dimensionless form

$$\frac{u(n,\,\delta n,\,h)}{\varepsilon_F} = \frac{3}{5}\Big(\frac{\delta n}{n}\Big)^{2/3}\delta n - v^2(n-\delta n) + \frac{\tilde{a}_{ad}}{2\pi v}\frac{(n-\delta n)\,\delta n}{n} + \frac{\tilde{a}_{dd}}{12\pi v}\frac{(n-\delta n)^2}{n} - \tilde{h}\,\delta n \quad (2.5)$$

Here, the energies are measured again in units of the Fermi energy of a fully polarized gas at the total density $\varepsilon_F = (6\pi^2 n)^{2/3}/(2m)$ and the tilde denotes dimensionless quantities, i.e. $\tilde{a}_{ad} = a_{ad}/a$ and $\tilde{h} = h/\varepsilon_F$. The minimum of the Landau free-energy is determined by the equation

$$\frac{\partial(u/\varepsilon_F)}{\partial\,\delta n} = \Big(\frac{\delta n}{n}\Big)^{2/3} + v^2 + \frac{\tilde{a}_{ad}}{2\pi v}\Big(1 - 2\frac{\delta n}{n}\Big) + \frac{\tilde{a}_{dd}}{6\pi v}\Big(\frac{\delta n}{n} - 1\Big) - \tilde{h} \stackrel{!}{=} 0\,. \quad (2.6)$$

From this expression we can calculate the asymptotics of the two critical fields h_c and h_s in the BEC-limit. The critical field h_c is defined by the condition of a vanishing imbalance $\delta n = 0$. Plugging this into Eq. (2.6) we obtain

$$h_c(v \to \infty) = \varepsilon_F\left(v^2 + \frac{1}{2\pi v}\Big[\frac{a_{ad}}{a} - \frac{a_{dd}}{6\,a}\Big]\right) + \mathcal{O}(v^{-2}) \quad (2.7)$$

On the other hand, the saturation field h_s is determined by the condition of a fully polarized gas $\delta n = n$. Together with Eq. (2.6) this leads to

$$h_s(v \to \infty) = \varepsilon_F\left(v^2 + 1 - \frac{a_{ad}/a}{2\pi v}\right) + \mathcal{O}(v^{-2}) \quad (2.8)$$

Apart from the interaction corrections the critical field h_c is thus given by minus one half of the molecular binding energy E_b, whereas the saturation field is higher by ε_F due to the presence of the excess Fermi sea. At unitarity, the values of h_c and h_s can be determined using variational and Monte-Carlo methods. As will be shown in chapter 3, the saturation field at unitarity is given by $h_s(v \to \infty) \simeq 0.80\varepsilon_F$. This value was obtained by Chevy [11] using a variational ansatz and has been confirmed by Monte-Carlo calculations [22, 23, 24]. The critical field $h_c(v \to \infty) \simeq 0.26\varepsilon_F$ at unitarity was calculated by Lobo et al. [22]. It is important to note that the range between h_c and h_s at unitarity is much larger than that found from a simple mean field analysis, which gives $h_c \simeq 0.32\varepsilon_F$ and $h_s = 0.5\varepsilon_F$ [25].

The qualitative structure of the zero temperature phase diagram as a function of the interaction parameter $v = 1/(k_F a)$ and the effective magnetic field h in units of the bare Fermi energy ε_F of the fully polarized gas is shown in Fig. 2.1. This phase diagram is simply constructed by extrapolating the asymptotics of the critical fields that have been derived above. Below h_c, the system is in the balanced superfluid phase (SF_0), where

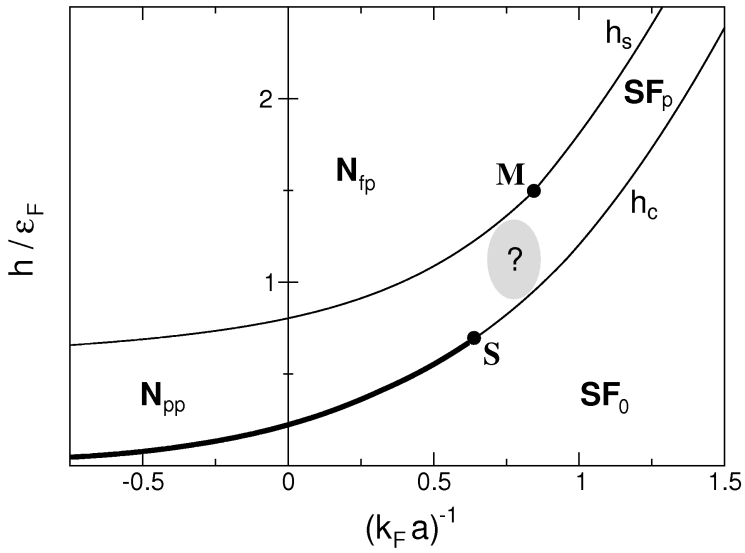

Figure 2.1: Qualitative phase diagram of the imbalanced Fermi gas as a function of the inverse coupling strength $(k_F a)^{-1}$ and the effective magnetic field h/ε_F. The thick line indicates a first order phase transition and the different phases are labeled as in [21], i.e. $N_{\rm fp}$: fully polarized normal phase, $N_{\rm pp}$: partially polarized normal phase, SF_0: balanced superfluid, $SF_{\rm p}$: polarized superfluid. The points M and S are discussed in the text. The precise structure of the phase diagram in the nontrivial regime $h_c < h < h_s$ is likely to contain unconventional superfluid phases in addition to the $N_{\rm pp}$ and $SF_{\rm p}$ phase, which are not shown in our figure. Apart from the $N_{\rm pp}$ and the $SF_{\rm p}$ phase, possible phases in the region between h_c and h_s that have been discussed in the literature are the FFLO-phase, the Sarma- or breached pair phase and various phase separated combinations thereof (for a review, see [18]). Moreover, the $N_{\rm pp}$ and $SF_{\rm p}$ phases are unstable with respect to p-wave pairing, at least in the weakly interacting limits.

the densities of both species are equal $n_\uparrow = n_\downarrow$. In the BCS-regime, the system enters a partially polarized ($n_\uparrow > n_\downarrow$), normal Fermi liquid phase (N_{pp}) above h_c. As mentioned above, this phase transition is of first order, because the polarization jumps from zero to a nonzero value. At unitarity, this first order transition to a normal state has been observed in experiments [26] at finite temperature. By contrast, the imbalanced Fermi gas is still superfluid above h_c in the BEC-regime ($v \to +\infty$). In this polarized superfluid phase (SF_p) all minority atoms are bound to bosonic molecules with majority atoms and are superfluid at zero temperature, whereas the excess majority atoms form a Fermi sea. The transition from SF_p to SF_0 at h_c in the BEC-regime is a continuous Lifshitz transition where the Fermi surface of the excess majority atoms vanishes, thus there has to be a splitting point S along the h_c line, where the first order transition on the BCS-side turns into a second order transition in the BEC-regime. Furthermore, this Lifshitz transition from SF_p to SF_0 is only sharp at zero temperature and turns into a smooth crossover at finite temperature. The nature of the phase diagram near the splitting point S has been discussed by Son and Stephanov [27] using an effective field theory. They have shown that the location of the point S is related to the shape of the dispersion relation of the fermionic excitations. In particular, the dispersion relation has its minimum at zero momentum for $v > v_S$ and at nonzero momenta for $v < v_S$. Within mean field theory, where the fermionic excitation spectrum has the usual BCS-form $E_{\mathbf{k}} = \sqrt{(\varepsilon_{\mathbf{k}} - \mu)^2 + \Delta^2}$, the splitting point S is thus related to the zero crossing of the chemical potential μ, which happens on the BEC-side of the resonance at $v \simeq 0.44$ in mean-field theory. The precise location of the splitting point S has been determined recently by us from a calculation of the fermionic excitation spectrum along the BCS-BEC crossover of the balanced gas [28]. It is located at $v_S \simeq 0.63$ and $h_c(v_S) = \Delta \simeq 0.6\varepsilon_F$, at considerably larger coupling strengths than predicted by mean-field theory (note the factor $2^{1/3}$-difference with the result in Ref. [28], which is due to the fact that the up-spin Fermi wave vector and not that of the balanced case appears in the definition of our coupling constant v).

The point M along the saturation field line h_s separates a regime where a single down-spin is a well defined fermionic quasiparticle from one, in which it is bound to a molecule with one of the majority Fermions. This critical point will be discussed extensively in chapter 3, where the $(N+1)$-particle problem that occurs infinitesimally below h_s is considered in detail. For a finite density of minority atoms, the point M appears as an endpoint of a line that separates a phase with a finite minority Fermi surface volume $\Omega_\downarrow \neq 0$ to its left from one with $\Omega_\downarrow = 0$ on the right side[5]. Using the generalized Luttinger theorem derived by Sachdev and Yang [29], the expected polarized superfluid (SF_p) phase on the molecular side has a condensate of 'dimers' plus an up-spin Fermi sea, whose volume $\Omega_\uparrow = (2\pi)^3(n_\uparrow - n_\downarrow)$ is set by the imbalance. This is consistent with the naive picture that the density of unpaired majority atoms is simply $n_\uparrow - n_\downarrow$ even though the 'dimers' in the vicinity of the transition are far from local $(\uparrow,\downarrow)$-pairs[6]. This part of the phase

[5] We note that the minority Fermi surface volume $\Omega_\downarrow$ vanishes also along the h_s-line on the BCS side to the left of M. This is again a continuous Lifshitz transition, which is sharp at zero temperature only. By contrast, the transition between the normal and the superfluid state at finite minority concentrations below the point M remains a phase transition at finite temperature.

[6] We note that the polarized superfluid phase is unstable with respect to p-wave pairing due to the

diagram has been explored experimentally by Shin et al. [31]. They find that the critical polarization $(\delta n/n)_c$, below which the imblanced gas is superfluid, approaches unity at an interaction strength $v \approx 0.74$. This point can be identified with the point M in our phase diagram in Fig. 2.1.

A nontrivial issue that has been neglected in the discussion so far is the question whether a gas of polarons or bound molecules is indeed stable at low but finite minority densities $n_\downarrow$. On the molecular side, the phase immediately below the saturation field line $h_s(v)$ is expected to be a superfluid of $(\uparrow,\downarrow)$-pairs at a very low density $n_\downarrow \to 0$ immersed in an up-spin Fermi sea. The fact that the atom-dimer repulsion $a_{ad} = 1.18\,a$ is much larger than the dimer-dimer repulsion $a_{dd} = 0.6\,a$, however indicates that a low density gas of molecules tends to phase separate from the up-spin Fermi gas. This phase separation has indeed been found from an extended BCS-description of the BCS-BEC crossover in an imbalanced gas [19, 25, 32, 33]. It has recently been seen also in the variational Monte Carlo calculations by Pilati and Giorgini [21]. Their results indicate that a section between $v_N \simeq 0.73$ and a triple point at $v_T \simeq 1.7$ along the h_s-line is actually a first order line, where the polarized superfluid disappears with a finite jump in density as the effective field h increases through h_s. The calculations in chapter 3 below show that the point M lies at $v_M \simeq 0.84$, right in the interval between v_N and v_T, thus the polaron to molecule transition would not be accessible at any finite minority density, at least not in an equilibrium situation. Clearly, our variational calculation for the single minority atom problem in chapter 3 cannot address the question of phase separation. An unexpected feature of the h_s-line in the presence of phase separation is the fact that the transition across h_s is predicted to be continuous up to v_N, first order between v_N and v_T and continuous again for $v > v_T$. The rather large value $v_T \simeq 1.7$ up to which phase separation is predicted also appears surprising. Indeed, in the region around $v = v_T \simeq 1.7$ our simple mean field model (2.5) for the molecules and the excess Fermions should be valid. In this model phase separation between a polarized superfluid phase and a fully polarized Fermi gas appears for coupling constants $v < v_{c,PS}$, below which the energy density (2.6) has a second minimum at full polarization. This occurs at

$$v_{c,PS} = \frac{3}{2\pi}\Big(\tilde{a}_{ad} - \frac{\tilde{a}_{dd}}{6}\Big)\,. \tag{2.9}$$

With the exact values $\tilde{a}_{ad} = 1.18$ and $\tilde{a}_{dd} = 0.6$ one obtains $v_{c,PS} = 0.516$, which is far beyond the predicted value $v_T \simeq 1.7$ and in a regime, where the simple expansion (2.5) is no longer valid. Thus, our simple mean field model does not reproduce the previous results [21, 25] for the triple point v_T. From our point of view, the question of phase separation at a finite minority atom concentration – and thus also the question if the point M is directly observable in experiments – remains open.

phonon-induced interaction between excess Fermions in the molecular condensate [30]. The same is true for the N_{pp} phase, where an attractive p-wave interaction between Fermions of the same species is mediated by the opposite species. At large imbalances, however, the energy scales associated with p-wave pairing are much smaller than the lowest temperatures that can be achieved in experiments.

2.2 Linear response theory of rf-spectroscopy

In experiments with ultracold, two-component Fermi gases a mixture of atoms in two different hyperfine states $|1\rangle$ and $|2\rangle$ is prepared. These two states are commonly denoted by the pseudospin indices $\uparrow$ and $\downarrow$ and interact via a s-wave contact potential with interaction strength g_{12}. In order to measure pairing correlations in such an interacting Fermi gas, a rf-pulse is applied that transfers atoms coherently form state $|2\rangle$ to an initially empty, third hyperfine state $|3\rangle$. This situation, depicted schematically in Fig. 2.2, is modeled by the Hamiltonian

$$H = H_0 + H_{\mathcal{T}}(t) \tag{2.10}$$

where the Hamiltonian H_0 describes the three hyperfine states and their mutual interactions

$$H_0 = \sum_{\mathbf{k},\,\sigma=1,2,3} \varepsilon_{\mathbf{k}} c^\dagger_{\mathbf{k}\sigma} c_{\mathbf{k}\sigma} + \sum_{\sigma\neq\sigma'} \frac{\bar{g}_{\sigma\sigma'}}{2V} \sum_{\mathbf{k}',\mathbf{k},\mathbf{q}} c^\dagger_{\mathbf{k}-\mathbf{q}\sigma} c^\dagger_{\mathbf{k}'+\mathbf{q}\sigma'} c_{\mathbf{k}'\sigma'} c_{\mathbf{k}\sigma} \ . \tag{2.11}$$

Here, $\sigma = 1,2,3$ indicates the three hyperfine states, $\varepsilon_{\mathbf{k}} = k^2/(2m)$ is the free Fermion dispersion and $\bar{g}_{\sigma\sigma'}$ denotes the bare interaction strength between the two different hyperfine levels σ and σ'. The external field that drives the transition between states $|2\rangle$ and $|3\rangle$ is described by the Hamiltonian

$$H_{\mathcal{T}}(t) = \mathcal{T} \int d^3x \left\{ e^{i(\mathbf{k}_L\cdot\mathbf{x}-\omega_L t)} \psi^\dagger_3(\mathbf{x})\, \psi_2(\mathbf{x}) \ + \ \text{h.c.} \right\} \tag{2.12}$$

where ω_L and $\mathbf{k}_L$ denote the frequency and momentum of the rf-photons and $\mathcal{T}$ is proportional to the dipole matrix element.

Now we want calculate the rf-current within linear response theory[7], which is a good approximation for small population transfers. The rf-current operator $\hat{I} := \dot{N}_3$ measures the rate of change of atoms in state $|3\rangle$ and – using the Heisenberg equation of motion – can be expressed as

$$\begin{aligned} \hat{I} \ &= \ \dot{N}_3 \ = \ i[H_0 + H_{\mathcal{T}}, N_3] \ = \ i[H_{\mathcal{T}}, N_3] \\ &= \ -i\mathcal{T} \int d^3x \left(e^{i(\mathbf{k}_L\cdot\mathbf{x}-\omega_L t)} \psi^\dagger_3(\mathbf{x})\psi_2(\mathbf{x}) - \ \text{h.c.} \right) \end{aligned} \tag{2.13}$$

Calculating the rf current in linear response [34] with respect to $H_{\mathcal{T}}$ leads to

$$I = \langle \dot{N}_3 \rangle = -i \int dt'\, \Theta(t-t') \left\langle [\dot{N}^I_3(t), H^I_{\mathcal{T}}(t')] \right\rangle \tag{2.14}$$

where the expectation value has to be taken in the initial state (i.e. the ground state of H_0) and the operators on the RHS are represented in the interaction picture with respect to the Hamiltonian H_0 defined in Eq. (2.11), i.e.

$$\mathcal{O}^I(t) = e^{iH_0 t} \mathcal{O} e^{-iH_0 t} = e^{i\sum_\sigma \mu_\sigma N_\sigma t} e^{iK_0 t} \mathcal{O} e^{-iK_0 t} e^{i\sum_\sigma \mu_\sigma N_\sigma t} \ . \tag{2.15}$$

[7] Note that the linear response theory for the rf-current is similar to simple theories of tunneling in superconductors, c.f. [34].

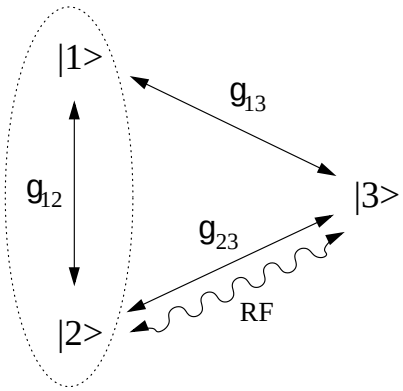

Figure 2.2: Schematic representation of rf spectroscopy. A two component Fermi gas is prepared using a mixture of Fermions in hyperfine states $|1\rangle$ and $|2\rangle$, interacting with coupling strength g_{12}. In order to probe pairing correlations in this two component gas, atoms in state $|2\rangle$ are transferred to an initially empty state $|3\rangle$ using a rf-transition. In a naive picture, the binding energy between two atoms in states $|1\rangle$ and $|2\rangle$ needs to be provided in order to transfer atoms from $|2\rangle$ to $|3\rangle$, giving rise to a shift of the bare rf-transition frequency by an amount proportional to the binding energy.

However, the interaction picture for the field operators is usually defined via the grand canonical Hamiltonian $K_0 = H_0 - \sum_\sigma \mu_\sigma N_\sigma$, in order to avoid dealing with a fixed particle number[8]

$$\psi_3^\dagger(\mathbf{x}, t) = e^{iK_0 t}\psi_3^\dagger(\mathbf{x})e^{-iK_0 t} \tag{2.16}$$

Thus, when switching to the interaction representation for the operators $H_\mathcal{T}$ and $\dot{N}_3$ in Eq. (2.14), one gets additional factors of the form $e^{i\mu_\sigma t}$ besides the replacement $\psi(\mathbf{x}) \to \psi(\mathbf{x}, t)$. After inserting the interaction picture operators for the rf-current (2.13) and the tunneling Hamiltonian (2.12) into Eq. (2.14) and evaluating the time integral, the rf-current, which is a function of the frequency of the applied rf-field, can be written as the imaginary part of the retarded rf-susceptibility in frequency space $\chi(\omega) = \chi'(\omega) + i\chi''(\omega)$

$$I(\omega_L) = 2\mathcal{T}^2\,\chi''(\omega = \mu_3 - \mu_2 - \omega_L)\,. \tag{2.17}$$

Here and in the following, the double-prime χ'' denotes the imaginary part of χ. The retarded susceptibility is given by[9]

$$\chi(\omega) = \int_{-\infty}^{\infty} dt\, e^{i\omega t}\chi(t) = -i\int_{-\infty}^{\infty} dt\, e^{i\omega t}\,\Theta(t)\big\langle[A(t), A^\dagger(0)]\big\rangle \tag{2.18}$$

with

$$A(t) = \int d^3x\, e^{i\mathbf{k}_L\cdot\mathbf{x}}\,\psi_3^\dagger(\mathbf{x}, t)\,\psi_2(\mathbf{x}, t)\ . \tag{2.19}$$

[8]Field operators in the 'grand canonical' interaction picture are indicated by the additional time argument instead of using the index ^{I}.

[9]Note that our definition of the susceptibility differs from the standard definition by a minus sign.

In the following two sections we use two different strategies in order to obtain information about the rf-spectra from equations (2.17) and (2.18). In section 2.2.1 we derive sum rules for the average rf-shift which hold for all interaction strengths $\bar{g}_{\sigma\sigma'}$, including final state interactions. This approach has been used before by Yu and Baym [35] for the weak coupling BCS-limit. In section 2.2.2 we derive an explicit expression for the susceptibility (2.18) in the case of vanishing final state interactions $\bar{g}_{13} = \bar{g}_{23} = 0$ and show how the rf-spectrum is related to the spectral function of the interacting Fermi gas. The results obtained in this section are similar to the expressions for the tunneling of electrons between a superconductor and a normal metal [34] and have been obtained previously by Kinnunen et al. [16], He et al. [17] and Ohashi et al. [36].

Note that we set the momentum of the incident rf-wave equal to zero $\mathbf{k}_L = 0$ in the remainder of this thesis. This is an excellent approximation, since $\mathbf{k}_L$ is orders of magnitude smaller than the momenta of the involved atoms.

2.2.1 Mean rf-shift in the presence of final state interactions

In this section our aim is to get an exact expression for the average (or mean) rf-shift including final state interactions. The mean rf-shift $\bar{\omega}$ is defined as the normalized first moment of the rf-spectrum $I(\omega)$

$$\bar{\omega} = \frac{\int d\omega\, \omega\, I(\omega)}{\int d\omega\, I(\omega)} = \frac{\int d\omega\, (\mu_3 - \mu_2 - \omega)\, \chi''(\omega)}{\int d\omega\, \chi''(\omega)} \tag{2.20}$$

Just as a side remark we note that $\omega(\equiv \omega_L)$ in the expression above doesn't really measure the real frequency of the rf-photon, since we have not included an energetic offset ω_{23} between the states $|2\rangle$ and $|3\rangle$ in our Hamiltonian H_0 in Eq. (2.11). Thus, ω corresponds to the difference between the photon frequency that is necessary to drive the transition in the presence of interactions and the bare transition frequency ω_{23}, which we have implicitly set to zero in our calculation.

Our remaining task is to calculate the zeroth and first moment of the retarded susceptibility's imaginary part $\chi''(\omega)$ defined in Eq. (2.18). This can be achieved by deriving sum rules using the peculiar analytic properties of $\chi(\omega)$. Indeed, the fact that the retarded susceptibility $\chi(\omega)$ is analytic in the upper half complex plane gives rise to exact relations between its real- and imaginary parts, famously known as Kramers-Kronig relations. Furthermore, the retarded susceptibility is completely determined by its imaginary part via the so called spectral representation

$$\chi(z) = \int_{-\infty}^{\infty} \frac{d\omega}{\pi} \frac{\chi''(\omega)}{\omega - z}\,. \tag{2.21}$$

From this relation we can infer the imaginary part $\chi''(\omega)$ of Eq. (2.18), which turns out to be given by

$$\chi''(\omega) = -\frac{1}{2} \int dt\, e^{i\omega t} \left\langle [A(t), A^\dagger(0)] \right\rangle . \tag{2.22}$$

This result can be verified easily by inserting it into the spectral representation (2.21). By a simple inverse Fourier transformation of (2.22) we get the 'generating function' of the

moments of $\chi''(\omega)$

$$\big\langle [A(t), A^\dagger(0)] \big\rangle = -\int \frac{d\omega}{\pi} e^{-i\omega t}\, \chi''(\omega) \tag{2.23}$$

Setting the time equal to zero ($t = 0$), we obtain the sumrule for the zeroth moment (i.e. the normalization) of the retarded susceptibility

$$\int \frac{d\omega}{\pi}\, \chi''(\omega) = -\big\langle [A, A^\dagger] \big\rangle = N_2 - N_3 \tag{2.24}$$

where N_2 and N_3 denote the total number of particles in states $|2\rangle$ and $|3\rangle$ before switching on the rf-field. In particular, we have $N_3 = 0$ in the situation considered here. We use this sumrule to normalize the rf-spectrum $I(\omega)$ to

$$\int d\omega\, I(\omega) \stackrel{!}{=} \frac{N_2}{V} = n_2 \tag{2.25}$$

i.e. using (2.17) the normalized rf-spectrum is defined by $I(\omega) = \chi''(\mu_3 - \mu_2 - \omega)/(\pi V)$.

The first moment can be obtained by differentiating Eq. (2.23) once with respect to the time t and setting $t = 0$ subsequently. This gives

$$\int \frac{d\omega}{\pi}\, \omega\, \chi''(\omega) = \big\langle [[K_0, A], A^\dagger] \big\rangle \tag{2.26}$$

where the Heisenberg equation of motion for the operator A has been used to replace $\dot{A}$ on the RHS. The double commutator can be calculated straightforwardly. Inserting $K_0 = H_0 - \sum_\sigma \mu_\sigma N_\sigma$ with H_0 from Eq. (2.11) leads to a number of terms that need to be evaluated. The kinetic energy terms give

$$\sum_{\sigma=1,2,3} \big\langle [[H_\sigma^{\rm kin} - \mu_\sigma N_\sigma, A], A^\dagger] \big\rangle = (\mu_3 - \mu_2)(N_2 - N_3)\,. \tag{2.27}$$

This expression cancels exactly with the first two terms on the RHS of (2.20), which simply reflects the fact that the mean rf-shift is zero when all interactions are switched off, as expected. The remaining calculation of the commutators with the interaction parts of H_0 can be simplified using the following observations. First of all, it is easily established that

$$[H_{\rm int}^{23}, A] = 0\,, \tag{2.28}$$

i.e. the interaction Hamiltonian between the states $|2\rangle$ and $|3\rangle$ drops out and doesn't affect the mean rf-shift. This is not really surprising, because the rf-field transfers the Fermions in a coherent superposition of states $|2\rangle$ and $|3\rangle$, thus they are all in the same state and cannot interact. The second simplification arises, if the interaction strengths $\bar{g}_{12}$ and $\bar{g}_{13}$ are equal. Precisely at this point one can show that all interaction effects cancel and the mean rf-shift is zero. We thus write the sum of $H_{\rm int}^{12}$ and $H_{\rm int}^{13}$ in the form

$$H_{\rm int}^{12} + H_{\rm int}^{13} = \big(\bar{g}_{12} - \bar{g}_{13}\big)\frac{H_{\rm int}^{12}}{\bar{g}_{12}} + \underbrace{\bar{g}_{13}\,\frac{H_{\rm int}^{12}}{\bar{g}_{12}} + H_{\rm int}^{13}}_{H_{\rm int}^{\rm invar}} \tag{2.29}$$

and use $[H_{\rm int}^{\rm invar}, A] = 0$. Thus we are left with the straightforward calculation of the double commutator $[[H_{\rm int}^{12}, A], A^\dagger]$, which in the end is the only term that contributes to the mean rf-shift. Collecting all results, we finally obtain

$$\bar{\omega} = \frac{\bar{g}_{12} - \bar{g}_{13}}{N_2 - N_3} \left(\frac{\langle H_{\rm int}^{13} \rangle}{\bar{g}_{13}} - \frac{\langle H_{\rm int}^{12} \rangle}{\bar{g}_{12}} \right) \tag{2.30}$$

A further simplification can be made using the fact that the state $|3\rangle$ is initially empty ($N_3 = 0$), which also implies that the interaction energy between the states $|1\rangle$ and $|3\rangle$ is zero, i.e. $\langle H_{\rm int}^{13} \rangle \equiv 0$. The mean rf-shift is thus given by

$$\bar{\omega} = -\frac{\bar{g}_{12} - \bar{g}_{13}}{\bar{g}_{12}} \frac{\langle H_{\rm int}^{12} \rangle}{N_2} \tag{2.31}$$

This expression shows that the mean rf-shift is indeed determined by the interaction energy in the Fermi gas, as expected naively. For attractive interactions, the rf-photons need to provide the difference of the binding energies[10] in the initial and final states in order to drive the transition. Furthermore, the mean rf-shift is zero if the interaction strengths $\bar{g}_{12}$ and $\bar{g}_{13}$ are equal.

In spite of its simplicity, there is one formal problem with Eq. (2.31) that needs to be resolved. Quite generally, contact interaction potentials of the form $V(\mathbf{x}) = g\delta(\mathbf{x})$ lead to momentum distributions that have a tail proportional to $\sim k^{-4}$ at large momenta $k \to \infty$. This fact has been elucidated recently in a series of papers by Tan [37, 38, 39]. As a consequence of this long tail the kinetic energy $\langle H_{\rm kin} \rangle \sim \Lambda$ as well as the potential energy $\langle H_{\rm int} \rangle \sim \Lambda$ formally diverge linearly with the momentum cutoff Λ, with their sum being finite, of course. One may thus wonder if the expression (2.31) is well defined and leads to physical results, if the interaction energy formally diverges. Interestingly it turns out, however, that the mean-rf shift is indeed finite because the bare coupling strengths $\bar{g}$ formally tend to zero and regularize the expression for the mean rf-shift. Indeed, as shown in the appendix, the bare couplings $\bar{g}_{\sigma\sigma'}$ are related to the physical s-wave scattering lengths $a_{\sigma\sigma'}$ via

$$\frac{1}{\bar{g}_{\sigma\sigma'}} = \frac{m}{4\pi a_{\sigma\sigma'}} - \int_{k<\Lambda} \frac{d^3k}{(2\pi)^3} \frac{1}{2\varepsilon_{\mathbf{k}}} \tag{2.32}$$

where $a_{\sigma\sigma'}$ is the s-wave scattering length between atoms in states $|\sigma\rangle$ and $|\sigma'\rangle$ and we have explicitly included the UV-cutoff $\Lambda \to \infty$. Plugging this result into (2.31) and expanding to leading order in the momentum cutoff Λ leads to

$$\bar{\omega} = \frac{\pi}{2} \frac{\langle H_{\rm int}^{12} \rangle}{\Lambda\, N_2} \left(\frac{1}{a_{13}} - \frac{1}{a_{12}} \right) \tag{2.33}$$

Now we need an expression for the interaction energy $\langle H_{\rm int} \rangle \sim \Lambda$, where the cutoff dependence is explicitly visible. One possibility is to use a result derived by Tan [37], who has

[10] The term 'binding energy' is used here in a rather general sense. It includes the binding energy of two-particle bound states as well as mean field interaction energies.

shown that the total energy $E = \langle H \rangle$ of a balanced Fermi gas with contact interaction is given by

$$E = 2\sum_{\mathbf{k}} \varepsilon_{\mathbf{k}} \left(n_{\mathbf{k}} - \frac{C}{k^4} \right) + V \frac{C}{4\pi m a} \,. \tag{2.34}$$

Here, the factor 2 comes from the spin degeneracy, a is the scattering length and C is the so called 'contact coefficient', which is determined by the asymptotics of the momentum distribution at large momenta[11]

$$n_{\mathbf{k}} \overset{k\to\infty}{\longrightarrow} \frac{C}{k^4} \,. \tag{2.35}$$

The result (2.34) is remarkable, since it shows that the total ground state energy of an ultracold gas with short range interactions is a function of the momentum distribution alone. From Tan's energy relation it is obvious, that the interaction energy contribution is determined by[12]

$$\begin{aligned} \langle H_{\mathrm{int}} \rangle &= E - \langle H_{\mathrm{kin}} \rangle \;=\; E - 2\sum_{\mathbf{k}} \varepsilon_{\mathbf{k}} n_{\mathbf{k}} \\ &= -2C \sum_{\mathbf{k}} \frac{\varepsilon_{\mathbf{k}}}{k^4} + C\frac{V}{4\pi m a} \\ &= -C\frac{V}{2\pi^2 m}\,\Lambda + C\frac{V}{4\pi m a} \,. \end{aligned} \tag{2.36}$$

Note that the second term is not cutoff dependent and thus irrelevant in the limit $\Lambda \to \infty$. Using Eq. (2.36) together with Eq. (2.33), we obtain a cutoff independent result for the mean rf-shift. Simultaneously, a different approach to make the cutoff dependence of $\langle H_{\mathrm{int}} \rangle$ explicit was utilized by Baym et al. [41], who used the fact that the interaction energy can be expressed as a derivative of the total ground state energy with respect to the inverse scattering length via

$$\langle H_{\mathrm{int}} \rangle = \bar{g}\frac{\partial E}{\partial \bar{g}} = \frac{2\Lambda}{\pi}\frac{\partial E}{\partial (1/a)} \tag{2.37}$$

Plugging this expression into (2.33) also leads to a cutoff independent expression for the mean rf-shift. The fact that both results (2.36) and (2.37) are equivalent follows from Tan's adiabatic theorem [37]

$$\frac{\partial (E/V)}{\partial (1/a)} = -\frac{C}{4\pi m} \,, \tag{2.38}$$

which relates to contact coefficient to the derivative of the ground state energy with respect to the inverse scattering length.

[11] Interestingly, the contact coefficient C shows up in many different contexts. For example, Braaten and Platter have shown that C is related to the probability that two Fermions with opposite spin are close to each other [40].

[12] We note that this result also holds for the imbalanced Fermi gas with $N_\uparrow \neq N_\downarrow$. In this case, the momentum distributions of the two Fermion species are different, but the asymptotics at large momenta are identical, because the asymptotics are determined by two particle physics. We will give an explicit example in section 3.1.3.

We obtain our final expression for the mean rf-shift using equations (2.36) and (2.33). In order to eliminate the dependence of the mean rf-shift $\bar{\omega} \sim \langle H_{\rm int}\rangle/N_2$ on the number of atoms in state $|2\rangle$ it is convenient to define a dimensionless contact coefficient s via

$$s = \frac{C}{k_{F2}^3\, k_{F1}}\,, \tag{2.39}$$

where the Fermi momenta are defined via the respective densities of the atoms in states $|1\rangle$ and $|2\rangle$ as $k_{F1}^3 = 6\pi^2 n_1$ and $k_{F2}^3 = 6\pi^2 n_2$. For balanced gases $n_1 = n_2 = n/2$, this definition reduces to the 'canonical' definition $s = C/k_F^4$ with $k_F^3 = 3\pi^2 n$. Using (2.39) our final result for the mean rf-shift is given by [42]

$$\frac{\bar{\omega}}{\varepsilon_{F1}} = -3\pi\, s \left(\frac{1}{k_{F1}a_{13}} - \frac{1}{k_{F1}a_{12}}\right)\,, \tag{2.40}$$

which holds for balanced, as well as imbalanced Fermi gases. It is interesting to note that the mean rf-shift $\bar{\omega}$ is well defined only in the presence of final state interactions $a_{13} \neq 0$. Indeed, as will be shown below, the rf-spectrum $I(\omega)$ decays at large frequencies like $\sim \omega^{-3/2}$ in the case of vanishing final state interactions, thus the first moment of $I(\omega)$ doesn't exist.

Mean rf-shift of the balanced Fermi gas in the BCS- and BEC-limits

We now employ Eq. (2.40) to calculate the mean rf-shifts of the balanced Fermi gas in the well known BCS- and BEC-limits. Using an extended BCS-theory for the crossover, the dimensionless contact coefficient is given by

$$s_{\rm BCS} = \frac{\Delta^2}{4\varepsilon_F^2}\,, \tag{2.41}$$

where $\varepsilon_F = (3\pi^2 n)^{2/3}/(2m)$ is the Fermi energy of the balanced gas. In the expression above Δ is the well known BCS gap-parameter. In the BCS-limit $a_{12} \to 0^-$ it is given by $\Delta_{\rm BCS} = 8\varepsilon_F \exp(-\pi/(2k_F|a_{12}|) - 2)$ (see e.g. [43]). One has to keep in mind however, that BCS-theory gives only a sub-leading correction to the ground state energy and thus to the mean rf-shift in the BCS-limit, where the Hartree term $\sim a_{12}n$ is the dominant contribution to the interaction energy. On the other hand one obtains $\Delta_{\rm BEC} = 4\varepsilon_F/\sqrt{3\pi k_F a_{12}}$ in the BEC-limit $a_{12} \to 0^+$. The mean rf-shift in the BEC-limit is thus given by

$$\bar{\omega} = 2E_b \left(1 - \frac{a_{12}}{a_{13}}\right)\,, \tag{2.42}$$

where $E_b = 1/(ma_{12}^2)$ is the binding energy of the molecule. This result is perfectly consistent with the mean rf-shift for bound-free transitions that follow from a detailed calculation of the rf-spectrum in the molecular limit by Chin and Julienne [44], who get

$$I(\omega) \sim \frac{(\omega - E_b)^{1/2}}{\omega^2(\omega + E_b' - E_b)}\,, \tag{2.43}$$

where $E_b = 1/(ma_{12}^2)$ and $E_b' = 1/(ma_{13}^2)$. The mean shift corresponding to this rf-spectrum is indeed given by Eq. (2.42).

Mean rf-shift of the unitary Fermi gas

At unitarity $a_{12} \to \infty$, the mean rf-shift can be expressed as

$$\bar{\omega} = -\frac{3\pi\, s}{2}\,\frac{v_{F1}}{a_{13}}\,, \tag{2.44}$$

where $v_{F1} = k_{F1}/m$ is the Fermi velocity of the atoms in state $|1\rangle$. For the case of a balanced $(1,2)$-Fermi gas, the dimensionless contact coefficient s can be calculated using Tan's adiabatic theorem (2.38) and numerical results for the ground state energy, for example. Recently, we obtained $s \simeq 0.08$ for the balanced, unitary gas at zero temperature [28], which is very close to the value $s \simeq 0.07$ for a strongly imbalanced gas (see Eq. (3.33)). This result is consistent with the experiments by Schunck et al. [13], who observe almost no change in the rf-spectrum when going from the balanced superfluid to the imbalanced normal phase at unitarity.

2.2.2 RF-spectrum in the case of no final state interactions

In this section we are going to evaluate the retarded susceptibility (2.18) in detail and show how it is connected to the spectral function of the interacting Fermi gas. In particular we focus on the situation of vanishing final state interactions ($\bar{g}_{13} = \bar{g}_{23} = 0$), where the following calculation is exact.

The explicit calculation of the retarded susceptibility in equation (2.18) is conveniently performed in the Matsubara representation [34, 45, 46], i.e. we calculate the Matsubara susceptibility $\chi(i\Omega_n)$ and obtain the retarded susceptibility by an analytic continuation to the real axis $\chi(\omega) = \chi(i\Omega_n \to \omega + i0^+)$, which can be inferred using a Lehmann representation of the susceptibilities. Using the Matsubara representation has the further advantage that we get an expression for the retarded susceptibility that is valid at arbitrary temperatures. The Matsubara susceptibility is given by

$$\chi(i\Omega_n) = \int_0^\beta d\tau\, e^{i\Omega_n\tau}\,\chi(\tau) = -\int_0^\beta d\tau\, e^{i\Omega_n\tau}\,\left\langle T_\tau A(\tau)A^\dagger(0)\right\rangle \tag{2.45}$$

where $\Omega_n = 2\pi n/\beta$ with $n \in \mathbb{Z}$ are bosonic Matsubara frequencies and T_τ denotes the imaginary time ordering symbol. Inserting the expressions for the operators (2.19) in Matsubara representation we get (note again that we set $\mathbf{k}_L = 0$)

$$\chi(i\Omega_n) = -\int_0^\beta d\tau\, e^{i\Omega_n\tau}\int d^3x\, d^3x'\,\left\langle T_\tau \bar{\psi}_3(\mathbf{x},\tau)\psi_2(\mathbf{x},\tau)\bar{\psi}_2(\mathbf{x}',0)\psi_3(\mathbf{x}',0)\right\rangle\,. \tag{2.46}$$

For the case of vanishing final state interactions, no vertex corrections need to be taken into account and the expectation value above can be factorized into two Matsubara Green's functions. The diagrammatic representation is shown in Fig. 2.3. After switching to momentum- and frequency space one thus gets

$$\chi(i\Omega_n) = \frac{1}{\beta}\sum_{\omega_m}\int\frac{d^3k}{(2\pi)^3}\mathcal{G}_3(\mathbf{k},i\omega_m)\mathcal{G}_2(\mathbf{k},i\omega_m + i\Omega_n) \tag{2.47}$$

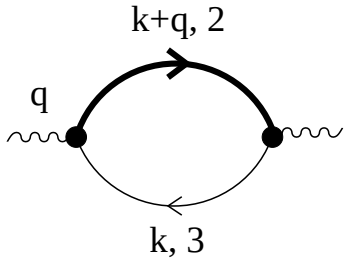

Figure 2.3: Diagrammatic representation of the rf-susceptibility. The bold line corresponds to the full Green's function of a Fermion in state $|2\rangle$ (i.e. dressed by interactions with state $|1\rangle$) and the thin line is the bare Green's function for a Fermion in state $|3\rangle$. Vertex corrections are absent in the case of vanishing final state interactions $\bar{g}_{13} = \bar{g}_{23} = 0$.

where $\omega_m = (2m+1)\pi/\beta$ with $m \in \mathbb{Z}$ are fermionic Matsubara frequencies. After replacing the Matsubara summation by a contour integral in the usual way[13] and performing the analytic continuation $i\Omega_m \to \omega + i0^+$ to real frequencies, we obtain the following expression for the imaginary part of the retarded susceptibility

$$\chi''(\omega) = \sum_{\mathbf{k}} \int \frac{d\Omega}{\pi} \, \mathrm{Im}G_3^R(\mathbf{k}, \Omega) \, \mathrm{Im}G_2^R(\mathbf{k}, \Omega + \omega) \big(n_F(\Omega + \omega) - n_F(\Omega) \big) \,, \tag{2.48}$$

and $n_F(\omega)$ denotes the Fermi distribution. Since the state $|3\rangle$ is not interacting with the other two, we can insert the free retarded Green's function for G_3^R, i.e.

$$\mathrm{Im}G_3^R(\mathbf{k}, \omega) = -\pi \, \delta(\omega - \varepsilon_{\mathbf{k}} - \omega_{23} + \mu_3) \tag{2.49}$$

where we have explicitly included the energy difference ω_{23} between the two hyperfine levels $|2\rangle$ and $|3\rangle$. Using Eq. (2.17), adopting the normalization condition (2.25) and using the fact that the state $|3\rangle$ is initially empty ($\mu_3 = 0$), we obtain our final expression for the rf-spectrum $I(\omega) = \chi''(\mu_3 - \mu_2 - \omega_{23} - \omega)/(\pi V)$

$$I(\omega) = \frac{1}{2\pi} \int \frac{d^3k}{(2\pi)^3} \, \mathcal{A}_2(\mathbf{k}, \varepsilon_{\mathbf{k}} - \omega - \mu_2) \; n_F(\varepsilon_{\mathbf{k}} - \omega - \mu_2) \tag{2.50}$$

where we have introduced the spectral function

$$\mathcal{A}_2(\mathbf{k}, \omega) = -2 \, \mathrm{Im}G_2^R(\mathbf{k}, \omega) \tag{2.51}$$

of Fermions in state $|2\rangle$ and the rf-frequency ω_L is measured with respect to the bare transition frequency, i.e. $\omega_L - \omega_{23} = \omega$. Using this convention, the rf-spectrum for a non-interacting Fermi gas in state $|2\rangle$ is a delta-peak at $\omega = \omega_L - \omega_{23} = 0$, corresponding to the bare rf-transition frequency.

[13] For details, see the similar calculation in section 2.3 below.

The spectral function $\mathcal{A}(\mathbf{k},\omega)$ contains all information about the single particle- and hole-excitations of the system. In particular, the momentum, energy and lifetime of these excitations can be obtained from it. In the following, we collect some properties of the spectral function which will be useful in later sections. First of all, $\mathcal{A}(\mathbf{k},\omega)$ can be decomposed into a sum of a particle- and a hole-part $\mathcal{A}(\mathbf{k},\omega) = \mathcal{A}_+(\mathbf{k},\omega) + \mathcal{A}_-(\mathbf{k},\omega)$, describing the particle- and the hole-excitations respectively. In terms of a Lehmann representation, these two parts can be expressed as

$$\mathcal{A}_+(\mathbf{k},\omega) = \frac{2\pi}{Z}\sum_{n,m} e^{-\beta E_n} \left|\langle m|c_{\mathbf{k}}^\dagger|n\rangle\right|^2 \delta(\omega - E_m + E_n) \tag{2.52}$$

$$\mathcal{A}_-(\mathbf{k},\omega) = \frac{2\pi}{Z}\sum_{n,m} e^{-\beta E_n} \left|\langle m|c_{\mathbf{k}}|n\rangle\right|^2 \delta(\omega + E_m - E_n)\,. \tag{2.53}$$

Here, the states $|n\rangle$ and $|m\rangle$ denote exact eigenstates of the interacting system with energies E_n and E_m, respectively, and Z is the canonical partition function. The spectral function is normalized as $\int \frac{d\omega}{2\pi}\mathcal{A}(\mathbf{k},\omega) = 1$ and the integral over the hole part $\mathcal{A}_-(\mathbf{k},\omega)$ gives the momentum distribution

$$\int \frac{d\omega}{2\pi}\mathcal{A}_-(\mathbf{k},\omega) = n(\mathbf{k}) \tag{2.54}$$

From Eqs. (2.52) and (2.53) it can be easily shown, that the particle- and the hole-part of the spectral function are related via a detailed balance condition

$$\mathcal{A}_-(\mathbf{k},\omega) = e^{-\beta\omega}\mathcal{A}_+(\mathbf{k},\omega) \tag{2.55}$$

From this follows, that the hole-part of the spectral function is given by

$$\mathcal{A}_-(\mathbf{k},\omega) = n_F(\omega)\mathcal{A}(\mathbf{k},\omega) \tag{2.56}$$

and thus the rf-spectrum (2.50) is a measure of the hole-part only. This is obvious from physical reasons, because the rf-transition removes particles from state $|2\rangle$, thereby creating hole-excitations in the interacting $(1,2)$-Fermi system.

RF-spectra in BCS theory

Now we are in a position to calculate the rf-spectra of ultracold Fermi gases using Eq. (2.50) and compare them directly to experiments. The only quantity that is needed as input is the spectral function $\mathcal{A}(\mathbf{k},\omega)$ of the interacting many-body system, which is usually known only approximately, however. One important example where the spectral function is known analytically is BCS-theory

$$\mathcal{A}_{BCS}(\mathbf{k},\omega) = 2\pi\left[u_{\mathbf{k}}^2\delta(\omega - E_{\mathbf{k}}) + v_{\mathbf{k}}^2\delta(\omega + E_{\mathbf{k}})\right]\,. \tag{2.57}$$

At zero temperature, this gives rise to an rf-spectrum of the form

$$I(\omega) = \frac{m^{3/2}}{\sqrt{2}\,\pi^2}\sqrt{\frac{\omega}{2} + \mu - \frac{\Delta^2}{2\omega}}\,\frac{\Delta^2}{2\omega^2}\,, \tag{2.58}$$

which has a sharp onset at $\omega_{\min} = \sqrt{\mu^2 + \Delta^2} - \mu$. In weak coupling, $\Delta \ll \mu \approx \varepsilon_F$, the onset corresponds to the condensation energy per particle $\omega_{\min} \simeq \Delta^2/(2\varepsilon_F)$ and the peak position is at $\omega_{\text{peak}} \simeq \frac{5}{8}\Delta^2/\varepsilon_F$. Furthermore, the rf-spectrum has a tail $\sim \omega^{-3/2}$ at large frequencies, thus the first moment doesn't exist.

As can be seen from Eq. (2.57), BCS-theory gives rise to a sharp fermionic single-particle excitation spectrum, i.e. the lifetime of the excitations is infinite for all momenta, even at finite temperature. The BCS-result is based on an approximate Hamiltonian, however, which neglects the effect of the collective Bogoluibov-Anderson mode on the fermionic excitation spectrum. Indeed, the interaction with Bogoliubov-Anderson phonons should lead to an appreciable lifetime-broadening of the fermionic quasiparticles and thus should have an observable effect on the rf-spectra. Some aspects of this question will be discussed in Appendix B.

2.3 Non-selfconsistent T-matrix approach for the imbalanced Fermi gas

In this section we formulate a theory that is capable of describing the normal phase of the attractively interacting, imbalanced Fermi gas above the Clogston-Chandrasekhar limit. In particular, our aim is to provide a qualitative as well as a quantitative understanding of the experimental results by Schunck et al. [13], who observed shifted rf-spectra in the normal phase of the imbalanced Fermi gas also in the normal state. Our starting point is the Hamiltonian

$$H = \sum_{\mathbf{k},\,\sigma=\uparrow,\downarrow} (\varepsilon_{\mathbf{k}} - \mu_\sigma)\, c^\dagger_{\mathbf{k}\sigma} c_{\mathbf{k}\sigma} + \frac{\bar{g}}{V} \sum_{\mathbf{k}',\mathbf{k},\mathbf{q}} c^\dagger_{\mathbf{q}-\mathbf{k}\uparrow} c^\dagger_{\mathbf{k}\downarrow} c_{\mathbf{k}'\downarrow} c_{\mathbf{q}-\mathbf{k}'\uparrow}\,. \tag{2.59}$$

describing a two-species Fermi gas with a contact interaction. We denote the majority atoms with $\uparrow$ and the minority atoms with $\downarrow$ in the remainder of this thesis, i.e. $n_\uparrow > n_\downarrow$. Furthermore, we use a grand-canonical description, where the population imbalance is imposed by applying different chemical potentials μ_σ for the two fermionic species. This can be described conveniently by introducing an effective magnetic field h that couples to the two different pseudo-spin states $\sigma = \uparrow, \downarrow$ via

$$\mu_{\uparrow,\downarrow} = \mu \pm h\,. \tag{2.60}$$

Note that this artificial magnetic field couples only to the "spin" of the uncharged atoms. For charged particles such as electrons, the orbital coupling of the magnetic field leads to the Meissner effect in the superconducting state and thus the coupling to the spin degree of freedom is effectively absent in the bulk. In that respect, ultracold atoms offer the unique possibility to study the Pauli-pair-breaking mechanism in its pure form.

In order to study the effects of pairing fluctuations on the single particle properties of the imbalanced Fermi gas in the normal phase, we employ a non-selfconsistent T-matrix approach. This method has been used widely in the literature to study the BCS-BEC crossover of the balanced gas above T_c [47, 48], or the normal phase of the attractive-U

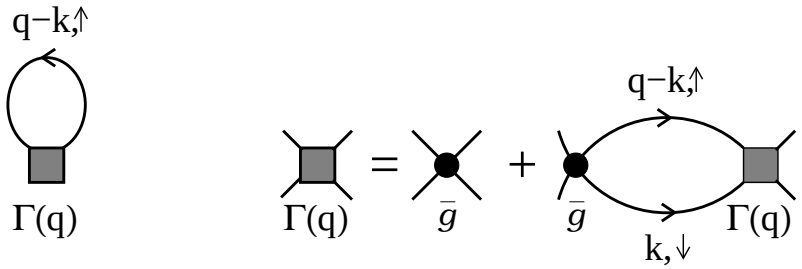

Figure 2.4: Left: diagram for the self-energy $\Sigma_\downarrow(\mathbf{k},\omega)$ of the minority species Green's function. Right: Bethe-Salpeter equation for the vertex function $\Gamma(\mathbf{q},\omega)$ in ladder approximation.

Hubbard model [49]. It has also been applied recently to study the strongly imbalanced Fermi gas at the saturation field [50]. In the non-selfconsistent T-matrix approach[14], a usual particle-particle ladder approximation is used to incorporate the effects of pairing in the vertex function (see e.g. [45, 51]) and the fermionic self-energy is calculated at the one-loop level, including the vertex corrections. The diagrams for the self-energy Σ and the vertex function Γ are shown in Fig. 2.4. In Matsubara representation, the corresponding analytic expressions are

$$\Sigma_\sigma(\mathbf{k}, i\omega_n) = \frac{1}{\beta}\sum_{\Omega_m}\int\frac{d^3q}{(2\pi)^3}\,\Gamma(\mathbf{q}, i\Omega_m)\mathcal{G}_{-\sigma}(\mathbf{q}-\mathbf{k}, i\Omega_m - i\omega_n) \tag{2.61}$$

$$\Gamma(\mathbf{q}, i\Omega_n) = \frac{1}{1/\bar{g} - L(\mathbf{q}, i\Omega_n)} \tag{2.62}$$

$$L(\mathbf{q}, i\Omega_n) = -\frac{1}{\beta}\sum_{\omega_m}\int\frac{d^3k}{(2\pi)^3}\,\mathcal{G}_\uparrow(\mathbf{q}-\mathbf{k}, i\Omega_n - i\omega_m)\mathcal{G}_\downarrow(\mathbf{k}, i\omega_m) \tag{2.63}$$

where $\mathcal{G}_\uparrow$ and $\mathcal{G}_\downarrow$ are the bare Matsubara-Green's functions of the majority- and minority Fermions, $\beta = 1/k_BT$ is the inverse temperature and the fermionic- and bosonic Matsubara frequencies are denoted by $\omega_n = (2n+1)\pi/\beta$ and $\Omega_n = 2\pi n/\beta$ respectively, with $n \in \mathbb{Z}$.

We evaluate the sums over Matsubara frequencies using standard techniques (see e.g. [34] and [45]), where the sums are represented as contour integrals over the complex coordinate $i\omega_m, i\Omega_m \to z$. We start by calculating the sum for the pair propagator $L(\mathbf{q}, i\Omega_n)$. As a function of z, the two Green's functions in (2.63) have poles on the real axis and at $z = i\Omega_n + \varepsilon$ with some $\varepsilon \in \mathbb{R}$, respectively. Thus, using the contour depicted in Fig. 2.5a, the Matsubara sum can be written as

$$L(\mathbf{q}, i\Omega_n) = \int\frac{d^3k}{(2\pi)^3}\oint_{\mathcal{C}_1}\frac{dz}{2\pi i}\,n_F(z)\,\mathcal{G}_\uparrow(\mathbf{q}-\mathbf{k}, i\Omega_n - z)\mathcal{G}_\downarrow(\mathbf{k}, z)\,, \tag{2.64}$$

[14] We note that the term "non-selfconsistent" refers to the fact, that all internal propagator lines in the diagrams are bare (i.e. non-interacting) Green's functions and the notion "T-matrix approach" is due to the replacement of the bare interaction vertex $\bar{g}$ with the scattering T-matrix of two particles in vacuum.

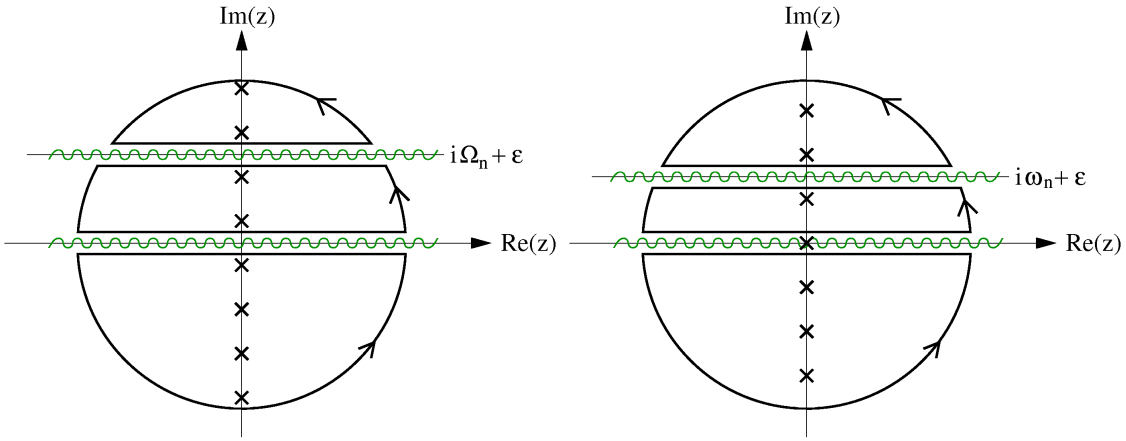

Figure 2.5: Contours for the evaluation of the Matsubara sums for the pair-propagator L (left) and the fermionic self-energy Σ (right). The radius of the circles is taken to infinity. The crosses mark the positions of the fermionic (left) and bosonic (right) Matsubara frequencies, i.e. the positions of the poles of $n_F(z)$ and $n_B(z)$.

where $n_F(z) = (\exp(\beta z) + 1)^{-1}$ is the Fermi distribution function which has poles at the fermionic Matsubara frequencies $i\omega_n$ with residuum $\mathrm{Res}[n_F(z), i\omega_n] = -\beta^{-1}$. The retarded pair propagator $L^R(\mathbf{q}, \Omega)$ is obtained via an analytic continuation $i\Omega_n \to \Omega + i0^+$ to real frequencies $\Omega \in \mathbb{R}$. Using $\mathcal{G}(\mathbf{k}, \Omega + i0^+) = G^R(\mathbf{k}, \Omega)$, $\mathcal{G}(\mathbf{k}, \Omega - i0^+) = G^A(\mathbf{k}, \Omega)$, where G_R and $G_A = G_R{}^*$ denote the retarded and advanced Green's functions respectively, and using $n_F(z + i\Omega_n) = n_F(z)$ we finally get

$$\begin{aligned} L^R(\mathbf{q}, \Omega) &= \int \frac{d^3k}{(2\pi)^3} \int_{-\infty}^{\infty} \frac{dz}{\pi}\, n_F(z) \Big[G^R_\uparrow(\mathbf{q}-\mathbf{k}, \Omega - z)\, \mathrm{Im} G^R_\downarrow(\mathbf{k}, z) \\ &\qquad - G^R_\downarrow(\mathbf{k}, z+\Omega)\, \mathrm{Im} G^R_\uparrow(\mathbf{q}-\mathbf{k}, -z) \Big] \\ &= \int \frac{d^3k}{(2\pi)^3} \frac{n_F(\mu_\uparrow - \varepsilon_{\mathbf{q}-\mathbf{k}}) - n_F(\varepsilon_{\mathbf{k}} - \mu_\downarrow)}{\Omega - \varepsilon_{\mathbf{k}} - \varepsilon_{\mathbf{q}-\mathbf{k}} + 2\mu + i0^+} \,. \end{aligned} \tag{2.65}$$

The 'retarded' vertex function is then straightforwardly defined via[15]

$$\Gamma^R(\mathbf{q}, \omega) = \frac{1}{\bar{g}^{-1} - L^R(\mathbf{q}, \omega)} \,. \tag{2.66}$$

Obviously, the integral in the definition (2.65) of the pair propagator diverges at large momenta and needs to be regularized. This can be achieved by replacing the bare interaction strength $\bar{g}$ in the vertex function with the scattering T-matrix of two Fermions in

[15] Albeit using the superscript ^{R}, the vertex function $\Gamma^R(\mathbf{q}, \omega)$ is not a retarded function in the usual sense. Indeed, $\Gamma^R(\mathbf{q}, \omega)$ can have poles in the upper half complex plane. The superscript ^{R} is just an indication that we have obtained the vertex function by an analytic continuation to $\omega + i0^+$.

vacuum, as shown in appendix A. We thus obtain

$$\Gamma^R(\mathbf{q},\omega) = \Big[\frac{m}{4\pi a} - L^R_{\rm reg}(\mathbf{q},\omega)\Big]^{-1}\,, \tag{2.67}$$

where the regularized pair propagator, given by

$$L^R_{\rm reg}(\mathbf{q},\omega) = L^R(\mathbf{q},\omega) + \int \frac{d^3k}{(2\pi)^3}\frac{1}{2\varepsilon_{\mathbf{k}}}\,, \tag{2.68}$$

is now well defined.

The Matsubara sum for the fermionic self-energy in Eq. (2.61) can be evaluated in a similar manner. In the following calculation we assume that the Vertex function $\Gamma(\mathbf{q},\omega)$ has poles or branch cuts only on the real axis. This assumption is crucial and intimately connected to the fact that our calculation is valid only for the non-superfluid, normal phase. Indeed, the appearance of a pole in the Vertex function in the upper half complex plane would signal the onset of superfluidity [45]. As will be discussed in the next section, the instability towards the superfluid phase occurs first at $\omega = 0$ and $\mathbf{q} = 0$, giving rise to the so called Thouless-criterion [52], which determines the boundary between the normal and the superfluid phase. Restricting ourselves to the normal phase, where the poles of the vertex function are on the real axis, the contour integral for the evaluation of the Matsubara sum is given by

$$\begin{aligned}\Sigma_\sigma(\mathbf{k},i\omega_n) &= \int \frac{d^3q}{(2\pi)^3}\Big[\oint_{\mathcal{C}_2}\frac{dz}{2\pi i}\,n_B(z)\,\Gamma(\mathbf{q},z)\mathcal{G}_{-\sigma}(\mathbf{q}-\mathbf{k},z-i\omega_n)\\ &\quad +\frac{1}{\beta}\,\Gamma(\mathbf{q},0)\mathcal{G}_{-\sigma}(\mathbf{q}-\mathbf{k},-i\omega_n)\Big]\,.\end{aligned} \tag{2.69}$$

Here, $n_B(z) = (\exp(\beta z)-1)^{-1}$ is the Bose distribution function which has poles at the bosonic Matsubara frequencies $i\Omega_n$ with residuum $\mathrm{Res}[n_B(z), i\Omega_n] = \beta^{-1}$ and the contour is depicted in Fig. 2.5b. Note that the term at $i\Omega_n = 0$ has to be included separately. After performing the analytical continuation to real frequencies and using $n_B(z+i\omega_n) = -n_F(z)$ we obtain the retarded fermionic self-energy

$$\begin{aligned}\Sigma^R_\sigma(\mathbf{k},\omega) &= \int \frac{d^3q}{(2\pi)^3}\int_{-\infty}^{\infty}\frac{dz}{\pi}\Big[n_B(z)\,G^A_{-\sigma}(\mathbf{q}-\mathbf{k},z-\omega)\,\mathrm{Im}\Gamma^R(\mathbf{q},z)\\ &\qquad -n_F(z)\,\Gamma^R(\mathbf{q},z+\omega)\,\mathrm{Im}G^R_{-\sigma}(\mathbf{q}-\mathbf{k},z)\Big]\,,\end{aligned} \tag{2.70}$$

where the separately included $i\Omega_n = 0$ term in (2.69) cancels exactly with the residue obtained by integrating above and below the pole of $n_F(z)$ at $z = 0$.

Within the non-selfconsistent T-matrix approach, the equations (2.65), (2.66) and (2.70) determine the properties of the imbalanced Fermi gas in the normal phase. We note however, that the chemical potential of the minority atoms in these equations has to be evaluated selfconsistently in order to get correct results in the whole crossover regime. Indeed, the chemical potential of the minority atoms in the BEC-limit is predominantly determined by the molecular binding energy, thus setting $\mu_\downarrow = \varepsilon_{F\downarrow}$ in the equations above

would lead to wrong results[16]. The chemical potential of the majority atoms $\mu_\uparrow$, however, does not need not be calculated selfconsistently for arbitrary coupling. Naively, this can be understood from the fact that in the BEC-regime all minority atoms are already paired, thus adding a further majority atom does not alter the ground state energy significantly in comparison to the non-interacting case. Recently, Veillette et al. [53] used a $1/N$-expansion to analyze the imbalanced gas at unitarity, which is equivalent to our T-matrix approximation in leading order. They did not determine the minority chemical potential self-consistently, however, and thus get $\mu_\downarrow \simeq -0.9\varepsilon_F$ at the saturation field at unitarity, which is 50% off the Monte-Carlo result $\mu_\downarrow \simeq -0.6\varepsilon_F$. Furthermore, their calculation breaks down at $(k_F a)^{-1} \approx 0.3$, where $\mu_\downarrow$ diverges in their approach.

In the following section we will discuss the properties of the vertex function in more detail. After that, we are going to calculate the fermionic spectral functions, thereby obtaining an explicit expression for the rf-spectrum of imbalanced Fermi gases in the normal phase at unitarity and zero temperature.

2.3.1 The Vertex function $\Gamma(\mathbf{q}, \Omega)$ at zero temperature

The vertex function $\Gamma(\mathbf{q}, \Omega)$ corresponds to the non-trivial part of the two-particle propagator. Its poles thus determine the dispersion relation of two-particle excitations of the imbalanced Fermi gas (see e.g. [54]). We start by discussing the poles of the vertex function (2.67) at zero temperature and zero momentum $\mathbf{q} = 0$. As mentioned previously, the chemical potential of the minority atoms $\mu_\downarrow$ in the imbalanced gas has to be calculated selfconsistently, in contrast to the majority chemical potential $\mu_\uparrow$. We thus set $\mu_\uparrow = \varepsilon_F$ in the expression (2.68) for the pair propagator (this approximation is exact close to the saturation field h_s), where $\varepsilon_F = k_F^2/(2m)$ is the Fermi energy associated with the density of the majority atoms, i.e. $k_F^3 = 6\pi^2 n_\uparrow$. After evaluating the integral we obtain

$$\begin{aligned}
\mathrm{Re}L^R_{\mathrm{reg}}(\mathbf{0},\omega) &= \frac{mk_F}{2\pi^2}\left[1+\sqrt{\tilde{\mu}_\downarrow}+\sqrt{|\lambda|}\begin{cases}\frac{1}{2}\ln\left|\frac{1-\sqrt{\lambda}}{1+\sqrt{\lambda}}\right|+\frac{1}{2}\ln\left|\frac{\sqrt{\tilde{\mu}_\downarrow}-\sqrt{\lambda}}{\sqrt{\tilde{\mu}_\downarrow}+\sqrt{\lambda}}\right| & \text{if } \lambda>0\\ \frac{\pi}{2}-\arctan\sqrt{\frac{1}{\lambda}}-\arctan\sqrt{\frac{\tilde{\mu}_\downarrow}{\lambda}} & \text{if } \lambda<0\end{cases}\right]\\
\mathrm{Im}L^R(\mathbf{0},\omega) &= \frac{mk_F}{2\pi^2}\,\frac{\pi}{2}\,\sqrt{\lambda}\,\Theta(\lambda)\left[\Theta(\tilde{\mu}_\downarrow-\lambda)-\Theta(\lambda-1)\right], \qquad (2.71)
\end{aligned}$$

where we have used the abbreviations $\lambda := (\varepsilon_F + \mu_\downarrow + \omega)/(2\varepsilon_F)$ and $\tilde{\mu}_\downarrow := \mu_\downarrow/\varepsilon_F$. Note that in case of a negative chemical potential of the minority atoms $\mu_\downarrow < 0$ (which happens in particular close to h_s), all terms where $\tilde{\mu}_\downarrow$ appears vanish identically in the expressions for the pair propagator above. For the case of positive $\mu_\downarrow$'s, the real part of the pair propagator has two poles at $\omega = \pm 2h$, as can be seen in Fig. 2.6. At a fixed magnetic field h, the corresponding vertex function $\Gamma(\mathbf{0}, \omega)$ has either two poles on the real axis in the region $-2h < \omega < 2h$, or two poles in the complex plane, depending on the interaction

[16] This situation is similar to the BCS-theory for the balanced crossover, where two equations (the gap-equation and the particle-number equation) are needed to determine all ground state properties. Setting $\mu = \varepsilon_F$ amounts to a neglect of the particle-number equation in this case.

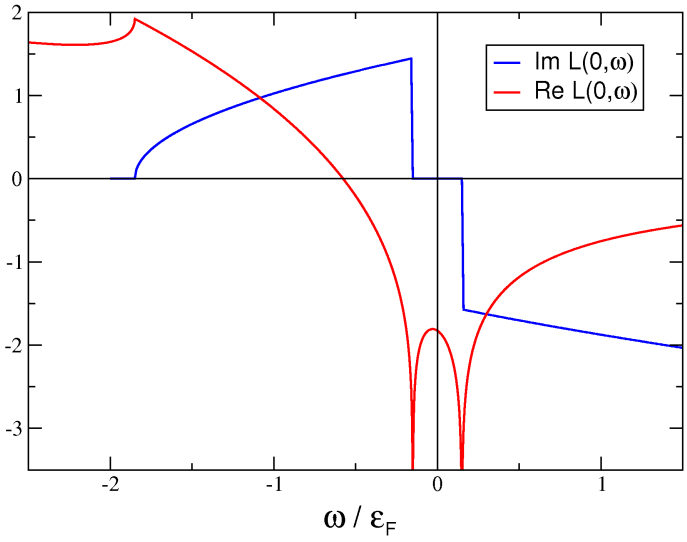

Figure 2.6: Real and imaginary part of the (regularized) pair propagator $L^R_{\rm reg}(\mathbf{q},\omega)$ at zero momentum $\mathbf{q}=0$ as a function of ω, for $2h=0.15\varepsilon_F$. The real part $\mathrm{Re}L^R_{\rm reg}(\mathbf{0},\omega)$ has two poles at $\omega=\pm 2h$, if the minority chemical potential as positive. For negative $\mu_\downarrow$'s, the pole at negative frequencies vanishes (this is an artefact of the theory and is discussed in more detail in the text).

strength[17]. Alternatively one can fix the interaction strength and vary the magnetic field h, thereby shifting the position of the poles.

In the BCS-limit ($a\to-\infty$) the poles of the vertex function jump into the complex plane right below the value of the magnetic field h, where the two poles on the real axis merge at $\omega=0$. This happens at very small magnetic fields in the BCS-limit. Expanding the vertex function in $h\ll\varepsilon_F$ leads to

$$\Gamma(\mathbf{0},0)=\frac{2\pi^2}{mk_F}\left[\frac{\pi}{2k_Fa}-2-\ln\frac{h}{4\varepsilon_F}+\mathcal{O}(h^2)\right]^{-1}. \tag{2.72}$$

The critical magnetic field $h_{\rm crit}$ below which the poles of Γ jump into the complex plane is thus given by

$$h^{\rm BCS}_{\rm crit} \;=\; 4\varepsilon_F\,\exp\left(-\frac{\pi}{2k_F|a|}-2\right) \;=\; \frac{\Delta_{\rm BCS}}{2} \tag{2.73}$$

corresponding to the lower critical field at the Clogston-Chandrasekhar transition[18]. The critical field $h_{\rm crit}$ where a pole in the vertex function appears at $\mathbf{q}=0$ and $\omega=0$ can thus be associated with the onset of superfluidity. This condition is known in the literature as

[17]Note that the term proportional to the inverse interaction strength $1/g$ in the vertex function (2.67) effectively shifts the real part of the pair propagator up or down, thereby shifting the position of the poles.

[18]Note that the value of $h_{\rm crit}$ is below the thermodynamical critical field $h_c=\Delta/\sqrt{2}$ and corresponds to the lower critical field of the first order phase transition from the superfluid to the normal state.

the *Thouless criterion* [52]. It is important to note, however, that away from the BCS-limit, the poles of the vertex function jump into the complex plane not at $\omega = 0$ but at slightly negative frequencies. This can be seen in Fig. 2.6, where the local maximum of the real part in the regime $-2h < \omega < 2h$ is slightly below $\omega = 0$. This would lead to a slightly lower critical field than the Thouless criterion. Nevertheless, because of the reasons to be explained in the following sub-section, we use the Thouless criterion to determine the boundary of the superfluid phase. At negative minority chemical potentials $\mu_\downarrow < 0$, the pole of the pair propagator at negative frequencies vanishes. This is an artefact of the theory and related to the fact, that the occupation number of the minority Fermion modes in the expression (2.65) for the pair propagator is identically zero at $T = 0$, which is obviously unphysical. Indeed, this has some consequences for our rf-spectra and other observables, as will be discussed in Sec. 2.3.2.

Thouless criterion

As mentioned above, the critical magnetic field below which the imbalanced Fermi gas is superfluid can be calculated from the condition that the vertex function has a pole at $\mathbf{q} = \mathbf{0}$ and $\omega = 0$, i.e.

$$\Gamma_R^{-1}(\mathbf{0}, 0) = 0\,. \tag{2.74}$$

There are several ways to understand how this condition arises. First of all it is easy to see that the Thouless criterion is equivalent to the BCS-gap equation at $\Delta = 0$, which determines the boundary of the superfluid phase within mean-field theory. Using Eqs. (2.74), (2.66) and (2.65) we obtain

$$\frac{1}{\bar{g}} = \int \frac{d^3k}{(2\pi)^3} \frac{\Theta(\varepsilon_\mathbf{k} - \mu_\uparrow) - \Theta(\mu_\downarrow - \varepsilon_\mathbf{k})}{2(\mu - \varepsilon_\mathbf{k})} \tag{2.75}$$

which is indeed equivalent to the BCS-gap equation for $\Delta = 0$.

A different way to understand the Thouless criterion is to study the response of the system to a fictitious external pairing field, which couples to the 'pairing operator' $\Delta_\mathbf{q} = \sum_\mathbf{k} c_{\mathbf{k}+\mathbf{q}\uparrow} c_{-\mathbf{k}\downarrow}$. Within a mean-field RPA calculation, the corresponding response function is given by [55]

$$\chi(\mathbf{q}, \omega) = \frac{\chi^{(0)}(\mathbf{q}, \omega)}{1 - \bar{g}\chi^{(0)}(\mathbf{q}, \omega)} \tag{2.76}$$

where the response function $\chi^{(0)}(\mathbf{q}, \omega)$ of the non-interacting system is given by our expression (2.65) for the pair propagator. The phase transition to a homogenous superfluid state is determined by a divergence of the static response function at $\mathbf{q} = 0$, i.e. $\bar{g}^{-1} - \chi^{(0)}(\mathbf{0}, 0) = 0$, which is equivalent to the Thouless criterion for our vertex function in ladder approximation. Actually, from this calculation it can be inferred, that an instability towards a superfluid phase with an inhomogeneous order parameter (such as the FFLO phase) can be obtained from a modified Thouless criterion, where the momentum $\mathbf{q}$ is kept at a non-zero value. Indeed, if the response function diverges at a finite momentum $\mathbf{q}$ before diverging at $\mathbf{q} = 0$, the response of the system to a modulated order parameter is stronger an thus the dominant instability.

On a more formal level, the Thouless criterion (2.74) is related to the spontaneous $U(1)$-symmetry breaking in the superfluid phase and the associated massless Goldstone Boson, i.e. the Bogoliubov-Anderson mode in the case of neutral superfluids. Indeed, the pole of the exact vertex function determines the dispersion relation of collective modes in the interacting Fermi gas. Thus, the appearance of a gapless Goldstone mode manifests itself through the presence of a pole in the vertex function at zero momentum and energy. Therefore, the Thouless criterion holds quite generally and is independent from our ladder approximation for the vertex function. In particular, it can be derived from an exact Ward identity related to the $U(1)$ gauge symmetry [56].

In Eq. (2.73) we have used the Thouless criterion already to calculate the critical field in the BCS-regime. In the opposite BEC-limit ($a \to \infty$) the asymptotic value of h_{crit}, obtained using the Thouless criterion, is given by

$$h_{\mathrm{crit}}^{\mathrm{BEC}} = |E_b|/2 + \varepsilon_F - \frac{4\,k_F a}{3\pi}\,\varepsilon_F + \mathcal{O}(a^2) \tag{2.77}$$

which corresponds to the saturation field (2.8) in the BEC-limit, as expected. However, the associated atom-dimer scattering length is given by $a_{ad}^{\mathrm{Born}} = 8/3a$ instead of the exact value $a_{ad} = 1.18a$. Thus, the ladder approximation for the vertex function takes the atom-dimer scattering only at the level of Born's approximation into account.

At unitarity we obtain $h_{\mathrm{crit}}(v \to \infty) \simeq 0.36\varepsilon_F$ for the value of the critical field. The instability torwards an FFLO phase occurs at a slightly higher field $h_{\mathrm{crit}}^{\mathrm{FFLO}}(v \to \infty) \simeq 0.40\varepsilon_F$. The critical field h_{crit} at arbitrary interaction strengths obtained from the Thouless criterion is plotted in the T-matrix phase diagram in Fig. 2.7 in Sec. 2.3.3.

The Vertex function for $\mu_\downarrow < 0$ at arbitrary momenta

As mentioned several times already, the chemical potential of the minority atoms $\mu_\downarrow$ has to be calculated selfconsistently in order to obtain correct results for all interaction strengths, especially in the BEC-limit. In the rest of this chapter we restrict ourselves to the case $\mu_\downarrow = \mu - h < 0$, where the chemical potential of the minority atoms is negative. This simplifies the calculations considerably but also leads to some unphysical results, as will be seen in Sec. 2.3.2. Nevertheless, albeit using this restriction, the calculation covers a large part of the phase diagram plotted in Fig. 4.2, in particular the normal phase in the region $h/\mu_\uparrow > 0.5$. As previously, we set $\mu_\uparrow = \varepsilon_F = k_F^2/(2m)$ with $k_F^3 = 6\pi^2 n_\uparrow$ and measure all energies in units of ε_F, i.e. in units of the Fermi energy of the non-interacting majority Fermi gas.

The regularized pair propagator (2.68) can be calculated analytically at zero temper-

ature. For the real and imaginary part we obtain

$$\begin{aligned}
\mathrm{Re}L^R_{\mathrm{reg}}(\mathbf{q},\omega) &= \int \frac{d^3k}{(2\pi)^3}\Big[\frac{\Theta(\varepsilon_{\mathbf{q}-\mathbf{k}}-\mu_\uparrow)}{\omega-\varepsilon_{\mathbf{k}}-\varepsilon_{\mathbf{q}-\mathbf{k}}+2\mu}+\frac{1}{2\varepsilon_{\mathbf{k}}}\Big] \\
&= \frac{mk_F}{(2\pi)^2}\Bigg[1-\frac{1-\lambda-q^2/4}{2q}\ln\left|\frac{\lambda-(1-q/2)^2}{\lambda-(1+q/2)^2}\right| \\
&\quad +\sqrt{|\lambda|}\begin{cases}\frac{1}{2}\ln\left|\frac{(1-\sqrt{\lambda})^2-q^2/4}{(1+\sqrt{\lambda})^2-q^2/4}\right| & \text{if } \lambda>0 \\ \pi-\arctan\frac{1+q/2}{\sqrt{|\lambda|}}-\arctan\frac{1-q/2}{\sqrt{|\lambda|}} & \text{if } \lambda<0\end{cases}\Bigg] \qquad (2.78) \\
\mathrm{Im}L^R(\mathbf{q},\omega) &= -\pi\int\frac{d^3k}{(2\pi)^3}\,\delta(\omega-\varepsilon_{\mathbf{k}}-\varepsilon_{\mathbf{q}-\mathbf{k}}+2\mu)\Theta(\varepsilon_{\mathbf{q}-\mathbf{k}}-\mu_\uparrow) \\
&= -\frac{mk_F}{8\pi}\,\Theta(\lambda)\Theta(\kappa+q\sqrt{\lambda}) \\
&\quad \times\Big[2\sqrt{\lambda}\Theta(\kappa-q\sqrt{\lambda})+(\sqrt{\lambda}+\kappa/q)\Theta(-\kappa+q\sqrt{\lambda})\Big] \qquad (2.79)
\end{aligned}$$

where we have defined $q = |\mathbf{q}|/k_F$ and k_F is the momentum associated to $\mu_\uparrow = \varepsilon_F = k_F^2/(2m)$, as defined above. The abbreviations λ and κ introduced in the expressions above are defined by

$$\lambda := \frac{1}{2}+\frac{\omega+\mu_\downarrow}{2\varepsilon_F}-\frac{|\mathbf{q}|^2}{4k_F^2} \qquad (2.80)$$

$$\kappa := \frac{\omega-2h}{2\varepsilon_F} \qquad (2.81)$$

Note that one of the two Fermi distribution functions from (2.65) has dropped out at zero temperature, since we have restricted ourselves to the case $\mu_\downarrow < 0$. Apart from simplifying further calculations, this leads to some unphysical results. Usually, the nominator of the integral for the pair propagator (2.65) is nonzero if both Fermion states are either occupied or empty, i.e. scattering can only take place if two particles or holes are present. For negative $\mu_\downarrow$'s, however, we have a situation where the occupation of the minority atom states in the pair propagator is always zero at $T = 0$. As a consequence, some universal properties of the interacting Fermi gas are flawed. For example, the tails in the momentum distributions at large momenta as well as the tails in the rf-spectra at large frequencies are missing. Furthermore, the majority atoms form a non-interacting Fermi gas, which is a good approximation only in the case of very strong imbalances $n_\uparrow \gg n_\downarrow$.

2.3.2 Spectral functions $\mathcal{A}_\sigma(\mathbf{k},\omega)$ at zero temperature

In this section we are going to calculate the spectral functions $\mathcal{A}_\sigma(\mathbf{k},\omega)$ for the two Fermion species $\sigma = \uparrow,\downarrow$ at zero temperature, using the non-selfconsistent T-matrix approach introduced above. We will consider only the case, where the chemical potential of the minority atoms is negative $\mu_\downarrow < 0$ (i.e. $h > \mu$). As mentioned previously, this includes the interesting regime close to the saturation field h_s and covers almost the whole normal phase

at unitarity. In terms of the fermionic self-energy $\Sigma(\mathbf{k},\omega)$, the spectral function can be expressed as

$$\begin{aligned}\mathcal{A}_\sigma(\mathbf{k},\omega) &= -2\ \mathrm{Im}\, G^R_\sigma(\mathbf{k},\omega) \\ &= \frac{-2\ \mathrm{Im}\,\Sigma^R_\sigma(\mathbf{k},\omega)}{(\omega-\varepsilon_{\mathbf{k}}+\mu_\sigma-\mathrm{Re}\,\Sigma^R_\sigma(\mathbf{k},\omega))^2+\left(\mathrm{Im}\,\Sigma^R_\sigma(\mathbf{k},\omega)\right)^2}\end{aligned} \tag{2.82}$$

Within our non-selfconsistent T-matrix approach, the real part of the self energy (2.70) at $T=0$ is given by

$$\begin{aligned}\mathrm{Re}\,\Sigma^R_\sigma(\mathbf{k},\omega) &= \int \frac{d^3q}{(2\pi)^3}\,\Theta(\mu_{-\sigma}-\varepsilon_q)\,\mathrm{Re}\Gamma^R(\mathbf{q}+\mathbf{k},\omega+\varepsilon_q-\mu_{-\sigma}) \\ &\quad -\int \frac{d^3q}{(2\pi)^3}\frac{dz}{\pi}\frac{\Theta(-z)\,\mathrm{Im}\Gamma^R(\mathbf{q},z)}{z-\omega-\varepsilon_{\mathbf{q}-\mathbf{k}}+\mu_{-\sigma}}\end{aligned} \tag{2.83}$$

whereas the imaginary part of the self energy can be written as

$$\mathrm{Im}\,\Sigma^R_\sigma(\mathbf{k},\omega)=\int\frac{d^3q}{(2\pi)^3}\,\left\{\Theta(\mu_{-\sigma}-\varepsilon_{\mathbf{q}})-\Theta(\mu_{-\sigma}-\omega-\varepsilon_{\mathbf{q}})\right\}\ \mathrm{Im}\Gamma^R(\mathbf{q}+\mathbf{k},\omega+\varepsilon_{\mathbf{q}}-\mu_{-\sigma})\,. \tag{2.84}$$

and the retarded, regularized vertex function (2.67) is given by

$$\Gamma^R(\mathbf{q},z)=\frac{1}{1/g-\mathrm{Re}\,L^R_{\mathrm{reg}}(\mathbf{q},z)-i\ \mathrm{Im}\,L^R(\mathbf{q},z)} \tag{2.85}$$

with $g=4\pi a/m$. The real- and imaginary-parts of the pair propagator L^R are given by (2.78) and (2.79).

Spectral function of the majority Fermions $\mathcal{A}_\uparrow(\mathbf{k},\omega)$

As explained above, the chemical potential $\mu_\downarrow$ for the minority Fermions has to be calculated selfconsistently in order to obtain correct results close to the saturation field h_s. Thus, in the regime where $\mu_\downarrow<0$, the occupation number of all minority Fermion modes in the expressions for the vertex function and self-energies is zero at $T=0$. The majority atoms thus respond as if no minority atoms were present and form an ideal Fermi gas. This can be seen easily from the equations (2.83) and (2.84) for the self energy of the majority atoms. If we set $\mu_\downarrow<0$, we get

$$\Sigma^R_\uparrow(\mathbf{k},\omega)=i0^-\,. \tag{2.86}$$

Clearly, this is an unphysical artefact of the self-consistent treatment of the minority chemical potential, which suppresses the occupation of all minority Fermion modes at zero temperature if $\mu_\downarrow<0$. Obviously, even for very small minority atom concentrations, the momentum distribution of the majority atoms should be smeared out and form a $\sim k^{-4}$ tail at large momenta due to the interaction with the minority atoms. The height of this tail should scale with the number of minority atoms, however. Thus, at very large

population imbalances, the treatment of the majority Fermions as an ideal Fermi gas is a fairly good approximation. This drawback has also one minor advantage. Indeed, within the T-matrix approach, setting the chemical potential of the majority atoms equal to the Fermi energy $\mu_\uparrow = \varepsilon_F$ is exact in the regime $\mu_\downarrow < 0$.

Spectral function of the minority Fermions $\mathcal{A}_\downarrow(\mathbf{k},\omega)$

For the discussion of the minority Fermion spectral function we restrict ourselves to the hole-part $\mathcal{A}_{\downarrow,-}(\mathbf{k},\omega)$, since this is the relevant quantity for calculating the rf-spectrum and the momentum distribution. At zero temperature, the hole-part (2.56) coincides with the full spectral function for negative frequencies $\omega < 0$ and is zero otherwise, i.e. $\mathcal{A}_-(\mathbf{k},\omega) = \Theta(-\omega)\mathcal{A}(\mathbf{k},\omega)$. Thus, we can restrict our calculation of the spectral function to negative frequencies in the following.

Note that in the case of negative frequencies $\omega < 0$, the vertex function in the expressions for the real- and imaginary-part of the self-energy in Eqs. (2.83) and (2.84) is evaluated only at negative frequencies $z < 0$. This simplifies the equations considerably, because one can easily show from Eq. (2.79) that the imaginary part of the pair propagator is zero at negative frequencies, i.e. $\mathrm{Im}\, L^R(\mathbf{q}, z<0) \equiv 0^+$. Thus, the real- and imaginary part of the vertex function at negative frequencies are given by

$$\mathrm{Im}\Gamma^R(\mathbf{q}, z<0) = \pi\,\delta\big(1/g - \mathrm{Re}\, L^R_{\mathrm{reg}}(\mathbf{q},z)\big) \tag{2.87}$$

$$\mathrm{Re}\Gamma^R(\mathbf{q}, z<0) = \frac{1}{1/g - \mathrm{Re}\, L^R_{\mathrm{reg}}(\mathbf{q},z)} \tag{2.88}$$

Due to the delta function in (2.87) expressions containing the imaginary part of the vertex function give a nonzero result only at those points, where the vertex function has a pole on the real axis at negative frequencies. Now, in the normal (non-superfluid) phase with $h > \mu$, the vertex function has a pole only at *positive* frequencies, as shown above in section 2.3.1. Thus, all terms in (2.83) and (2.84) which involve the imaginary part of the vertex function $\mathrm{Im}\Gamma^R(\mathbf{q}, z<0)$ vanish and we are finally left with

$$\mathrm{Im}\,\Sigma^R_\downarrow(\mathbf{k},\omega) = 0^- \tag{2.89}$$

$$\mathrm{Re}\,\Sigma^R_\downarrow(\mathbf{k},\omega) = \int \frac{d^3q}{(2\pi)^3}\,\Theta(\mu_\uparrow - \varepsilon_q)\,\frac{1}{1/g - \mathrm{Re}\, L^R_{\mathrm{reg}}(\mathbf{q}+\mathbf{k}, \omega + \varepsilon_q - \mu_\uparrow)} \tag{2.90}$$

The hole-part of the minority species spectral function at zero temperature is thus simply given by

$$\mathcal{A}_{\downarrow,-}(\mathbf{k},\omega) = 2\pi\,\Theta(-\omega)\;\delta\big(\omega - \varepsilon_{\mathbf{k}} + \mu_\downarrow - \mathrm{Re}\,\Sigma^R_\downarrow(\mathbf{k},\omega)\big)\,. \tag{2.91}$$

We mention once more, that this expression is only valid in the normal, non-superfluid phase and for negative minority-species chemical potentials $\mu_\downarrow < 0$. For positive $\mu_\downarrow$'s, the pair-propagator has a finite imaginary part at negative frequencies and the simplifications used above are no longer valid.

The dispersion relation $E_{\mathbf{k}}$ of the minority species' fermionic excitations is given by the zeros of the argument of the delta function in Eq. (2.91). In particular, the dispersion

relation is defined by the roots $\omega = E_{\mathbf{k}} - \mu_\downarrow$, i.e. it is a solution of the equation

$$E_{\mathbf{k}} = \varepsilon_{\mathbf{k}} + \mathrm{Re}\,\Sigma^R_\downarrow(\mathbf{k}, E_{\mathbf{k}} - \mu_\downarrow) \tag{2.92}$$

At zero temperature, the hole-spectral function (2.91) can thus be written in terms of the dispersion relation of the excitations $E_{\mathbf{k}}$ as

$$\mathcal{A}_{\downarrow,-}(\mathbf{k},\omega) = 2\pi\,\Theta(-\omega)\;Z(\mathbf{k})\;\delta(\omega - E_{\mathbf{k}} + \mu_\downarrow) \tag{2.93}$$

and the quasiparticle weight $Z(\mathbf{k})$ is given by

$$Z(\mathbf{k}) = \left|1 - \partial_\omega \mathrm{Re}\,\Sigma^R_\downarrow(\mathbf{k},\omega)\Big|_{\omega = E_{\mathbf{k}} - \mu_\downarrow}\right|^{-1}. \tag{2.94}$$

Using Eqs. (2.90) and (2.92), we solve for the excitation energies $E_{\mathbf{k}}$ numerically. At unitarity $a \to \infty$ we find that the dispersion relation of the polaron can be parameterized using a binding energy and an effective mass as

$$E_{\mathbf{k}} = -|\epsilon_b| + \frac{m}{m^*}\varepsilon_{\mathbf{k}} \tag{2.95}$$

with excellent accuracy for $k \lesssim 0.5 k_F$. Here $\epsilon_b = -0.6066\varepsilon_F = \mu_\downarrow\big|_{h=h_s}$ is the binding energy of the polaron at unitarity, which is independent of the field h (i.e. independent of the imbalance) in the regime $h > \mu$ within the non-selfconsistent T-matrix approach. For the effective mass of the polaron at unitarity we get $m^* = 1.17m$, which is also independent of the imbalance. These values have been found previously by Combescot et al. [50] and are in good agreement with the recent experimental results $\epsilon_b \simeq -0.64(7)$ [57] and $m^*/m = 1.17(10)$ [58]. Furthermore, we find that the quasiparticle weight $Z(k)$ at unitarity for momenta $k \lesssim 0.4 k_F$ can be parameterized with very good accuracy as

$$Z(k) = Z_0 - \zeta\left(\frac{k}{k_F}\right)^2 \tag{2.96}$$

where the coefficients $Z_0 = 0.78$ and $\zeta = 0.14$ are independent of the imbalance. For momenta $k \gtrsim 0.4 k_F$ the quadratic dependence is no longer valid.

2.3.3 Momentum distribution of the minority Fermions

The momentum distribution of the minority Fermions at zero temperature in the regime $\mu_\downarrow < 0$ can be calculated using the spectral function (2.93) via Eq. (2.54). From this we obtain

$$\begin{aligned} n_\downarrow(\mathbf{k}) &= \int_{-\infty}^{\infty} \frac{d\omega}{2\pi} A_{\downarrow,-}(\mathbf{k},\omega) \\ &= \int_{-\infty}^{0} d\omega\, Z(\mathbf{k})\;\delta(\omega - E_{\mathbf{k}} + \mu_\downarrow) \\ &= Z(\mathbf{k})\,\Theta(\mu_\downarrow - E_{\mathbf{k}}) \end{aligned} \tag{2.97}$$

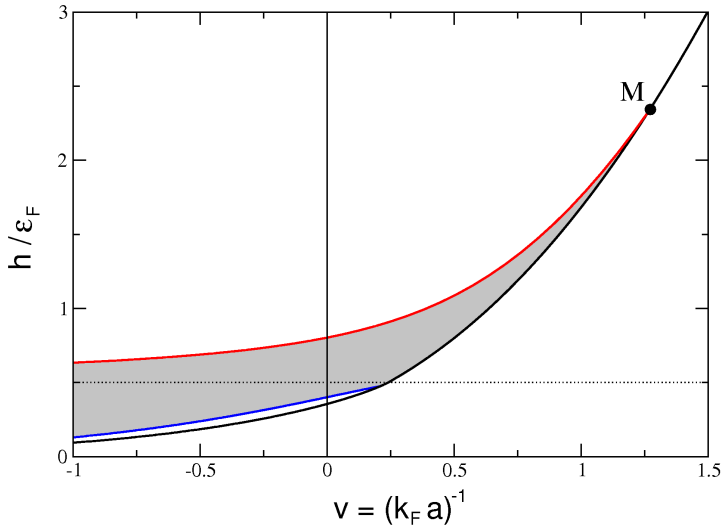

Figure 2.7: Phase boundaries within the T-matrix approach (compare with Fig. 2.1). The grey region represents the partially polarized normal phase $N_{\rm pp}$. The red line marks the saturation field h_s obtained using Eq. (2.99), the black line was obtained using the Thouless criterion (2.74). The blue line marks the phase boundary of the FFLO phase, obtained using the modified Thouless criterion. In the region above the dotted line $h/\varepsilon_F = 0.5$, the minority Fermion chemical potential is negative $\mu_\downarrow < 0$.

This expression for the momentum distribution of the minority atoms can be used to obtain the saturation field h_s, where the minority Fermion density vanishes. Indeed, the chemical potential of the minority Fermion at h_s is given by $\mu_\downarrow(h = h_s) = E_{\mathbf{0}}$. Using Eq. (2.92) we obtain

$$\mu_\downarrow\big|_{h=h_s} = \Sigma^R_\downarrow(\mathbf{0}, 0) \tag{2.98}$$

and thus the saturation field h_s is given by the exact expression

$$\frac{h_s}{\varepsilon_F} = \frac{1}{2}\left(1 - \frac{\Sigma^R_\downarrow(\mathbf{0}, 0)}{\varepsilon_F}\right) . \tag{2.99}$$

Using this equation and the self-energy from our T-matrix approximation, we calculate the saturation field h_s for all interaction strengths numerically. The result is plotted in the T-matrix phase diagram in Fig. 2.7. It turns out that the $h_s(v)$ curve intersects with the critical field $h_{\rm crit}$ from the Thouless criterion at an interaction strength $v = (k_F a)^{-1} = 1.27$ and lies below $h_{\rm crit}$ for $v > 1.27$. In this regime, the vertex function has poles in the complex plane and the calculation of h_s using Eq.(2.99) breaks down.

From Eq. (2.97) it is obvious, that the momentum distribution of the minority Fermions at zero temperature has no tail at large momenta, since $n^\downarrow_{\mathbf{k}} = 0$ if $\frac{m}{m^*}\varepsilon_{\mathbf{k}} > |\epsilon_b| + \mu_\downarrow$. Again, this is an artefact of the selfconsistent calculation of the minority chemical potential in the regime $\mu_\downarrow < 0$. Nevertheless, we expect that the main features are reasonably well

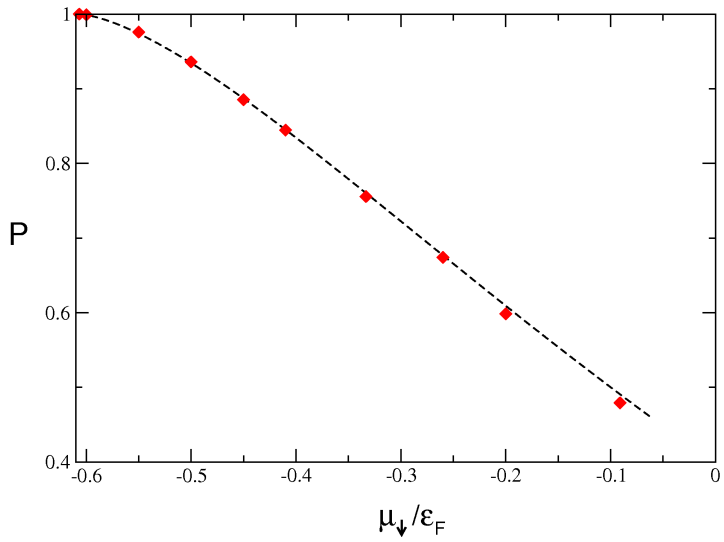

Figure 2.8: Polarization $P = (n_\uparrow - n_\downarrow)/(n_\uparrow + n_\downarrow)$ of the imbalanced Fermi gas at unitarity and $T = 0$ as a function of the minority chemical potential $\mu_\downarrow$, obtained by integrating the momentum distribution (2.97). The dashed line corresponds the approximate result, obtained using Eq. (2.100).

described within this approach. Using the approximate expansions (2.95) and (2.96) for the dispersion relation and the quasiparticle weight at unitarity, we get

$$n_\downarrow(\mathbf{k}) \approx \left(Z_0 - \zeta \frac{k^2}{k_F^2}\right) \Theta\left(\mu_\downarrow + |\varepsilon_b| - \frac{m}{m^*}\varepsilon_\mathbf{k}\right) \tag{2.100}$$

which is a good description for $k_{F\downarrow} \lesssim 0.4 k_F$, i.e. for large imbalances.

We can use the minority momentum distribution (2.97) to calculate the population imbalance $P = (n_\uparrow - n_\downarrow)/(n_\uparrow + n_\downarrow)$ as a function of the minority chemical potential. The result is plotted in Fig. 2.8 and shows that the chemical potential of the minority Fermions is indeed negative for a large range of polarizations at unitarity.

2.3.4 RF-spectra of the minority Fermions

In the absence of final state interactions, the rf-spectrum for the minority Fermions can be calculated using Eq. (2.50). At zero temperature, using the result (2.93) for the hole-part of the minority species' spectral function in the regime $\mu_\downarrow < 0$, we obtain

$$\begin{aligned} I(\omega) &= \frac{1}{2\pi} \int \frac{d^3k}{(2\pi)^3}\, A_\downarrow(\mathbf{k}, \varepsilon_\mathbf{k} - \omega - \mu_\downarrow)\, n_F(\varepsilon_\mathbf{k} - \omega - \mu_\downarrow) \\ &= \int \frac{d^3k}{(2\pi)^3} Z(\mathbf{k})\, \delta(\varepsilon_\mathbf{k} - E_\mathbf{k} - \omega)\, \Theta(\omega + \mu_\downarrow - \varepsilon_\mathbf{k}) \end{aligned} \tag{2.101}$$

The rf-response is nonzero at frequencies which coincide with the energy difference between the kinetic energy of the Fermion in the final state and the excitation energy $E_{\mathbf{k}}$. Using the approximate expression (2.95) for the excitation energies $E_{\mathbf{k}}$ at unitarity, the rf-spectrum can be written as

$$\begin{aligned} I(\omega) &= \int \frac{d^3k}{(2\pi)^3}\, Z(\mathbf{k})\, \delta\!\left(\frac{m^*-m}{m^*}\varepsilon_{\mathbf{k}} + |\epsilon_b| - \omega\right)\, \Theta(\omega+\mu_\downarrow-\varepsilon_{\mathbf{k}}) \\ &\sim \int d\varepsilon\, \sqrt{\varepsilon}\, Z(\sqrt{\varepsilon})\, \delta\!\left(\frac{m^*-m}{m^*}\varepsilon + |\epsilon_b| - \omega\right)\, \Theta(\omega+\mu_\downarrow-\varepsilon) \\ &\sim Z(\sqrt{\varepsilon_0})\, \sqrt{\varepsilon_0}\, \Theta(\omega+\mu_\downarrow-\varepsilon_0) \end{aligned} \tag{2.102}$$

with

$$\varepsilon_0 = \frac{m^*}{m^*-m}(\omega - |\epsilon_b|)\,. \tag{2.103}$$

Using Eq. (2.96) for the quasiparticle weight, the rf-spectrum of the minority Fermions in the regime $\mu_\downarrow < 0$ at unitarity is approximately given by

$$I(\omega) \sim \left(Z_0 - \zeta\,\frac{m^*}{m^*-m}\frac{\omega-|\varepsilon_b|}{\varepsilon_F}\right)\, \sqrt{\frac{m^*}{m^*-m}(\omega-|\epsilon_b|)}\;\; \Theta\!\left(\frac{m^*}{m}|\epsilon_b| + \frac{m^*-m}{m}\mu_\downarrow - \omega\right) \tag{2.104}$$

Note that there is no tail in the rf-spectrum at $T=0$ at large frequencies, since the unit step function cuts off the integral and thus $I(\omega)$ is identically zero for all frequencies $\omega > \omega_{\max} = \frac{m^*}{m}|\epsilon_b| + \frac{m^*-m}{m}\mu_\downarrow$. Again, this is an artefact of the selfconsistent calculation of the minority species' chemical potential $\mu_\downarrow$ within the T-matrix approach. Indeed, it has been shown recently by Schneider et al. [59], that the rf-spectra should have a tail $\sim C/\omega^{3/2}$ proportional to the contact coefficient C, which has been introduced in Sec. 2.2.1. The sharp drop of the minority rf-spectrum at zero temperature in the normal phase is related to the fact the minority atoms form a Fermi-liquid. Indeed, close to the Fermi surface a Landau Fermi liquid at zero temperature has a spectral function of the form

$$\mathcal{A}_{\mathrm{FL}}(\mathbf{k},\omega) = Z\delta(\omega - \varepsilon^*_{\mathbf{k}} + \mu) + \mathcal{A}_{\mathrm{inc}}(\mathbf{k},\omega)\,, \tag{2.105}$$

where the 'coherent' delta-function contribution comes from the infinite-lifetime excitations at the Fermi momentum and the renormalized dispersion is parametrized by an effective mass, i.e. $\varepsilon^*_{\mathbf{k}} = k^2/(2m^*)$. The second term describes the incoherent part of the spectral function. Repeating the calculation for the rf-spectrum with this spectral function gives rise to a sharp drop of $I(\omega)$ at $\omega = \mu(m^*-m)/m$, as above. Thus, apart from missing the small tails at high frequencies, the qualitative form of the spectrum (2.104) is correct.

The minority rf-spectrum has a sharp onset at $\omega_{\min} = |\epsilon_b|$, corresponding to the 'binding energy' of the down-Fermion to the majority Fermi sea. This coincides again with the naive expectation, that the rf-field has to provide the binding energy in order to transfer atoms to the empty hyperfine state. The width of the rf-spectrum is given by

$$\Delta\omega \;=\; \omega_{\max} - \omega_{\min} \;=\; \frac{m^*-m}{m}(|\epsilon_b| + \mu_\downarrow)\,. \tag{2.106}$$

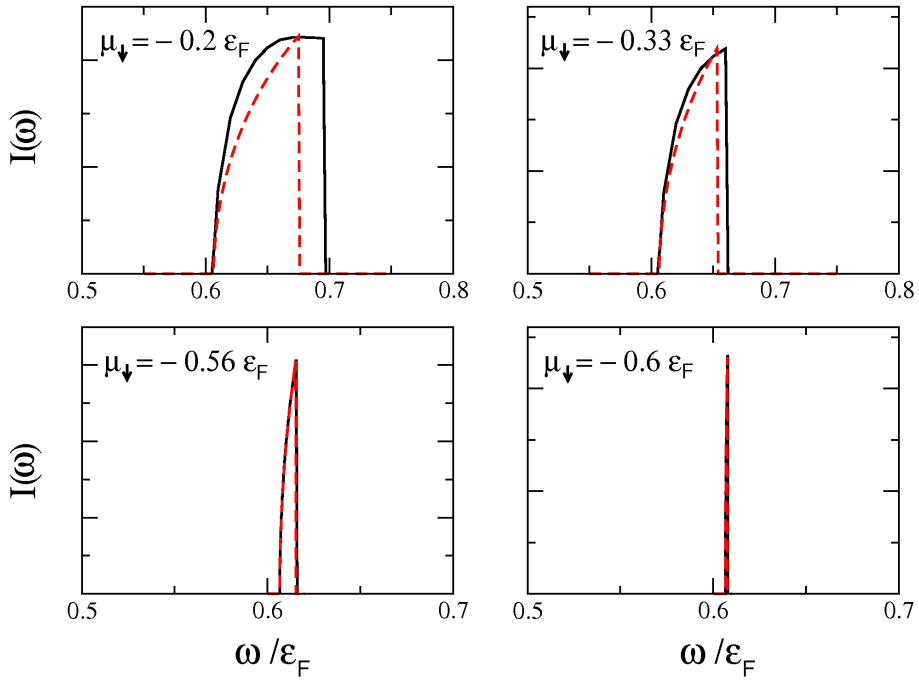

Figure 2.9: Minority Fermion rf-spectra in the normal phase at unitarity and zero temperature, plotted for population imbalances. The red dashed line corresponds to the approximate spectra obtained using Eq. (2.104).

The width of the spectral line is a direct measure of the effective mass m^* and of the population imbalance P. Indeed, for $m^* \to m$ or $P \to 1$ (i.e. $\mu_\downarrow \to -|\epsilon_b|$) the width of the spectral line goes to zero.

The numerically obtained results for the rf-spectra (2.101) are plotted in Fig. 2.9. These spectra cannot be compared directly with the experimentally measured ones, because we have calculated the rf-spectra at zero temperature, whereas the experiments are performed at relatively high temperatures on the order of $0.1T_F$. As mentioned above, the sharp upper cutoff in the rf-spectra is related to the presence of a sharp Fermi surface at zero temperature and thus cannot be resolved in the experimentally measured spectra at finite temperature. Indeed, at finite temperature, this discontinuity is washed out due to thermal excitations.

2.4 Conclusions

In this chapter we have calculated the spectral functions and the rf-response of imbalanced Fermi gases in the normal phase at zero temperature, using a T-matrix approach. One important conclusion that can be drawn from this calculation is, that the shift of the minority rf-spectrum in the normal phase of the imbalanced Fermi gas is essentially due

to the *Hartree* shift of the minority species' chemical potential and *not* an effect of two-particle pairing. Actually, after the first rf-measurements on imbalanced Fermi gases came up, it was widely believed that the minority rf-shift is due to pre-formed pairs in the normal phase. This is not true, however. Indeed, if the minority rf-shift would be a pairing effect, the paired majority atoms should show the same rf-response as the minority atoms because of symmetry. Apart from the unpaired "excess"-Fermion peak at $\omega = 0$, the rf-spectrum of the majority atoms should show a second peak that is identical to the minority rf-spectrum and arises from the paired majority atoms. Our calculations show no signs of such a pairing in the normal phase, however. Thus, the binding energy of the minority atoms in the normal phase of the imbalanced Fermi gas is a polaronic effect. Only for strong enough interactions on the BEC-side of the Feshbach resonance, where the formation of a molecular bound state is possible, the pairing is of a two-particle nature. In this case, the ground state of the many-body system is no longer a normal Fermi-liquid but a superfluid of condensed molecules. This polaron-to-molecule transition will be discussed extensively in the subsequent chapter 3. Recent rf-measurements of the imbalanced Fermi gas [57] directly validate this picture. Indeed, in the normal phase where polaronic binding is present, no overlap between the minority and the majority rf-spectra is seen. In the superfluid phase, however, where molecules are formed, the rf-spectra of the two species overlap (apart from the rf-response of the unpaired majority atoms).

Chapter 3

Polaron to molecule transition in strongly imbalanced Fermi gases

As already mentioned in Sec. 2.1, the phase diagram of strongly interacting two-component Fermi gases with a population imbalance is rather complicated and poorly understood. In fact, reliable theoretical results exist only for two limiting cases. The first one is the trivial limit of zero imbalance, i.e. the balanced Fermi gas, which has been studied extensively in the BCS-BEC crossover literature (see [4] and references therein). The other limit, on which we will will focus in this chapter, corresponds to the extremely imbalanced gas close to the saturation field h_s. Here one encounters the situation of a single minority atom interacting with a Fermi sea of majority atoms. This problem is especially interesting, because a quantum phase transition from a normal (Fermi liquid) phase to a superfluid phase of Bose-condensed molecules is expected to occur at finite but arbitrary low concentration of minority atoms, if the interaction strength is tuned from the BCS to the BEC regime via a Feshbach resonance. Within the $(N+1)$-particle problem, this phase transition can be understood in a simple picture as follows. In the case of attractive interactions, the minority atom dresses itself with a cloud of majority atoms and forms a Landau quasiparticle. This quasiparticle is usually called *polaron* in the literature, in analogy to a polaron in solid state physics, where an electron dresses itself with a cloud of phonons (see e.g. [60]). Quite generally, the associated polaron energy for low momenta $\mathbf{p} \ll k_F$ is of the form

$$E(\mathbf{p}) = A\varepsilon_F + \frac{\mathbf{p}^2}{2m^*} \ , \tag{3.1}$$

where the first term corresponds to a 'binding energy' (i.e. $A < 0$) due to the attractive interaction between the minority atom and the Fermi sea and the second term represents the kinetic energy of the quasiparticle, where the effect of the dressing cloud is described by an effective mass $m^* > m$. Here and in the following, the Fermi energy is defined by $\varepsilon_F = k_F^2/(2m)$ with a Fermi momentum k_F that is related to the up-spin density by the standard relation $n_\uparrow = k_F^3/(6\pi^2)$ for a single component Fermi gas. Since we are interested in the limit of vanishing down-spin density $n_\downarrow \to 0$, these are the relevant energy

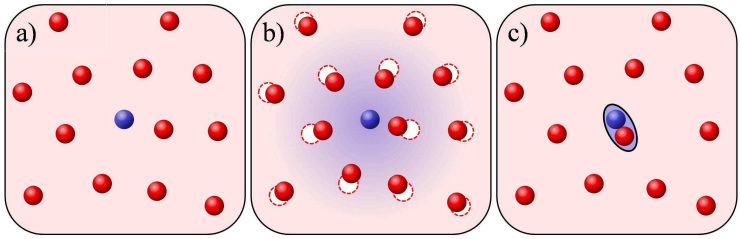

Figure 3.1: Cartoon of the polaron to molecule transition in the $(N+1)$-particle problem. a): noninteracting case; b): for attractive interactions, the minority atom forms a polaron by dressing itself with a cloud of majority atoms; c): beyond a critical interaction strength, the minority atom forms a molecular bound state with one of the majority atoms. Picture taken from [57].

and momentum scales. Theoretical values for the binding energy and the effective mass of the polaron have been determined from variational Monte-Carlo calculations by Lobo et al. [22] as well as from a T-matrix approximation by Combescot et al. [50] and in the previous chapter of the present thesis (see Eq. (2.95)). Quite recently, the properties of the polaron have been studied also in experiments. For the binding energy and the effective mass at unitarity they obtain $A = -0.64(7)$ [57] and $m^*/m = 1.17(10)$ [58], in rather good agreement with the theoretical results.

Beyond a critical interaction strength however, the minority atom forms a molecular bound state with one of the majority atoms and thus can no longer propagate as an independent fermionic quasiparticle[1]. This transition has been discussed previously by Prokof'ev and Svistunov [23, 24]. At finite minority concentrations one expects a Bose-Einstein-condensate of molecules. A cartoon picture of the polaron to molecule transition is shown in Fig. 3.1.

A major step torwards a theoretical understanding of the $(N+1)$-particle problem was put forward by Chevy [11], who introduced a simple variational wave function that captures the essential physics of a single down-Fermion immersed in an up-Fermi sea. This ansatz works very well on the BCS-side of the Feshbach resonance up to the unitary point and slightly beyond, as long as the minority atom forms a polaron with the Fermi-sea. However – as will be discussed in detail below – it turns out that Chevy's wave function is not capable of describing the BEC-regime of the $(N+1)$-particle problem properly. In particular, it doesn't capture the phase transition from polaronic-binding to a molecular two-body bound state. In the following sections we discuss the limitations of Chevy's

[1]Obviously, this critical interaction strength lies on the BEC-side of the Feshbach resonance, since a molecular bound state in the two body problem is only present at positive scattering lengths $a > 0$. As will be shown below, the formation of the two-body bound state is possible only beyond a critical interaction strength $(k_F a)_c^{-1} > 0.84$. Interestingly, the molecule formation is *more difficult* in the presence of a Fermi sea, than in its absence. This is in contrast to the usual Cooper problem [61], where a bound state between to weakly interacting Fermions arises only if a Fermi sea is present. This issue is discussed in App. C, where we analyze the Cooper problem in a spin polarized environment.

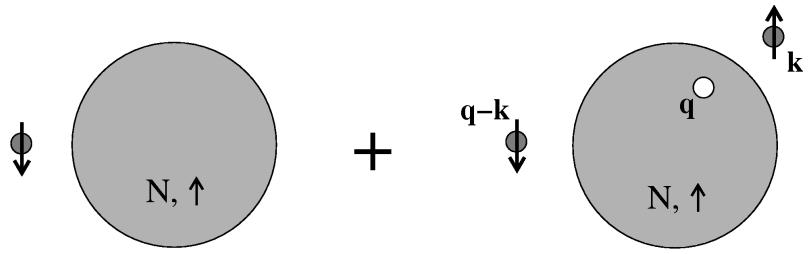

Figure 3.2: Pictorial representation of Chevy's variational wave function (3.4). The large grey circle represents the Fermi sea of the majority atoms.

ansatz and propose a complementary variational wave function, that leads to a correct description of the molecular bound-state within the $(N+1)$-particle problem and allows to pin down the polaron to molecule transition point.

3.1 Chevy's ansatz and its problems in the BEC-regime

The $(N+1)$-particle problem that will be discussed in the following is based on the standard model for ultracold two-species Fermi gases interacting via a contact interaction, defined by the Hamiltonian

$$H = \sum_{\mathbf{k},\,\sigma} \varepsilon_{\mathbf{k}} c^\dagger_{\mathbf{k}\sigma} c_{\mathbf{k}\sigma} + \frac{g_0}{V} \sum_{\mathbf{k}_1,\mathbf{k}_2,\mathbf{k}_3,\mathbf{k}_4} c^\dagger_{\mathbf{k}_1\uparrow} c^\dagger_{\mathbf{k}_2\downarrow} c_{\mathbf{k}_3\downarrow} c_{\mathbf{k}_4\uparrow} \delta_{\mathbf{k}_1+\mathbf{k}_2,\mathbf{k}_3+\mathbf{k}_4} \ . \tag{3.2}$$

Here, $c^\dagger_{\mathbf{k}\sigma}$ and $c_{\mathbf{k}\sigma}$ are the creation and destruction operators for Fermions with momentum $\mathbf{k}$ in the pseudo-spin state σ and $\varepsilon_{\mathbf{k}} = k^2/(2m)$ denotes the dispersion relation of free Fermions with mass m. As shown in appendix A, the bare interaction strength g_0 is related to the physical s-wave scattering length a via

$$\frac{1}{g_0} = \frac{m}{4\pi a} - \frac{1}{V} \sum_{\mathbf{k}} \frac{1}{2\varepsilon_{\mathbf{k}}} \ . \tag{3.3}$$

A simple variational wave function for the (N+1)-particle problem of a single down-spin Fermion interacting with a sea of spin-up Fermions was introduced by Chevy [11]. It is based on an expansion up to a single particle-hole excitation around the unperturbed Fermi sea and takes the form

$$|\psi_0\rangle = \Big(\phi_0\, c^\dagger_{\mathbf{0}\downarrow} + \sum_{\mathbf{k},\mathbf{q}}{}' \phi_{\mathbf{kq}}\, c^\dagger_{\mathbf{q}-\mathbf{k}\downarrow} c^\dagger_{\mathbf{k}\uparrow} c_{\mathbf{q}\uparrow}\Big) |FS^N_\uparrow\rangle \ . \tag{3.4}$$

Here and in the following sums on $\mathbf{k}$ and $\mathbf{q}$ with a prime are restricted to $k > k_F$ and $q < k_F$, respectively and the N-particle Fermi sea of up-atoms is denoted by $|FS^N_\uparrow\rangle$. Pictorially, this variational ansatz is shown in Fig. 3.2.

Although the ansatz (3.4) is restricted to single particle-hole excitations, which is difficult to justify for strongly interacting Fermi systems[2], Monte Carlo calculations [21, 23, 24] have shown that this variational wave function gives very accurate results for the ground state energy of the polaron, in particular at unitarity, where the scattering length a is infinite. On a formal level, the truncation of the particle-hole expansion after the first term has been analyzed by Combescot and Giraud [62], who have shown that higher order terms with more than one particle-hole excitation interfere destructively. In fact, this interference is perfect if the hole-momentum $\mathbf{q}$ in the first order term is pinned at $\mathbf{q} = 0$ and justifies the restriction to a single particle-hole excitation, if an expansion in hole wavevectors is legitimate[3]. In fact, however, the accuracy of Chevy's ansatz at unitarity is probably a coincidence, because the wave function smoothly interpolates between the weak coupling BCS- and BEC-limits, where it gives the correct leading-order behavior of the ground state energy, as will be shown in the next section. Furthermore, the results for other quantities such as the quasiparticle residue of the minority atom are not very accurate (see Fig. 3.4 below).

3.1.1 Ground state energy

A variational upper bound to the ground state energy of the polaron using Chevy's ansatz (3.4) can be obtained by taking the coefficients ϕ_0 and $\phi_{\mathbf{kq}}$ in the wave function (3.4) as an infinite set of variational parameters. Calculating the minimum of $\langle\psi_0|\hat{H}|\psi_0\rangle$ with respect to these variational parameters under the constraint of a normalized wave function leads to the two coupled equations [11]

$$\left(E - \frac{g_0}{V}N\right)\phi_0 = \frac{g_0}{V}\sum_{\mathbf{kq}}{}' \phi_{\mathbf{kq}} \tag{3.5}$$

$$\left(E - \varepsilon_{\mathbf{k}} - \varepsilon_{\mathbf{q}-\mathbf{k}} + \varepsilon_{\mathbf{q}}\right)\phi_{\mathbf{kq}} = \frac{g_0}{V}\phi_0 + \frac{g_0}{V}\sum_{\mathbf{k}}{}' \phi_{\mathbf{kq}}\,, \tag{3.6}$$

where the ground state energy E is measured with respect to the N-particle Fermi sea, thus E is equivalent to the chemical potential of the down-Fermion $\mu_\downarrow \equiv E$. Solving (3.6) for $\phi_{\mathbf{kq}}$ leads to

$$\phi_{\mathbf{kq}} = \frac{\phi_0}{V}\frac{\chi(\mathbf{q}; E)}{E - \varepsilon_{\mathbf{k}} - \varepsilon_{\mathbf{q}-\mathbf{k}} + \varepsilon_{\mathbf{q}}} \tag{3.7}$$

where we have defined

$$\chi(\mathbf{q}; E) := \left[\frac{1}{g_0} - \frac{1}{V}\sum_{|\mathbf{k}|>k_F}\frac{1}{E - \varepsilon_{\mathbf{k}} - \varepsilon_{\mathbf{q}-\mathbf{k}} + \varepsilon_{\mathbf{q}}}\right]^{-1}. \tag{3.8}$$

The divergence of the integral in the expression above can be regularized using Eq. (3.3), i.e. by replacing the bare interaction strength g_0 with the physical s-wave scattering length

[2] Note that from an energetic point of view it would be favorable to create a larger number of particle-hole excitations close to the Fermi surface, instead of a single one with large momentum transfer.

[3] Pinning the hole-wavevector at $\mathbf{q} = 0$ is a bad approximation in the BEC-regime. This issue will be discussed at the end of Sec. 3.1.1.

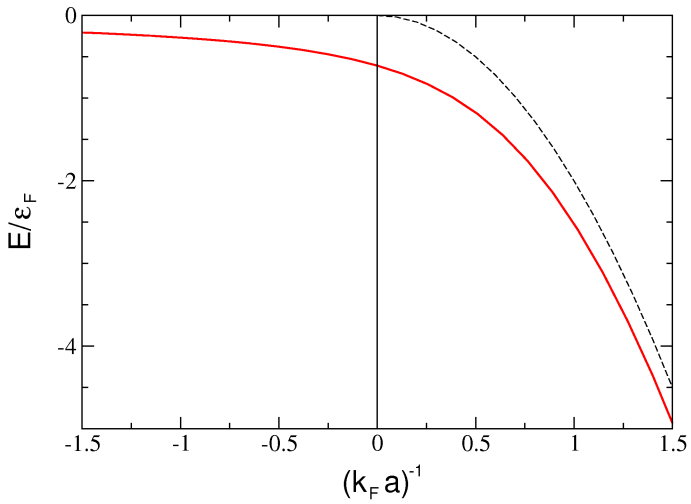

Figure 3.3: Ground state energy E in units of the Fermi energy ε_F as a function of the inverse coupling $(k_F a)^{-1}$. Note that $E \equiv \mu_\downarrow$ is measured with respect to the Fermi sea. The red solid line corresponds to the result obtained using Chevy's wave function, the black dashed line corresponds to the energy of the molecular bound state $E_b = -1/(ma^2)$.

a. Note that $\chi(\mathbf{q}; E)$ has essentially the same form as the (real part of the) vertex function (2.66) studied in detail in Sec. 2.3.1 and thus can be calculated analytically.

Using Eq. (3.5) one gets the following implicit equation for the ground state energy

$$E = \frac{1}{V} \sum_{|\mathbf{q}|<k_F} \chi(\mathbf{q}; E)\,. \tag{3.9}$$

This equation thus determines the variational upper bound for the ground state energy of a single down-Fermion immersed in an up-Fermi sea as a function of the interaction strength. The numerically obtained result is shown in Fig. 3.3. In particular, the chemical potential of the down-Fermion at unitarity is given by $\mu_\downarrow = -0.6066\varepsilon_F$, which is in good agreement with the fixed-node Monte Carlo result $\mu_\downarrow = -0.594\varepsilon_F$ of Pilati and Giorgini [21] and the diagrammatic Monte-Carlo result $\mu_\downarrow = -0.615\varepsilon_F$ of Prokof'ev and Svistunov [23].

In the two weak coupling BCS- and BEC-limits the ground state energy $E \equiv \mu_\downarrow$ can be calculated analytically within Chevy's variational approach. In the BCS-regime $a \to 0^-$, the dominant contribution to the ground state energy comes from $\chi(\mathbf{q}; E) \approx 4\pi a/m$, thus the chemical potential of the down-Fermion is given by its mean field value $\mu_\downarrow/\varepsilon_F = 4/(3\pi)\, k_F a$, as expected. A bit more interesting is the BEC-limit $a \to 0^+$. In this regime the two-particle bound state dominates the ground state behavior. We thus expand the integral in Eq. (3.8) for large energies $|E| \gg \varepsilon_F$ and small momenta $\mathbf{q}$, which is very accurate in the BEC-regime. In this case Eq. (3.9) simplifies to (in dimensionless form

and after taking the thermodynamic limit)

$$\frac{E}{\varepsilon_F} \approx \frac{4}{\pi}\int_0^1 dq \frac{q^2}{\frac{1}{k_F a} - \sqrt{-\frac{E/\varepsilon_F}{2}} + \sqrt{-\frac{2}{E/\varepsilon_F}\,\frac{q^2}{8}}} \tag{3.10}$$

where momenta $\mathbf{q}$ are measured in units of k_F. In the BEC-limit $(k_F a)^{-1} \to \infty$, this equation leads to[4]

$$E_{\text{Chevy}} \overset{a\to 0^+}{=} E_b - \varepsilon_F/2 + \mathcal{O}(a)\,, \tag{3.11}$$

where $E_b = -1/(ma^2)$ denotes the binding energy of the two particle bound state. Thus, Chevy's wave function seems to describe the molecule formation correctly. However, it turns out that the constant term $\sim \varepsilon_F/2$ in (3.11) is wrong by a factor of two. Indeed, a simple mean field analysis shows, that the correct asymptotic behavior of the ground state energy in the BEC-limit is given by

$$E \overset{a\to 0^+}{=} E_b - \varepsilon_F + g_{ad} n_\uparrow + \mathcal{O}(a^2)\,, \tag{3.12}$$

where the leading contribution is again the molecular binding energy E_b. The constant contribution ε_F is due to the removal of one up-Fermion from the Fermi-sea in order to form the molecule and the third term accounts for the mean field repulsion between the molecule and the Fermi-sea. Its interaction strength $g_{ad} = 3\pi a_{ad}/m$ is related to the exact atom-dimer scattering length $a_{ad} = 1.18\,a$ that has first been calculated by Skorniakov and Ter-Martirosian [63] for neutron-deuteron scattering (in the context of ultracold gases, this result has been re-derived by Petrov et. al. [20]).

The fact that the result (3.11) for the ground state energy differs from the correct asymptotics by $\varepsilon_F/2$ is a first indication that Chevy's variational ansatz breaks down in the BEC-regime. The reason for this discrepancy can be traced back easily to the structure of Chevy's wave function. Indeed, a closer inspection of (3.4) shows that the dominant terms in the BEC-limit are those, where the hole-momentum $\mathbf{q} = 0$ vanishes, i.e.

$$\sum_{\mathbf{k}}{}' \phi_{\mathbf{k},\mathbf{0}}\, c^\dagger_{-\mathbf{k}\downarrow} c^\dagger_{\mathbf{k}\uparrow} c_{\mathbf{0}\uparrow} |FS^N_\uparrow\rangle\ . \tag{3.13}$$

In the BEC-regime this term corresponds to the molecular bound-state wave function of an up- and a down-Fermion with opposite momenta in the presence of a Fermi sea[5]. From an energetic point of view this part of the wave function is not optimal however, since it creates a hole in the center of the ↑-Fermi-sphere. Energetically it would be favorable to replace the punctured N-particle Fermi-sphere with a (N-1)-particle Fermi sea, i.e.

$$c_{\mathbf{0}\uparrow}|FS^N_\uparrow\rangle \ \longrightarrow\ |FS^{N-1}_\uparrow\rangle\ , \tag{3.14}$$

[4] We note that the inclusion of the q-dependent term in the denominator of Eq. (3.10) is crucial in order to obtain the constant term $\sim \varepsilon_F$ in the asymptotics of the ground state energy (3.11). This term is missing in the analysis of Combescot et al. [50], see their Eq. (9).

[5] The presence of the up-Fermi sea leads to a slight modification of the 'free' molecular wave function on length scales $x \gtrsim k_F^{-1}$. However, this modification is not important in the BEC-regime $k_F a \ll 1$, where the interparticle spacing $\sim k_F^{-1}$ is much larger than the typical size of the molecule $\sim a$.

which would lead to a ground state energy that is lower by ε_F. However, within Chevy's ansatz (3.4) this would require the inclusion of an arbitrary number of particle-hole excitations in order to reshuffle the Fermi-sea in such a way that the hole vanishes.

The fact that Chevy's wave function gives an incorrect description of the $(N+1)$-particle problem in the BEC-regime becomes even more apparent if one takes a closer look at the quasiparticle residue $Z_\downarrow$ of the minority atom.

3.1.2 Quasiparticle residue

From a many body point of view, the relevant quantity that characterizes the polaron as well defined quasi-particle is the so called quasiparticle residue $Z_\downarrow$ of the minority atom. Quite generally, the quasiparticle residue gives the probability amplitude that a particle with momentum $\mathbf{k}$ propagates without being scattered. It is directly related to the Green's function

$$iG(\mathbf{p}, t>0) = \langle c_{\mathbf{p}}(t) c^\dagger_{\mathbf{p}}(0)\rangle \,. \tag{3.15}$$

Indeed, the probability amplitude for propagation as a proper quasiparticle is determined by the pole and the corresponding residue of the Green's function in the lower half complex plane [45]

$$G(\mathbf{k},t) \overset{\gamma t \gg 1}{\approx} G_R(\mathbf{k},t) = \int \frac{d\omega}{2\pi} \frac{e^{-i\omega t}}{\omega - \varepsilon_{\mathbf{k}} + \mu - \Sigma_R(\mathbf{k},\omega)} \,. \tag{3.16}$$

Let's assume that the retarded Green's function has a simple pole in the LHP at $\omega = E_{\mathbf{k}} - i\gamma_{\mathbf{k}} - \mu$, with $\gamma_{\mathbf{k}} > 0$, i.e.

$$E_{\mathbf{k}} = \varepsilon_{\mathbf{k}} + \mathrm{Re}\,\Sigma_R(\mathbf{k}, E_{\mathbf{k}} - i\gamma_{\mathbf{k}} - \mu) \tag{3.17}$$

$$\gamma_{\mathbf{k}} = -\mathrm{Im}\,\Sigma_R(\mathbf{k}, E_{\mathbf{k}} - i\gamma_{\mathbf{k}} - \mu) \tag{3.18}$$

Closing the contour in the LHP gives

$$G_R(\mathbf{k},t) = -i \frac{e^{-i(E_{\mathbf{k}} - i\gamma_{\mathbf{k}} - \mu)t}}{1 - \partial_\omega \Sigma_R(\mathbf{k}, E_{\mathbf{k}} - i\gamma_{\mathbf{k}} - \mu)} \,. \tag{3.19}$$

In a Fermi liquid state the imaginary part of the self energy vanishes right at the Fermi momentum[6] k_F, which is defined by $E_{\mathbf{k}_F} = \mu$, and thus we have $\gamma_{\mathbf{k}} = 0^+$. The quasiparticle residue Z is then defined by

$$Z = \lim_{t\to\infty} |G_R(\mathbf{k}_F, t)| = \frac{1}{|1 - \partial_\omega \Sigma_R(\mathbf{k}_F, 0)|} \tag{3.20}$$

where the absolute value was taken in order to remove the oscillating term. The quasiparticle residue Z is also related to the discontinuity of the momentum distribution $n(\mathbf{p})$ of the Fermions at $\mathbf{k}_F$. It was already shown by Migdal [64] that

$$Z = n(k_F - 0^+) - n(k_F + 0^+) \tag{3.21}$$

[6]Note that this is a general discussion of the quasiparticle residue. In the following we are interested in the properties of the minority Fermion, thus $k_F \equiv k_{F\downarrow} \to 0$ for the $(N+1)$-particle problem considered in this chapter.

Indeed, at zero temperature and infinitesimally close to k_F, where $\gamma_{\mathbf{k}} = 0$ we get

$$\begin{aligned} n(\mathbf{k}) &= \int \frac{d\omega}{2\pi} \mathcal{A}(\mathbf{k},\omega)\Theta(-\omega) \\ &\overset{k\to k_F}{\approx} \int d\omega\, \delta\left(\omega - \varepsilon_{\mathbf{k}} + \mu - \mathrm{Re}\,\Sigma_R(\mathbf{k},\omega)\right)\Theta(-\omega) \\ &\approx Z(k_F)\,\Theta(\mu - E_{\mathbf{k}}) \end{aligned} \tag{3.22}$$

with the quasiparticle residue $Z(k_F) \equiv Z$ from Eq. (3.20). From this expression it is obvious that the Fermi momentum $\mathbf{k}_F$ is related to the chemical potential μ via $\mu = E_{\mathbf{k}_F}$ or equivalently, using Eq. (3.17), by

$$\mu = \varepsilon_{\mathbf{k}_F} + \mathrm{Re}\,\Sigma_R(\mathbf{k}_F, 0)\,. \tag{3.23}$$

Furthermore, the discontinuity of the momentum distribution at the Fermi momentum is given by

$$\lim_{\delta\to 0}\left[n(k_F - \delta) - n(k_F - \delta)\right] \;=\; Z \;=\; \frac{1}{|1 - \partial_\omega \Sigma_R(\mathbf{k}_F, 0)|} \tag{3.24}$$

In the case of Chevy's wave function (3.4), where the Fermi momentum of the down particle is zero, the quasiparticle residue of the down-Fermion can be obtained via the jump in the momentum distribution at $\mathbf{k} = 0$. It is given by

$$Z_\downarrow = |\phi_0|^2 \tag{3.25}$$

and can be calculated by inserting the coefficients $\phi_{\mathbf{kq}}$ from Eq. (3.7) into the normalization condition of the wave function $1 = |\phi_0|^2 + \sum_{\mathbf{kq}} |\phi_{\mathbf{kq}}|^2$. From this one obtains

$$\frac{1}{|\phi_0|^2} = 1 + \frac{1}{V^2}\sum_{\mathbf{k},\mathbf{q}}{}' \frac{\chi^2(\mathbf{q}; E)}{\left(E - \varepsilon_{\mathbf{k}} - \varepsilon_{\mathbf{q}-\mathbf{k}} + \varepsilon_{\mathbf{q}}\right)^2}\,. \tag{3.26}$$

The result for the minority Fermion quasiparticle residue is shown in Fig. 3.4 together with recent experimental results. Apparently, Chevy's ansatz for the polaron predicts a finite $Z_\downarrow$ of the minority atom for all interaction strengths, even deep in the BEC-regime where a molecular bound state with one of the majority atoms is formed. In this regime, however, the quasiparticle residue is expected to vanish, because the minority atom can no longer propagate as a free particle. Indeed $Z_\downarrow$ vanishes identically beyond the critical interaction strength of molecule formation, which is consistent with recent experiments [57]. Actually, $Z_\downarrow$ can be viewed as the order parameter of the polaron to molecule transition.

The numerical value of $Z_\downarrow$ at unitarity $v = 0$ is $Z_\downarrow(v = 0) \simeq 0.78$ within Chevy's ansatz. This is much larger than the experimentally observed value $Z_\downarrow = 0.39(9)$ which is likely to be a lower bound, however [57]. Apparently, the expansion up to a single particle-hole excitation considerably overestimates the quasiparticle residue even though it gives reliable results for the ground state energy and the effective mass.

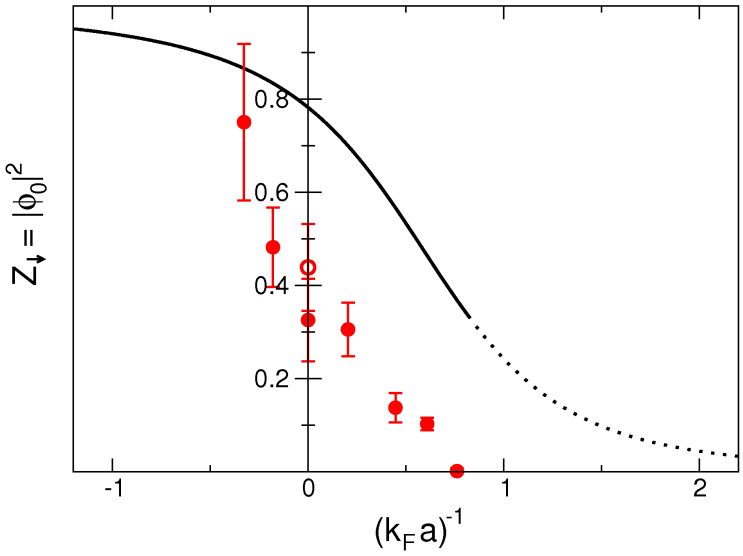

Figure 3.4: Quasiparticle residue $Z_\downarrow$ of the minority Fermion as function of $(k_F a)^{-1}$, calculated using Chevy's variational ansatz (3.4). In the regime where the ansatz (3.4) breaks down, $Z_\downarrow$ is drawn as dotted line. The red dots correspond to the experimentally measured quasiparticle residue from the MIT group [57] at a minority concentration of 5%.

3.1.3 Momentum distribution and contact coefficient

Another interesting quantities are the momentum distributions of the two Fermion species. A simple calculation using Chevy's ansatz shows that they are given by

$$n^{\downarrow}_{\mathbf{p}} = |\phi_0|^2 \delta_{\mathbf{p},0} + \sum_{|\mathbf{q}|<k_F} |\phi_{\mathbf{q}-\mathbf{p},\mathbf{q}}|^2 \Theta(|\mathbf{q}-\mathbf{p}| - k_F) \tag{3.27}$$

$$n^{\uparrow}_{\mathbf{p}} = \Theta(k_F - p)\left[1 - \sum_{|\mathbf{k}|>k_F} |\phi_{\mathbf{kp}}|^2\right] + \Theta(p - k_F) \sum_{|\mathbf{q}|<k_F} |\phi_{\mathbf{pq}}|^2 \tag{3.28}$$

Note that the wave-function coefficients $\phi_{\mathbf{kq}}$ from Eq. (3.7) scale as $\sim V^{-1}$ an thus the tails of the momentum distributions of both species scale as one over volume. This is a trivial consequence of the fact that we have only one minority atom present and thus the minority atom density is given by V^{-1}. Furthermore, the asymptotics of momentum distributions for both species at large momenta are identical and given by

$$n^{\uparrow,\downarrow}_{\mathbf{p}} \overset{p\to\infty}{\longrightarrow} \sum_{|\mathbf{q}|<k_F} |\phi_{\mathbf{pq}}|^2 \,. \tag{3.29}$$

The contact coefficient C that has been introduced in sec 2.2.1 can now be calculated according to (2.35) via

$$C = \lim_{k\to\infty} k^4 n_{\mathbf{k}} = \lim_{k\to\infty} k^4 \sum_{\mathbf{k}}{}' |\phi_{\mathbf{kq}}|^2 = \frac{m^2|\phi_0|^2}{V^2} \sum_{\mathbf{q}}{}' |\chi(\mathbf{q}; E)|^2 \tag{3.30}$$

Now it is easy to see that Chevy's ansatz for the strongly imbalanced gas obeys the adiabatic theorem (2.38). Indeed, the interaction energy within Chevy's ansatz is given by

$$\langle H_{\text{int}} \rangle = -\Lambda \frac{m}{2\pi^2} \frac{|\phi_0|^2}{V} \sum_{\mathbf{q}}{}' |\chi(\mathbf{q}; E)|^2 \,. \tag{3.31}$$

Using Tan's relation for the interaction energy from Eq. (2.36), the contact coefficient is given by

$$C = -\frac{2\pi^2 m}{\Lambda V} \langle H_{\text{int}} \rangle = \frac{m^2|\phi_0|^2}{V^2} \sum_{\mathbf{q}}{}' |\chi(\mathbf{q}; E)|^2 \,, \tag{3.32}$$

which is equivalent to the result (3.30) obtained from the asymptotics of the momentum distribution, thus Chevy's ansatz obeys the adiabatic theorem. Right at unitarity the dimensionless contact coefficient s, defined in (2.39), can be obtained numerically from (3.32) and is given by [65]

$$s = \frac{C}{k_F \, 6\pi^2/V} = 0.072 \,. \tag{3.33}$$

Note again that the factor V comes from the fact that the minority atom density is given by $n_\downarrow = V^{-1}$. The results for the dimensionless contact coefficient as a function of the scattering length are shown in Fig. 3.11 on page 67, together with the results from our variational ansatz for the BEC-regime.

3.1.4 Minority spectral function and rf-response

In principle, a variational ansatz like (3.4) for the ground state of an interacting many-body system contains no dynamical information. Indeed, in order to calculate the single particle spectral function $\mathcal{A}(\mathbf{k}, \omega)$ it is necessary to know the excited states[7] of the system, as can be seen immediately from the Lehmann representation of the spectral function in Eqs. (2.52) and (2.53). However, the $(N+1)$-particle problem is an exception to this general rule, because the knowledge of the ground state wave function suffices to calculate the hole part of the minority spectral function $\mathcal{A}^-_\downarrow(\mathbf{k}, \omega)$ at zero temperature, which is given by

$$\mathcal{A}^-_\downarrow(\mathbf{k}, \omega) = 2\pi \sum_m |\langle m|c_{\mathbf{k}\downarrow}|0\rangle|^2 \, \delta(\omega + E_m - E_0) \,. \tag{3.34}$$

This is because the excited states $|m\rangle$ are eigenstates of the *non-interacting* Hamiltonian of the fully polarized majority gas, if the single minority atom is removed from the system.

[7] In particular one has to know the excited states with single particle/hole excitations.

Using Chevy's ansatz (3.4) for the ground state wave function $|0\rangle$ and the equation above, the hole part of the minority spectral function at zero temperature is given by

$$\mathcal{A}_{\downarrow}^{-}(\mathbf{p},\omega) = 2\pi|\phi_0|^2\delta(\omega)\delta_{\mathbf{p},0} + 2\pi \sum_{|\mathbf{q}|<k_F} |\phi_{\mathbf{q}-\mathbf{p},\mathbf{q}}|^2 \Theta(|\mathbf{q}-\mathbf{p}|-k_F)\delta(\omega+\varepsilon_{\mathbf{q}-\mathbf{p}}-\varepsilon_{\mathbf{q}}) \quad (3.35)$$

Note that by convention ω is measured with respect to the chemical potential $\mu_{\downarrow}$. It can be seen immediately that this expression for the spectral function satisfies Eq. (2.54), i.e. it gives the momentum distribution of the minority atom (3.27) when integrated over the frequency ω and divided by 2π. Furthermore, from the delta-function in the last term of Eq. (3.35) it can be inferred that for a given momentum $\mathbf{p}$, the spectral function is non-zero in the interval $-\varepsilon_{\mathbf{p}} - pk_F/m < \omega < -\varepsilon_{\mathbf{p}} + pk_F/m$.

The minority rf-spectrum at zero temperature can now be calculated by plugging the spectral function from Eq. (3.35) into Eq. (2.50)

$$I_{\downarrow}(\omega) = \frac{|\phi_0|^2}{V}\,\delta(\omega+\mu_{\downarrow}) + V\int' \frac{d^3k\,d^3q}{(2\pi)^6}\,|\phi_{\mathbf{kq}}|^2\,\delta(\varepsilon_{\mathbf{q}-\mathbf{k}}+\varepsilon_{\mathbf{k}}-\varepsilon_{\mathbf{q}}-\omega-\mu_{\downarrow})\,, \quad (3.36)$$

where the prime on the integration symbol indicates the restriction of the integration area to $k > k_F$ and $q < k_F$. The rf-spectrum exhibits a sharp peak $\sim Z_{\downarrow}\delta(\omega+\mu_{\downarrow})$ proportional to the quasiparticle residue, as expected in an exact description. This peak has been obtained already in the T-matrix calculation in Sec. 2.3.2. Note that the factor V^{-1} in the first term comes from the normalization of the rf-spectrum (2.25). The second term is non-zero for $\omega > -\mu_{\downarrow}$ and leads to the tail in the rf-spectrum, which is missing in the T-matrix calculation. As will be shown right below, this tail is proportional to the contact coefficient $C \sim V^{-1}$ at large frequencies. The scaling of the tail $\sim V^{-1}$ is again due to the normalization condition of the Rf-spectrum, thus the tail doesn't vanish in the thermodynamic limit if the Rf-spectrum is properly normalized. Indeed, if we calculate the normalized spectral weight of the peak (first term) and of the tail (second term) of the rf-spectrum in Eq. (3.36) using the normalization condition $1 = |\phi_0|^2 + \sum_{\mathbf{kq}}|\phi_{\mathbf{kq}}|^2$, we immediately see that spectral weight of the tail is given by $1 - Z_{\downarrow}$, which is $\sim 22\%$ at unitarity.

At large frequencies $\omega \to \infty$, the rf-spectrum can be calculated explicitely and we get

$$I_{\downarrow}(\omega\to\infty) \approx V\int' \frac{d^3k\,d^3q}{(2\pi)^6}\,|\phi_{\mathbf{kq}}|^2\,\delta(2\varepsilon_{\mathbf{k}}-\omega)\,. \quad (3.37)$$

From Eq. (3.29) we know that the q-integral in the above expression gives the asymptotics of the momentum distribution at large momenta. After evaluating the k-integral the tail of the rf-spectrum can thus be expressed as

$$I_{\downarrow}(\omega\to\infty) \approx \frac{1}{4\pi^2\sqrt{m}}\,\frac{C}{\omega^{3/2}}\,, \quad (3.38)$$

where C is the contact coefficient introduced above.

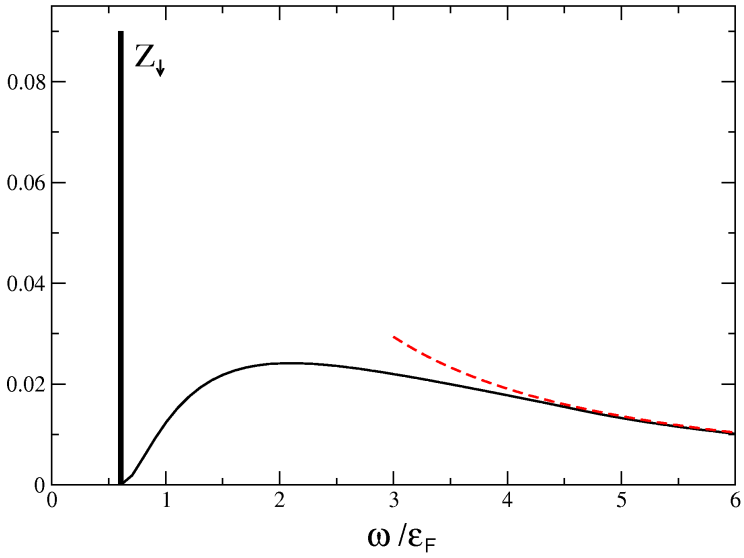

Figure 3.5: Minority rf-spectrum at unitarity, obtained within Chevy's ansatz from (3.36) and normalized to unity. The red dashed line marks the asymptotics (3.38) at large frequencies. The delta-function contribution is indicated by the thick vertical line and has a weight equal to $Z_\downarrow = |\phi_0|^2 \simeq 0.78$.

3.1.5 Equivalence of Chevy's ansatz to a non-selfconsistent T-matrix approach

It turns out that Chevy's variational ansatz for the polaron problem is formally equivalent to the non-selfconsistent T-matrix approach for the imbalanced Fermi gas from Sec. 2.3, as far as equilibrium properties such as the ground state energy and the quasiparticle residue at the saturation field h_s (i.e. where the minority density vanishes) are concerned. This equivalence was observed already by Combescot et al. [50] and will be briefly discussed in this section.

Within Chevy's ansatz, the chemical potential[8] of the minority Fermion $\mu_\downarrow$ is determined by Eq. (3.9). On the other hand, within the T-matrix approach the chemical potential $\mu_\downarrow$ at the saturation field h_s is given by the self-energy at zero momentum and frequency[9]. Using Eq. (2.90) this leads to the equation

$$\begin{aligned} \mu_\downarrow &= \Sigma^R_\downarrow(\mathbf{0},0) \\ &= \int_{q<k_F} \frac{d^3q}{(2\pi)^3} \left[\frac{1}{g_0} + \int_{k>k_F} \frac{d^3k}{(2\pi)^3} \frac{1}{\varepsilon_{\mathbf{k}} + \varepsilon_{\mathbf{q}-\mathbf{k}} - \varepsilon_{\mathbf{q}} - \mu_\downarrow} \right]^{-1} \end{aligned} \tag{3.39}$$

[8] Note again that the ground state energy E of the polaron measured with respect to the N-particle Fermi sea is equivalent to the minority Fermion chemical potential $\mu_\downarrow \equiv E$.

[9] At the saturation field h_s the chemical potential $\mu_\downarrow$ is negative for all interaction strengths, which simplifies the T-matrix calculations considerably. See the discussion in Sec. 2.3.2.

which is identical to Chevy's result (3.9). The same is true for the quasiparticle residue $Z_\downarrow$ of the minority Fermion. Within Chevy's ansatz $Z_\downarrow$ is given by Eqs. (3.25) and (3.26). The T-matrix approach at the saturation field h_s leads to

$$\begin{aligned} Z_\downarrow^{-1} &= \left| 1 - \frac{\partial}{\partial\omega} \mathrm{Re}\, \Sigma_\downarrow^R(\mathbf{0},0) \right| \\ &= 1 + \frac{1}{V^2} \sum_{\substack{q<k_F \\ k>k_F}} \frac{\left(\varepsilon_{\mathbf{k}} + \varepsilon_{\mathbf{q}-\mathbf{k}} - \varepsilon_{\mathbf{q}} - \mu_\downarrow\right)^{-2}}{\left(\frac{1}{g_0} + \frac{1}{V}\sum_{k'>k_F} \frac{1}{\varepsilon_{\mathbf{k}'} + \varepsilon_{\mathbf{q}-\mathbf{k}'} - \varepsilon_{\mathbf{q}} - \mu_\downarrow}\right)^2}, \end{aligned} \tag{3.40}$$

which is again equivalent to the result obtained using Chevy's ansatz.

Apart from leading to the same results, the T-matrix approach has one crucial advantage over Chevy's wave function, however. While Chevy's ansatz suggests that it is valid in the whole BCS-BEC crossover regime, the T-matrix approach has the ability to predict its own breakdown via the Thouless criterion, that has been discussed in Sec. 2.3.1. Indeed, we have found in Sec. 2.3.2 that the critical chemical potential from the Thouless criterion crosses the chemical potential obtained using Eq. (3.39) at a critical interaction strength

$$\left(\frac{1}{k_F a}\right)_{\mathrm{crit}} = 1.27\,. \tag{3.41}$$

which can be identified with the point M in the phase diagram 2.1.

The equivalence of Chevy's wave function to the T-matrix approach shows, that there is a critical point M on the BEC side of the Feshbach resonance beyond which the ansatz (3.4) is no longer valid. Indeed, we have already seen above that Chevy's ansatz leads to a polaronic ground state for all interaction strengths and is not capable of describing the molecule formation correctly. In the rest of this chapter our aim is to find a complementary variational ansatz that is valid on the BEC-side of the point M and which correctly describes the formation of the molecular ground state. This will allow us to pin down the transition point M with a higher accuracy than the T-matrix result (3.41).

3.2 Variational ansatz for the BEC-regime

In order to describe the physics of bound state formation in the regime $v \gg 1$, we propose a variational ansatz for the (N+1)-body problem that complements the ansatz (3.4) describing a Fermi polaron with a finite quasiparticle residue. Our ansatz gives the exact behavior (3.12) of the ground state energy in the BEC-limit up to linear order in a. The associated variational wave function

$$|\psi_0\rangle = \Big(\sum_{\mathbf{k}}{}' \xi_{\mathbf{k}}\, c^\dagger_{-\mathbf{k}\downarrow} c^\dagger_{\mathbf{k}\uparrow} + \sum_{\mathbf{k}',\mathbf{k},\mathbf{q}}{}' \xi_{\mathbf{k}'\mathbf{k}\mathbf{q}}\, c^\dagger_{\mathbf{q}-\mathbf{k}-\mathbf{k}'\downarrow} c^\dagger_{\mathbf{k}'\uparrow} c^\dagger_{\mathbf{k}\uparrow} c_{\mathbf{q}\uparrow} \Big) |FS^{N-1}_\uparrow\rangle \tag{3.42}$$

is a natural generalization of the Chevy ansatz and is constructed by adding a $(\uparrow,\downarrow)$-pair to a $(N-1)$-particle Fermi sea of $\uparrow$-Fermions, together with the leading term in an expansion in particle-hole excitations. Again, sums on $\mathbf{k}, \mathbf{k}'$ and $\mathbf{q}$ are restricted to

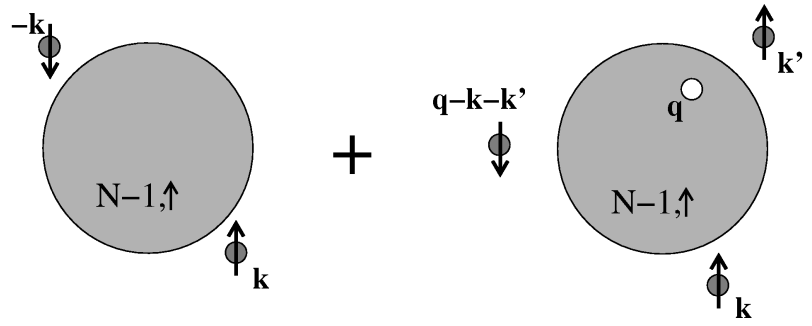

Figure 3.6: Pictorial representation of the variational wave function (3.42) for the molecular ground state.

$k, k' > k_F$ and $q < k_F$, respectively. The first term accounts for the formation of the molecule in the presence of the ↑-Fermi sea and gives the correct next-to-leading-order ground state energy in the BEC-limit, avoiding the problem of creating a hole in the ↑-Fermi sea. The single particle-hole excitation in the second term describes the leading order contribution to the interaction of the dimer with the Fermi sea apart from Pauli-blocking effects, that are already accounted for in the first term. An important feature brought about by the inclusion of the second term in Eq. (3.42) is that it amounts to an exact treatment of the three-particle problem. Indeed, as will be shown in detail in Sec. 3.2.6, the set of coupled equations (3.63)-(3.66) that determine the coefficients of the variational many-body wave function reduce, in the three-particle limit, precisely to the integral equation for the exact solution of the three-body problem by Skorniakov and Ter-Martirosian [63]. As a result, the exact atom-dimer scattering length $a_{ad} = 1.18a$ appears in the asymptotic behavior of the ground state energy (3.12), giving rise to the correct next-to-next-to-leading order behavior of the ground state energy in the BEC-limit.

Obviously, the ansatz (3.42) is not capable of describing the whole range of scattering lengths correctly. In particular, it does not capture the weak coupling BCS-limit $a \to 0^-$. Indeed, the ↓-Fermion in the first term is always added at momenta $k > k_F$, leading to a ground state energy that is too high by ε_F in the weak coupling limit. Our ansatz (3.42) is therefore complementary to the Chevy wave function (3.4), which correctly describes the situation at weak coupling up to and slightly beyond the unitarity limit.

From a physical point of view, the two variational wave functions (3.4) and (3.42) characterize very different ground states. Chevy's ansatz describes a Fermi polaron with a finite quasiparticle residue, which allows to build a normal Fermi liquid at a finite concentration of the down-spin Fermions, provided that interactions between the quasiparticles have no attractive channels. By contrast, the wave function (3.42) describes a bosonic molecule interacting with a Fermi sea. At a finite concentration $n_\downarrow \neq 0$, the resulting ground state is expected to be a superfluid of condensed bosonic molecules, coexisting with unpaired majority Fermions. The critical coupling v_M, where the ground state energies of the two variational wave functions intersect, is thus expected to separate a normal

fluid from a superfluid ground state of the attractive Fermi gas in the limit of very strong imbalance.

3.2.1 The two-channel model

The variational ansatz (3.42) is based on the single channel model (3.2) that describes the attractive interactions between the two pseudo-spin states. For computational purposes, however, it turns out to be easier to start from the more general two-channel model [66], which is defined by the Hamiltonian

$$H = \sum_{\mathbf{p}} \left(\frac{\varepsilon_{\mathbf{p}}}{2} + \nu_0 \right) b^\dagger_{\mathbf{p}} b_{\mathbf{p}} + \sum_{\mathbf{p},\sigma} \varepsilon_{\mathbf{p}} c^\dagger_{\mathbf{p},\sigma} c_{\mathbf{p},\sigma} + \frac{g_0}{\sqrt{V}} \sum_{\mathbf{p}',\mathbf{p}} \left(b^\dagger_{\mathbf{p}} c_{\mathbf{p}-\mathbf{p}',\uparrow} c_{\mathbf{p}',\downarrow} \; + \; h.c. \right) \; . \tag{3.43}$$

Here, $b^\dagger_{\mathbf{p}}$ denotes the bosonic creation operator of a molecule with momentum $\mathbf{p}$ and $c^\dagger_{\mathbf{p},\sigma}$ are the fermionic creation operators for the two species $\sigma = \uparrow, \downarrow$. The free particle dispersion is denoted by $\varepsilon_{\mathbf{p}} = p^2/(2m)$ and the factor $1/2$ in the first term accounts for the factor two in the molecule to single Fermion mass ratio.

The two particle problem: relating the bare couplings to physical parameters

In order see how the bare detuning ν_0 and the Feshbach coupling strength g_0 in the two-channel model are related to the physical s-wave scattering length a and the interaction range r_0, we study the two particle problem briefly. The ground state wave function of an up- and a down-Fermion in the two channel model can be obtained from the ansatz

$$|\psi\rangle = \left(\eta b^\dagger_{\mathbf{0}} + \sum_{\mathbf{k}} \xi_{\mathbf{k}} c^\dagger_{\mathbf{k}\uparrow} c^\dagger_{-\mathbf{k}\downarrow} \right) |0\rangle \, , \tag{3.44}$$

which is an eigenstate of the Hamiltonian (3.43) with energy E if the coefficients η and $\xi_{\mathbf{k}}$ satisfy the equations

$$(E - \nu_0)\eta \;\; = \;\; \frac{g_0}{\sqrt{V}} \sum_{\mathbf{k}} \xi_{\mathbf{k}} \tag{3.45}$$

$$(E - 2\varepsilon_{\mathbf{k}})\, \xi_{\mathbf{k}} \;\; = \;\; \frac{g_0}{\sqrt{V}} \eta \tag{3.46}$$

as can be checked easily by calculating $H|\psi\rangle = E|\psi\rangle$ and equating the coefficients. These two equations can be combined to

$$E - \nu_0 = \frac{g_0^2}{V} \sum_{\mathbf{k}} \frac{1}{E - 2\varepsilon_{\mathbf{k}}} \, . \tag{3.47}$$

The integral on the RHS diverges for large momenta, thus the bare detuning needs to be regularized in the usual way via

$$\nu_0 = \nu + \frac{g_0^2}{V} \sum_{\mathbf{k}} \frac{1}{2\varepsilon_{\mathbf{k}}} \, . \tag{3.48}$$

Evaluating the integral in the thermodynamic limit finally leads to the eigenvalue equation

$$E - \nu = \frac{g_0^2 m}{4\pi}\sqrt{-Em}\,. \tag{3.49}$$

We are looking for the energy of the molecular bound state of the two Fermions, which is parameterized as[10] $E = -E_b = -\kappa^2/m$. Plugging this into the above equation we get

$$-\frac{\kappa^2}{m} - \frac{g_0^2 m}{4\pi}\,\kappa - \nu = 0\,. \tag{3.50}$$

On the other hand, the scattering amplitude of two particles with vanishing relative momentum $\mathbf{k}$ is given by

$$f(k \to 0) = \frac{1}{-1/a + r_0 k^2/2 - ik + \mathcal{O}(k^3)} \tag{3.51}$$

where a is the s-wave scattering length and r_0 is the interaction range. Bound states are determined by the poles of the scattering amplitude in the upper half complex plane at $k = i\kappa$, with a binding energy given by $E = -\kappa^2/m$. This leads to the equation

$$-r_0\frac{\kappa^2}{2} + \kappa - \frac{1}{a} = 0 \tag{3.52}$$

Comparing the coefficients of equations (3.50) and (3.52) we finally get the following relations between the bare couplings ν_0 and g_0 of the two-channel model and the physical parameters a and r_0

$$\frac{\nu_0}{g_0^2} = -\frac{m}{4\pi a} + \frac{1}{V}\sum_{\mathbf{p}}\frac{1}{2\varepsilon_{\mathbf{p}}}\,, \tag{3.53}$$

$$r_0 = -\frac{8\pi}{g_0^2 m^2}\,. \tag{3.54}$$

Note that the effective range of the interaction r_0 is *negative*. Indeed, this counterintuitive result holds for all zero-range potentials [67]. Furthermore, we note that the two-channel Hamiltonian (3.43) is equivalent to a single channel model in the interesting limit where the effective range r_0 goes to zero, i.e. $k_F r_0 \ll 1$ (i.e. for broad Feshbach resonances), as can be seen easily by integrating out the bosonic degrees of freedom.

Variational ansatz in the two-channel model

The corresponding variational ansatz to (3.42) in the two-channel model has two additional terms ($\sim \eta_0$, $\eta_{\mathbf{kq}}$) where the closed-channel state is occupied

$$\begin{aligned}|\psi_0\rangle = \Big(&\eta_0\, b_{\mathbf{0}}^\dagger + {\sum_{\mathbf{k}}}'\,\xi_{\mathbf{k}}\, c_{-\mathbf{k}\downarrow}^\dagger c_{\mathbf{k}\uparrow}^\dagger + {\sum_{\mathbf{k},\mathbf{q}}}'\,\eta_{\mathbf{kq}}\, b_{\mathbf{q}-\mathbf{k}}^\dagger c_{\mathbf{k}\uparrow}^\dagger c_{\mathbf{q}\uparrow} \\ &+ {\sum_{\mathbf{k}',\mathbf{k},\mathbf{q}}}'\,\xi_{\mathbf{k}'\mathbf{kq}}\, c_{\mathbf{q}-\mathbf{k}-\mathbf{k}'\downarrow}^\dagger c_{\mathbf{k}'\uparrow}^\dagger c_{\mathbf{k}\uparrow}^\dagger c_{\mathbf{q}\uparrow}\Big)|FS_\uparrow^{N-1}\rangle\,.\end{aligned} \tag{3.55}$$

[10] Note that the two Fermions have the same mass m, thus the reduced mass is given by $m_r = m/2$.

The ground state energy can now be obtained variationally by evaluating the expectation value of the Hamilton operator (3.43) in the state (3.55) and determining the minimum with respect to the infinite set of variational parameters $\eta_0, \xi_{\mathbf{k}}, \eta_{\mathbf{kq}}$ and $\xi_{\mathbf{k'kq}}$. The constraint of a normalized variational wave function is included conveniently using a Lagrange multiplier E, which serves as trial ground state energy. The variational method thus leads to the four coupled equations

$$\frac{\partial}{\partial \eta_0^*}\Big(\langle\psi_0|\hat{H}|\psi_0\rangle - E\langle\psi_0|\psi_0\rangle\Big) = 0 \tag{3.56}$$

$$\frac{\partial}{\partial \xi_{\mathbf{k}}^*}\Big(\langle\psi_0|\hat{H}|\psi_0\rangle - E\langle\psi_0|\psi_0\rangle\Big) = 0 \tag{3.57}$$

$$\frac{\partial}{\partial \eta_{\mathbf{kq}}^*}\Big(\langle\psi_0|\hat{H}|\psi_0\rangle - E\langle\psi_0|\psi_0\rangle\Big) = 0 \tag{3.58}$$

$$\frac{\partial}{\partial \xi_{\mathbf{k'kq}}^*}\Big(\langle\psi_0|\hat{H}|\psi_0\rangle - E\langle\psi_0|\psi_0\rangle\Big) = 0 \tag{3.59}$$

The derivatives with respect to the complex conjugate parameters lead to the conjugate equations, which contain no additional information. The expectation values can be evaluated straightforwardly and one obtains

$$\langle\psi_0|\psi_0\rangle = |\eta_0|^2 + {\sum_{\mathbf{k}}}' |\xi_{\mathbf{k}}|^2 + {\sum_{\mathbf{kq}}}' |\eta_{\mathbf{kq}}|^2 + 2{\sum_{\mathbf{k'kq}}}' |\xi_{\mathbf{k'kq}}|^2 \tag{3.60}$$

$$\begin{aligned}\langle\psi_0|\hat{H}_0|\psi_0\rangle = {} & (\nu_0 - \varepsilon_F)|\eta_0|^2 + {\sum_{\mathbf{k}}}' |\xi_{\mathbf{k}}|^2(2\varepsilon_{\mathbf{k}} - \varepsilon_F) \\ & + {\sum_{\mathbf{kq}}}' |\eta_{\mathbf{kq}}|^2(\nu_0 + \varepsilon_{\mathbf{q-k}}/2 + \varepsilon_{\mathbf{k}} - \varepsilon_{\mathbf{q}} - \varepsilon_F) \\ & + 2{\sum_{\mathbf{k'kq}}}' |\xi_{\mathbf{k'kq}}|^2(\varepsilon_{\mathbf{q-k-k'}} + \varepsilon_{\mathbf{k}} + \varepsilon_{\mathbf{k'}} - \varepsilon_{\mathbf{q}} - \varepsilon_F)\end{aligned} \tag{3.61}$$

$$\begin{aligned}\langle\psi_0|\hat{H}_{\mathrm{int}}|\psi_0\rangle = {} & -\frac{g_0}{\sqrt{V}}\eta_0^* {\sum_{\mathbf{k}}}' \xi_{\mathbf{k}} + \frac{g_0}{\sqrt{V}} {\sum_{\mathbf{kq}}}' \xi_{\mathbf{k}}^*\eta_{\mathbf{kq}} - \frac{g_0}{\sqrt{V}} {\sum_{\mathbf{k'kq}}}' (\eta_{\mathbf{kq}}^* - \eta_{\mathbf{k'q}}^*)\xi_{\mathbf{k'kq}} \\ & + \text{h.c.}\end{aligned} \tag{3.62}$$

Note that the energy in the above equations is evaluated with respect to the N-particle Fermi sea instead of the $(N-1)$-particle sea, which explains the occurrence of the $\sim \varepsilon_F$ terms in Eq. (3.61). This choice allows for a direct comparison with the results obtained using Chevy's ansatz. Furthermore, since the N-particle Fermi sea has been used as reference scale, the ground state energy E is equivalent to the chemical potential $\mu_\downarrow \equiv E$

of the single down-spin. Finally, the four coupled variational equations are given by

$$(E+\varepsilon_F-\nu_0)\,\eta_0 = -\frac{g_0}{\sqrt{V}}\sum_{\mathbf{k}}{}' \xi_{\mathbf{k}} \tag{3.63}$$

$$(E+\varepsilon_F-2\varepsilon_{\mathbf{k}})\,\xi_{\mathbf{k}} = -\frac{g_0}{\sqrt{V}}\eta_0+\frac{g_0}{\sqrt{V}}\sum_{\mathbf{q}}{}' \eta_{\mathbf{kq}} \tag{3.64}$$

$$\left(E+\varepsilon_F-\nu_0-\frac{\varepsilon_{\mathbf{q}-\mathbf{k}}}{2}-\varepsilon_{\mathbf{k}}+\varepsilon_{\mathbf{q}}\right)\eta_{\mathbf{kq}} = \frac{g_0}{\sqrt{V}}\xi_{\mathbf{k}}-\frac{2g_0}{\sqrt{V}}\sum_{\mathbf{k}'}{}' \xi_{\mathbf{k}'\mathbf{kq}} \tag{3.65}$$

$$\left(E+\varepsilon_F-\varepsilon_{\mathbf{q}-\mathbf{k}-\mathbf{k}'}-\varepsilon_{\mathbf{k}'}-\varepsilon_{\mathbf{k}}+\varepsilon_{\mathbf{q}}\right)\xi_{\mathbf{k}'\mathbf{kq}} = -\frac{g_0}{2\sqrt{V}}\left(\eta_{\mathbf{kq}}-\eta_{\mathbf{k}'\mathbf{q}}\right) \tag{3.66}$$

3.2.2 No particle-hole excitation

Before providing a full solution to the equations (3.63)-(3.66), we investigate a simplified version of the variational problem and neglect the effect of particle-hole excitations for the moment, i.e. we set $\eta_{\mathbf{kq}}=0$ and $\xi_{\mathbf{k}'\mathbf{kq}}=0$. In this case the ground state energy is determined solely by the equations (3.63) and (3.64), which are essentially equivalent to the two equations (3.45) and (3.46) for the exact solution of the two-body problem. The only difference is the restriction of the $\mathbf{k}$-sum to momenta larger than k_F, which accounts for the Pauli blocking of the Fermi sea. Without the inclusion of particle-hole excitations our variational ansatz is thus analogous to Cooper's problem [61] (see also App. C), where the ground state energy of two Fermions with zero total momentum in the presence of a Fermi sea is studied. Plugging Eq. (3.63) into (3.64) one obtains the equation

$$(E+\varepsilon_F-2\varepsilon_{\mathbf{k}})\,\xi_{\mathbf{k}} = \frac{g_0^2}{E+\varepsilon_F-\nu_0}\frac{1}{V}\sum_{\mathbf{k}}{}' \xi_{\mathbf{k}}\ . \tag{3.67}$$

This integral equation is easily soluble since it has a trivially separable kernel. Setting the RHS equal to a constant we get the condition

$$\frac{E+\varepsilon_F-\nu_0}{g_0^2} = \frac{1}{V}\sum_{\mathbf{k}}{}' \frac{1}{E+\varepsilon_F-2\varepsilon_{\mathbf{k}}}\ . \tag{3.68}$$

Since we are interested in broad Feshbach resonances, where the long range physics is determined solely by the s-wave scattering length a, we take the zero range limit $r_0\to 0$ (or equivalently $g_0\to\infty$, see Eq. (3.54)). Furthermore we use Eq. (3.53) to renormalize the bare coupling constants and obtain

$$\frac{m}{4\pi a} = \frac{1}{V}\sum_{\mathbf{k}}{}' \frac{1}{E+\varepsilon_F-2\varepsilon_{\mathbf{k}}}+\frac{1}{V}\sum_{\mathbf{p}}\frac{1}{2\varepsilon_{\mathbf{p}}}\ . \tag{3.69}$$

Note again that the prime on the summation symbol indicates the restriction of the integration area to $|\mathbf{k}|>k_F$. Evaluating the integrals explicitly in the thermodynamic limit, (3.69) reduces to the transcendental equation (in dimensionless form, i.e. measuring

energies in units of ε_F)

$$\frac{\pi}{2k_F a} = 1 + \sqrt{-\frac{E+\varepsilon_F}{2\varepsilon_F}}\ \arctan\left(\sqrt{-\frac{E+\varepsilon_F}{2\varepsilon_F}}\right) . \tag{3.70}$$

The numerical results for the ground state energy obtained from Eq. (3.70) are shown in Fig. 3.10. As discussed in equation (3.12), the dominant contribution to the ground state energy in the BEC-limit ($a \to 0^+$) comes from the molecular binding energy. In this limit an approximate analytical solution to Eq. (3.70) can be obtained by setting $E = E_b - \varepsilon_F + \delta$ and expanding to leading order in δ. As a result we get

$$E = E_b - \varepsilon_F + \frac{8\pi a}{m} n_\uparrow + \mathcal{O}(a^2) . \tag{3.71}$$

Comparing this result with Eq. (3.12), the effective atom-dimer scattering length within this approximation turns out to be given by $a_{ad} = (8/3)a$. This is exactly the result for atom-dimer scattering in Born approximation, which, however, is far from the exact value $a_{ad} = 1.18a$.

We note that the transcendental equation (3.70) is exactly equivalent to the Thouless criterion $\Gamma^{-1}(\mathbf{k} = 0, \omega = 0) = 0$ that was obtained in section 2.3.1, where only the particle-particle ladder for the vertex function was taken into account. Formally, this can be understood from the fact that the Thouless criterion for the vertex function in the particle-particle ladder approximation is equivalent to the BCS-gap equation, which in turn gives the same result as the Cooper problem, which is equivalent to the ansatz discussed in this subsection.

3.2.3 Full solution of the variational problem

Now we turn to the solution of the full variational problem, thus including the effect of a single particle hole excitation. In this case, the equations (3.63)-(3.66) can be reduced to a single integral equation for the coefficients $\eta_{\mathbf{kq}}$ as follows. First of all, we insert equation (3.63) in (3.64) and (3.66) in (3.65). In order to perform the zero range limit $r_0 \to 0$ already at an early stage we multiply Eq. (3.65) with $1/g_0^2$ and define $\tilde{\xi}_{\mathbf{k}} = \xi_{\mathbf{k}}/(g_0\sqrt{V})$. This leads to the two coupled equations

$$E_{\mathbf{k}}\tilde{\xi}_{\mathbf{k}} = -\frac{g_0^2}{\nu_0}\frac{1}{V}{\sum_{\mathbf{k}}}' \tilde{\xi}_{\mathbf{k}} + \frac{1}{V}{\sum_{\mathbf{q}}}' \eta_{\mathbf{kq}} \tag{3.72}$$

$$\alpha_{\mathbf{kq}}\eta_{\mathbf{kq}} = \tilde{\xi}_{\mathbf{k}} - \frac{1}{V}{\sum_{\mathbf{k}'}}' \frac{\eta_{\mathbf{k}'\mathbf{q}}}{E_{\mathbf{k}'\mathbf{kq}}} \tag{3.73}$$

where the zero range limit has been taken already and the coefficients are defined as

$$E_{\mathbf{k}} := E + \varepsilon_F - 2\varepsilon_{\mathbf{k}} \tag{3.74}$$

$$E_{\mathbf{k}'\mathbf{kq}} := E + \varepsilon_F - \varepsilon_{\mathbf{q}-\mathbf{k}-\mathbf{k}'} - \varepsilon_{\mathbf{k}'} - \varepsilon_{\mathbf{k}} + \varepsilon_{\mathbf{q}} \tag{3.75}$$

$$\alpha_{\mathbf{kq}} := -\frac{\nu_0}{g_0^2} - \frac{1}{V}{\sum_{\mathbf{k}'}}' \frac{1}{E_{\mathbf{k}'\mathbf{kq}}} \tag{3.76}$$

The integral equation (3.72) for the coefficients $\tilde{\xi}_{\mathbf{k}}$ has a trivial kernel and can be solved formally

$$\tilde{\xi}_{\mathbf{k}} = -\frac{c}{E_{\mathbf{k}}} + \frac{1}{V}\sum_{\mathbf{q}}{}' \frac{\eta_{\mathbf{kq}}}{E_{\mathbf{k}}} \tag{3.77}$$

where the constant c is given by

$$c = \frac{g_0^2}{\nu_0}\frac{1}{V}\sum_{\mathbf{k}}{}' \tilde{\xi}_{\mathbf{k}} = \frac{1}{V^2}\sum_{\mathbf{kq}}{}' \frac{\eta_{\mathbf{kq}}}{\gamma\, E_{\mathbf{k}}} \tag{3.78}$$

and we have defined

$$\gamma := \frac{\nu_0}{g_0^2} + \frac{1}{V}\sum_{\mathbf{k}}{}' \frac{1}{E_{\mathbf{k}}} \tag{3.79}$$

By inserting $\tilde{\xi}_{\mathbf{k}}$ from Eq. (3.77) into Eq. (3.73) the four coupled equations (3.63)-(3.66) finally reduce to a single homogeneous Fredholm equation of the second kind[11]

$$\frac{1}{V^2}\sum_{\mathbf{k}',\mathbf{q}'}{}' \mathcal{K}(E;\mathbf{k},\mathbf{q};\mathbf{k}',\mathbf{q}')\ \eta_{\mathbf{k}'\mathbf{q}'} = 0\,. \tag{3.80}$$

The associated Kernel $\mathcal{K}(E;\mathbf{k},\mathbf{q};\mathbf{k}',\mathbf{q}')$ is given by

$$\mathcal{K}(E;\mathbf{k},\mathbf{q};\mathbf{k}',\mathbf{q}') = \frac{V\delta_{\mathbf{k},\mathbf{k}'}}{E_{\mathbf{k}}} - \frac{1}{\gamma E_{\mathbf{k}} E_{\mathbf{k}'}} - \alpha_{\mathbf{kq}} V^2 \delta_{\mathbf{k},\mathbf{k}'}\,\delta_{\mathbf{q},\mathbf{q}'} - \frac{V\delta_{\mathbf{q},\mathbf{q}'}}{E_{\mathbf{k}'\mathbf{kq}}} \tag{3.81}$$

Now, the ground state energy can be obtained in a rather straightforward manner. The homogeneous integral equation (3.80) has a nontrivial solution only if the Fredholm determinant of the Kernel vanishes ($\det_F \mathcal{K} = 0$). Since an analytic solution to this problem is hardly possible, we evaluate the Fredholm determinant numerically by discretizing the integral equation and calculating the determinant of the corresponding homogeneous linear equation system. Schematically this works in the following way[12]

$$\begin{aligned}
\int dx' \mathcal{K}(x,x')u(x') &= 0 \\
&\downarrow \\
\sum_{m=1}^{N} \Delta x\, \mathcal{K}(x_n,x_m)u(x_m) &= 0 \qquad \forall\ n \in \{1,\ldots,N\} \\
&\downarrow \\
\det \mathcal{K}(x_n,x_m) &\stackrel{!}{=} 0
\end{aligned}$$

[11] We note that the description within the two-channel model allowed us to reduce the problem to a single integral equation for the coefficients $\eta_{\mathbf{kq}}$. Within the single-channel model, we would get an equation for the coefficients $\xi_{\mathbf{k'kq}}$, which is in principle equivalent but much harder to solve numerically due to the third momentum dependence.

[12] Note that we use a Gauss-Legendre quadrature instead of an equidistant discretization in our calculation. This leads to a much faster convergence with less sampling points.

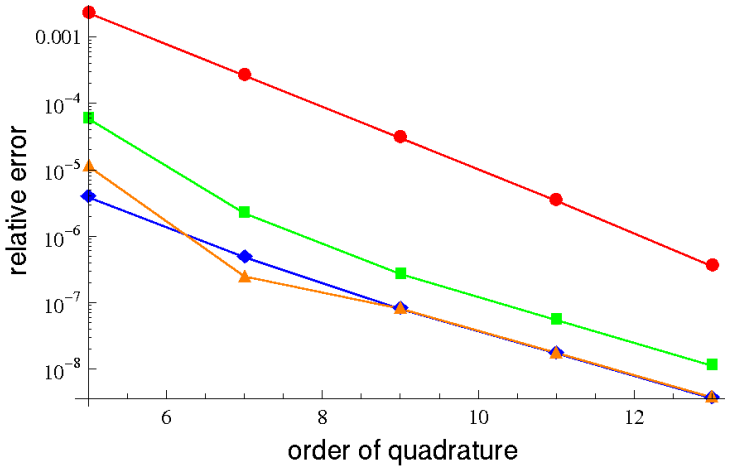

Figure 3.7: Relative error of the ground state energy in the ($\mathbf{q} = 0$)-approximation as a function of the order m of the Gauss-Legendre quadrature, plotted for different interaction strengths. The ground state energy at order $m = 15$ (in the ($\mathbf{q} = 0$)-approximation) has been taken as reference value, i.e. we plot $|E^{(m)}_{\mathbf{q}=0}/E^{(15)}_{\mathbf{q}=0} - 1|$. Red with circles: unitarity; green with squares: $\nu = \pi/(2k_F a) = 1$; blue with diamonds: $\nu = 2$; orange with up-triangles: $\nu = 3$. At order $m = 11$ the relative error at unitarity is already below 10^{-5}.

The root of the determinant then determines the ground state energy E. For an efficient numerical calculation of the Fredholm determinant we need to reduce the dimensionality of the integral equation, however[13]. In the following, this will be done in two ways. At first approximately, by pinning to hole-wavevector at $\mathbf{q} = 0$. This leads to an one-dimensional integral equation, which is easy to solve numerically. Secondly, we show how the numerical solution to the full variational problem can be obtained by reducing (3.80) to a three-dimensional integral equation. This is possible because in an isotropic system the scalar coefficients $\eta_{\mathbf{kq}} \equiv \eta(k, q, \cos\theta_{\mathbf{kq}})$ only depend on the magnitude of the two momenta $\mathbf{k}$ and $\mathbf{q}$, as well as the angle between them.

Evaluation of the ground state energy in the ($\mathbf{q} = 0$)-approximation

Pinning the hole wavevector $\mathbf{q}$ in Eq. (3.80) at $\mathbf{q} = 0$ leads to the simplified integral equation

$$\frac{1}{V}\sum_{\mathbf{k}'}{}' \left(\frac{V\delta_{\mathbf{k},\mathbf{k}'}\, n_\uparrow}{E_{\mathbf{k}}} - \frac{n_\uparrow}{\gamma E_{\mathbf{k}} E_{\mathbf{k}'}} - \frac{1}{E_{\mathbf{k}'\mathbf{k}0}} - \alpha_{\mathbf{k}0} V\delta_{\mathbf{k},\mathbf{k}'} \right) \eta_{\mathbf{k}'0} = 0 \tag{3.82}$$

[13] A simple discretization of the integral equation (3.80) in cartesian coordinates with only ten points per axis would already lead to a $10^6 \times 10^6$ matrix, the determinant of which can hardly be evaluated on a usual computer in reasonable time.

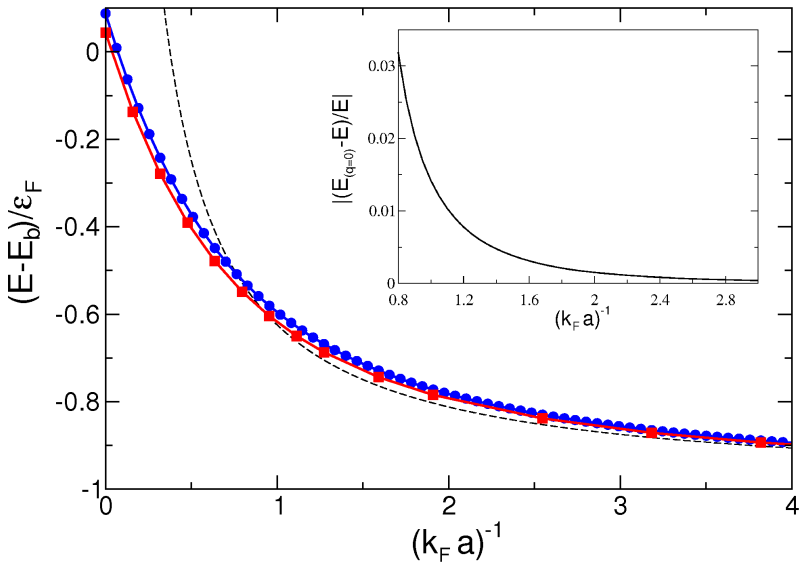

Figure 3.8: Ground state energy (binding energy E_b subtracted) as a function of the inverse interaction parameter $(k_F a)^{-1}$. The blue line with dots corresponds to the $(\mathbf{q} = 0)$-approximation, the red line with squares are the results from the full solution of the variational problem. The inset shows the error of the $(\mathbf{q} = 0)$-approximation with respect to the full solution, which is at most 3% in the regime $(k_F a)^{-1} \gtrsim 0.8$, where the ansatz (3.55) is valid.

where the factors $n_\uparrow$ arise from the remaining $\mathbf{q}'$-integral, i.e. $(1/V)\sum_{\mathbf{q}}{}' 1 = n_\uparrow$. Since $\eta_{\mathbf{k}'0}$ depends only on the magnitude of $\mathbf{k}'$, we switch to spherical coordinates and choose a frame where $\mathbf{k}$ points in z-direction and the polar angle θ' corresponds to the angle between $\mathbf{k}'$ and $\mathbf{k}$. In dimensionless form one obtains

$$\int_1^\infty dk' \left\{ \frac{2\delta(k-k')}{3\tilde{E}_{\mathbf{k}}} - \tilde{\alpha}_{\mathbf{k}0}\delta(k-k') - \frac{4k'^2}{3\tilde{\gamma}\tilde{E}_{\mathbf{k}}\tilde{E}_{\mathbf{k}'}} - \int_{-1}^{1} d\cos\theta' \frac{k'^2}{\tilde{E}_{\mathbf{k}'\mathbf{k}0}} \right\} \eta_{\mathbf{k}'} \tag{3.83}$$

where the energies and momenta are measured in units of ε_F and k_F. The angular integral in the equation above can be evaluated analytically. The Fredholm determinant of (3.83) can now be evaluated numerically as sketched above. The discretization of the integral using a Gauss-Legendre quadrature [68] of order[14] $m \approx 10$ already leads to very accurate results, as can be seen from Fig. 3.7. If a simple rectangular equidistant quadrature is applied, more than 200 sampling points are needed to reach the same level of accuracy. The results for the ground state energy are shown in Fig. 3.8.

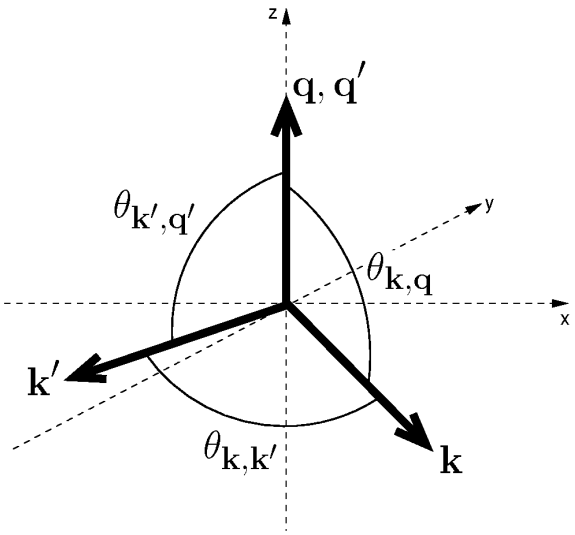

Figure 3.9: Coordinate frame for evaluating the integral in Eq. (3.86). In the text we use the abbreviated notation $\theta_{\mathbf{kq}} \equiv \theta$ and $\theta_{\mathbf{k'q'}} \equiv \theta'$.

Full solution of the variational problem

We now proceed with the solution of the full variational problem. As mentioned above, we need to reduce the six-dimensional integral equation (3.80) to a three dimensional integral equation of the form

$$\int_{k_F}^{\infty} dk' \int_0^{k_F} dq' \int_{-1}^{1} d\cos\theta' \; \mathcal{K}(E; k, q, \cos\theta; k', q', \cos\theta') \; \eta(k', q', \cos\theta') = 0 \qquad (3.84)$$

where $k = |\mathbf{k}|$, $q = |\mathbf{q}|$ and θ denotes the angle between $\mathbf{k}$ and $\mathbf{q}$. We start by writing the original integral equation (3.80) in dimensionless form and take the thermodynamic limit

$$\begin{aligned} 0 \;=\; \int\limits_{|\mathbf{q}'|<1} d^3q' \int\limits_{|\mathbf{k}'|>1} d^3k' \Bigg\{ & \frac{\delta^{(3)}(\mathbf{k}-\mathbf{k}')}{2\pi\tilde{E}_{\mathbf{k}}} - \frac{1}{4\pi^2\tilde{\gamma}\tilde{E}_{\mathbf{k}}\tilde{E}_{\mathbf{k}'}} - \tilde{\alpha}_{\mathbf{k'q'}}\delta^{(3)}(\mathbf{q}-\mathbf{q}')\delta^{(3)}(\mathbf{k}-\mathbf{k}') \\ & - \frac{\delta^{(3)}(\mathbf{q}-\mathbf{q}')}{2\pi\tilde{E}_{\mathbf{k'kq}}} \Bigg\} \; \eta_{\mathbf{k'q'}} \; . \end{aligned} \qquad (3.85)$$

Here, $\tilde{E} = E/\varepsilon_F$ and $\tilde{\alpha} = \alpha 2\pi^2/(k_F m)$ (same for $\tilde{\gamma}$) and the momenta are measured in units of k_F, but are denoted with the same symbols. Since $\eta_{\mathbf{kq}}$ and $\tilde{\alpha}_{\mathbf{kq}}$ depend only on the lengths and the angle between $\mathbf{k}$ and $\mathbf{q}$, the first three terms on the RHS can be brought easily to the form (3.84). Only the last term needs a more careful analysis, since $E_{\mathbf{k'kq}}$ depends on the magnitudes and angles between the three momenta $\mathbf{k}'$, $\mathbf{k}$ and $\mathbf{q}$. At

[14] The order m of the quadrature is equal to the number of support points.

first, we evaluate the d^3k' integral of the last term using spherical coordinates in the frame depicted in Fig. 3.9, where $\mathbf{q} \equiv \mathbf{q}'$ is taken along the z-axis and $\mathbf{k}$ lies in the xz-plane, WLOG (i.e. $\varphi_{\mathbf{k}} = 0$ in spherical coordinates). Inserting $E_{\mathbf{k'kq}}$ from Eq. (3.75) explicitly, the d^3k' integral of the last term on the RHS of Eq. (3.85) takes the form

$$\int_1^\infty dk' k'^2 \int_{-1}^1 d\cos\theta' \int_0^{2\pi} d\varphi'_k \frac{\eta(k', q', \cos\theta')/(2\pi)}{\tilde{E} - 2k^2 - 2k'^2 - 2kk'\cos\theta_{\mathbf{k},\mathbf{k}'} + 2kq\cos\theta + 2k'q'\cos\theta'} \tag{3.86}$$

Since $\mathbf{q} \equiv \mathbf{q}'$, we can express the angle between $\mathbf{k}$ and $\mathbf{k}'$ as

$$\cos\theta_{\mathbf{kk}'} = \cos\theta\cos\theta' + \cos\varphi'_k \sin\theta\sin\theta' \ , \tag{3.87}$$

and perform the $d\varphi'_k$ integral directly. Thus, we find the kernel $\mathcal{K}$ of the dimension-reduced integral equation (3.84) in dimensionless form to be given by

$$\begin{aligned}
\mathcal{K} \;=\; & \frac{q'^2}{\tilde{E}_k}\delta(k-k') - \frac{2q'^2k'^2}{\tilde{\gamma}\tilde{E}_k\tilde{E}_{k'}} - \delta(k-k')\delta(q-q')\delta(\cos\theta - \cos\theta')\tilde{\alpha}(k', q', \cos\theta) \\
& + k'^2\delta(q-q')\Bigg\{ \Big(2k^2 + 2k'^2 + 2kk'\cos\theta\cos\theta' - 2qk\cos\theta - 2q'k'\cos\theta' - \tilde{E}\Big)^2 \\
& - \big(2kk'\big)^2\big(1-\cos^2\theta\big)\big(1-\cos^2\theta'\big)\Bigg\}^{-1/2}
\end{aligned} \tag{3.88}$$

The integrals (3.76) and (3.79) for the coefficients $\tilde{\alpha}_{\mathbf{kq}}$ and $\tilde{\gamma}$ in the above expression for the kernel $\mathcal{K}$ can be evaluated analytically. For the sake of completeness, we give here the results without derivation[15]

$$\tilde{\gamma} \;=\; -\frac{\pi}{2k_F a} + 1 - \sqrt{\frac{\tilde{E}+1}{2}}\,\mathrm{arctanh}\sqrt{\frac{\tilde{E}+1}{2}} \tag{3.89}$$

$$\tilde{\alpha}_{\mathbf{kq}} \;=\; \frac{\pi}{2k_F a} - \frac{1}{2}\left[1 - \frac{1-\lambda-\mu^2}{4\mu}\ln\left|\frac{\lambda-(1-\mu)^2}{\lambda-(1+\mu)^2}\right| + \sqrt{|\lambda|}\ \mathcal{F}\right] \tag{3.90}$$

with

$$\mathcal{F} = \begin{cases} \frac{1}{2}\ln\left|\frac{(1-\sqrt{\lambda})^2-\mu^2}{(1+\sqrt{\lambda})^2-\mu^2}\right| & \text{if } \ \lambda > 0 \\ \\ \pi - \arctan\frac{1+\mu}{\sqrt{|\lambda|}} - \arctan\frac{1-\mu}{\sqrt{|\lambda|}} & \text{if } \ \lambda < 0 \end{cases} \tag{3.91}$$

and

$$\lambda \;=\; \frac{\tilde{E} + 1 - |\mathbf{k}-\mathbf{q}|^2/2 - k^2 + q^2}{2} \tag{3.92}$$

$$\mu \;=\; \frac{|\mathbf{k}-\mathbf{q}|}{2} \tag{3.93}$$

[15] Note again that ˜ denotes the dimensionless quantities, i.e. $\tilde{\gamma} = \gamma\ 2\pi^2/(mk_F)$.

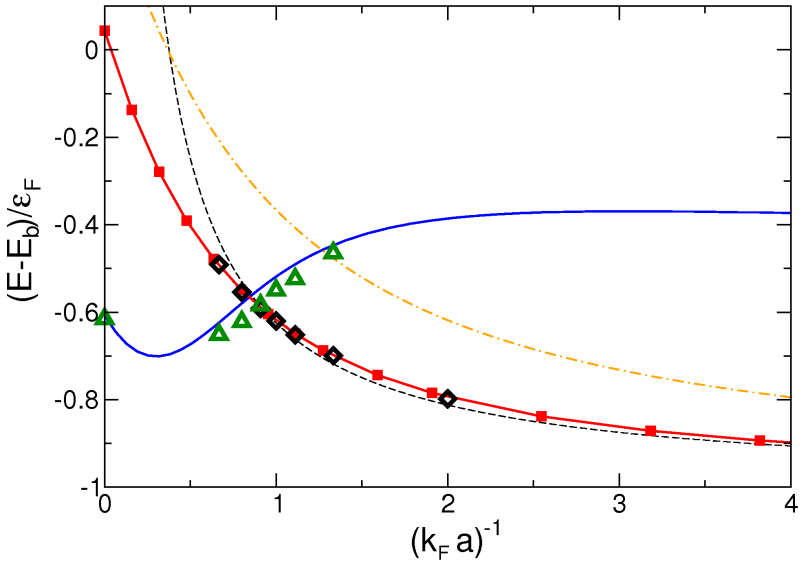

Figure 3.10: Groundstate energy $E - E_b$ (binding energy $E_b = -1/(ma^2)$ subtracted) of a single down-Fermion immersed in an up-spin Fermi sea in units of the Fermi energy ε_F as function of the inverse interaction strength $(k_F a)^{-1}$. Blue solid line: Chevy's ansatz (3.4); red line with full squares: ansatz Eq. (3.42); black dashed line: BEC-asymptotics (3.12); orange dash-dotted line: Thouless criterion (3.70). The open black diamonds and green triangles correspond to the QMC results for the molecule- and the polaron energy from Prokof'ev and Svistunov [23]. For $(k_F a)^{-1} > 0.84$ our variational ansatz (3.55) leads to a lower ground state energy than Chevy's ansatz (3.4). This point marks the phase transition from a polaron to a molecular state. Picture taken from [65].

In order to perform the numerical calculation of the Fredholm determinant we change the variables k and k' in the integral equation (3.84) and its corresponding kernel (3.88) to the new variables $y = 1/k$ and $y' = 1/k'$ and discretize the resulting integral equation using a Gauss-Legendre quadrature with eleven sampling points for the k and q integrals and four points for the $\cos\theta$ integral, leading to an absolute error of order 10^{-4} of the ground state energy at the unitarity point, where the convergence is slowest. The results are shown in Fig. 3.10. For $(k_F a)^{-1} = 0.84$, our variational ansatz leads to a lower ground state energy than Chevy's ansatz. It is quite remarkable, that our variational results are in perfect agreement with diagrammatic Monte-Carlo results from Prokof'ev and Svistunov [23].

3.2.4 Quasiparticle residue and contact coefficient

As shown previously, Chevy's ansatz for the polaron problem leads to a finite quasiparticle residue $Z_\downarrow$ of the minority atom for all interaction strengths, implying that there is always a finite probability that the down-Fermion can propagate freely. However, in the regime where the minority particle forms a molecule with one of the up-Fermions, it is clear that

it can no longer propagate as a free particle, thus the quasiparticle residue $Z_\downarrow$ has to vanish identically. From this point of view $Z_\downarrow$ can be interpreted as order parameter for the transition from the polaron to the molecular state. In the following we show that our ansatz indeed leads to a vanishing quasiparticle residue for the minority Fermion, thus implying that the intersection point of the ground state energies obtained using Chevy's ansatz and our ansatz for the molecule marks the position of a first order quantum phase transition.

Since the variational ground state wave function does not allow to calculate the full down-spin Green's function, the definition (3.20) of the quasiparticle residue is not applicable. Instead, we use the standard connection between $Z_\downarrow$ and the jump in the momentum distribution at the Fermi momentum $k_{F\downarrow}$, which is zero in the limit of a single down-spin. The momentum distribution of the $\downarrow$-Fermion within the variational ansatz (3.55) is given by

$$n^\downarrow_{\mathbf{p}} = |\xi_{\mathbf{p}}|^2 + 2\sum_{\mathbf{k'kq}}{}' \left|\xi_{\mathbf{k'kq}}\right|^2 \delta_{\mathbf{p},\mathbf{q}-\mathbf{k'}-\mathbf{k}} \tag{3.94}$$

and is normalized via

$$1 = \sum_{\mathbf{p}} n^\downarrow_{\mathbf{p}} = \sum_{\mathbf{k}}{}' |\xi_{\mathbf{k}}|^2 + 2\sum_{\mathbf{k'kq}}{}' \left|\xi_{\mathbf{k'kq}}\right|^2 \ . \tag{3.95}$$

The normalization condition requires the coefficients to scale with the system volume as $\xi_{\mathbf{k}} \sim 1/\sqrt{V}$ and $\xi_{\mathbf{k'kq}} \sim 1/V^{3/2}$. Since an upper bound to the quasiparticle residue $Z_\downarrow$ is given by the momentum distribution at $\mathbf{p} = 0$ and $\xi_{\mathbf{p}} \equiv 0$ for $p < k_F$, we find that

$$Z_\downarrow \leq n^\downarrow_{\mathbf{p}=0} = 2\sum_{\mathbf{k'kq}}{}' \left|\xi_{\mathbf{k'kq}}\right|^2 \delta_{\mathbf{q},\mathbf{k'}+\mathbf{k}} \sim \frac{1}{V} \, . \tag{3.96}$$

As a result, the quasiparticle residue $Z_\downarrow$ of the molecular wave function scales inversely with the volume of the system and thus vanishes in the thermodynamic limit. This is in contrast to Chevy's wave function, where $Z_\downarrow = |\phi_0|^2$ is always finite. The two wave functions (3.4) and (3.42) therefore describe qualitatively different ground states. In particular, no sharp peak is expected in the minority rf-spectrum at coupling strengths $v > v_M$, consistent with the experimental observation [57]. This point will be discussed in more detail in the subsequent section.

In the $\mathbf{q} = 0$ approximation, which captures the essential properties of the variational ansatz (3.42), the quasiparticle residue $Z_\downarrow$ in fact vanishes identically. Indeed,

$$Z_\downarrow \leq 2\sum_{\mathbf{k}}{}' |\xi_{-\mathbf{k}\mathbf{k}0}|^2 = 0 \ , \tag{3.97}$$

since, as can be seen from Eq. (3.66), the coefficients $\xi_{-\mathbf{k}\mathbf{k}0} \propto \eta_{\mathbf{k}0} - \eta_{-\mathbf{k}0} = 0$ vanish because $\eta_{\mathbf{k}0}$ only depends on the length of $\mathbf{k}$.

In Fig. 3.11 we plot the dimensionless contact coefficient s, which has been defined in Eq. (2.39), for the two variational wave functions (3.4) and (3.55), using the adiabatic theorem (2.38). Quite generally, the ground state energy density $u = E/V$ of the strongly

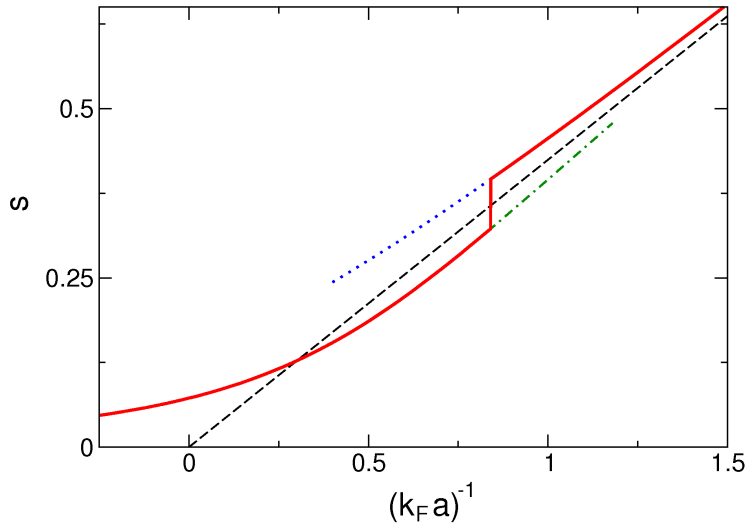

Figure 3.11: Dimensionless contact coefficient s, calculated using the adiabatic theorem (2.38) and the ground state energies from the two variational wave functions (3.4) and (3.55). The black dashed line indicates the BEC-asymptotics $s_{\mathrm{BEC}} = 4v/3\pi$.

imbalanced Fermi gas can be expanded in powers of the minority density $n_\downarrow$. The definition of the minority atom chemical potential $\mu_\downarrow$ implies that this expansion is of the form

$$u = \frac{3}{5}\varepsilon_{F\uparrow} n_\uparrow + \mu_\downarrow n_\downarrow + \dots \tag{3.98}$$

where the first term is simply the energy of a non-interacting gas of spin-up Fermions. The dimensionless contact coefficient s defined in Eq. (2.39) for a strongly imbalanced Fermi gas can thus be obtained from the derivative

$$s = \frac{1}{3\pi}\frac{\partial(-\mu_\downarrow/\varepsilon_F)}{\partial v} \tag{3.99}$$

of the negative down-spin chemical potential in units of the majority Fermi energy with respect to the coupling constant v. Since $\mu_\downarrow$ is precisely the energy E associated with adding a single down-spin, our result for the ground state energy of the $(N+1)$-particle problem immediately gives the contact density of an almost fully polarized attractive Fermi gas (note that this applies even on the molecular side $v > v_M$, where the single added down-spin is not a propagating quasiparticle). Because the ground state energies of the two variational wave functions as a function of the inverse interaction strength cross with a finite slope, the contact coefficient jumps at the critical point M, indicating a first order transition.

3.2.5 Minority spectral function and rf-response

As in Sec. 3.1.4 we can calculate the hole-part of the minority spectral function $\mathcal{A}_\downarrow^-(\mathbf{k},\omega)$ and the minority rf-spectrum at zero temperature using the variational ansatz (3.55) for

the BEC regime. For simplicity we use the approximation $\xi_{\mathbf{k'kq}} = 0$, i.e. we do not include particle hole excitations. This approximation gives the correct results for large frequencies and momenta, because the molecule formation is described already by the $\xi_{\mathbf{k}}$ term alone. Using Eq. (3.34) the hole-part of the minority spectral function at $T = 0$ in the BEC regime is thus given by

$$\mathcal{A}_{\downarrow}^{-}(\mathbf{k},\omega) = 2\pi|\xi_{\mathbf{k}}|^2\,\Theta(k-k_F)\,\delta(\omega+\varepsilon_{\mathbf{k}}) \tag{3.100}$$

We note that $|\xi_{\mathbf{k}}|^2 = n_k^{\downarrow}$ equals the minority momentum distribution in this approximation. Furthermore, the inclusion of the $\xi_{\mathbf{k'kq}}$ term in the ground state wave function would give rise to non-zero spectral weight in the regime $\omega < \varepsilon_F$ and $k < k_F$. The minority rf-spectrum can be obtained straightforwardly from the spectral function above and can be expressed as

$$I_{\downarrow}(\omega) = \int \frac{d^3k}{(2\pi)^3}\,|\xi_{\mathbf{k}}|^2\Theta(k-k_F)\,\delta(2\varepsilon_k-\omega-\mu_{\downarrow})\,. \tag{3.101}$$

The coefficients $\xi_{\mathbf{k}}$ have been determined in Eq. (3.67) as $\xi_{\mathbf{k}} \sim (\mu_{\downarrow}+\varepsilon_F-2\varepsilon_{\mathbf{k}})^{-1}$, apart from a normalization factor. In the molecular limit, where $\mu_{\downarrow} \simeq E_b = -1/(ma^2)$, the rf-spectrum thus takes the form

$$I_{\downarrow}(\omega) \sim \sqrt{\frac{\omega+\mu_{\downarrow}}{2}}\,\frac{\Theta(\frac{\omega+\mu_{\downarrow}}{2}-\varepsilon_F)}{(\omega-\varepsilon_F)^2}\,. \tag{3.102}$$

Note that the ε_F terms are a remnant of the Pauli blocking of the molecular wave function for $k < k_F$ and lead to a sharp cutoff of the rf-spectrum at low frequencies (deep in the molecular limit the ε_F-terms are negligible, however). This cutoff is washed out, if particle hole excitations ($\xi_{\mathbf{k'kq}} \neq 0$) are taken into account.

Compared to the result for the polaron rf-spectrum in Sec. 3.1.4, the sharp peak at $\omega = -\mu_{\downarrow}$ is missing on the molecular side of the transition. However, the tail of the rf-spectrum at large frequencies is again determined by

$$I_{\downarrow}(\omega\to\infty) \approx \frac{1}{4\pi^2\sqrt{m}}\,\frac{C}{\omega^{3/2}}\,. \tag{3.103}$$

3.2.6 Three particle limit

As mentioned previously, our variational ansatz (3.55) solves the three particle problem exactly, since it corresponds to the most general three particle state that one can write down. In this section we show explicitly how the connection between our result and the exact solution of the three Fermion problem by Skorniakov and Ter-Martirosian can be established.

If we take our variational wave function (3.55) and reduce the $(N-1)$-particle Fermi sea to a single Fermion, it is clear that only the $\mathbf{q} = 0$ term survives in the ansatz. Now, if we start from our integral equation (3.80) for the full variational problem and take the

limit of a one particle Fermi sea, i.e. we set $\mathbf{q} = 0$ and take $k_F \to 0$, it is easy to see that one arrives at the equation (in the thermodynamic limit)

$$\alpha_{\mathbf{k}0}\,\eta_{\mathbf{k}0} = -\int \frac{d^3k'}{(2\pi)^3}\frac{\eta_{\mathbf{k}'0}}{E_{\mathbf{k}'\mathbf{k}0}}\ . \tag{3.104}$$

Note that the first two terms from Eq. (3.81) vanish in the limit $k_F \to 0$ due to the lack of the Delta-functions in the d^3q' integral. Inserting the coefficients $\alpha_{\mathbf{k}0}$ and $E_{\mathbf{k}'\mathbf{k}0}$ from equations (3.76) and (3.75) explicitly (keeping in mind that the $\mathbf{k}$-integration covers the whole $\mathbb{R}^3$ in the limit $k_F \to 0$), equation (3.104) takes the form

$$\left(\frac{1}{a} - \sqrt{\frac{3k^2}{4} - mE}\right)\eta_{\mathbf{k}} \ = \ \int \frac{d^3k'}{(2\pi)^3}\frac{4\pi\,\eta_{\mathbf{k}'}}{k^2 + k'^2 + \mathbf{k}\cdot\mathbf{k}' - mE}\ . \tag{3.105}$$

The above equation corresponds to the Schrödinger equation for the relative wave function between the molecule and the third Fermion in the three particle problem. It is exactly equivalent to the one derived by Skorniakov and Ter-Martirosian [63] for the three nucleon problem with total spin $S = 3/2$ and total pseudospin $T = 1/2$ (see Eq. (29) in [63]), which corresponds exactly to our problem[16].

3.3 Conclusions

Using two complementary variational wave functions we have shown that a phase transition from a polaronic ground state to a molecular bound state shows up in the $(N+1)$-particle problem at an interaction strength $v_M \approx 0.84$. Our result is close to the value $v_M \approx 0.90$ obtained from exact diagrammatic quantum Monte-Carlo simulations [23, 24]. The little discrepancy is entirely due to the fact that the variational ansatz (3.4) for the polaronic side of the transition is not precise near v_M, as can be seen from Fig. 3.10.

The analysis of the polaron to molecule transition in this chapter leaves two important questions open: what is the nature of the transition and what are its implications for the phase diagram of the strongly imbalanced gas? Now for the case of a single minority Fermion in an up-spin Fermi sea, the transition from a polaronic to a molecular state is a first order transition, where the quasiparticle residue $Z_\downarrow$ exhibits a discontinuous jump from a finite value to zero at the critical coupling $v_M \simeq 0.9$. This is a result of the fact that the energies of the two ground states, which have different quantum numbers, cross with a finite slope at v_M (see Fig. 3.10.). It is important to note that this crossing is not an artefact of extending the different variational states beyond their domain of validity. Indeed, as shown by Prokof'ev and Svistunov [23, 24], both the polaronic and the molecular state exist as stable excitations for $v > v_M$ or $v < v_M$ respectively because the phase space for decay vanishes linearly with the magnitude of the energy difference. Both states are thus reachable as metastable configurations coming from the weak coupling or the molecular side, as expected for a first order transition.

[16] Note that in the case $S = 3/2$ the spin part of the wave function only gives rise to an unimportant overall prefactor.

Concerning the implications for the phase diagram, the results for the minority atom chemical potential $\mu_\downarrow \equiv E$ in this chapter completely determine the saturation field line $h_s(v)$ as a function of $v = (k_F a)^{-1}$ in the phase diagram shown in Fig. 2.1. This is because the effective magnetic field is determined by $h = (\mu_\uparrow - \mu_\downarrow)/2$ and the majority chemical potential $\mu_\uparrow = \varepsilon_F$ is equal to the Fermi energy at h_s, where $\varepsilon_F = (6\pi^2 n)^{2/3}/(2m)$ and $n = n_\uparrow$. The saturation field is thus given by

$$h_s(v) = \frac{\varepsilon_F}{2}\left(1 - \frac{\mu_\downarrow(v)}{\varepsilon_F}\right) . \tag{3.106}$$

One open question that has been mentioned at the end of Sec. 2.1 cannot be answered within the $(N+1)$-particle problem, however, namely if phase separation occurs at finite minority atom concentrations close to the point M. This question is interesting from a theoretical point of view but not important for experiments, because the mixing entropy disfavors phase separated states at finite temperature.

Chapter 4

Quench dynamics of Heisenberg spin chains

The experimental ability to control systems of ultracold atoms with high accuracy and prepare states with high fidelity triggered lots of theoretical work on so called quantum quench problems recently. In a quantum quench problem, the system under consideration is described by a Hamiltonian $H(g)$ that is dependent on a parameter g, such as the interaction strength for example. Initially, the system is prepared in the ground state of the Hamiltonian with respect to a given parameter g_0. At time $t = 0$ the parameter g is suddenly 'quenched' to a different value $g \neq g_0$ and the subsequent time evolution of the system is studied. Up to now mainly questions concerning thermalization of quenched quantum systems have been addressed. Obviously, the unitary time evolution of a pure initial state can never lead to a thermal mixed-state. Nevertheless, it was suggested that the expectation values of *local* observables after large evolution times can be expressed in terms of a thermal average at an effective temperature corresponding to the energy of the initial state [69, 70, 71, 72].

The first experimental realization of a quantum quench problem with ultracold atoms was reported by Greiner *et al.* [73] in 2002. In this experiment, ultracold bosonic atoms were loaded into an optical lattice at a lattice depth where the ground state is superfluid. Then, the lattice depth was ramped up rapidly to a value, where the equilibrium ground state is a Mott-insulator. After this interaction quench Greiner *et al.* observed collapse and revival oscillations of the order parameter. Deep in the Mott-insulating regime, this can be understood rather easily in terms of a single site Hamiltonian. Indeed, in that case the time evolution of the initial on-site coherent state is governed by the interaction term $\sim U$ alone, leading to a phase factor that is periodic if Ut is an integer multiple of 2π.

The following theoretical work was triggered partly by a recent experiment with ultracold atoms in optical lattices, which has demonstrated the control of super-exchange interactions in such systems for the first time [74]. In particular, a one-dimensional array of decoupled double wells was generated by superposition of lasers with different wavelengths. Atoms in two different hyperfine states (which we refer to as pseudospin "up" and "down" in the following) were loaded into the lattice and manipulated in such a way,

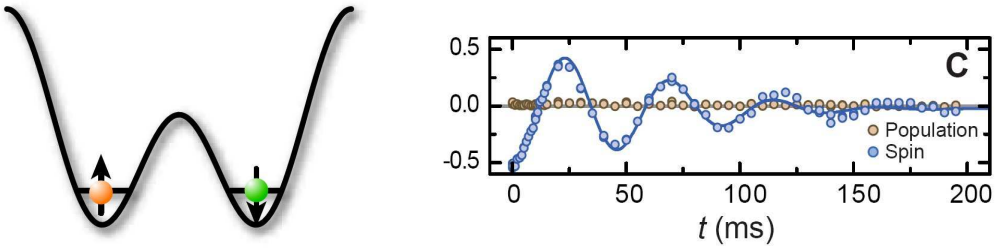

Figure 4.1: Left: schematic picture of the experimental setup studied by Trotzky et al. [74]. Right: results. Both pictures were taken from [74].

that in each left well a spin up atom and in each right well a spin down atom was present (see Fig. 4.1). This initial state corresponds to a perfectly Néel ordered state of the spins in the array of decoupled double wells

$$|\psi_{\text{Néel}}\rangle = |\uparrow\downarrow\uparrow\downarrow \ \cdots \ \uparrow\downarrow\rangle \tag{4.1}$$

Deep in the Mott-insulating regime, i.e. at large lattice depths, where double occupancies of a single well are heavily suppressed by the strong on-site repulsion of the atoms, the simplest theoretical description for each double well is provided by a two-site Heisenberg model

$$H = J\,\mathbf{S}_1 \cdot \mathbf{S}_2 = \frac{J}{2}\left(S_1^+ S_2^- + h.c.\right) + J S_1^z S_2^z \ . \tag{4.2}$$

The Heisenberg model accounts for the interaction of localized spins via virtual second order hopping processes, commonly known as superexchange interactions. The superexchange coupling $J \sim t^2/U$ is related to the hopping t and onsite-interaction U of the atoms in the double well[1]. Since the initial state $|\psi(0)\rangle = |\uparrow\downarrow\rangle$ is coupled solely to the state $|\downarrow\uparrow\rangle$ via the Hamiltonian (4.2), it is sufficient to diagonalize the Hamiltonian in the subspace of those two states. The eigenstates are the singlet $|s\rangle = (|\uparrow\downarrow\rangle - |\downarrow\uparrow\rangle)/\sqrt{2}$ and the triplet-state $|t\rangle = (|\uparrow\downarrow\rangle + |\downarrow\uparrow\rangle)/\sqrt{2}$ with respective eigenenergies $E_s = -3J/4$ and $E_t = J/4$. Obviously, after preparation of the initial state, the system will start to oscillate between the singlet- and the triplet state

$$|\psi(t)\rangle = \frac{1}{\sqrt{2}}\, e^{iJt/4}\left(e^{-iJt/2}|t\rangle + e^{iJt/2}|s\rangle\right) \tag{4.3}$$

with a characteristic frequency given by the exchange coupling J. Indeed, such oscillations have been observed in the experiment, the results of which are shown in Fig. 4.1.

In the subsequent sections we are going to study the many-body analogon of the above mentioned singlet-triplet oscillations in the double-well, i.e. instead of a double well we

[1]The coupling between neighboring double wells can be neglected if the potential barriers between the double wells are large enough.

focus on a Heisenberg chain with $N \to \infty$ sites and nearest neighbor superexchange coupling. Experimentally, this situation can be realized easily by ramping down the barriers between the initially decoupled double wells.

The outline of this chapter is as follows. In Sec. 4.1 we present the basic XXZ-model, which is a generalization of the isotropic spin-1/2 Heisenberg chain to anisotropic spin-spin couplings, and discuss approximative and numerical methods to study the time evolution of the initial Néel state. A slightly different model for a spin-chain, the so called XZ-model, is analyzed in Sec. 4.2. It has the advantage of being analytically diagonalizable and shows a similar behavior in the time evolution of the Néel state as the XXZ-model. In Sec. 4.3 we discuss the time evolution of weakly antiferromagnetically ordered initial states. In particular, we focus on the applicability of Luttinger liquid theory, which has been extremely successful in describing the equilibrium properties of 1D systems. Finally, in Sec. 4.4, the time evolution of the Néel state in higher dimensional XXZ-models is considered.

4.1 XXZ-Model

As mentioned above, the Heisenberg model provides an effective description of two component Bose- or Fermi gases in optical lattices deep in the Mott insulating regime[2]. In the following, we are going to study the time evolution of a Néel state (4.1) in the one-dimensional, anisotropic spin-1/2 Heisenberg- (or XXZ-) chain, defined by the Hamiltonian

$$\begin{aligned} H_{\mathrm{XXZ}} &= J \sum_{\ell} \left(S^x_\ell S^x_{\ell+1} + S^y_\ell S^y_{\ell+1} + \Delta\, S^z_\ell S^z_{\ell+1} \right) \\ &= J \sum_{\ell} \left[\frac{1}{2} \left(S^+_\ell S^-_{\ell+1} + S^-_\ell S^+_{\ell+1} \right) + \Delta\, S^z_\ell S^z_{\ell+1} \right] \end{aligned} \tag{4.4}$$

where the index ℓ labels the lattice sites and the spin operators S^x, S^y and S^z obey the usual angular momentum algebra $[S^x, S^y] = iS^z$ on a given lattice site and commute if taken at different sites. The spin raising and lowering operators are defined as $S^\pm = S^x \pm iS^y$. In the rest of this thesis we take J to be positive.

The XXZ-Hamiltonian is a slight generalization of the usual isotropic ($\Delta = 1$) Heisenberg model and has some interesting properties. First of all it is an integrable model and can be solved exactly using the Bethe-ansatz [76]. The zero temperature phase diagram of the XXZ-Hamiltonian is shown in Fig. 4.2. Since the total magnetization $S^z_{\mathrm{tot}} = \sum_\ell S^z_\ell$ is a conserved quantity in the XXZ-model and we start from an initial Néel state, which has zero total magnetization, we restrict our discussion to the line $S^z_{\mathrm{tot}} = 0$ in the phase diagram. Here, the ground state has antiferromagnetic order in z-direction if $\Delta > 1$ and ferromagnetic order if $\Delta < -1$. In the regime $|\Delta| < 1$, the ground state of the XXZ-model is paramagnetic. At finite temperatures no long range order exists in the one dimensional XXZ-chain. This is true for any one dimensional system at finite temperature with short range interactions. In the limit $\Delta \to \infty$, the XXZ-chain reduces to an antiferromagnetic

[2]For details see for example [4, 75].

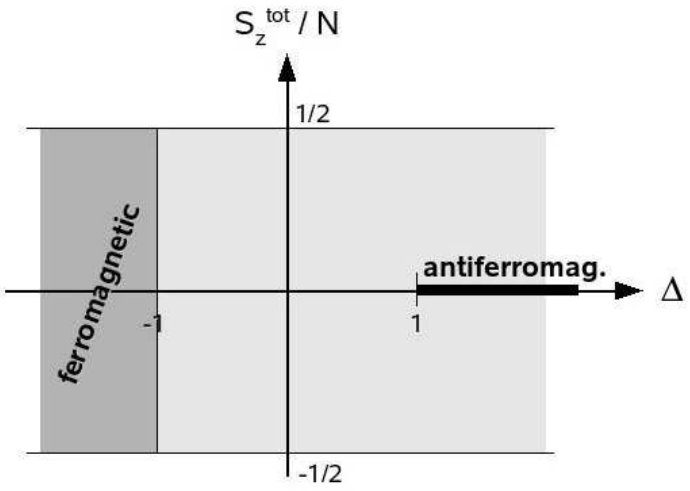

Figure 4.2: Zero temperature phase diagram of the XXZ-Hamiltonian (4.4) with $J > 0$ as function the anisotropy parameter Δ and of the total magnetization per lattice site.

Ising model, where the Néel state is one of the two degenerate ground states which are related via a translation by one lattice site. From this point of view the time evolution of a Néel state is equivalent to a quench of the XXZ-chain from $\Delta_0 = \infty$ to a finite value of the anisotropy Δ.

Our goal is to study the relaxation timescales in the XXZ-chain that are a consequence of the quantum quench from the initial Néel state. In principle, we have to calculate the unitary time evolution of the initial state, i.e.

$$|\psi(t)\rangle = e^{iH_{\mathrm{XXZ}}t}|\psi_{\mathrm{N\acute{e}el}}\rangle\,. \tag{4.5}$$

This is a non-trivial problem, however, because we are dealing with an interacting many-body system. Since it is practically impossible to study the time evolution of the full wave function in the thermodynamic limit, we focus on one particular observable, namely the staggered magnetization

$$m_s = \frac{1}{N}\sum_{\ell}(-1)^{\ell}\langle S^z_{\ell}\rangle\ , \tag{4.6}$$

where N denotes the number of lattice sites. The staggered magnetization m_s is the order parameter of the antiferromagnetic phase and takes its maximal value for a Néel state (4.1), where $|m_s| = 1/2$. Contrary, a state with ferromagnetically aligned spins has $m_s = 0$. In contrast to spin-spin correlation functions, the staggered magnetization is well suited to extract nontrivial relaxation timescales from our quench problem. This is in part a consequence of the light-cone effect, which leads to a rather generic behavior of spin-spin correlation functions and will be discussed in more detail later.

To get more insight into the problem under consideration and for certain practical calculations it is useful to map the XXZ-Hamiltonian (4.4) to a model of spinless Fermions

on a lattice using the well known Jordan-Wigner transform [77]

$$\begin{aligned} S_\ell^z &= n_\ell - 1/2 \\ S_\ell^+ &= c_\ell^\dagger \exp\Big(i\pi \sum_{j<\ell} n_j\Big) \\ S_\ell^- &= c_\ell \exp\Big(-i\pi \sum_{j<\ell} n_j\Big) \,. \end{aligned} \tag{4.7}$$

Here, the fermionic operators c_ℓ and $c_\ell^\dagger$ obey the standard anti-commutation relations and $n_\ell = c_\ell^\dagger c_\ell$ counts the number of Fermions on site ℓ. The idea of this transformation becomes clear when one realizes that the string operators ensure the commutativity of the spin operators at different lattice sites. Using this transformation, the XXZ-Hamiltonian (4.4) maps to a model of spinless Fermions on a lattice with nearest neighbor interactions

$$H_{\rm XXZ} = -\frac{J}{2} \sum_\ell \Big\{ c_\ell^\dagger c_{\ell+1} + c_{\ell+1}^\dagger c_\ell - 2\Delta (n_\ell - 1/2)(n_{\ell+1} - 1/2) \Big\} \,. \tag{4.8}$$

Note that we have used a sublattice rotation $c_j \to (-1)^j c_j$ on every other site to transform the antiferromagnetic exchange coupling in the xy-plane to a ferromagnetic exchange[3], i.e. $J \to -J$ and $\Delta \to -\Delta$. We note that the Néel state and the staggered magnetization m_s are invariant with respect to this sublattice rotation, thus the time evolution of $m_s(t)$ is invariant as well. In the fermionized picture, the Néel state (4.1) corresponds to a state with one Fermion at every second lattice site, i.e. spin-up corresponds to an occupied site and spin-down to an empty site[4].

Before procceding, we prove that the time evolution of the staggered magnetization $m_s(t)$ following a quench from the Néel state is invariant with respect to a change of sign of the exchange coupling $J \to -J$ and/or of the anisotropy $\Delta \to -\Delta$. This is a remarkable property, because it means that $m_s(t)$ is the same in a ferromagnetic and in an antiferromagnetic spin-chain, which have a completely different excitation spectrum, however. Above, we have already argued, that $m_s(t)$ is invariant with respect to a combined change of sign of J and Δ. Now we show that $m_s(t)$ is also invariant with respect to a change of J alone. Indeed, the change $J \to -J$ is equivalent to a time reversal transformation of the time evolution operator. We thus get

$$\begin{aligned} m_s(t,-J) &= \langle\psi_{\rm Néel}|\, T^{-1} e^{iHt} T\, m_s\, T^{-1} e^{-iHt} T\, |\psi_{\rm Néel}\rangle \\ &= \langle\psi_{\rm Néel}|\, T^{-1} e^{iHt} T_r\, m_s\, T_r^{-1} e^{-iHt} T\, |\psi_{\rm Néel}\rangle \\ &= \langle\psi_{\rm Néel}|\, T^{-1} T_r e^{iHt}\, m_s\, e^{-iHt} T_r^{-1} T\, |\psi_{\rm Néel}\rangle \\ &= \langle\psi_{\rm Néel}|\, e^{iHt}\, m_s\, e^{-iHt}\, |\psi_{\rm Néel}\rangle \quad = \quad m_s(t,J) \end{aligned} \tag{4.9}$$

[3] We note that this transformation is not necessary for the subsequent calculations. Its only purpose is to bring the kinetic energy term in the fermionized Hamiltonian to the conventional form.

[4] A similar setup with Bosons instead of Fermions at every second lattice site and on-site interactions instead of nearest neighbor interactions was studied by Cramer et al. [78]. Note however, that their model exhibits no quantum phase transition, because the equilibrium ground state for Bosons is always superfluid at half filling.

where T and T_r denote the time-reversal and lattice translation operators and we have used the facts that $T^{-1}m_sT = T_r^{-1}m_sT_r = -m_s$, the Hamiltonian is translation invariant and the Néel state is invariant under the combination of time reversal and lattice translation.

4.1.1 Free Fermion limit ($\Delta = 0$)

The fermionized Hamiltonian (4.8) is especially useful to study the limit $\Delta = 0$, which is commonly known as the XX-limit, where the XXZ-chain maps to a model of free Fermions. Going over to momentum representation via[5]

$$c_\ell = \frac{1}{\sqrt{L}} \sum_{k=-\pi}^{\pi} \exp(-ik\ell)\, c_k \ , \tag{4.10}$$

the fermionized Hamiltonian (4.8) with $\Delta = 0$ becomes diagonal

$$H_{\mathrm{XX}} = \sum_{k=-\pi}^{\pi} \varepsilon_k\, c_k^\dagger c_k \qquad \text{with} \qquad \varepsilon_k = -J\cos(k) \tag{4.11}$$

and the staggered magnetization (4.6) is given by

$$m_s = \frac{1}{N}\sum_{\ell}(-1)^\ell \langle c_\ell^\dagger c_\ell\rangle = \frac{1}{L}\sum_{k=-\pi}^{\pi} \langle c_{k+\pi}^\dagger c_k\rangle \ . \tag{4.12}$$

In this special case the time evolution of the staggered magnetization starting from an initial Néel state can be calculated exactly

$$\begin{aligned} m_s(t) &= \frac{1}{L}\sum_{k=-\pi}^{\pi} \langle\psi_{\text{Néel}}|c_{k+\pi}^\dagger(t)c_k(t)|\psi_{\text{Néel}}\rangle \\ &= \int_{-\pi}^{\pi}\frac{dk}{2\pi} e^{i2Jt\cos(k)}\langle\psi_{\text{Néel}}|c_{k+\pi}^\dagger c_k|\psi_{\text{Néel}}\rangle \\ &= \frac{1}{2}\mathcal{J}_0(2Jt)\,, \end{aligned} \tag{4.13}$$

where we have used that $\langle\psi_{\text{Néel}}|c_{k+\pi}^\dagger c_k|\psi_{\text{Néel}}\rangle = 1/2$ and $\mathcal{J}_0$ denotes the zeroth Bessel function of the first kind. At times $Jt \gg 1$, the asymptotic behavior is given by

$$m_s(t) \overset{Jt\gg 1}{\approx} \sqrt{\frac{1}{4\pi Jt}}\,\cos(2Jt - \pi/4) \tag{4.14}$$

Thus, the staggered magnetization oscillates with a characteristic frequency $\sim 2J$ and decays algebraically as $\sim 1/\sqrt{t}$. The oscillations can be viewed as the many body analogon

[5] We set the lattice spacing to unity throughout, thus the length L of the chain equals the number of lattice sites N.

of the singlet-triplet oscillations in the two site model. The connected spin-spin correlation function can be calculated equally easy in the free Fermion limit. We obtain

$$\langle S_0^z S_\ell^z \rangle - \langle S_0^z \rangle \langle S_\ell^z \rangle = \frac{1}{4} \left(\delta_{\ell,0} - \mathcal{J}_\ell^2(2Jt) \right) \ , \tag{4.15}$$

where $\mathcal{J}_\ell$ denote the Bessel functions of the first kind.

For finite anisotropies $\Delta \neq 0$ it is no longer possible to calculate the exact time evolution of the staggered magnetization analytically in a simple way, since one deals with an interacting many-body problem. In this case, one has to use approximations or resort to numerical simulations. We mention however, that it might be possible to calculate $m_s(t)$ exactly using the Bethe ansatz. Using this method, it would be necessary to evaluate the expression

$$m_s(t) = \sum_{n,n'} \langle \psi_0 | n \rangle \langle n' | \psi_0 \rangle e^{i(E_n - E_{n'})t} \langle n | \hat{m_s} | n' \rangle \tag{4.16}$$

where $\{|n\rangle\}$ denotes a full set of Bethe eigenstates with corresponding eigenenergies E_n, which are in principle known exactly. However, the calculation of the overlap of the initial state with the Bethe-eigenstates and of matrix elements of the staggered magnetization operator is a highly non-trivial task, which we did not attempt in this thesis.

4.1.2 Time-dependent mean-field theory

In this section, as a first step to analyze the interacting many-body problem, we employ a simple time-dependent mean field theory to account for the interaction term in (4.8)[6]. We expand the interaction term to linear order in fluctuations δn_ℓ around the mean density

$$n_\ell = \langle n_\ell \rangle + \delta n_\ell \, . \tag{4.17}$$

The mean field value of the Fermion density at site ℓ is related to the staggered magnetization via (note the time dependence)

$$\langle n_\ell \rangle = \frac{1}{2} + (-1)^\ell m_s(t) \tag{4.18}$$

Using this approach, the Hamiltonian (4.8) reduces to the time dependent mean-field Hamiltonian in momentum space, given by

$$H_{\mathrm{MF}}(t) = -J \sum_{k=-\pi}^{\pi} \left\{ \cos(k) c_k^\dagger c_k + 2\Delta m_s(t) c_{k+\pi}^\dagger c_k \right\} \tag{4.19}$$

Note that the time dependent mean field $m_s(t) = L^{-1} \sum_k \langle c_{k+\pi}^\dagger(t) c_k(t) \rangle$ has to be evaluated selfconsistently.

In order to calculate the time evolution of the staggered magnetization within this mean field Hamiltonian, we map (4.19) to a pseudospin model as follows. Since the

[6] After we had obtained the tMFT results which are presented in this section, a preprint of Hastings and Levitov appeared on the arXiv [79], who had studied the same problem using exactly the same method.

symmetry of the initial Néel state is always present in the mean-field Hamiltonian, the unit cell is effectively doubled and we can employ a reduced zone scheme by restricting the pseudo-momentum to the interval $|k| < \pi/2$. Furthermore, we define pseudospin operators via

$$\sigma_k^x = c_{k+\pi}^\dagger c_k + c_k^\dagger c_{k+\pi} \tag{4.20}$$
$$\sigma_k^y = i\, c_{k+\pi}^\dagger c_k - i\, c_k^\dagger c_{k+\pi} \tag{4.21}$$
$$\sigma_k^z = c_k^\dagger c_k - c_{k+\pi}^\dagger c_{k+\pi} \tag{4.22}$$

The mean-field Hamiltonian (4.19) thus maps to the pseudospin Hamiltonian

$$H_{\mathrm{MF}} = -J \sum_{k=-\pi/2}^{\pi/2} \{\cos(k)\, \sigma_k^z + 2\Delta m_s(t)\, \sigma_k^x\} \tag{4.23}$$

and the staggered magnetization $m_s(t)$ in the pseudospin formulation is given by

$$m_s(t) = \frac{1}{L} \sum_{k=-\pi/2}^{\pi/2} \langle \sigma_k^x(t) \rangle \ . \tag{4.24}$$

In the pseudospin model, the initial Néel state corresponds to a state where all spins point in x-direction, i.e. $\langle \sigma_k^x \rangle_0 = 1$. The Heisenberg equations of motion for the pseudospin operators are now easily obtained and take the form

$$\partial_t \langle \sigma_k^x \rangle = -2\varepsilon_k \langle \sigma_k^y \rangle \tag{4.25}$$
$$\partial_t \langle \sigma_k^y \rangle = 2\varepsilon_k \langle \sigma_k^x \rangle + 4\Delta m_s(t) \langle \sigma_k^z \rangle \tag{4.26}$$
$$\partial_t \langle \sigma_k^z \rangle = -4\Delta m_s(t) \langle \sigma_k^y \rangle \ . \tag{4.27}$$

Note again, that the staggered magnetization $m_s(t)$ has to be evaluated selfconsistently via Eq. (4.24). In order to calculate the time evolution of the staggered magnetization, we solve the equations of motion for the pseudo-spin operators numerically using the Euler method. The results are shown in Fig. 4.3.

In the paramagnetic regime $\Delta < 1$, the numerics shows that the staggered magnetization decays *faster* if Δ is increased. This result is somewhat surprising, because naively one would expect that a repulsive nearest neighbor interaction between the Fermions would stabilize the initial Néel order. This argument doesn't work however, since we have shown earlier that the time evolution of the staggered magnetization is invariant with respect to $J \to -J$ and/or $\Delta \to -\Delta$. Thus replacing the repulsive with an attractive interaction doesn't change $m_s(t)$. From the pseudospin formulation of the mean-field Hamiltonian it becomes clear, why the staggered magnetization decays faster if the anisotropy Δ is increased. In the free Fermion limit $\Delta = 0$ the pseudospins precess independently around the z-axis, each with a different precession frequency due to the different Zeeman field for every spin. The total spin in x-direction, which equals the staggered magnetization in the Heisenberg model, thus decays due to the dephasing of the individual spins. Now, if the

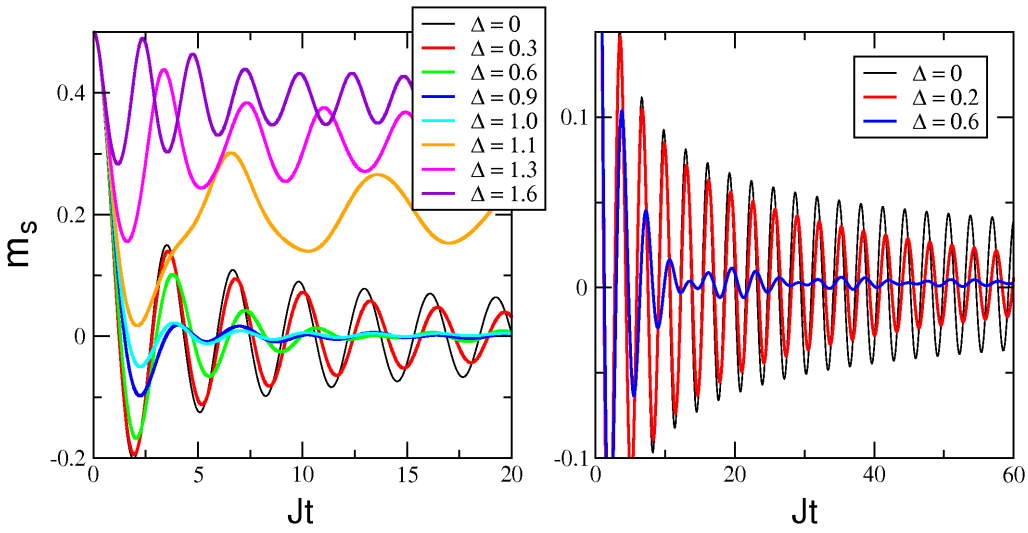

Figure 4.3: Time evolution of the staggered magnetization $m_s(t)$ in the XXZ-chain for various anisotropy parameters Δ, starting from an initial Néel state. The results shown in this picture were obtained within our time dependent mean-field theory. For easy axis anisotropies ($\Delta > 1$) our tMFT predicts a saturation of the staggered magnetization in the long time limit $t \to \infty$.

anisotropy Δ is nonzero, the precession axis is slightly tilted in the x-z-plane, thus reducing the projection of the pseudospins on the x-axis, which amounts to a smaller staggered magnetization.

In the antiferromagnetic regime $\Delta > 1$, our mean field theory predicts a saturation of the staggered magnetization at a nonzero value at large times. The saturation value

$$\bar{m} = \lim_{T\to\infty} \frac{1}{T} \int_0^T dt\, m_s(t) \tag{4.28}$$

can be inferred from a time averaged Hamiltonian, because we know from our numerics that the staggered magnetization exhibits decaying oscillations around the saturation value in the easy axis regime at large times. Since the saturation value of the staggered moment $\bar{m}$ is simply a time average over $m_s(t)$, we attempt to calculate $\bar{m}$ selfconsistently with a time averaged Hamiltonian

$$\bar{H} = \sum_k \{\varepsilon_k \sigma_k^z - 2J_z \bar{m} \sigma_k^x\} \tag{4.29}$$

which is almost trivially soluble. Using (4.29) for the dynamics of the Néel state and the Baker-Campbell-Haussdorff formula, we obtain

$$m_s(t) = \frac{1}{2} - \int \frac{dk}{2\pi} \frac{2J^2 \cos^2(k)}{4J_z^2 \bar{m}^2 + J^2 \cos^2(k)} \sin^2\Big(\sqrt{4J_z^2 \bar{m}^2 + J^2 \cos^2(k)}\, t\Big) \tag{4.30}$$

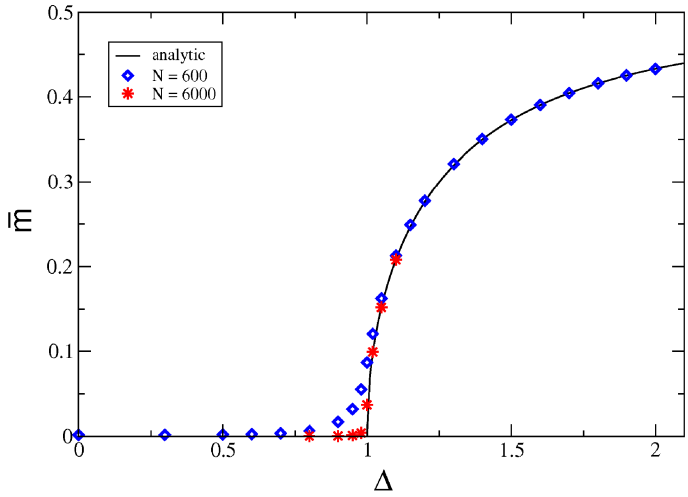

Figure 4.4: Saturation value of the staggered magnetization $\bar{m}$ as a function of the anisotropy parameter Δ, obtained within our time dependent mean field theory. The solid line corresponds to the result (4.32), whereas the dots are obtained from the full numerical solution of the mean field equations for N spins. Close to the isotropic point $\Delta = 1$, the numerics shows a finite size rounding of the transition.

corresponding to a saturation value of the staggered moment given by

$$\bar{m} = \frac{1}{2} - \int \frac{dk}{2\pi} \frac{J^2 \cos^2(k)}{4J_z^2 \bar{m}^2 + J^2 \cos^2(k)} = \frac{\bar{m} J_z/J}{\sqrt{1 + (2\bar{m} J_z/J)^2}} \,. \tag{4.31}$$

Solving for $\bar{m}$, we get the following analytic expression for the saturation value of the staggered moment as function of the anisotropy parameter Δ

$$\bar{m} = \frac{1}{2}\sqrt{1 - \frac{1}{\Delta^2}} \tag{4.32}$$

As can be seen from a comparison with numerically obtained saturation values from the full solution of the mean-field equations in Fig. 4.4, the expression (4.32) is essentially exact.

4.1.3 Numerical simulations

The time dependent mean-field theory described in the previous section is a simple method to study the time evolution of the staggered magnetization in the XXZ-chain at finite anisotropies Δ. Nevertheless, these results should be taken with care, since it is known that mean field theories for low dimensional systems are problematic due to the increased importance of quantum fluctuations and may lead to wrong conclusions. Thus, it is necessary to complement the findings in the previous section with exact results in order to validate or invalidate our time dependent mean-field theory. Since an exact solution of

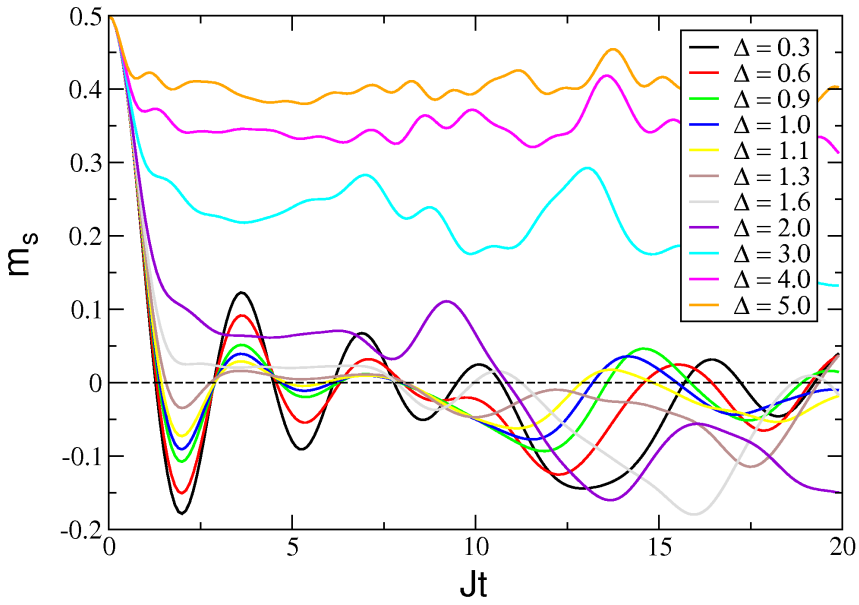

Figure 4.5: Numerical simulation of the time evolution of the staggered magnetization $m_s(t)$ in a XXZ-chain with $N = 12$ spins and open boundary conditions, starting from an initial Néel state. The different curves correspond to various anisotropies Δ.

the full interacting system is out of question, the next best thing to try is a numerical simulation of the problem. However, an exact numerical calculation can be handled only for small sized chains with up to 20 spins. This has the disadvantage, that the simulation runs into Poincaré recurrences after rather short evolution times. Fortunately, there exist quite sophisticated numerical techniques for 1D systems commonly known under the collective name 'density matrix renormalization group' (DMRG)[7], which can be used for controlled simulations of large (in some situations even infinite) size spin chains. These methods are based on matrix product state decompositions and allow to follow the time evolution of the infinite chain as long as the entanglement entropy remains sufficiently small. In the following we present results obtained using both techniques.

Direct numerical solution of the Schrödinger equation for a small spin chain

The easiest way to simulate a small sized spin chain is a brute force method using the Euler algorithm to solve the Schrödinger equation directly. This is simply achieved via a discretization of the time derivative by replacing it with the differential quotient and calculating the state of the system iteratively using the discretized Schrödinger equation

$$|\psi(t+\delta t)\rangle = |\psi(t)\rangle - i\,\frac{\delta t}{\hbar}\,\hat{H}_{\mathrm{XXZ}}|\psi(t)\rangle\ . \tag{4.33}$$

[7]For a review see [80].

This method has the disadvantage that very small time steps δt need to be chosen in order to keep the error during the time evolution small[8]. In particular we have taken $J\,\delta t = 10^{-4}$ for the data shown in Fig. 4.5. The state of the system is conveniently expanded in the basis of the S^z_ℓ eigenstates. Since the total magnetization is a conserved quantity, the dimension of the Hilbert space corresponding to our problem of an initial Néel state for a chain with N spins is given by

$$\dim(\mathcal{H}) = \binom{N}{N/2} . \tag{4.34}$$

which is slightly smaller than 2^N and reduces the computational effort a little bit. The numerical results for a chain with $N = 12$ spins and open boundary conditions are shown in Fig. 4.5. Obviously, the small system size becomes apparent after evolution times on the order of $Jt \simeq 10$, where the first recurrence seems to appear. Comparing the numerical simulation of the finite size chain with the mean-field results from the previous section shows qualitative agreement for easy plane anisotropies $\Delta < 1$, i.e. with increasing Δ the oscillations of the staggered magnetization decay faster. Interestingly, the situation is different in the easy axis regime $\Delta > 1$. A comparison of the results for $\Delta = 1.6$ shows a fast decay of the staggered magnetization without oscillations up to times $Jt = 5$ in the numerical simulation of the finite size chain (at larger times, a comparison is no longer trustworthy due to the recurrence in the finite chain at $Jt = 10$). In contrast, mean-field theory predicts a large saturation value even at such moderate easy axis anisotropies, together with a fast oscillation around the saturation value. This is a first indication that the time dependent mean-field theory leads to questionable results in the easy axis regime. In particular, the numerical results for the finite size chain at moderate easy axis anisotropies seem to indicate that $m_s(t)$ decays to zero also for $\Delta > 1$. Unfortunately, the numerical simulation cannot rule out the possibility of a saturation of the staggered magnetization for easy axis anisotropies because of the early appearance of Poincaré recurrences.

DMRG results

In the following we present numerical results on the time evolution of the staggered magnetization in the XXZ-chain starting from an initial Néel state, which were obtained using the above mentioned DMRG technique. This method is far better suited to study infinite spin chains, especially if the initial state is sufficiently uncorrelated such that the entanglement entropy is small. The number of matrix product states which have to be taken into account for an accurate description of the system's state within the DMRG-method is directly proportional to the entanglement entropy, which is defined as the von Neumann entropy of an arbitrary sub-system of the total system, i.e. $S = \mathrm{Tr}(\rho_A \log_2 \rho_A)$, where ρ_A is the reduced density matrix of the subsystem A. Since this entropy usually increases

[8] A direct numerical diagonalization of the Hamiltonian would be better suited to study the time evolution of finite size spin chains, because no time-slicing error is introduced that way. Furthermore one avoids the problem of violating unitarity due to the discretization. In our case this is not relevant however, since the Poincaré recurrences reduce the interesting time window to a size, where the time slicing error can be kept small with little effort.

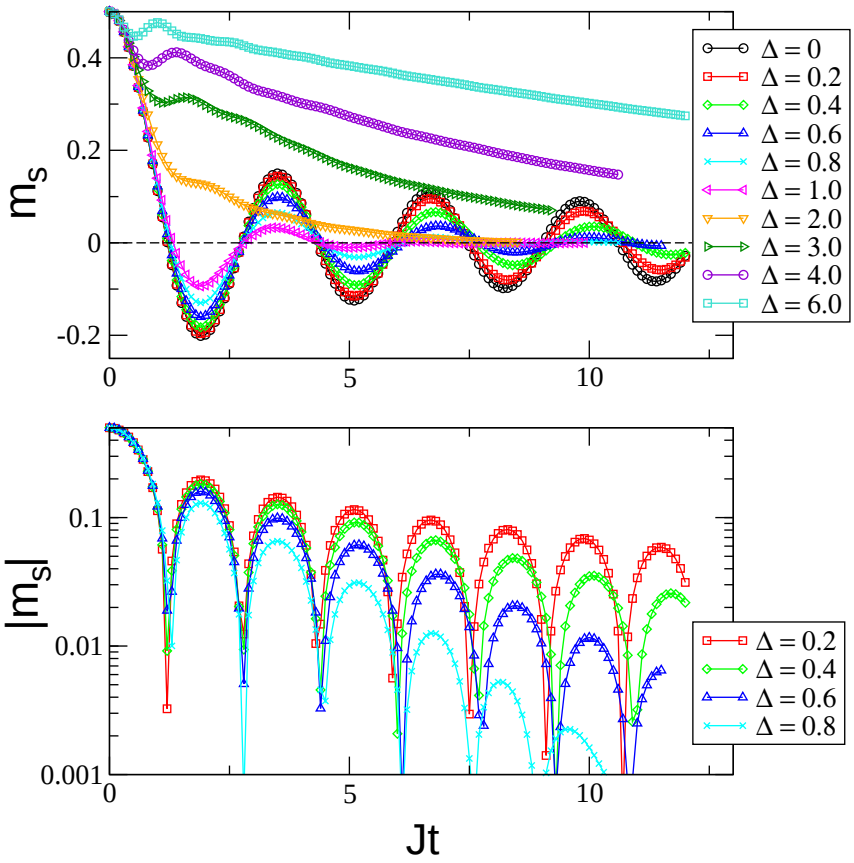

Figure 4.6: Numerical calculation of the time evolution of the staggered magnetization $m_s(t)$ in an infinite size XXZ-chain using the DMRG method, starting from an initial Néel state. The different curves correspond to various anisotropies Δ. The lower panel shows $m_s(t)$ on a logarithmic scale, indicating exponential relaxation for intermediate times.

linearly in time for Heisenberg spin chains, this method works particularly well to follow the evolution up to intermediate times on the order of $Jt \simeq 15$ for infinite size chains. The results which are shown in Fig. 4.6 were obtained by Peter Barmettler in course of a collaboration on this problem setup. For the details on the method see Peter's thesis [81] or our papers [82] and [83] and the references therein.

The DMRG results in Fig. 4.6 show several interesting features. First of all, the behavior of the staggered magnetization in the easy axis regime $\Delta > 1$ is different from the findings of our time-dependent mean-field theory. In particular, $m_s(t)$ shows hardly any oscillations and decays exponentially in the numerically accessible time window instead of having a tendency to saturate as expected from tMFT. These results also agree with the findings from the numerical simulation of the finite size spin chain at short times. In the easy plane regime $\Delta < 1$, the DMRG-results seem to agree qualitatively with the tMFT data. A quantitative analysis of the data shows however, that tMFT leads

to an *algebraic* decay of the oscillations, whereas DMRG shows *exponential* relaxation at intermediate times. Surprisingly, for $0.6 < \Delta < 1$ DMRG predicts a relaxation of the staggered magnetization that seems to be *faster* than exponential.

We have extracted the relaxation timescales from fits to the numerical data at sufficiently large times using

$$m_s(t) \sim e^{-t/\tau_1} \tag{4.35}$$

in the easy axis regime $\Delta \gtrsim 1$, and fits of the form

$$m_s(t) \sim e^{-t/\tau_2} \cos(\omega t + \phi) \tag{4.36}$$

in the easy plane regime $\Delta \lesssim 1$. Note that this fit is only valid at intermediate timescales in the easy plane regime, because the numerics shows an accelerated relaxation for $\Delta \gtrsim 0.6$ at large times, as mentioned above. Close to the critical point, the behavior of $m_s(t)$ in the XXZ-model is rather complicated and cannot be reliably fitted with one of the functions above. The relaxation times and the oscillation period are plotted in Fig. 4.7. It is interesting to note that the relaxation is fastest close to the critical point[9] $\Delta = 1$. In the easy axis regime this can be understood using a simple phase space argument. Naively, the initial state can be considered as a source of quasiparticles at $t = 0$. In order to equilibrate, these quasiparticles need to scatter. Since the gap of the quasiparticle excitations vanishes at the critical point, the phase space for scattering is largest and thus the relaxation should be fastest at the critical point. We also mention that, as far as the staggered magnetization m_s is concerned, our results are in agreement with a thermalization scenario, because the equilibrium expectation value of m_s at finite temperature is zero in $1D$. This is not true for correlation functions in general, however.

4.2 XZ-Model

The previous numerical investigations of the time evolution of the staggered magnetization $m_s(t)$ following a quench in the XXZ-chain revealed an interesting crossover in the relaxation dynamics at the isotropic point $\Delta = 1$ of the XXZ-model, but were not suitable to draw any conclusions on the behavior of $m_s(t)$ at large times. The mean field theory discussed in Sec. 4.1.2 predicts a saturation of the staggered magnetization in the easy axis regime, which is presumably wrong, whereas the DMRG-numerics in Sec. 4.1.3 indicates exponential relaxation of $m_s(t)$, although the accessible time scales do not suffice to rule out saturation at long times for large anisotropies. In order to circumvent these drawbacks, we look for a slightly different, analytically treatable model, that shows a similar behavior of $m_s(t)$ as the XXZ-model in the easy axis regime $\Delta > 1$ as far as the time evolution of the Néel state is concerned. A suitable candidate is the so called XZ-chain,

[9] We mention that this is exactly the opposite as one would expect from the notion of "critical slowing down", which holds only for small perturbations from equilibrium, however.

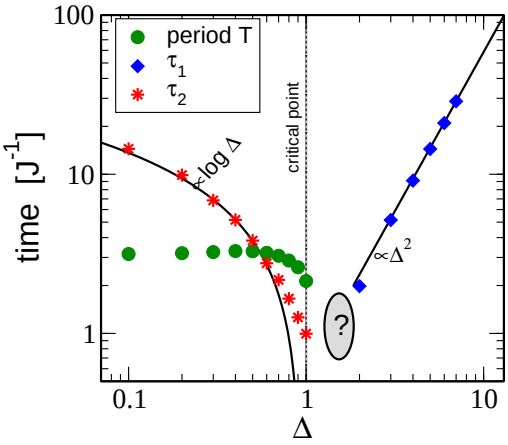

Figure 4.7: Numerically extracted timescales for the quench from a Néel state in the XXZ-model as a function of the anisotropy Δ. The relaxation times τ_1 and τ_2 have been obtained from an exponential fit to the numerical data of the staggered magnetization $m_s(t)$. Note that in the easy plane regime $\Delta < 1$, the exponential fit from which τ_1 is extracted is only valid in the intermediate time regime. The green dots correspond to the period of the oscillations of $m_s(t)$ in the easy plane regime.

defined by the Hamiltonian

$$H_{\mathrm{XZ}} = J \sum_{\ell} \left(2\, S^x_\ell S^x_{\ell+1} + \Delta\, S^z_\ell S^z_{\ell+1} \right) \tag{4.37}$$

$$= H_{\mathrm{XXZ}} + \frac{J}{2} \sum_{\ell} \left(S^+_\ell S^+_{\ell+1} + S^-_\ell S^-_{\ell+1} \right) \ . \tag{4.38}$$

This Hamiltonian differs from the XXZ-chain (4.4) by the appearance the terms $S^+_\ell S^+_{\ell+1} + h.c.$ that violate the conservation of the total magnetization in z-direction S^z_{tot}, but in the limit $\Delta \gg 1$ one expects that the time evolution of the staggered magnetization in this model is similar to that in the XXZ model. In particular, it is obvious that the time evolution of the Néel state (4.1) in both models is equivalent for short times, since the additional terms in the XZ-Hamiltonian give zero when acting on a Néel state. The XZ-model as defined above also has a quantum phase transition at $\Delta_c = 2$ with long-range-order in the ground state z-correlations for $\Delta > \Delta_c$ and thus resembles the XXZ-chain in that respect. The situation is different in the regime $\Delta < \Delta_c$ however, where the ground state of the XZ-model has LRO in the x-correlations, whereas the XXZ-model has a paramagnetic ground state.

In contrast to the XXZ-model, the XZ-model can be diagonalized analytically by applying the Jordan-Wigner transform in a rotated frame of reference. Using the transformation defined in Eq. (4.7) after a $\pi/2$ rotation around the x-axis (i.e. $S^z_\ell \to S^y_\ell$) and going over to momentum representation via (4.10) we map the Hamiltonian of the XZ-model to the

fermionic Hamiltonian

$$H_{\mathrm{XZ}} = \frac{J}{2}\sum_{k=-\pi}^{\pi}\left\{(\Delta+2)\cos(k)c_k^\dagger c_k + \frac{i}{2}(\Delta-2)\sin(k)\left(c_k^\dagger c_{-k}^\dagger + c_k c_{-k}\right)\right\} . \tag{4.39}$$

In this form, the Hamiltonian can be diagonalized straightforwardly using a Bogoliubov transformation to a new set of fermionic creation- and annihilation-operators α_k and $\alpha_k^\dagger$ with the standard fermionic anti-commutation relations $\{\alpha_k, \alpha_q^\dagger\} = \delta_{k,q}$, that are related to the original Jordan-Wigner Fermion operators via

$$\begin{bmatrix} c_{-k} \\ c_k^\dagger \end{bmatrix} = \begin{bmatrix} \cos\theta_k & -i\sin\theta_k \\ -i\sin\theta_k & \cos\theta_k \end{bmatrix}\begin{bmatrix} \alpha_{-k} \\ \alpha_k^\dagger \end{bmatrix} = M_\Delta \begin{bmatrix} \alpha_{-k} \\ \alpha_k^\dagger \end{bmatrix} , \tag{4.40}$$

where the constraint $\theta_{-k} = -\theta_k$ needs to be imposed in order to preserve the fermionic anti-commutation relations of the c_k-operators. Using (4.40), we finally obtain the diagonalized XZ-Hamiltonian

$$H_{\mathrm{XZ}} = \sum_{k=-\pi}^{\pi} E_k\left(\alpha_k^\dagger\alpha_k - \frac{1}{2}\right) \qquad \text{with} \qquad E_k = J\sqrt{1+\Delta^2/4+\Delta\cos(2k)} \tag{4.41}$$

together with the equation that determines the rotation angle θ_k of the Bogoliubov transformation

$$\tan(2\theta_k) = \frac{2-\Delta}{2+\Delta}\tan(k) . \tag{4.42}$$

The next step is to calculate the time evolution of the Jordan-Wigner Fermion operators following the quantum quench. The time dependence of the Bogoliubov-quasiparticle operators follows trivially from (4.41). Thus, the time evolution of the JW-operators in momentum space can be immediately obtained using the Bogoliubov transformation (4.40)

$$\begin{bmatrix} c_{-k}(t) \\ c_k^\dagger(t) \end{bmatrix} = M_\Delta \begin{bmatrix} e^{-iE_k t} & 0 \\ 0 & e^{iE_k t} \end{bmatrix} M_\Delta^{-1}\begin{bmatrix} c_{-k} \\ c_k^\dagger \end{bmatrix} \tag{4.43}$$

where M_Δ is the Bogoliubov-transformation matrix that has been defined in Eq. (4.40). Note that M_Δ depends on the anisotropy parameter Δ via Eq. (4.42).

Since the initial Néel state is the ground state of the XZ-Hamiltonian (4.39) with $\Delta = \Delta_0 \to \infty$, we express the time dependent (Heisenberg-) Jordan-Wigner Fermion operators $c_k(t)$ after the quench (i.e. at $t > 0$) in terms of the Bogoliubov-quasiparticle operators $\alpha_k^{(0)}$ that diagonalize the Hamiltonian (4.39) for the *initial* value $\Delta = \Delta_0$ before the quench. We thus get

$$\begin{bmatrix} c_{-k}(t) \\ c_k^\dagger(t) \end{bmatrix} = M_\Delta \begin{bmatrix} e^{-iE_k t} & 0 \\ 0 & e^{iE_k t} \end{bmatrix} M_\Delta^{-1} M_{\Delta_0}\begin{bmatrix} \alpha_{-k}^{(0)} \\ \alpha_k^{(0)\dagger} \end{bmatrix} \tag{4.44}$$

This mapping allows us to evaluate all expectation values as ground state expectation values with respect to the Bogoliubov-quasiparticle operators $\alpha_k^{(0)}$ that diagonalize the

initial Hamiltonian, i.e. $\alpha_k^{(0)}|GS(t<0)\rangle = 0$. Writing down Eq. (4.44) explicitly, we get the following expression for the time dependence of the JW-Fermion operators after the quantum quench

$$\begin{aligned} c_k(t) &= \Big(e^{-iE_k t}\cos(\theta_k)\cos(\theta_k-\theta_k^{(0)}) + e^{iE_k t}\sin(\theta_k)\sin(\theta_k-\theta_k^{(0)})\Big)\,\alpha_k^{(0)} \\ &+ i\Big(e^{iE_k t}\sin(\theta_k)\cos(\theta_k-\theta_k^{(0)}) - e^{-iE_k t}\cos(\theta_k)\sin(\theta_k-\theta_k^{(0)})\Big)\,\alpha_k^{(0)\,\dagger}\ . \quad (4.45) \end{aligned}$$

Here, the angle $\theta_k^{(0)}$ that corresponds to the initial state is given by $2\theta_k^{(0)} = -k$ in the case of an initial Néel state (i.e. $\Delta_0 \to \infty$).

Although the Jordan-Wigner transform makes an analytic diagonalization of the XZ-Hamiltonian possible, it introduces complications to the calculation of the staggered magnetization. In terms of the Jordan-Wigner Fermions the staggered magnetization (4.6) is no longer a local operator, because the spin operators S_ℓ^z have the Jordan-Wigner strings attached (remember that we had to rotate our frame of reference by $\pi/2$ around the x-axis in order to be able to diagonalize $H_{\rm XZ}$ using the standard definition (4.7) of the Jordan-Wigner transform), i.e.

$$S_\ell^z = \frac{i}{2}(c_\ell - c_\ell^\dagger)\exp\Big(i\pi\sum_{j<\ell} n_j\Big) \quad (4.46)$$

Thus it is no longer tractable to calculate the staggered magnetization as defined in Eq. (4.6). Because of that, we use an equivalent definition of the staggered magnetization which probes the long-range antiferromagnetic order

$$m_s^2 = \lim_{n\to\infty}(-1)^n\langle S_\ell^z S_{\ell+n}^z\rangle \quad (4.47)$$

where ℓ can be set to any value due to the translational invariance of the spin chain in the thermodynamic limit (later we take $\ell = 0$ for convenience). In terms of Jordan-Wigner Fermions the S^zS^z-correlation function is given by [84]

$$\begin{aligned} \langle S_\ell^z S_{\ell+n}^z\rangle &= -\frac{1}{4}\big\langle (c_\ell - c_\ell^\dagger)\,\exp\Big(i\pi\sum_{j=\ell}^{\ell+n-1} n_j\Big)\,(c_{\ell+n} - c_{\ell+n}^\dagger)\big\rangle \\ &= -\frac{1}{4}\big\langle (c_\ell - c_\ell^\dagger)\prod_{\ell\le j<\ell+n}(1-2n_j)\,(c_{\ell+n} - c_{\ell+n}^\dagger)\big\rangle \\ &= -\frac{1}{4}(-1)^n\big\langle (c_\ell^\dagger - c_\ell)\prod_{\ell\le j<\ell+n}(c_j^\dagger - c_j)(c_j^\dagger + c_j)\,(c_{\ell+n}^\dagger - c_{\ell+n})\big\rangle \\ &= \frac{1}{4}(-1)^n\big\langle (c_\ell^\dagger + c_\ell)\prod_{\ell<j<\ell+n}(c_j^\dagger - c_j)(c_j^\dagger + c_j)\,(c_{\ell+n}^\dagger - c_{\ell+n})\big\rangle \quad (4.48) \end{aligned}$$

where the last line follows from $(c_\ell^\dagger - c_\ell)^2 = -1$. The last equation can be written in a more compact form by introducing the Majorana-Fermion operators

$$A_\ell = c_\ell^\dagger + c_\ell \qquad \text{and} \qquad B_\ell = c_\ell^\dagger - c_\ell \quad (4.49)$$

In this notation the S^zS^z-correlation function is given by

$$\langle S_0^z S_n^z\rangle = \frac{1}{4}(-1)^n\langle A_0B_1A_1B_2A_2\ldots B_{n-1}A_{n-1}B_n\rangle \tag{4.50}$$

As is obvious from Wick's theorem (see e.g. [46]), the basic building blocks of the correlation function (4.50) are the pairwise contractions $\langle A_iB_j\rangle$, $\langle A_iA_j\rangle$ and $\langle B_iB_j\rangle$ between all Majorana operators. Indeed, the correlation function (4.50) can be written as a Pfaffian of pairwise contractions (c.f. [85] and references therein)

$$\langle S_0^z S_n^z\rangle = \tfrac{(-1)^n}{4}\,\mathrm{Pf}\,\begin{vmatrix} \langle A_0A_1\rangle & \langle A_0A_2\rangle & \cdots & \langle A_0A_{n-1}\rangle & \langle A_0B_1\rangle & \langle A_0B_2\rangle & \cdots & \langle A_0B_n\rangle \\ & \langle A_1A_2\rangle & \cdots & \langle A_1A_{n-1}\rangle & \langle A_1B_1\rangle & \langle A_1B_2\rangle & \cdots & \langle A_1B_n\rangle \\ & & \ddots & \vdots & \vdots & & \ddots & \vdots \\ & & & \langle A_{n-2}A_{n-1}\rangle & \langle A_{n-2}B_1\rangle & \cdots & & \langle A_{n-2}B_n\rangle \\ & & & & \langle A_{n-1}B_1\rangle & \langle A_{n-1}B_2\rangle & \cdots & \langle A_{n-1}B_n\rangle \\ & & & & & \langle B_1B_2\rangle & \langle B_1B_3\rangle\ \cdots & \langle B_1B_n\rangle \\ & & & & & & \langle B_2B_3\rangle\ \cdots & \langle B_2B_n\rangle \\ & & & & & & \ddots & \vdots \\ & & & & & & & \langle B_{n-1}B_n\rangle \end{vmatrix} \tag{4.51}$$

This expression is further simplified in the thermodynamic limit, where all pairwise contractions depend only on the distance between the Majorana operators due to the translational invariance. Using (4.10), (4.45) and (4.49), we are now able to calculate the time dependent pairwise contractions between the Majorana operators following the quantum quench and thus get an explicit expression for the time evolution of staggered magnetization via (4.47) and (4.51). In particular, after a tedious but straightforward calculation, we obtain the following expressions for the contractions in the thermodynamic limit (define $\phi_k \doteq \theta_k - \theta_k^{(0)}$)

$$a_{j-\ell+1} \doteq \langle A_jB_\ell\rangle = \int_{-\pi}^{\pi}\frac{dk}{2\pi}\,e^{-ik(j-\ell)}e^{i2\theta_k}\left[\cos(2\phi_k) - i\sin(2\phi_k)\cos(2E_kt)\right] \tag{4.52}$$

$$b_{j-\ell} \doteq \langle A_jA_\ell\rangle = \langle B_jB_\ell\rangle = \int_{-\pi}^{\pi}\frac{dk}{2\pi}\,e^{-ik(j-\ell)}\sin(2E_kt)\sin(2\phi_k) \qquad \forall j\neq\ell \tag{4.53}$$

we note that the above expressions have been derived before by Sengupta, Powell and Sachdev [86] in the context of quench problems in the transverse field Ising-model. In terms of the above coefficients a_n and b_n for the pairwise contractions, which depend explicitly on time, the Pfaffian (4.51) now takes the simplified form

$$\langle S_0^z(t) S_n^z(t)\rangle = \tfrac{(-1)^n}{4}\,\mathrm{Pf}\,\begin{vmatrix} b_{-1} & b_{-2} & \cdots & b_{-(n-1)} & a_0 & a_{-1} & \cdots & a_{-(n-1)} \\ & b_{-1} & \cdots & b_{-(n-2)} & a_1 & a_0 & \cdots & a_{-(n-2)} \\ & & \ddots & \vdots & \vdots & & \ddots & \vdots \\ & & & b_{-1} & a_{n-2} & \cdots & & a_{-1} \\ & & & & a_{n-1} & a_{n-2} & \cdots & a_0 \\ & & & & & b_{-1} & b_{-2}\ \cdots & b_{-(n-1)} \\ & & & & & & b_{-1}\ \cdots & b_{-(n-2)} \\ & & & & & & \ddots & \vdots \\ & & & & & & & b_{-1} \end{vmatrix} \tag{4.54}$$

The integrals for the coefficients a_n and b_n in the defining equations (4.52) and (4.53) simplify considerably for three special cases:

- $\mathbf{t = 0}$: In this somewhat trivial limit the evaluation of the Pfaffian gives the staggered magnetization of the initial state via (4.47). The coefficients a_n and b_n at $t = 0$ are given by

$$a_n = \int_{-\pi}^{\pi} \frac{dk}{2\pi}\, e^{-ik(n-1)} e^{i2\theta_k^{(0)}} \overset{\text{Néel}}{=} \delta_{n,0} \tag{4.55}$$

$$b_n = 0 \tag{4.56}$$

- $\mathbf{t \to \infty}$: The behavior of the staggered magnetization at large times $t \to \infty$ is particularly interesting, since this is precisely the regime which is not accessible numerically. Indeed, as will be shown below, the Szegö lemma allows us to get a rigorous result for long time limit of the staggered magnetization $m_s(t \to \infty)$ in the XZ-model. At $t \to \infty$, the coefficients a_n and b_n take the form

$$a_n = \int_{-\pi}^{\pi} \frac{dk}{2\pi}\, e^{-ik(n-1)} e^{i2\theta_k} \cos(2\phi_k) \tag{4.57}$$

$$b_n = 0 \tag{4.58}$$

  where the time-dependent oscillating terms vanish due to the Riemann-Lebesgue lemma.

- **Quench from the Néel state to the critical point**: For the special case of a quench from the Néel state ($\Delta_0 = \infty$) to the critical point ($\Delta = 2$), i.e. for $\theta_k^{(0)} = -k$ and $\theta_k = 0$, the integrals can be evaluated explicitly and we get

$$a_n = \begin{cases} (\delta_{n,0} + \delta_{n,2})/2 + (-1)^{n/2}\,(n-1)\,\dfrac{\mathcal{J}_{n-1}(4Jt)}{4Jt} & \text{for } n \text{ even} \\ 0 \qquad \text{for } n \text{ odd} \end{cases} \tag{4.59}$$

$$b_n = \begin{cases} i(-1)^{n/2}\, n\, \dfrac{\mathcal{J}_n(4Jt)}{4Jt} & \text{for } n \text{ even} \quad (n \neq 0) \\ 0 \qquad \text{for } n \text{ odd} \end{cases} \tag{4.60}$$

4.2.1 Staggered magnetization $m_s(t \to \infty)$ in the long time limit

As we have shown above in Eqs. (4.57) and (4.58), the coefficients of the Pfaffian (4.54) simplify considerably in the long time limit $t \to \infty$. In particular, since the coefficients b_n vanish, the Pfaffian reduces to a Toeplitz determinant, as can be seen easily by applying Wick's theorem to (4.50) for the case $b_n \equiv 0$ (see [84]). The staggered magnetization is thus given by

$$m_s^2(t \to \infty) = \lim_{n\to\infty} \frac{1}{4} \begin{vmatrix} a_0 & a_{-1} & \cdots & a_{-(n-1)} \\ a_1 & a_0 & \cdots & a_{-(n-2)} \\ \vdots & & \ddots & \vdots \\ a_{n-1} & \cdots & & a_0 \end{vmatrix} \tag{4.61}$$

The reduction of the Pfaffian to a Toeplitz determinant in the case of vanishing b_n contractions can also be inferred by using the fact that the Pfaffian is equivalent to the square

root of the determinant of the antisymmetric $2n \times 2n$ matrix (apart from a sign, which is obvious in our case) obtained by mirroring the triangular scheme (4.54) at the main diagonal. Thus, for $b_n \equiv 0$ one is left with

$$m_s^2(t \to \infty) = \lim_{n\to\infty} \frac{1}{4}\sqrt{\begin{vmatrix} 0 & \mathcal{A}_n \\ -\mathcal{A}_n^T & 0 \end{vmatrix}} = \lim_{n\to\infty} \frac{1}{4}\sqrt{(\det \mathcal{A}_n)^2} = \lim_{n\to\infty} \frac{1}{4}|\det \mathcal{A}_n| \tag{4.62}$$

where $\mathcal{A}_n$ is the $n \times n$-Toeplitz matrix built from the coefficients a_j, i.e. the matrix shown in equation (4.61). In order to calculate the asymptotics $n \to \infty$ of the Toeplitz determinant in Eq. (4.61), we apply Szegös lemma, which can be stated as follows:

> ***Szegö's Lemma [87]:*** *Let $\alpha(k)$ be the generating function of the $n \times n$-Toeplitz matrix $\mathcal{A}_n$, i.e. the coefficients a_ℓ of the Toeplitz matrix*
>
> $$\mathcal{A}_n = \begin{bmatrix} a_0 & a_{-1} & \cdots & a_{-(n-1)} \\ a_1 & a_0 & \cdots & a_{-(n-2)} \\ \vdots & & \ddots & \vdots \\ a_{n-1} & \cdots & & a_0 \end{bmatrix} \tag{4.63}$$
>
> *are obtained via the Fourier-integral*
>
> $$a_\ell = \int_{-\pi}^{\pi} \frac{dk}{2\pi} e^{-i\ell k}\alpha(k) \ . \tag{4.64}$$
>
> *If α has no singularities in the integration interval and has winding number zero, i.e. $\arg\alpha(k+2\pi) - \arg\alpha(k) = 0$, then the asymptotic behavior of the Toeplitz matrix $\mathcal{A}_n$ for large n is given by*
>
> $$\lim_{n\to\infty} \det(\mathcal{A}_n) = \exp\left[n \int_{-\pi}^{\pi} \frac{dk}{2\pi} \log\alpha(k)\right] F(\alpha) \tag{4.65}$$
>
> *where* log *denotes the natural logarithm and the function F contains subleading corrections of order $\mathcal{O}(n^0)$.*

In our case, the generating function $\alpha(k) = e^{ik}e^{i2\theta_k}\cos(2\phi_k)$ can be read off directly from (4.57). For a quench from the Néel state ($2\theta_k^{(0)} = -k$) it can be simplified to

$$\alpha(k) = e^{ik}\frac{\Delta + 2\cos(2k)}{(\Delta+2)\cos(k) - i(\Delta-2)\sin(k)} \tag{4.66}$$

The generating function has no singularities and winding number zero in the easy axis regime $\Delta > 2$, thus we can apply Szegös lemma in order to obtain the staggered magnetization at $t \to \infty$. The integral in Eq. (4.65) using the generating function (4.66) can be calculated analytically and we obtain finally

$$m_s^2(t \to \infty) = \lim_{n\to\infty} \frac{1}{4}\left[\frac{1 + \sqrt{1 - 4/\Delta^2}}{2}\right]^n \tag{4.67}$$

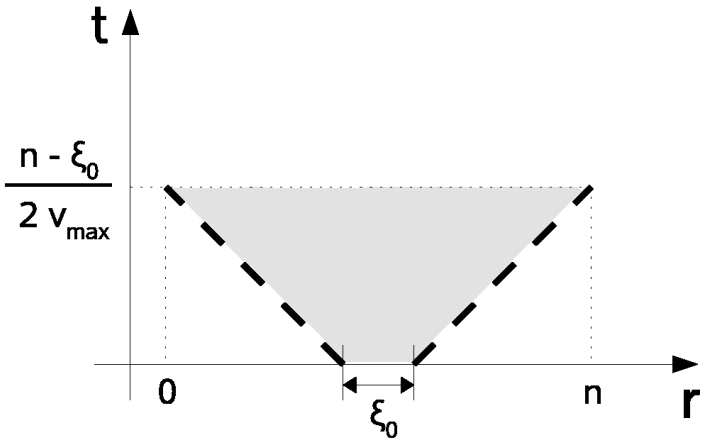

Figure 4.8: Cartoon of the light-cone in quantum mechanical spin systems. Two initially uncorrelated spins at a distance n are not causally connected up to a time given by the light-cone condition $t = (n - \xi_0)/(2v_{\max})$, where $v_{\max}$ is the maximum (classical) speed of the quasiparticles and ξ_0 is the correlation length of the initial state.

Thus, the staggered magnetization $m_s(t \to \infty)$ in the XZ-model vanishes at long times for any finite $\Delta > 2$, if we start from an initial Néel state.

4.2.2 Staggered magnetization $m_s(t)$ and the light-cone trick

In the section above we have shown how the staggered magnetization can be calculated explicitly in the long time limit by the application of Szegö's lemma to obtain the asymptotics of the Toeplitz determinant (4.61) for $n \to \infty$. Now we are interested not only in the long time limit, but in the full time evolution of the staggered magnetization in the XZ-model. Unfortunately, Szegö's lemma as stated above cannot be applied in this case, since the contractions b_n do not vanish and thus the Pfaffian (4.54) does not reduce to a Toeplitz determinant. In this section we use a trick based on the so called horizon- or light-cone effect to calculate the time evolution of $m_s(t)$ semi-analytically. However, an analytic solution of this problem might be possible via a generalization of Szegö's lemma to block Toeplitz determinants, as will be shown in the subsequent section 4.2.3.

The light-cone trick is based on an observation by Lieb and Robinson [88], who have shown that information in quantum spin systems with finite range interactions propagates with a finite group velocity. From this follows, that correlations in a spin chain can only build up within a 'light-cone' determined by the maximal group velocity of the quasiparticles. Or stated otherwise, two initially uncorrelated spins are not causally connected up to a time which is given by the ratio of the distance between the two spins to the maximal group velocity of the quasiparticles. Calabrese and Cardy [89] have constructed an intuitive picture of this situation, which holds quite generally and works extremely well.

The main message can be summed up in three points:

- In the context of a quench problem, the initial state is a source of quasiparticles which propagate through the system with a finite (classical) group velocity $v = \partial E_k/\partial k$. Here, E_k denotes the dispersion relation of the quasiparticles, which is given by Eq. (4.41) in our case.
- Quasiparticles originating from points that are separated by a distance which is *larger* than the correlation length ξ_0 of the initial state are *incoherent* and lead to the *relaxation* of local observables.
- Quasiparticles originating from *closely* separated points, i.e. two points within the correlation length ξ_0 of the initial state, are *entangled* and *induce correlations* between local observables.

The situation is sketched in the cartoon in Fig. 4.8. It needs to be mentioned however, that the light cone is not perfectly sharp in a quantum mechanical system. Nevertheless, the corrections are exponentially small [88] and can be safely neglected for our purpose.

Our initial Néel state is completely uncorrelated, i.e. the correlation length ξ_0 defined via the connected correlation function

$$G_{zz}(n) \;=\; \langle S_0^z S_n^z\rangle - \langle S_0^z\rangle\langle S_n^z\rangle \;\sim\; e^{-n/\xi_0} \tag{4.68}$$

is identically zero for the Néel state: $\xi_0^{\text{Néel}} \equiv 0$. Thus, two spins at a distance of n lattice sites are not causally connected up to a time given by the light-cone condition

$$t = \frac{n}{2v_{\max}} = \frac{n}{4J} \tag{4.69}$$

where $v_{\max} = 2J$ is the maximum group velocity for our quasiparticles with dispersion (4.41). In order to calculate the time evolution of the staggered magnetization starting from a Néel state it is thus sufficient to evaluate the Pfaffian in Eq. (4.54) for a *finite* size n numerically, as long as we are interested in times smaller than $Jt < n/4$

$$m_s^2(t)\Big|_{Jt<\frac{n}{4}} = (-1)^n\langle S_0^z S_n^z\rangle \tag{4.70}$$

This means that the size of the Pfaffian that we have to evaluate numerically increases linearly in time. If we want to follow the time evolution of the staggered magnetization starting from an initial Néel state up to times $Jt = 10$, we need to evaluate the Pfaffian corresponding to an antisymmetric 80×80 matrix. Since the light-cone is not perfectly sharp, we increase the distance between the spins by two lattice spacings as compared to the light-cone condition in the numerical calculation. Using this method, we follow the time evolution up to $Jt = 40$ for arbitrary anisotropies Δ and up to $Jt = 100$ for a quench to the critical point $\Delta = \Delta_c = 2$. The results are plotted in Fig. 4.9. In order to show how well the light-cone trick works, we have plotted the staggered magnetization evaluated using Eq. (4.70) for different fixed distances between the spins as a function of time in Fig. 4.10. As can be seen in the figure, the result for a fixed distance r starts to deviate

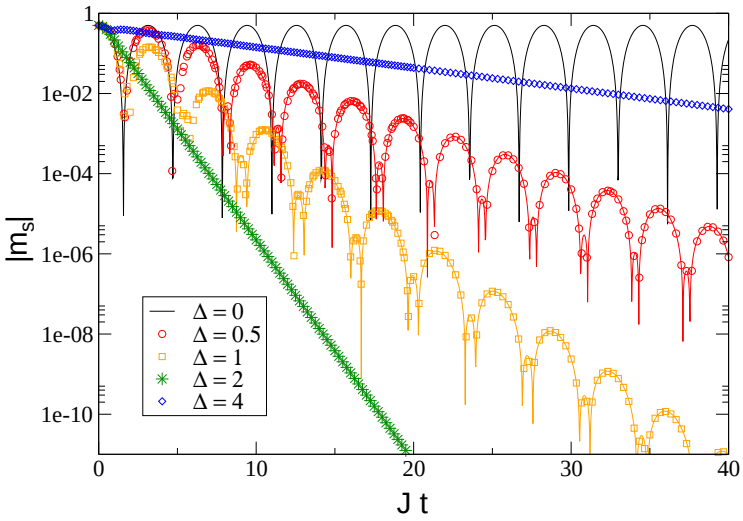

Figure 4.9: Time evolution of the staggered magnetization $m_s(t)$ at different anisotropies starting from an initial Néel state in the XZ-model, calculated semi-analytically using the light-cone trick. The solid lines for $\Delta < 2$ are fits to the numerical data using Eq. (4.72).

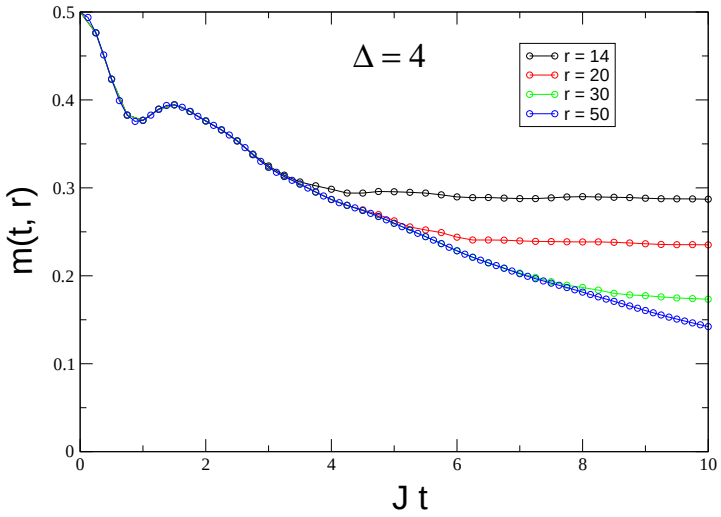

Figure 4.10: Time evolution of the staggered magnetization $m_s(t)$ at $\Delta = 4$, evaluated using Eq. (4.70) for different distances r between the spins. The results start to deviate from the true $m_s(t)$ curve precisely at the times given by the light-cone condition (4.69).

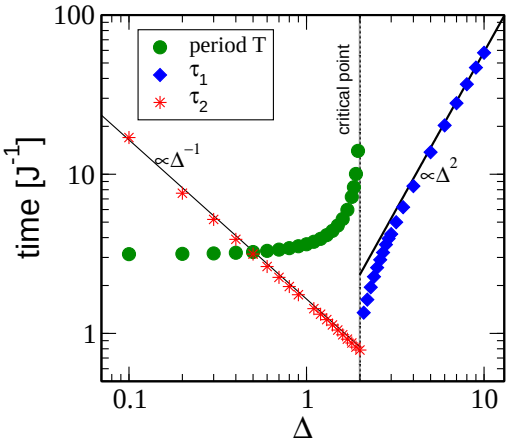

Figure 4.11: Numerically extracted timescales for the quench from a Néel state in the XZ-model as a function of the anisotropy Δ. The relaxation times τ_1 and τ_2 have been obtained from an exponential fit to the numerical data of the staggered magnetization $m_s(t)$. The green dots correspond to the period of the oscillations of $m_s(t)$ in regime $\Delta < \Delta_c$.

from the true time evolution of the staggered magnetization $m_s(t)$ precisely at the times given by the light-cone condition (4.69).

We note that the above mentioned method also works for a general quench problem, where a ground state with arbitrary Δ_0 is chosen. One has to keep in mind however, that for a general quench the light-cone condition (4.69) has to be modified, since the correlation length ξ_0 of the initial state is usually nonzero. Indeed, the distance between the two spins in Eq. (4.70) has to be increased by ξ_0 in order to obtain reliable results. This means that the computational effort increases considerably, if the correlation length of the initial state is large. Thus, the light-cone method for calculating $m_s(t)$ works well for sufficiently uncorrelated initial states, i.e. quenches with $\Delta_0 \gg 1$, but breaks down for quenches with Δ_0 close to the critical value $\Delta_c = 2$, where the correlation length of the initial state diverges.

From the results shown in Figs. 4.9 and 4.12 it can be seen that the staggered magnetization $m_s(t)$ after a quench from the Néel state in the XZ-model indeed behaves similarly as in the XXZ-model for large anisotropies $\Delta > \Delta_c$, i.e. $m_s(t)$ decays exponentially without oscillations. For $\Delta < \Delta_c$ the behavior is a little bit different than in the XXZ-model. In this regime we find again exponentially decaying oscillations, but the oscillation period increases upon approaching the critical point. Furthermore, in the limit $\Delta = 0$ the time evolution of $m_s(t)$ can again be calculated exactly, as in the XX-model. From this we obtain

$$m_s(t) \overset{\Delta=0}{=} \frac{1}{2} \cos^2(Jt)\,, \tag{4.71}$$

i.e. the staggered magnetization in the XZ-model steadily oscillates without decaying in

the limit $\Delta = 0$.

As for the XXZ-model, we have extracted the relaxation times using exponential fits to the numerical data of $m_s(t)$. In the easy axis regime $\Delta > \Delta_c$, we use the same simple exponential fit as for the XXZ data. In the regime $\Delta < \Delta_c$ however, we use a fitting function of the form

$$m_s(t) \sim e^{-t/\tau_2} \left(\cos^2(\omega t) - \text{const.}\right) \tag{4.72}$$

where the constant is usually small and positive. Note that this function fits the XZ-data perfectly for all times $Jt \gtrsim 5$ and all anisotropies $\Delta < \Delta_c$, in contrast to the XXZ-model, where an accelerated decay is observed close to the critical point. The relaxation times and the oscillation period are shown in Fig. 4.11. As can be seen from this figure, the minimum of the relaxation time in the XZ-model is right at the critical point $\Delta_c = 2$.

4.2.3 A possible route to an exact analytic solution

As mentioned in the previous section, there exists a possible route to an exact analytical calculation of the time evolution of the staggered magnetization in the XZ-model, which is sketched in this section. This method is based on a generalization of Szegö's lemma to block-Toeplitz determinants that has been found by Widom [90]. Using this approach, the computation reduces to a Wiener-Hopf factorization problem of the matrix-valued generating function for the coefficients of the block-Toeplitz matrix, which we weren't able to solve, unfortunately. Nevertheless, since the method itself is interesting on its own and might be useful for related problems, we present it here briefly.

We want to obtain a general expression for the time evolution of the staggered magnetization $m_s(t)$ in the XZ-model following a quantum quench, i.e. we have to evaluate the Pfaffian defined in Eq. (4.54) in the limit $n \to \infty$. We recall that Pfaffians can be written as the square root of the determinant of the antisymmetric $2n \times 2n$ matrix (apart from a sign, which is obvious in our case) obtained by mirroring the triangular scheme (4.54) at the main diagonal. Since in our case we have $b_{-i} = -b_i$, the correlator (4.50) can be written as the square root of a block-Toeplitz determinant

$$\langle S_0^z(t) S_n^z(t)\rangle = \frac{1}{4}(-1)^n \begin{vmatrix} C & D \\ -D^T & C \end{vmatrix}^{1/2} \tag{4.73}$$

where the Toeplitz matrices C and D have coefficients b_n and a_n respectively. Alternatively, by shuffling rows and columns, we can write

$$\langle S_0^z(t) S_n^z(t)\rangle = \frac{1}{4}(-1)^n \det(T_n)^{1/2} \tag{4.74}$$

with a $n \times n$ block-Toeplitz matrix T_n with 2×2 matrix coefficients τ_i:

$$T_n = \begin{bmatrix} \tau_0 & \tau_{-1} & \cdots & \tau_{-(n-1)} \\ \tau_1 & \tau_0 & \cdots & \tau_{-(n-2)} \\ \vdots & & \ddots & \vdots \\ \tau_{n-1} & \cdots & & \tau_0 \end{bmatrix} \qquad \tau_i = \begin{pmatrix} b_i & a_i \\ -a_{-i} & b_i \end{pmatrix} \tag{4.75}$$

All coefficients τ_i of the block-Toeplitz determinant T_n are completely specified by the 2×2 matrix-valued generating function $\tau(k)$, whose Fourier coefficients are equal to τ_i:

$$\tau_\ell = \int_{-\pi}^{\pi} \frac{dk}{2\pi} e^{-ik\ell}\, \tau(k) \qquad\qquad \tau(k) = \begin{pmatrix} \lambda(k) & \mu(k) \\ -\mu(-k) & \lambda(k) \end{pmatrix} \tag{4.76}$$

and the coefficients of the generating function are obtained from Eqs. (4.52) and (4.53), in particular

$$\lambda(k) = \sin(2\phi_k)\sin(2E_k t) \tag{4.77}$$

$$\mu(k) = e^{i(k+2\theta_k)}(\cos(2\phi_k) - i\sin(2\phi_k)\cos(2E_k t)) \tag{4.78}$$

and $\mu(-k) = \mu^*(k)$. Now we can use the equivalent of Szegö's lemma for block-Toeplitz determinants [90], which is applicable if $\det \tau(k) \neq 0$ and $\det \tau(k)$ has winding number zero (i.e. $\arg\det \tau(k=0) - \arg\det \tau(k=2\pi) = 0$). In our case the matrix function $\tau(k)$ from Eq. (4.76) is unitary and has $\det \tau(k) = 1$, thus all prerequisites for applying Widom's theorem are met. This theorem provides an asymptotic formula for block Toeplitz determinants and reads as follows

$$\lim_{n\to\infty} \det(T_n) = G[\tau(k)]^n\, E[\tau(k)] \tag{4.79}$$

with

$$G[\tau(k)] = \exp\left[\int_{-\pi}^{\pi} \frac{dk}{2\pi} \log\det \tau(k)\right] \tag{4.80}$$

$$E[\tau(k)] = \det(T_\infty[\tau(k)]T_\infty[\tau^{-1}(k)]) \tag{4.81}$$

In our case the leading order term is unity, i.e. $G[\tau(k)] = 1$, because we have $\det \tau(k) = 1$. This result has to hold because of physical reasons obviously, otherwise $m_s(t)$ would be zero or infinity at all times. In order to obtain the time evolution of the staggered magnetization at arbitrary times, we have to evaluate the sub-leading corrections $E[\tau]$. Unfortunately the expression (4.81) is not very useful for explicit calculations. Nevertheless, Widom was able to prove another theorem, which gives an explicit expression for the logarithmic derivative of $E[\tau]$ and can be used for explicit calculations. In order to be able to apply this theorem directly to our problem, it is convenient to make a change of variables. In particular, we write the generating function $\tau(k)$ as a function of the complex variable $z = e^{ik}$. Now suppose $\tau^{-1}(z)$ (which is equivalent to $\tau^\dagger(z)$ in our case) has the left and right Wiener-Hopf factorizations

$$\tau^{-1}(z) = u_+(z)u_-(z) = v_-(z)v_+(z) \tag{4.82}$$

where u_+ and v_+ (u_- and v_-) are analytic inside (outside) the unit circle, i.e. u_+ and v_+ (u_- and v_-) have only positive (negative) Fourier coefficients as functions of k. Furthermore let $\tau(z)$ be a differentiable function of a parameter t. Then Widom's theorem [90] states that

$$\frac{d}{dt}\log E[\tau] = \frac{i}{2\pi}\oint_\Xi dz\, tr\left\{[(\partial_z u_+)u_- - (\partial_z v_-)v_+]\,\partial_t \tau\right\} \tag{4.83}$$

where Ξ denotes the unit circle and we have chosen the time t as the parameter. Since we now from our numerics that the staggered magnetization $m_s(t)$ decays exponentially at large times, the expression (4.83) should tend to a constant value at large times.

The remaining problem is to find the Wiener-Hopf factorization in Eq. (4.82) of the generating function $\tau(z)$. The only situation where an analytical factorization seems to be possible is the quench from the Néel state to the critical point $\Delta_c = 2$ of the XZ-model, where the expressions for the coefficients μ and λ in Eqs. (4.77) and (4.78) of the generating function simplify considerably. At the critical point $\Delta = 2$ we get (again $z = e^{ik}$)

$$\lambda(z) = \frac{-i}{2}(z - z^{-1}) \sin(J_z t(z + z^{-1})) \tag{4.84}$$

$$\mu(z) = \frac{z}{2}\left\{z + z^{-1} - (z - z^{-1}) \cos(J_z t(z + z^{-1}))\right\} \tag{4.85}$$

Note that these functions have an essential singularity at $z = 0$. If we would have just a pole of finite order n at the origin, the Wiener-Hopf factorization could be performed easily by factoring out the singularity by a multiplication with z^n.

Albeit we haven't been able to solve the Wiener-Hopf factorization problem for the matrix-valued generating function τ, the above formulation of the problem can be employed to justify the light-cone trick used in the previous section. Indeed, there is another theorem by Widom [90] which states that $E[\tau]$ is given by

$$E[\tau] = G[\tau]^\ell \det T_\ell[\tau^{-1}] \tag{4.86}$$

if the Fourier coefficients τ_m vanish for $m > \ell$ or $m < \ell$ for some fixed ℓ. Thus one only needs to calculate the determinant of a finite Toeplitz matrix T_ℓ in order to obtain the determinant of T_∞. This is precisely what we do when using the light-cone trick at intermediate times, where ℓ scales linearly with time. Indeed, it can be shown that the coefficients τ_m are exponentially small for $m > \ell$ at a given time t.

4.2.4 Relation between the XXZ- and XZ-model in the regime $\Delta \gg 1$

The comparison between the results for the XXZ- and XZ-model in Fig. 4.12 shows, that the time evolution of the staggered magnetization in both models is almost indistinguishable at large anisotropies $\Delta \gg 1$. In the following we're going to clarify this observation by comparing the excitation spectra of the two models.

As has been shown in the previous section, the dispersion relation of the excitations in the XZ-model for $\Delta > 2$ is given by

$$E_{\mathrm{xz}}(k) = J\sqrt{1 + \Delta^2/4 + \Delta \cos(2k)}. \tag{4.87}$$

For the XXZ chain, the dispersion relation of elementary excitations can be calculated using the Bethe-ansatz [76]. In the antiferromagnetic regime ($\Delta > 1$) one can write down

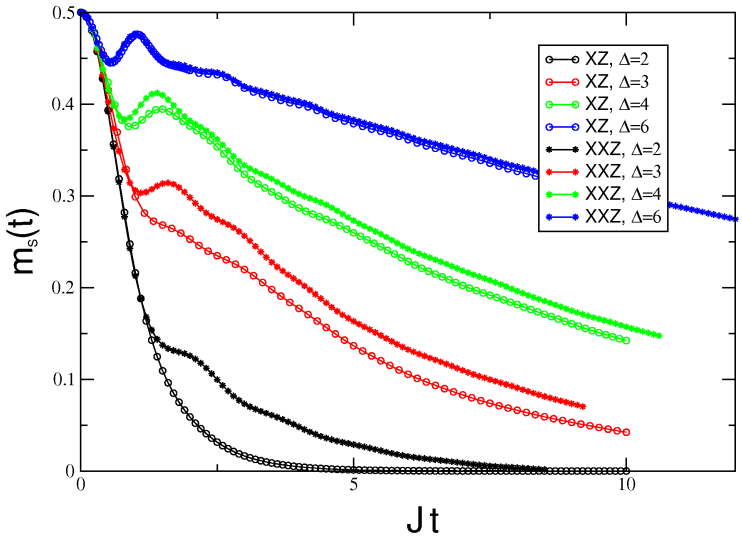

Figure 4.12: Comparison between the results for the time evolution of the staggered magnetization $m_s(t)$ following a quench from the Néel state in the XXZ- and XZ-model.

a parametric representation (define $\Delta = \cosh(\lambda)$)

$$E_{\mathrm{xxz}}(\alpha) = 2\pi \sinh(\lambda) \sum_{n=-\infty}^{\infty} \frac{e^{-in\alpha}}{\cosh(n\lambda)} \tag{4.88}$$

$$k(\alpha) = -2\pi \int_0^{\alpha} d\alpha' \sum_{n=-\infty}^{\infty} \frac{e^{-in\alpha'}}{\cosh(n\lambda)} \tag{4.89}$$

A plot of both dispersion relations for different values of Δ is shown in Fig.4.13.

Now, one can easily establish that the dispersion relations of both models are asymptotically the same in the regime $\Delta \gg 1$, where we get

$$E(k) = \frac{\Delta}{2} + \cos(2k) + \mathcal{O}(1/\Delta). \tag{4.90}$$

Since the energy difference between the initial Néel-state and the ground state in the regime $\Delta \gg 1$ is small, the dynamics is completely determined by the elementary excitations, which have identical dispersions in both models, up to corrections $\sim 1/\Delta$. Thus it is not surprising that the time evolution of the staggered magnetization in both models is almost equivalent for large Δ.

4.3 Weakly antiferromagnetically ordered initial states and Luttinger-Liquid theory

As an introduction to our discussion of quenches from correlated antiferromagnetic states (i.e. quenches with $\Delta_0 < \infty$), we consider the time evolution of weakly antiferromagnetic

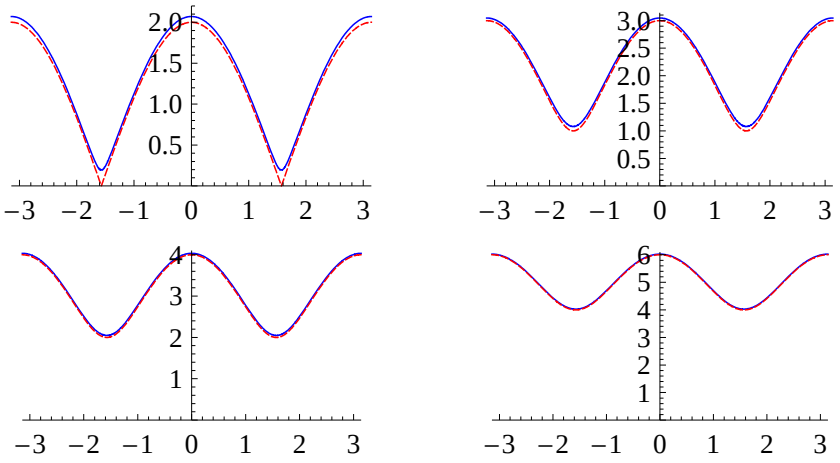

Figure 4.13: Dispersion relation of excitations in the XXZ-model (blue) and in the XZ-model (red,dashed) for different values of Δ ($\Delta = 2, 4, 6, 10$ from top left to bottom right).

spin density wave (SDW) states under the XX-Hamiltonian (4.11) in the first part of this section. This will provide a benchmark for the results obtained within Luttinger-liquid theory in the second part of this section and allows for a brief discussion of the applicability of effective low energy theories to the particular type of quench problems studied in this thesis.

In the fermionic picture, antiferromagnetic SDW states can be written in analogy to a BCS state as

$$|\mathrm{SDW}\rangle = \prod_{-\pi/2 < k \leq \pi/2} (u_k c_k^\dagger + v_k c_{k+\pi}^\dagger)|0\rangle \ . \tag{4.91}$$

In particular, the SDW state reduces to a Néel state for $u_k = v_k = 1/\sqrt{2}$. The time evolution of the staggered magnetization $m_s(t)$ in the XX-model (4.11) starting from a SDW state at $t = 0$ is thus determined by the coefficients u_k and v_k and Eq. (4.12) via

$$\begin{aligned} m_s(t) &= \frac{1}{L} \sum_{k=-\pi}^{\pi} \langle \mathrm{SDW}| c_{k+\pi}^\dagger(t) c_k(t) |\mathrm{SDW}\rangle \\ &= \int_{-\pi}^{\pi} \frac{dk}{2\pi} e^{-i2\epsilon_k t} u_k v_k \ , \end{aligned} \tag{4.92}$$

where we have taken the thermodynamic limit in last equality. In the following we consider weakly antiferromagnetic SDW states, where

$$u_k v_k = \frac{\Delta_s}{2\sqrt{\epsilon_k^2 + \Delta_s^2}} \, . \tag{4.93}$$

Here, Δ_s denotes the SDW-gap and $\epsilon_k = -J \cos k$ is the free Fermion dispersion relation. For a weak SDW state with $\Delta_s \ll J$ there are two main contributions to the integral in

equ. (4.92). The first comes from the square root singularity in the vicinity of the two Fermi points $k_f = \pm\pi/2$, whereas the second one comes from the square root singularity of the density of states at $k = 0$. Writing down these two contributions separately one obtains

$$\begin{aligned} m_s(t) &\approx \frac{\Delta_s}{2J} J_0(2Jt) + \frac{\Delta_s}{\pi J} K_0(2\Delta_s t) \\ &\approx \frac{1}{\sqrt{4\pi Jt}} \left\{ \sqrt{\frac{\Delta_s}{J}} e^{-2\Delta_s t} + \frac{\Delta_s}{J} \cos(2Jt - \pi/4) \right\} \end{aligned} \tag{4.94}$$

and the second equality holds for large times $t \gg 1/\Delta_s$. Here, the first term is simply the result of the linearized dispersion near the Fermi points, or stated otherwise, what one would obtain from Luttinger-liquid theory. The algebraically decaying oscillations which dominate the long time behavior are a result of contributions from the band edges, hence are a lattice effect and thus cannot be captured within a Bosonization approach. From this simple calculation it becomes clear that even for the time evolution of a very weak SDW-state ($\Delta_s \ll J$), where the deviation of the momentum distribution from a Fermi distribution is significant only close to the Fermi points and a linearization of the dispersion relation seems viable, Luttinger liquid theory gives reasonable results only in the very restricted time interval $\Delta_s^{-1} \ll t \ll \Delta_s^{-1} \ln(J/\Delta_s)$.

Although we have argued above that Luttinger liquid theory is not expected to correctly describe the time evolution of the staggered magnetization following a quantum quench, we briefly discuss the predictions of LL-theory for a quench from correlated initial states to the gapless phase $\Delta < 1$ in this section. In the paramagnetic regime $\Delta < 1$, the bosonized form of the XXZ model (4.4) up to irrelevant terms is given by the Luttinger liquid Hamiltonian [91]

$$H_{LL} = \frac{u}{2\pi} \int dx \left\{ K \left(\pi \Pi(x)\right)^2 + \frac{1}{K} \left(\partial_x \phi(x)\right)^2 \right\} . \tag{4.95}$$

The bosonized form of the staggered magnetization is given by $m_s \sim \langle \cos(2\phi) \rangle_{x=0}$, where we have used translational invariance. The remaining problem amounts to computing the time evolution of $\langle \cos(2\phi) \rangle$, starting from a state where the field ϕ is initially locked near 0 or $\pi/2$. We mention that this is essentially the dual of the dephasing problem studied in [92], and thus we expect an exponential decay of m_s with a characteristic timescale $\tau \sim 1/(K\Delta_s)$. A convenient technique to solve this problem is the truncated Wigner method [93], which is exact for quadratic Hamiltonians such as (4.95). Using this approach, the time dependent expectation value of the staggered magnetization can be written as a functional integral over the Wigner transform $\varrho_W(\phi_0, \dot{\phi}_0)$ of the initial density matrix:

$$\begin{aligned} \langle \cos(2\phi) \rangle &= \int \mathcal{D}\phi(t) \int \mathcal{D}(\phi_0, \dot{\phi}_0)\, \varrho_W(\phi_0, \dot{\phi}_0)\, \cos(2\phi)\, \delta(\ddot{\phi} - u^2 \partial_x^2 \phi) \\ &= \int \mathcal{D}(\phi_0, \dot{\phi}_0)\, \varrho_W(\phi_0, \dot{\phi}_0) \cos(2\phi_{\mathrm{cl}}(x,t)) \end{aligned} \tag{4.96}$$

Here, the functional $\delta-$distribution ensures that one integrates only over solutions of the classical equations of motion and $\phi_{\rm cl}(x,t)$ denotes the classical solution to the 1D wave equation corresponding to the initial conditions $\phi_0(x)$ and $\dot{\phi}_0(x)$. The speed of sound is denoted by u. We have also used the fact that the operator $\cos(\phi)$ is diagonal in the $\phi-$representation. The classical solution $\phi_{\rm cl}(t)$ of the 1D wave equation can be explicitly constructed using D'Alembert's formula

$$\phi_{\rm cl}(x,t) = \frac{1}{2}\left[\phi_0(x-ut) + \phi_0(x+ut) + \frac{1}{u}\int_{x-ut}^{x+ut} dx' \dot{\phi}_0(x')\right] \tag{4.97}$$

After switching to a dual field representation using $Ku\partial_x\theta = \dot{\phi}$, we get

$$\begin{aligned}\langle\cos(2\phi)\rangle \quad \sim \quad & \int \mathcal{D}(\phi_0,\theta_0)\, \varrho_W(\phi_0,\theta_0)\, \cos\Big[\phi_0(x-ut) + \phi_0(x+ut) \\ & + K\theta_0(x+ut) - K\theta_0(x-ut)\Big]\end{aligned} \tag{4.98}$$

Since in the initial state ϕ is locked near $\phi_0 = 0$, we factor out the ϕ dependent part of the integral obtaining

$$m_s(t) \sim \left\langle \cos K(\theta(ut) - \theta(-ut))\right\rangle_0 , \tag{4.99}$$

where the brackets with the index 0 denote the expectation value taken with respect to the initial state. In principle, the expectation value in Eq. (4.99) has to be calculated for the ground state of the sine-Gordon model in the gapped phase, which is a nontrivial problem. Alternatively, Eq. (4.99) can be evaluated within a semiclassical analysis, where the gap of the initial state is relatively large. In this case, the cos-term in the sine-Gordon model can be expanded around the minimum, thereby obtaining the Hamiltonian of a massive scalar field. In particular, we take the ground state of the LL-Hamiltonian (4.95) with an additional mass-term $\sim \Delta_s\phi^2$ as initial state. Since this is a quadratic theory, Eq. (4.99) can be simplified via

$$\begin{aligned} m_s(t) \quad &\sim \quad \mathrm{Re}\left\langle e^{iK(\theta(ut)-\theta(-ut))}\right\rangle_0 \\ &= \quad \exp -\frac{K^2}{2}\left\langle(\theta(ut)-\theta(-ut))^2\right\rangle_0 \end{aligned} \tag{4.100}$$

After inserting the mode expansions of the dual field

$$\theta(x) = \sqrt{\frac{\pi}{2uKL}}\sum_q \frac{\sqrt{\omega_q}}{q}\left(b_q\, e^{iqx} + b_q^\dagger\, e^{-iqx}\right) \tag{4.101}$$

with the dispersion relation $\omega_q^2 = (uq)^2 + \Delta_s^2$, we obtain

$$\begin{aligned} m_s(t) \quad &\sim \quad \exp -K\int_0^\Lambda dq\, \frac{\sqrt{q^2+\Delta_s^2/u^2}}{q^2}\sin^2(qut) \\ &\sim \quad \exp(-\pi K\Delta_s t/2)\ . \end{aligned} \tag{4.102}$$

The last line holds for $\Delta_s t \gg 1$, where Δ_s again denotes the gap of the initial state. Luttinger-liquid theory thus predicts an exponential decay of the staggered magnetization, but it misses the oscillations of $m_s(t)$, which are a lattice effect. Furthermore, LL-theory predicts a slowing down of the exponential decay as one gets closer to the Heisenberg point $K = 1/2$ (the free Fermion limit corresponds to $K = 1$). Interestingly, this behavior is in accordance with the naive picture of critical slowing down. We also mention, that LL-theory doesn't respect the exact symmetry of the time evolution under $J_z \to -J_z$, which in LL-theory corresponds to $K \to 1/K$.

4.4 Quench dynamics in higher dimensions

So far we have discussed the time evolution of the staggered magnetization starting from an initial Néel state only in one dimensional spin chains. Obviously, it would be interesting to study the same setup in higher dimensional systems. Unfortunately there are not as many sophisticated analytical tools available to study this problem in $D > 1$. In the following section we use the simplest approach to study our quench problem in higher dimensional models, namely spin-wave theory, where a Holstein-Primakoff transformation is utilized to obtain an approximate description of the Heisenberg model in terms of non-interacting spin-wave excitations. This approach should work reasonably well if the initial Néel state is energetically not far from the equilibrium ground state after the quench and thus the density of excitations is low, i.e. for $\Delta \gg 1$. In the subsequent section we compare the results with a thermalization scenario.

4.4.1 Quench from a Néel state using Holstein-Primakoff theory

We start from a D-dimensional, anisotropic, antiferromagnetic Heisenberg model with nearest neighbor interactions on a cubic lattice

$$H = J \sum_{\langle \ell, m \rangle} \left\{ \frac{1}{2} \left(S^+_\ell S^-_m + h.c. \right) + \Delta \, S^z_\ell S^z_m \right\} . \tag{4.103}$$

The cubic lattice is bipartite, thus we express the spin operators in terms of two Holstein-Primakoff Bosons (see e.g. [75]), one for each sublattice. On sublattice A (index ℓ) we take

$$S^z_\ell = S - a^\dagger_\ell a_\ell \ , \qquad S^-_\ell \approx \sqrt{2S}\, a^\dagger_\ell \tag{4.104}$$

and on sublattice B (index m)

$$S^z_m = -S + b^\dagger_m b_m \ , \qquad S^-_m \approx \sqrt{2S}\, b_m \tag{4.105}$$

with a_ℓ and b_m as bosonic annihilation operators and $S = 1/2$ for the spin-1/2 models under consideration. By inserting these expressions in equ. (4.103), retaining only quadratic terms and switching to momentum representation we obtain (setting the lattice constant to unity)

$$H \approx -J\Delta S^2 N z/2 + zJ\Delta S \sum_{\mathbf{k}} \left\{ a^\dagger_{\mathbf{k}} a_{\mathbf{k}} + b^\dagger_{\mathbf{k}} b_{\mathbf{k}} + \lambda_{\mathbf{k}} \left(a^\dagger_{\mathbf{k}} b^\dagger_{-\mathbf{k}} + a_{\mathbf{k}} b_{-\mathbf{k}} \right) \right\} , \tag{4.106}$$

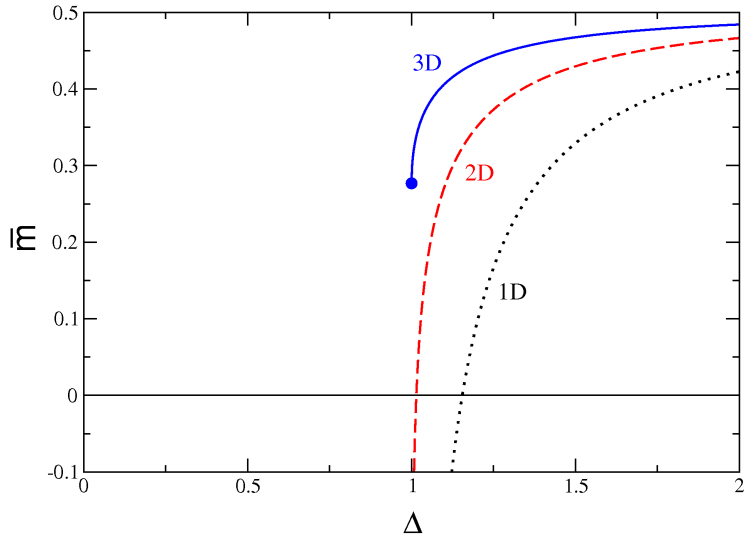

Figure 4.14: Saturation value $\bar{m}$ of the staggered moment at long times $t \to \infty$ for different dimensions D as a function of the anisotropy Δ, obtained using the Holstein-Primakoff approach. Black dotted line: D=1; red dashed line: D=2; blue solid line: D=3. In three dimensions the saturation value at the isotropic point $\Delta = 1$ is finite and given by $\bar{m} = 0.277$.

where z is the number of nearest neighbors, i.e. $z_{1D} = 2$, $z_{2D} = 4$ and $z_{3D} = 6$ on a cubic lattice. Furthermore, $k_{i=x,y,z} \in \{-\pi/2, \pi/2\}$ and

$$\lambda_{\mathbf{k}} = \frac{2}{z\Delta} \sum_{i=x,y,z} \cos(k_i)\,. \tag{4.107}$$

The staggered magnetization expressed in terms of the HP-Bosons is given by

$$m_s = \frac{1}{N}\sum_{\ell\in A} S^z_\ell - \frac{1}{N}\sum_{m\in B} S^z_m = S - \frac{1}{N}\sum_{\mathbf{k}} \left(a^\dagger_{\mathbf{k}} a_{\mathbf{k}} + b^\dagger_{\mathbf{k}} b_{\mathbf{k}}\right)\,. \tag{4.108}$$

Now we want to calculate the time evolution of the staggered magnetization $m_s(t)$ under the Hamiltonian (4.106), starting from an initial Néel state. The Néel state is the ground state of the Hamiltonian (4.106) for $\Delta \to \infty$, i.e. it satisfies $a_{\mathbf{k}}|\psi(0)\rangle = b_{\mathbf{k}}|\psi(0)\rangle = 0$. Because of that it is convenient to calculate the time evolution of $m_s(t)$ directly with the Hamiltonian (4.106) instead of diagonalizing it first using a Bogoliubov transformation. Using the Baker-Campbell-Hausdorff formula we get

$$\langle a^\dagger_{\mathbf{k}}(t) a_{\mathbf{k}}(t)\rangle_{\text{Néel}} = \langle b^\dagger_{\mathbf{k}}(t) b_{\mathbf{k}}(t)\rangle_{\text{Néel}} = \frac{\lambda^2_{\mathbf{k}}}{1-\lambda^2_{\mathbf{k}}} \sin^2\left(zJ\Delta S\sqrt{1-\lambda^2_{\mathbf{k}}}\, t\right) \tag{4.109}$$

Thus, using the Holstein-Primakoff approach, we obtain the following expression for the

time evolution of the staggered magnetization in a spin-1/2 Heisenberg model ($S = 1/2$) after a quench from the Néel state

$$m_{s,\mathrm{HP}}(t) = \frac{1}{2} - 2\int_{-\pi/2}^{\pi/2} \frac{d^D k}{(2\pi)^D} \frac{\lambda_{\mathbf{k}}^2}{1-\lambda_{\mathbf{k}}^2} \sin^2\left(\frac{zJ\Delta}{2}\sqrt{1-\lambda_{\mathbf{k}}^2}\, t\right) \tag{4.110}$$

The saturation value of the staggered magnetization

$$\begin{aligned} \bar{m} &= \lim_{T\to\infty} \frac{1}{T}\int_0^T dt\, m_s(t) \\ &= \frac{1}{2} - \int_{-\pi/2}^{\pi/2} \frac{d^D k}{(2\pi)^D} \frac{\lambda_{\mathbf{k}}^2}{1-\lambda_{\mathbf{k}}^2} \end{aligned} \tag{4.111}$$

is shown in Fig. 4.14 for the dimensions D=1,2 and 3. As can be seen from this figure, the HP-approach breaks down at the Heisenberg point $\Delta = 1$ in one and two dimensions, leading to an unphysical divergence of the saturation value of the staggered magnetization. In $D = 3$ the HP approach gives a finite saturation value of $\bar{m} = 0.277$ at the Heisenberg point. In contrast to the 1D case, where we suspect from the analysis in the previous sections that the staggered magnetization doesn't saturate at a finite value at long times, the saturation predicted by spin-wave theory in the 3D case is likely to be correct. Indeed, within a thermalization scenario, the staggered magnetization should saturate at a value corresponding to a thermal state at a temperature related to the energy of the initial state. We will take a closer look at this scenario in the following section.

4.4.2 Comparison with a thermalization scenario in 3D

In the section above we have calculated the saturation value of the staggered magnetization $\bar{m}$ using the Holstein-Primakoff spin-wave theory. Now we want to see if $\bar{m}$ can be inferred from a thermalization scenario in the three dimensional case. As mentioned previously, one naively expects that local observables should thermalize after a quantum quench. Thus, after long evolution times $t \to \infty$, the expectation values of local observables should coincide with a thermal average at an effective temperature $T_{\mathrm{eff}} = 1/\beta_{\mathrm{eff}}$ corresponding to the energy of the initial state $|\psi_0\rangle$. More precisely, the effective temperature is determined by

$$\langle\psi_0|\hat{H}|\psi_0\rangle \stackrel{!}{=} \frac{1}{Z}\,\mathrm{Tr}\left[\hat{H}e^{-\beta_{\mathrm{eff}}\hat{H}}\right]. \tag{4.112}$$

In the following we are going to compare the results for the saturation value of the staggered magnetization $\bar{m}$ after a quench from the Néel state with the thermal expectation value at an effective temperature given by the equation above. All calculations are performed within the framework of spin-wave theory in order to get comparable results.

As a first step we need to diagonalize the Hamiltonian (4.106) in order to calculate the thermal averages. This can be achieved easily using a Bogoliubov transformation to a new set of bosonic operators $\alpha_{\mathbf{k}}$ and $\beta_{\mathbf{k}}$, defined by

$$a_{\mathbf{k}} = \alpha_{\mathbf{k}} \cosh\theta_k + \beta_{-\mathbf{k}}^\dagger \sinh\theta_k \tag{4.113}$$

$$b_{-\mathbf{k}}^\dagger = \alpha_{\mathbf{k}} \sinh\theta_k + \beta_{-\mathbf{k}}^\dagger \cosh\theta_k\,. \tag{4.114}$$

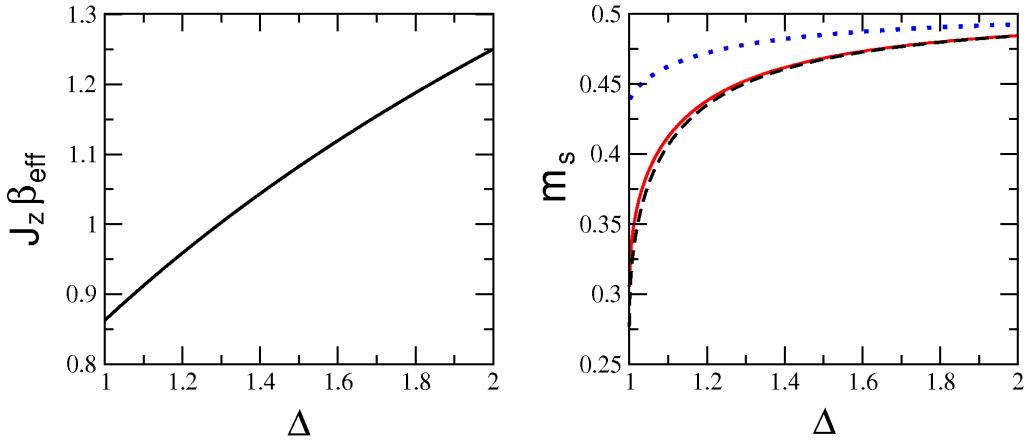

Figure 4.15: Effective temperature β_{eff} and staggered magnetization m_s for the $3D$ antiferromagnetic Heisenberg model on a cubic lattice, calculated within spin-wave theory. Left: β_{eff} of the initial Néel state as a function of the anisotropy Δ in units of $J_z^{-1} = (J\Delta)^{-1}$, calculated using (4.112). Right: staggered magnetization as function of the anisotropy. Blue dotted line: equilibrium value of m_s at zero temperature; red solid line: equilibrium value of m_s at temperature β_{eff} corresponding to the initial Néel state; black dashed line: saturation value $\bar{m}$ of the staggered magnetization after a quench from the Néel state (4.111).

The angle θ_k is determined by

$$\tanh 2\theta_k = -\lambda_{\mathbf{k}} \tag{4.115}$$

and $\lambda_{\mathbf{k}}$ has been defined in Eq. (4.107). The diagonalized Hamiltonian reads

$$H = -\frac{zNJ\Delta}{2} S(S+2^{1-D}) + zNJ\Delta S \int_{-\pi/2}^{\pi/2} \frac{d^D k}{(2\pi)^D} \sqrt{1-\lambda_{\mathbf{k}}^2} \left(\alpha_{\mathbf{k}}^\dagger \alpha_{\mathbf{k}} + \beta_{\mathbf{k}}^\dagger \beta_{\mathbf{k}} + 1\right) . \tag{4.116}$$

At finite temperatures, the number of Bogoliubov quasiparticle excitations is determined by the Bose-Einstein distribution function

$$\langle \alpha_{\mathbf{k}}^\dagger \alpha_{\mathbf{k}} \rangle_\beta = \langle \beta_{\mathbf{k}}^\dagger \beta_{\mathbf{k}} \rangle_\beta = n_B(E_{\mathbf{k}}) = \left(\exp\left[\beta\, zSJ\Delta \sqrt{1-\lambda_{\mathbf{k}}^2}\right] - 1 \right)^{-1} . \tag{4.117}$$

Using this result it is straightforward to show, that the staggered magnetization in thermal equilibrium is given by

$$\langle m_s \rangle_\beta = \frac{1}{2} - \int_{-\pi/2}^{\pi/2} \frac{d^D k}{(2\pi)^D} \left(\frac{1 + 2n_B(E_{\mathbf{k}})}{\sqrt{1-\lambda_{\mathbf{k}}^2}} - 1 \right) \tag{4.118}$$

The (inverse) effective temperature β_{eff} corresponding to the initial Néel state can now be calculated using (4.112), (4.116), (4.117) and $\langle \psi_{\text{Néel}} | H | \psi_{\text{Néel}} \rangle = -zNJ\Delta S^2/2$. For the $3D$

case, where HP works reasonably well, the numerical results for the effective temperature β_{eff} and the staggered magnetization m_s are shown in Fig. 4.15. It seems that in $3D$ a thermalization scenario is indeed valid, at least as far as m_s is concerned. Apart from a small region close to the critical point $\Delta = 1$, the saturation value $\bar{m}$ after the quench and the equilibrium value m_s at the effective temperature practically coincide.

4.5 Conclusions

In this chapter we have calculated the time evolution of the staggered magnetization in spin-1/2 Heisenberg chains starting from an initial Néel state, using different methods and approximations. We have conjectured that the staggered magnetization vanishes *exponentially* (at least at intermediate time scales) for all finite anisotropies $0 < \Delta < \infty$ in the XXZ- as well as in the XZ-chain and the corresponding relaxation time exhibits a *minimum* close to or at the critical point, where a quantum phase transition to an antiferromagnetically ordered state occurs. Furthermore, we have observed a crossover from oscillating to non-oscillating behavior of the staggered magnetization in both models as the critical point is crossed.

Appendix A

Regularization of the bare interaction strength

In this appendix we show briefly, how the UV-divergence associated with the contact interaction $V(\mathbf{x}) = g_0\delta(\mathbf{x})$ is regularized[1]. This can be done by replacing the bare interaction potential with the low energy limit of the scattering T-matrix of two particles in vacuum, which is well defined even if the potential is singular. The T-matrix is related to the scattering amplitude f via

$$T = -\frac{4\pi}{m} f \tag{A.1}$$

In the low energy limit $k \to 0$, where the scattering amplitude is given by

$$f(k) = \frac{1}{-a^{-1} - ik} \tag{A.2}$$

The T-matrix is thus simply related to the s-wave scattering amplitude

$$T \xrightarrow{k\to 0} \frac{4\pi a}{m} \tag{A.3}$$

The remaining task is to replace the bare interaction V with the T-matrix (A.3). This can be done using the Lippmann-Schwinger equation for the T-matrix of two particles in vacuum

$$T = V + V\chi^{(0)}T\,, \tag{A.4}$$

which takes an arbitrary number of repeated scattering events between the two particles into account. Here, $\chi^{(0)}$ denotes the propagator of the two particles in vacuum. In case of a contact interaction, the T matrix depends only on the total momentum and energy of the two colliding particles. In particular we get

$$T(q) = g_0 + g_0 \int \frac{d^4k}{(2\pi)^4} G(q-k)G(k)T(q) \tag{A.5}$$

[1] Usually, a more physical interaction potential with a finite range r_0 would lead to a natural momentum cutoff $\Lambda \sim r_0^{-1}$.

in momentum space, where G denotes the single-particle propagator. Taking the limit of vanishing 4-momentum $q \to 0$ one obtains

$$T(0) = g_0 - g_0\, T(0) \int \frac{d^3k}{(2\pi)^3} \frac{1}{2\varepsilon_{\mathbf{k}}} \tag{A.6}$$

Using $T(0) = \frac{4\pi a}{m}$ from above, we finally arrive at

$$\frac{1}{g_0} = \frac{m}{4\pi a} - \int \frac{d^3k}{(2\pi)^3} \frac{1}{2\varepsilon_{\mathbf{k}}} \tag{A.7}$$

This expression can be used to remove the UV-divergences in all ill-defined expressions that arise due to the use of the contact potential.

Appendix B

BCS-BEC crossover at $T = 0$: lifetime of fermionic excitations

Two types of low energy quasiparticle excitations are present in the BCS-BEC crossover problem at temperatures below the superfluid transition, namely gapped fermionic single particle excitations with a BCS-like dispersion and the collective Bogoliubov-Anderson mode, which is a phonon excitation of the condensate with a linear dispersion relation. A description of the BCS-BEC crossover in terms of effectively non-interacting quasiparticles is only feasible, if the lifetime of these two excitation branches is sufficiently large. At zero temperature, where no interaction with thermally excited quasiparticles takes place, the only lifetime limiting process is the decay of a quasiparticle into a bunch of low energy excitations. These processes need to obey the kinematic constraints from energy- and momentum-conservation, however. For example, as long as the energy of a phonon doesn't exceed twice the fermionic excitation gap, it cannot decay into a fermionic particle- and a hole-excitation. The only other process that can lead to a finite phonon lifetime is Beliaev-damping [94], which is only possible if the non-linear part of the phonon dispersion is positive, i.e. the dispersion bends slightly upward. Even if this is the case, Beliaev-damping is negligible in the long-wavelength limit. In this appendix we want to ask the question, to what extent the lifetime of the fermionic single particle excitations is limited by the interactions. It is clear that the fermionic excitations have to be sharp at the minimum of the dispersion, because at this point it is energetically not possible for the fermionic excitations to decay.

Our starting point is the standard Hamiltonian of a two-component Fermi gas with an attractive ($\bar{g} < 0$) contact interaction

$$H = \sum_{\mathbf{k},\sigma} (\varepsilon_{\mathbf{k}} - \mu) n_{\mathbf{k}\sigma} + \frac{\bar{g}}{V} \sum_{\mathbf{q},\mathbf{k}',\mathbf{k}} c^{\dagger}_{\mathbf{k}+\mathbf{q}\uparrow} c^{\dagger}_{-\mathbf{k}\downarrow} c_{-\mathbf{k}'\downarrow} c_{\mathbf{k}'+\mathbf{q}\uparrow} \,. \tag{B.1}$$

The superfluid correlations of the ground state are very well described by the reduced BCS-Hamiltonian

$$H_{\mathrm{BCS}} = \sum_{\mathbf{k},\sigma} (\varepsilon_{\mathbf{k}} - \mu) n_{\mathbf{k}\sigma} + \frac{\bar{g}}{V} \sum_{\mathbf{k}',\mathbf{k}} c^{\dagger}_{\mathbf{k}\uparrow} c^{\dagger}_{-\mathbf{k}\downarrow} c_{-\mathbf{k}'\downarrow} c_{\mathbf{k}'\uparrow} \,, \tag{B.2}$$

which only takes zero momentum pairs (i.e. $\mathbf{q} = 0$) into account. Unfortunately, this approximate Hamiltonian is not capable of describing the collective Bogoliubov-Anderson mode, which is connected to the spontaneous $U(1)$-symmetry breaking of the superfluid ground state. The Bogoliubov-Anderson mode is a sound mode that is related to density fluctuations of the condensate, which cannot be described without including finite momentum pairs. However, the reduced BCS-Hamiltonian has the advantage of being exactly diagonalizable. In terms of the fermionic BCS-quasiparticle operators $\alpha_{\mathbf{k}\sigma}$ it takes the form

$$H_{\mathrm{BCS}} = E_0^{\mathrm{BCS}} + \sum_{\mathbf{k}\sigma} E_{\mathbf{k}}\, \alpha^\dagger_{\mathbf{k}\sigma}\alpha_{\mathbf{k}\sigma}\,, \tag{B.3}$$

where $E_{\mathbf{k}} = \sqrt{(\varepsilon_{\mathbf{k}} - \mu)^2 + \Delta^2}$ denotes the standard BCS-quasiparticle dispersion. The quasiparticle operators $\alpha_{\mathbf{k}\sigma}$ are related to the original fermionic operators via a Bogoliubov transformation

$$c_{\mathbf{k}\uparrow} = u_{\mathbf{k}}\alpha_{\mathbf{k}\uparrow} + v_{\mathbf{k}}\alpha^\dagger_{-\mathbf{k}\downarrow} \tag{B.4}$$

$$c_{-\mathbf{k}\downarrow} = -v_{\mathbf{k}}\alpha^\dagger_{\mathbf{k}\uparrow} + u_{\mathbf{k}}\alpha_{-\mathbf{k}\downarrow}\,, \tag{B.5}$$

where the coefficients are given by $u_k^2 = (1 + \frac{\varepsilon_{\mathbf{k}}-\mu}{E_{\mathbf{k}}})/2$ and $v_k^2 = 1 - u_k^2$. Note that the reduced BCS-Hamiltonian (B.2) cannot be mapped to (B.3) directly by simply applying the Bogoliubov transformation. Indeed, a direct mapping is only possible if a mean field decomposition of the interaction term in Eq. (B.2) is used beforehand. The interaction term in the reduced BCS-Hamiltonian corresponds to an *infinite* range interaction, however, thus the mean field treatment is essentially *exact*[1].

In the following we are interested in the lifetime of fermionic excitations in a neutral, superfluid Fermi system at zero temperature. The dispersion and the lifetime of single particle excitations are determined by the poles of the Green's function

$$G_\sigma(\mathbf{k}, t - t') = -i\langle T\big\{c_{\mathbf{k}\sigma}(t)c^\dagger_{\mathbf{k}\sigma}(t')\big\}\rangle\,, \tag{B.6}$$

where the time argument denotes operators in the Heisenberg picture. In order to incorporate the superfluid correlations of the ground state without having to deal with anomalous Green's functions, we use the Bogoliubov transformation that has been defined in Eqs. (B.4) and (B.5) above, and express the fermionic Green's function G from Eq. (B.6) in terms of the BCS-quasiparticle Green's functions $\mathcal{G}_\sigma(\mathbf{k}, t - t') = -i\langle T\big\{\alpha_{\mathbf{k}\sigma}(t)\alpha^\dagger_{\mathbf{k}\sigma}(t')\big\}\rangle$

$$G_\sigma(\mathbf{k}, \omega) = u_k^2\,\mathcal{G}_\sigma(\mathbf{k}, \omega) - v_k^2\,\mathcal{G}_{-\sigma}(-\mathbf{k}, -\omega) \tag{B.7}$$

This mapping directly relates the lifetime of fermionic excitations to the lifetime of BCS-quasiparticles. Within a description in terms of the reduced BCS-Hamiltonian alone, the lifetime of the BCS-quasiparticles (and thus also the lifetime of the fermionic excitations) is obviously infinite, i.e. $\mathrm{Im}\mathcal{G}^R_\sigma(\mathbf{k}, \omega) = -\pi\delta(\omega - E_{\mathbf{k}})$. Together with Eq. (B.6) this leads to the BCS-approximation for the fermionic spectral function, see Eq. (2.57).

[1] For a more rigorous analysis of this mapping see [95].

The residual interaction

$$H_{\rm res} = H - H_{\rm BCS} = \frac{\bar{g}}{V} \sum_{\mathbf{k}',\mathbf{k},\mathbf{q}\neq 0} c^\dagger_{\mathbf{k}+\mathbf{q}\uparrow} c^\dagger_{-\mathbf{k}\downarrow} c_{-\mathbf{k}'\downarrow} c_{\mathbf{k}'+\mathbf{q}\uparrow} \,, \tag{B.8}$$

that has been neglected in BCS-theory, describes interactions between BCS-quasiparticles and their coupling to the collective Bogoliubov-Anderson mode. When expressed in terms of the Bogoliubov quasiparticle operators, the residual interaction gives rise to three different types of quasiparticle interactions $H_{\rm res} = H_{40} + H_{31} + H_{22}$

$$H_{40} = \frac{1}{V} \sum_{\mathbf{k},\mathbf{k}',\mathbf{q}\neq 0} V^{(4,0)}_{\mathbf{k}'\mathbf{k}\mathbf{q}}\ \alpha_{\mathbf{k}\uparrow}\alpha_{-\mathbf{k}-\mathbf{q}\downarrow}\alpha_{-\mathbf{k}'\downarrow}\alpha_{\mathbf{k}'+\mathbf{q}\uparrow} + \text{h.c.} \tag{B.9}$$

$$H_{31} = \frac{1}{V} \sum_{\mathbf{k},\mathbf{k}',\mathbf{q}\neq 0,\sigma} V^{(3,1)}_{\mathbf{k}'\mathbf{k}\mathbf{q}}\ \alpha^\dagger_{\mathbf{k}\sigma}\alpha_{\mathbf{k}-\mathbf{q}\sigma}\alpha_{-\mathbf{k}'\downarrow}\alpha_{\mathbf{k}'+\mathbf{q}\uparrow} + \text{h.c.} \tag{B.10}$$

$$\begin{aligned} H_{22} = \frac{1}{V} \sum_{\mathbf{k},\mathbf{k}',\mathbf{q}\neq 0} \Big[& V^{(2,2),\uparrow\downarrow,1}_{\mathbf{k}'\mathbf{k}\mathbf{q}}\ \alpha^\dagger_{\mathbf{q}-\mathbf{k}\uparrow}\alpha^\dagger_{\mathbf{k}\downarrow}\alpha_{\mathbf{k}'\downarrow}\alpha_{\mathbf{q}-\mathbf{k}'\uparrow} \\ & + V^{(2,2),\uparrow\downarrow,2}_{\mathbf{k}'\mathbf{k}\mathbf{q}}\ \alpha^\dagger_{\mathbf{k}\uparrow}\alpha^\dagger_{-\mathbf{k}'\downarrow}\alpha_{\mathbf{q}-\mathbf{k}'\downarrow}\alpha_{\mathbf{k}-\mathbf{q}\uparrow} + V^{(2,2),\uparrow\uparrow}_{\mathbf{k}'\mathbf{k}\mathbf{q}}\ \alpha^\dagger_{\mathbf{k}+\mathbf{q}\uparrow}\alpha^\dagger_{\mathbf{k}'\uparrow}\alpha_{\mathbf{k}'+\mathbf{q}\uparrow}\alpha_{\mathbf{k}\uparrow} \\ & + V^{(2,2),\downarrow\downarrow}_{\mathbf{k}'\mathbf{k}\mathbf{q}}\ \alpha^\dagger_{\mathbf{k}+\mathbf{q}\downarrow}\alpha^\dagger_{\mathbf{k}'\downarrow}\alpha_{\mathbf{k}'+\mathbf{q}\downarrow}\alpha_{\mathbf{k}\downarrow} \Big] \end{aligned} \tag{B.11}$$

corresponding to four-wave annihilation, quasiparticle decay and quasiparticle scattering. The associated vertices are given by

$$V^{(4,0)}_{\mathbf{k}'\mathbf{k}\mathbf{q}} = g_0\, v_{\mathbf{k}+\mathbf{q}} v_{\mathbf{k}} u_{\mathbf{k}'} u_{\mathbf{k}'+\mathbf{q}} \tag{B.12}$$

$$V^{(3,1)}_{\mathbf{k}'\mathbf{k}\mathbf{q}} = g_0\, \left(v_{\mathbf{k}'} v_{\mathbf{k}'+\mathbf{q}} v_{\mathbf{k}} u_{\mathbf{k}-\mathbf{q}} - u_{\mathbf{k}'} u_{\mathbf{k}'+\mathbf{q}} u_{\mathbf{k}} v_{\mathbf{k}-\mathbf{q}} \right) \tag{B.13}$$

$$V^{(2,2),\uparrow\downarrow,1}_{\mathbf{k}'\mathbf{k}\mathbf{q}} = g_0\, \left(u_{\mathbf{q}-\mathbf{k}} u_{\mathbf{k}} u_{\mathbf{k}'} u_{\mathbf{q}-\mathbf{k}'} + v_{\mathbf{q}-\mathbf{k}} v_{\mathbf{k}} v_{\mathbf{k}'} v_{\mathbf{q}-\mathbf{k}'} \right) \tag{B.14}$$

$$V^{(2,2),\uparrow\downarrow,2}_{\mathbf{k}'\mathbf{k}\mathbf{q}} = g_0\, \left(u_{\mathbf{k}} u_{\mathbf{k}'-\mathbf{q}} v_{\mathbf{k}'} v_{\mathbf{k}-\mathbf{q}} + v_{\mathbf{k}} v_{\mathbf{k}'-\mathbf{q}} u_{\mathbf{k}'} u_{\mathbf{k}-\mathbf{q}} \right) \tag{B.15}$$

$$V^{(2,2),\uparrow\uparrow}_{\mathbf{k}'\mathbf{k}\mathbf{q}} = g_0\, u_{\mathbf{k}+\mathbf{q}} u_{\mathbf{k}'+\mathbf{q}} v_{\mathbf{k}} v_{\mathbf{k}'} \tag{B.16}$$

$$V^{(2,2),\downarrow\downarrow}_{\mathbf{k}'\mathbf{k}\mathbf{q}} = g_0\, v_{\mathbf{k}+\mathbf{q}} v_{\mathbf{k}'+\mathbf{q}} u_{\mathbf{k}} u_{\mathbf{k}'} \tag{B.17}$$

The only process that limits the lifetime of BCS-quasiparticles at zero temperature is quasiparticle decay. A simple second order perturbation theory calculation with H_{31} shows, that there is a broad range around the minimum of the dispersion relation where the BCS-quasiparticle has an infinite lifetime. This is simply because the decay into three quasiparticles is suppressed by energy and momentum conservation (i.e. the quasiparticle has to have at least an initial energy of 3Δ, otherwise the decay is impossible). However, this is *not* the dominant contribution to the lifetime close to the dispersion minimum. Indeed, it is possible that a BCS-quasiparticle emits a Bogoliubov-Anderson phonon. This process has a much less restrictive phase space constraint than the decay into three quasiparticles. In order to estimate this contribution, we need to know how the BCS-quasiparticles couple to the collective Bogoliubov-Anderson mode. Quite generally,

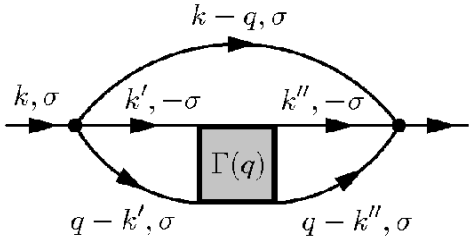

Figure B.1: Dominant contribution to the BCS-quasiparticle self-energy at $T = 0$.

collective modes show up as pole in the vertex function corresponding to the scattering of two quasiparticles. In the case of the Bogoliubov-Anderson mode this can be understood from the fact that a phonon can be considered as a bound state of two elementary excitations with non-vanishing total momentum. As shown already by Galitskii [96], the vertex function $\Gamma(\mathbf{q}, \omega)$ for the scattering of an up- and a down- BCS-quasiparticle has a pole at $\omega^2 = c_s^2 q^2$ corresponding to the Bogoliubov-Anderson phonon mode, where c_s is the sound velocity. Within a diagrammatic formulation, the leading order self-energy contribution corresponding to the emission of a Bogoliubov-Anderson phonon is shown in Fig. B.1. Apart from combinatorial factors, the BCS-quasiparticle self-energy is thus given by

$$\begin{aligned}\Sigma_\uparrow(\mathbf{k}, i\omega_k) &= \frac{1}{\beta^3}\sum_{\{\omega_n\}}\int \frac{d^3q\, d^3k'\, d^3k''}{(2\pi)^9} V^{(1,3)}_{-\mathbf{k'kq}} V^{(3,1)}_{-\mathbf{k''kq}}\, \mathcal{G}_\uparrow(\mathbf{k}-\mathbf{q}, i\omega_k - i\omega_q)\mathcal{G}_\downarrow(\mathbf{k'}, i\omega_{k'}) \\ &\times \mathcal{G}_\uparrow(\mathbf{q}-\mathbf{k'}, i\omega_q - i\omega_{k'})\Gamma(\mathbf{q}, i\omega_q)\mathcal{G}_\downarrow(\mathbf{k''}, i\omega_{k''})\mathcal{G}_\uparrow(\mathbf{q}-\mathbf{k''}, i\omega_q - i\omega_{k''}) \quad \text{(B.18)}\end{aligned}$$

Evaluating the Matsubara summations, setting $T = 0$ and performing the analytic continuation $i\omega_k \to \omega + i\delta$, we obtain the retarded self-energy

$$\begin{aligned}\Sigma^R_\uparrow(\mathbf{k}, \omega) &= \int \frac{d^3q\, d^3k'\, d^3k''}{(2\pi)^9} V^{(1,3)}_{-\mathbf{k'kq}} V^{(3,1)}_{-\mathbf{k''kq}}\, \Gamma(\mathbf{q}, \omega - E_{\mathbf{k}-\mathbf{q}} + i\delta) \\ &\times \mathcal{G}_\downarrow(\mathbf{k'}, \omega - E_{\mathbf{k}-\mathbf{q}} - E_{\mathbf{q}-\mathbf{k'}} + i\delta)\mathcal{G}_\downarrow(\mathbf{k''}, \omega - E_{\mathbf{k}-\mathbf{q}} - E_{\mathbf{q}-\mathbf{k''}} + i\delta) \quad \text{(B.19)}\end{aligned}$$

The important contribution to the imaginary part of the self energy comes from the pole of the Vertex function $\Gamma(\mathbf{q}, \omega)$ at $\omega = c_s|\mathbf{q}|$ and is given by

$$\begin{aligned}\mathrm{Im}\Sigma^R_\uparrow(\mathbf{k}, \omega) &= \int \frac{d^3q\, d^3k'\, d^3k''}{(2\pi)^9} V^{(1,3)}_{-\mathbf{k'kq}} V^{(3,1)}_{-\mathbf{k''kq}}\, Z_{\mathrm{BA}}(q)\, \delta(\omega - E_{\mathbf{k}-\mathbf{q}} - c_s|\mathbf{q}|) \\ &\times \mathrm{Re}\mathcal{G}_\downarrow(\mathbf{k'}, \omega - E_{\mathbf{k}-\mathbf{q}} - E_{\mathbf{q}-\mathbf{k'}})\, \mathrm{Re}\mathcal{G}_\downarrow(\mathbf{k''}, \omega - E_{\mathbf{k}-\mathbf{q}} - E_{\mathbf{q}-\mathbf{k''}}) \quad \text{(B.20)}\end{aligned}$$

where $Z_{BA}(q)$ is the quasiparticle weight of the Bogoliubov-Anderson mode and we have neglected the terms originating from the imaginary parts of the two Green's functions, because they give rise to the stronger 3Δ constraint that has been discussed above. Assuming that the real part of the self-energy is small, we evaluate the self-energy on-shell at $\omega = E_{\mathbf{k}}$ and extract from (B.20) the – expected – kinematic constraint

$$E_{\mathbf{k}} = E_{\mathbf{k}-\mathbf{q}} + c_s|\mathbf{q}|\,. \quad \text{(B.21)}$$

For fermionic excitations with an energy close to the dispersion minimum it is clear that only the emission of long wavelength (i.e. low-energy) phonons is possible. Expanding the kinematic constraint for small phonon momenta we get the condition

$$|\nabla E_{\mathbf{k}}| > c_s \tag{B.22}$$

for the emission of a phonon, i.e. the emission of a phonon is *impossible* as long as the group velocity $|\partial_k E_k|$ of the quasiparticle excitations is *smaller* than the sound velocity. Thus, the spectral function of the fermionic single-particle excitations exhibits a sharp peak in the interval

$$\frac{|k - k_F|}{k_F} < \frac{c_s}{2v_F}\,\frac{\Delta}{\varepsilon_F} \tag{B.23}$$

around the dispersion minimum.

Apart from this region close to the dispersion minimum, the fermionic excitations have a finite liftime which scales as $\sim (k_F a)^2$ in the weak coupling limit. This lifetime broadening has observable consequences on the rf-spectra. Indeed, the sharpness of the onset of the rf-spectra is determined by the quasiparticle width at $\mathbf{k} = 0$. A more detailed discussion of this issue can be found in Ref. [28].

Appendix C

The Cooper problem in a spin-polarized Fermi gas

In this appendix we briefly analyze the Cooper problem of two interacting Fermions in a spin-polarized environment. Suppose we have a spin-polarized Fermi sea of noninteracting up-Fermions and we add one more up-Fermion and one down-Fermion, which are interacting via a pseudopotential with interaction strength $g = 4\pi a/m$. Due to Pauli blocking, the up-Fermion has to be added at a momentum $|\mathbf{k}| > k_F$, where $k_F = (6\pi^2 n_\uparrow)^{1/3}$ denotes the Fermi-momentum of the up-Fermi-sea. The down-Fermion can be added at arbitrary momenta, however. In the non-interacting limit it is thus energetically favorable to add the down-Fermion at $\mathbf{k}_\downarrow = 0$ and the up-Fermion at $|\mathbf{k}_\uparrow| = k_F$ (without loss of generality we add the up-Fermion at momentum $\mathbf{k}_\uparrow = k_F \mathbf{e}_z$). Note that this 'Cooper-pair' has a total momentum of $\mathbf{Q} = \mathbf{k}_\uparrow + \mathbf{k}_\downarrow = k_F \mathbf{e}_z$ per construction. In the center of mass frame, the Schrödinger equation for the ground state energy of the two interacting Fermions takes the form

$$\frac{1}{g_0} = \frac{1}{V} \sum_{\mathbf{q}} \frac{1}{E_r - 2\varepsilon_{\mathbf{q}}} \tag{C.1}$$

with $\mathbf{q} = (\mathbf{k}_\uparrow - \mathbf{k}_\downarrow)/2$ as the relative momentum between the two Fermions. Here E_r is the ground state energy in the CM-frame (i.e. without the kinetic energy of the center of mass motion) and $\varepsilon_{\mathbf{q}} = q^2/(2m)$ denotes the dispersion relation of the Fermions. The bare interaction strength g_0 is regularized in the standard form via (A.7).

In the usual Cooper problem, the $\mathbf{q}$-sum in (C.1) is restricted to $|\mathbf{q}| < k_F$ due to the presence of a Fermi sea for both Fermion species. In the case of a spin-polarized up-Fermi sea, virtual scattering processes are restricted to $|\mathbf{k}_\uparrow| > k_F$ and we get the following condition for the $\mathbf{q}$-sum in (C.1)

$$|\mathbf{k}_\uparrow| = \left| \frac{k_F}{2} \mathbf{e_z} + \mathbf{q} \right| > k_F \,. \tag{C.2}$$

The Schrödinger equation (C.1) can thus be written as

$$\frac{1}{g_0} = \frac{1}{V} \sum_{|\mathbf{p}| > k_F} \frac{1}{E_r - 2\varepsilon_{\mathbf{p} - \mathbf{e}_z k_F/2}} \,. \tag{C.3}$$

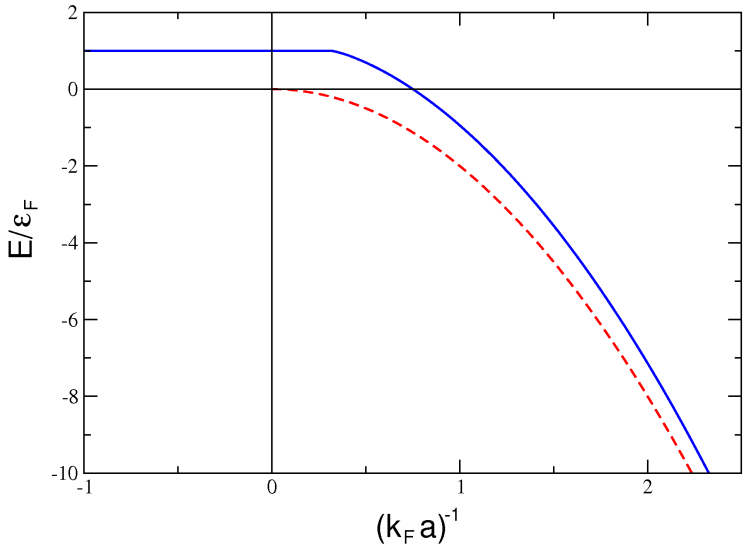

Figure C.1: Blue line: ground-state energy of a Cooper-pair in a spin polarized Fermi sea in units of ε_F, as function of the inverse coupling strength $(k_F a)^{-1}$. The dashed red line marks the two-particle bound-state energy $E_b = -1/(ma^2)$ in the absence of a Fermi sea.

In fig. C.1 we plot the ground state energy of the Cooper pair, i.e. the numerical solution of (C.3) *plus* the kinetic energy of the center of mass motion, as function of $v = (k_F a)^{-1}$. For $v < \pi^{-1}$ the ground state energy is the same as in the non-interacting case. For $v > \pi^{-1}$, however, the two Fermions form a two-particle bound state. Naively this should happen when the binding energy of the two particle bound state is larger than the Fermi energy $|E_b| = (ma^2)^{-1} > \varepsilon_F$, , i.e. $v > 1/\sqrt{2}$, because in this case it is energetically favorable to lift the down-Fermion to an energy above ε_F and form a bound state in a relative $(\mathbf{q}, -\mathbf{q})$-configuration with zero total momentum. This estimate is in reasonable agreement with the result for the position of the critical point M from chapter 3, where we have found $v_M \simeq 0.84$. For the case considered in this appendix, however, the situation is a little bit different because the total momentum of the pair is finite and conserved.

Now it is also clear why molecule formation is more difficult in the presence of a polarized Fermi sea than in its absence. Indeed, the minority Fermion has to overcome an energy gap $\sim \varepsilon_F$ in order to form a bound state with one of the majority Fermions. Energetically, this process is favorable only if the binding energy is larger then the energy gap.

Appendix D

Papers

On the following pages we reprint the four most relevant of the papers that were published in the context of this thesis:

- M. Punk and W. Zwerger
  "Theory of rf-Spectroscopy of Strongly Interacting Fermions"
  Phys. Rev. Lett. **99**, 170404 (2007).

- M. Punk, P.T. Dumitrescu, and W. Zwerger
  "Polaron-to-molecule transition in a strongly imbalanced Fermi gas"
  Phys. Rev. A **80**, 053605 (2009).

- R. Haussmann, M. Punk, and W. Zwerger
  Spectral functions and rf-response of ultracold fermionic atoms
  Phys. Rev. A **80**, 063612 (2009).

- P. Barmettler, M. Punk, V. Gritsev, E. Demler, and E. Altman
  "Relaxation of Antiferromagnetic Order in Spin-1/2 Chains Following a Quantum Quench"
  Phys. Rev. Lett. **102**, 130603 (2009).

PRL 99, 170404 (2007) PHYSICAL REVIEW LETTERS week ending 26 OCTOBER 2007

Theory of rf-Spectroscopy of Strongly Interacting Fermions

M. Punk and W. Zwerger

Physik-Department, Technische Universität München, James-Franck-Str., D-85748 Garching, Germany

(Received 5 July 2007; published 25 October 2007)

We show that strong pairing correlations in Fermi gases lead to the appearance of a gaplike structure in the rf spectrum, both in the balanced superfluid and in the normal phase above the Clogston-Chandrasekhar limit. The average rf shift of a unitary gas is proportional to the ratio of the Fermi velocity and the scattering length with the final state. In the strongly imbalanced case, the rf spectrum measures the binding energy of a minority atom to the Fermi sea of majority atoms. Our results provide a qualitative understanding of recent experiments by Schunck *et al.*

DOI: 10.1103/PhysRevLett.99.170404 PACS numbers: 03.75.Ss, 05.30.Fk, 32.30.Bv

According to the 50 yr old microscopic theory of Bardeen, Cooper, and Schrieffer, the phenomenon of superfluidity in a system of fermions is connected with the formation of bound pairs. In the weak coupling limit, where the formation of pairs and their condensation appears simultaneously, the transition to the superfluid state is associated with the appearance of a gap in the fermionic excitation spectrum. For strong coupling, however, this simple connection is no longer valid and bound pairs of fermions may exist even in the normal state. This phenomenon is well known from the pseudogap phase in high temperature superconductors, where a d-wave pairing gap appears on the Fermi surface at temperatures far above the superconducting transition temperature [1]. A much simpler example is realized by ultracold fermions near a Feshbach resonance, which provide a perfectly controllable model system to study the effects of strong pairing interactions [2]. In the case of an equal population of the two hyperfine states undergoing pairing, the ground state is superfluid at arbitrary values of the scattering length. A microscopic signature of pairing in ultracold Fermi gases has first been obtained by Chin *et al.* [3] through rf spectroscopy. The rf field drives transitions between one of the hyperfine states $|2\rangle = |\downarrow\rangle$ which is involved in the pairing and an empty hyperfine state $|3\rangle$ which lies above it by an energy $\hbar\omega_{23}$ due to the magnetic field splitting of the bare atom hyperfine levels. In the absence of any interactions, the spectrum exhibits a sharp peak at $\omega = \omega_{23}$. Pairing between the two lowest hyperfine states $|1\rangle$ and $|2\rangle$ leads to an upward shift of this resonance. The shift essentially follows the two-particle binding energy on the BEC-side of the crossover but stays finite on the BCS side, where the appearance of a bound Cooper pair is a many-body effect [3]. A theoretical explanation of these observations can be given by extending the BCS description of pairing to the strong coupling regime and neglecting interactions involving state $|3\rangle$ [4,5]. In a homogeneous system, the resulting rf spectrum exhibits a peak at energies around Δ^2/μ, which is of the order of the energy gap $\Delta \approx 0.5\varepsilon_F$ at the unitarity point. Since pairing appears already in the normal state above T_c, the rf shift does not directly measure the superfluid order, however [5]. The importance of understanding the relation between rf spectra and the nature of the many-body states involved, is underlined by recent experiments in imbalanced gases [6]. There, a shift in the rf spectrum is observed which hardly changes between the balanced superfluid and a normal ground state beyond a critical population imbalance, where superfluidity is destroyed by a sufficiently large mismatch of the Fermi energies even at $T = 0$ (this is the analog of the Clogston-Chandrasekhar limit in superconductors). In this Letter, we present a theory of rf shifts in both balanced and imbalanced Fermi gases, which provides a qualitative understanding of these observations. In particular, we show that the average frequency shift in the balanced superfluid at unitarity (i.e., at infinite scattering length) is linear in the Fermi velocity and inversely proportional to the scattering length a_{13}. In the nonsuperfluid state beyond the Clogston-Chandrasekhar limit, pair fluctuations give rise to sharp peaks in the rf spectrum which are associated with the binding of $\uparrow\downarrow$ -pairs even in the absence of long range phase coherence.

Within linear response theory, which is adequate for rf pulses short compared to the Rabi oscillation period of the bare 2–3 transition, the number of particles transferred from state $|2\rangle$ to state $|3\rangle$ per unit time is given by

$$I(\omega) \sim \int dt d^3x d^3x' e^{i(\mu_3-\mu_\downarrow-\omega_L)t}\langle[\psi_3^\dagger(x,t)\psi_\downarrow(x,t), \psi_\downarrow^\dagger(x',0)\psi_3(x',0)]\rangle, \quad (1)$$

where $\omega = \omega_L - \omega_{23}$ denotes the detuning of the rf field from the bare 2–3 transition. Since particles in state $|3\rangle$ have a nonvanishing interaction with those in states $|1\rangle$ and $|2\rangle$ [7], the response function in Eq. (1) does not factorize into one particle functions, making a full calculation of the spectrum very difficult. Nevertheless, near $T = 0$, where only a single peak is observed in the rf spectrum, its position can be determined from a sum rule approach [8]. In particular, the first moment $\bar{\omega} = \int d\omega \omega I(\omega) / \int d\omega I(\omega)$ is given by

$$\hbar\,\bar{\omega} = \frac{\bar{g}_{12} - \bar{g}_{13}}{N_2 - N_3}\left(\frac{\langle H'_{13}\rangle}{\bar{g}_{13}} - \frac{\langle H'_{12}\rangle}{\bar{g}_{12}}\right). \quad (2)$$

Here H'_{13} and H'_{12} denote the interaction Hamiltonians between the respective states, while N_2 and N_3 denote the total number of particles in states $|2\rangle$ and $|3\rangle$. The $\bar{g}_{ij}$ are the bare interaction constants arising in the pseudopotential interaction Hamiltonian

$$H'_{ij} = \bar{g}_{ij}\int d^3x \psi_i^\dagger(x)\psi_j^\dagger(x)\psi_j(x)\psi_i(x). \quad (3)$$

They are related to their renormalized values $g_{ij} = 4\pi\hbar^2 a_{ij}/m$ by

$$\frac{1}{\bar{g}} = \frac{1}{g} - \int \frac{d^3k}{(2\pi)^3}\frac{1}{2\varepsilon_{\mathbf{k}}}, \quad (4)$$

where a_{ij} are the s-wave scattering lengths between states i and j, m is the mass of the particles and $\varepsilon_{\mathbf{k}} = \hbar^2k^2/2m$ the single particle energy. Note that the interaction g_{23} between states 2 and 3 drops out quite generally, because H'_{23} and H_{RF} commute. Moreover, there is no shift of the rf peak if the interaction strengths g_{12} and g_{13} are equal, a case, where all interaction effects are cancelled exactly [8,9]. Since $\langle H'_{13}\rangle$ is of order N_3, the first term in (3) is negligible compared to the second term if $N_2 \gg N_3$. The average shift of the rf spectrum then simplifies to

$$\hbar\,\bar{\omega} = \frac{\langle H'_{12}\rangle}{N_2}\left(\frac{\bar{g}_{13}}{\bar{g}_{12}} - 1\right) \to \frac{\langle H'_{12}\rangle}{N_2\Lambda}\,\frac{\pi}{2}\left(\frac{1}{a_{13}} - \frac{1}{a_{12}}\right). \quad (5)$$

Here, the second form is obtained by expanding $1 - \bar{g}_{13}/\bar{g}_{12}$ to leading order in the upper cutoff Λ of the momentum integral in (4). Evidently, for vanishing interactions $\bar{g}_{13} = g_{13} \equiv 0$ with state 3, the rf shift just measures the (negative) interaction energy per particle in the state 2. Within a pseudopotential description, however, the interaction energy $\langle H'_{12}\rangle \sim \Lambda$ diverges linearly with the cutoff. It is thus sensitive to the range of the interactions, which is set equal to zero in the pseudopotential. In terms of the spectrum $I(\omega)$, this divergence shows up as a slow decay $I(\omega) \sim \omega^{-3/2}$ at large frequencies, leading to a divergent first moment, as is easily seen within a BCS description with a constant gap Δ. Remarkably, for finite interactions $g_{13} \neq 0$, the second form of (5) gives a result for the frequency shift which is well defined and finite in the limit $\Lambda \to \infty$. As shown by Tan [10], the total energy of the balanced gas can be obtained from the momentum distribution $n_{\mathbf{k}}$ via $E = 2\sum_k \varepsilon_{\mathbf{k}}(n_{\mathbf{k}} - C/k^4)$ up to a constant, which is irrelevant for the calculation of the limit $\langle H'_{12}\rangle/\Lambda$. Here C is the constant arising in the asymptotic behavior $\lim n_{\mathbf{k}} = C/k^4$ of the momentum distribution at large momenta. Evidently, the interaction contribution to the total energy is just $\langle H'_{12}\rangle = -2C\sum_k \varepsilon_{\mathbf{k}}/k^4 \sim -C\Lambda$. Introducing a dimensionless constant s via $C = sk_F^4$, the shift of the rf spectrum

$$\hbar\,\bar{\omega} = s\frac{4\varepsilon_F^2}{n_2}\left(\frac{1}{g_{12}} - \frac{1}{g_{13}}\right) \quad (6)$$

of the balanced gas is completely determined by the universal constant s, the Fermi energy $\varepsilon_F = \hbar^2k_F^2/(2m)$ of the balanced, noninteracting gas and the renormalized interaction constants g_{12} and g_{13}. The expression is finite for all coupling strengths g_{12} and evolves smoothly from the BCS to the Bose-Einstein condensation (BEC) limit. Within an extended BCS description of the ground state wave function, the product $s^{(0)}4\varepsilon_F^2 \equiv \Delta^2$ is precisely the square of the gap parameter. In weak coupling, our result then coincides with that obtained by Yu and Baym [8], except for the mean field shift, which is not contained in the reduced BCS Hamiltonian. In the BEC-limit, where the BCS ground state becomes exact, the asymptotic behavior $\Delta_{\mathrm{BEC}} = 4\varepsilon_F/\sqrt{3\pi k_F a_{12}}$ gives $\hbar\bar{\omega} = 2\varepsilon_b(1 - a_{12}/a_{13})$, where $\varepsilon_b = \hbar^2/ma_{12}^2$ is the two-particle binding energy. It is straightforward to show that this is precisely the average shift for bound-free transitions following from a detailed calculation of the rf spectrum in the molecular limit by Chin and Julienne [11]. The most interesting regime is that around the unitarity limit $1/g_{12} = 0$. At this point, the average rf shift is given by $\bar{\omega} = -0.46v_F/a_{13}$, which varies like the *square root* of the Fermi energy $\varepsilon_F = mv_F^2/2$. The constant $s = 0.098$ is obtained from the recent calculations of the crossover thermodynamics by Haussmann *et al.* [12]. Our result for the homogeneous gas can be compared directly with locally resolved rf spectra by Shin *et al.* [13]. Accounting for the enhancement of the local Fermi velocity at the trap center by a factor ≈ 1.25 due to the attractive interactions, the predicted average shift $\bar{\omega} = 2\pi \times 28.9$ kHz [14] is considerably larger than the measured position of the peak near 15 kHz. This is probably due to the fact, that $\bar{\omega}$ has a considerable contribution from the higher frequency part of the spectrum. A crucial prediction of our theory is the linear behavior of the average rf shift with the Fermi momentum. Experimentally, the spatial resolution necessary to distinguish this from the naive ε_F scaling has not yet been achieved [13].

To discuss the situation with a finite imbalance, it is convenient to introduce two distinct chemical potentials for the states undergoing pairing, defined by $\mu_\uparrow = \mu + h$ and $\mu_\downarrow = \mu - h$. Since the ground state of the spin balanced gas is a superfluid with a gap for fermionic excitations, it will be stable over a finite range $h < h_c$ of the chemical potential difference. In the BCS limit, the associated Clogston-Chandrasekhar critical field $h_c = \Delta_{\mathrm{BCS}}/\sqrt{2}$ is exponentially small. Near the unitarity point, the absence of a second energy scale implies that the critical field h_c beyond which a nonzero polarization appears, is on the order of the bare Fermi energy ε_F of the balanced two-component Fermi gas. From fixed node diffusion Monte Carlo calculations the resulting numerical value in the continuum case at unitarity is $h_c = 0.96\mu \approx 0.4\varepsilon_F$ [15]. The phase for $h > h_c$ is a nonsuperfluid, polarized

PRL 99, 170404 (2007) PHYSICAL REVIEW LETTERS week ending 26 OCTOBER 2007

mixture of the different spin states. For large enough fields, the system will eventually be completely spin polarized. At unitarity, the associated saturation field h_s was determined by Chevy [16] using a variational calculation of the energy change $\mu_\downarrow$ associated with adding a single $\downarrow$-particle to a Fermi sea of $\uparrow$-particles. This leads to an upper bound $\mu_\downarrow \leq -0.60\mu_\uparrow$ at the unitarity point, where $\mu_\uparrow = 2^{2/3}\varepsilon_F$ is the Fermi energy of the completely spin polarized gas. The saturation field thus obeys the inequality $h_s \geq 0.8\mu_\uparrow = 1.27\varepsilon_F$. At unitarity, therefore, there is a wide regime $h_c < h < h_s$ of an intermediate phase between the balanced superfluid and a fully polarized gas. While superfluidity is quenched in this phase, the strong interactions between particles in states $|1\rangle$ and $|2\rangle$ still give rise to large frequency shifts in the rf spectrum, as will be shown below. To study the effect of pairing fluctuations on the imbalanced Fermi gas above the Clogston-Chandrasekhar limit, we calculate the pair-fluctuation spectrum from the two-fermion Green function, using a non-self-consistent T-matrix approach, similar to the approach by Combescot *et al.* [17]. Such a perturbative analysis is reasonable, since the states which are coupled through the interaction Hamiltonian are separated by an energy gap of width $2h$. A usual ladder approximation is used to incorporate the effects of the attractive $\uparrow\downarrow$-interaction on the vertex part, whereas the self-energy is calculated at the one-loop level, including vertex corrections. The basic equations for the polarization loop L, vertex part Γ and self-energy part of the minority species $\Sigma_\downarrow$ are given by (see Fig. 1, we take units such that $\hbar = 1$)

$$L(\mathbf{q}, i\Omega_n) = -\frac{1}{\beta}\sum_{\omega_m}\int \frac{d^3k}{(2\pi)^3}\mathcal{G}_\uparrow^{(0)}(\mathbf{q}-\mathbf{k}, i\Omega_n - i\omega_m) \times \mathcal{G}_\downarrow^{(0)}(\mathbf{k}, i\omega_m), \tag{7}$$

$$\Gamma(\mathbf{q}, i\Omega_n) = \frac{1}{1/\bar{g} - L(\mathbf{q}, i\Omega_n)}, \tag{8}$$

$$\Sigma_\downarrow(\mathbf{k}, i\omega_n) = \frac{1}{\beta}\sum_{\Omega_m}\int \frac{d^3q}{(2\pi)^3}\Gamma(\mathbf{q}, i\Omega_m) \times \mathcal{G}_\uparrow^{(0)}(\mathbf{q}-\mathbf{k}, i\Omega_m - i\omega_n), \tag{9}$$

where $\mathcal{G}_\uparrow^{(0)}$ and $\mathcal{G}_\downarrow^{(0)}$ are the bare Matsubara-Green's functions of the majority and minority component, and $\beta = 1/k_BT$ is the inverse temperature. $\omega_n = (2n+1)\pi/\beta$ and $\Omega_n = 2\pi n/\beta$ with $n \in \mathbb{Z}$ denote fermionic and bosonic Matsubara frequencies, respectively. After evaluating the Matsubara summation and analytic continuation, the vertex part can be calculated analytically at $T = 0$. In the regime $h > \mu$ (i.e., essentially beyond the Clogston-Chandrasekhar field $h > h_c \approx 0.96\mu$), one obtains for $\mathbf{q} = 0$, $\omega > -2\mu$

$$\Gamma^R(\mathbf{0}, \omega) = \frac{2\pi^2}{mk_{F\uparrow}}\left\{-\frac{\pi}{2k_{F\uparrow}|a|} - 1 + \frac{1}{2}\sqrt{\frac{\omega+2\mu}{2\mu_\uparrow}} \times \left[\ln\left|\frac{1+\sqrt{\frac{\omega+2\mu}{2\mu_\uparrow}}}{1-\sqrt{\frac{\omega+2\mu}{2\mu_\uparrow}}}\right| + i\pi\Theta(\omega-2h)\right]\right\}^{-1}, \tag{10}$$

where $\Theta(x)$ is the unit step function and $k_{F\uparrow}$ is defined via $k_{F\uparrow} = \sqrt{2m\mu_\uparrow}/\hbar$. For $h > \mu$ the retarded vertex $\Gamma^R(\mathbf{q} = 0, \omega)$ has a single pole on the real axis at $\omega_0^+ = 2h - \Omega_+$ with $\Omega_+ > 0$ (note that for $h < \mu$ the vertex has two real poles). Physically, this pole describes an excitation in which two fermions with opposite spin and vanishing total momentum form a pair at the Fermi energy of the majority component with binding energy Ω_+. A similar structure was first discussed for weak coupling by Aleiner and Altshuler [18] in the context of small superconducting grains. Remarkably, as shown in Fig. 2, the pair binding energy in units of $\mu_\uparrow$ is constant for $h > \mu$ and agrees well with the value $0.6\mu_\uparrow$ for the binding energy of a single down spin in the presence of a Fermi sea of majority atoms as calculated by Chevy [16]. The retarded self-energy for the minority component in the normal state is given by

$$\Sigma_\downarrow^R(\mathbf{k}, \omega) = \int \frac{d^3q}{(2\pi)^3}\frac{dz}{\pi}\{n_B(z)G_{A,\uparrow}^{(0)}(\mathbf{q}-\mathbf{k}, z-\omega) \times \mathrm{Im}\Gamma^R(\mathbf{q}, z) - n_F(z)\mathrm{Im}G_{R,\uparrow}^{(0)}(\mathbf{q}-\mathbf{k}, z) \times \Gamma^R(\mathbf{q}, z+\omega)\}, \tag{11}$$

with n_B and n_F denoting the Bose and Fermi distributions.

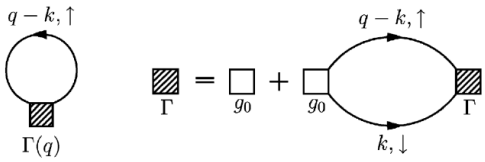

FIG. 1. Lowest order self-energy diagram for the minority component ($\downarrow$) Green's function and Bethe-Salpeter equation for the vertex part in ladder approximation.

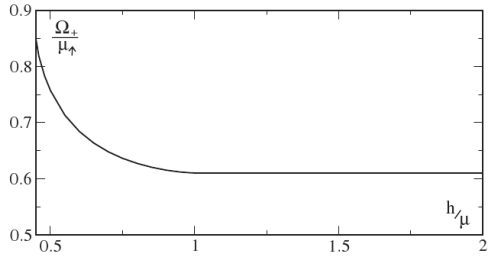

FIG. 2. Pair binding energy Ω_+ in units of $\mu_\uparrow$ at unitarity as a function of h at $T = 0$. For $h > \mu$ the binding energy is constant and given by $\Omega_+ = 0.61\mu_\uparrow$.

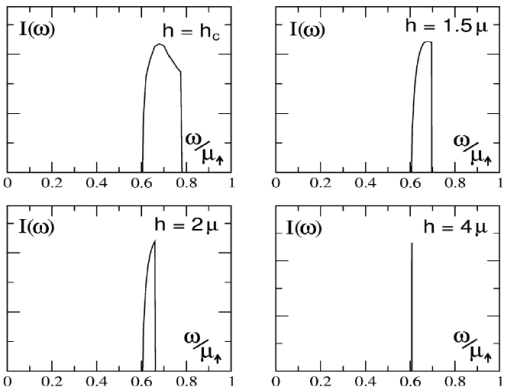

FIG. 3. rf spectra at unitarity for different imbalances at $T = 0$ (Intensity in arbitrary units; $h_c = 0.96\mu$).

This result enables us to calculate rf spectra explicitly in the limit of vanishing g_{23} and g_{13}, where the expectation value in Eq. (2) can be factorized. In this case, one obtains [4,5]

$$I(\omega) \sim \int \frac{d^3k}{(2\pi)^3} \mathrm{Im} G_{\downarrow}^{R}(\mathbf{k}, \varepsilon_{\mathbf{k}} - \omega - \mu_{\downarrow}) n_F(\varepsilon_{\mathbf{k}} - \omega - \mu_{\downarrow}),$$

if state $|3\rangle$ is initially empty. In Fig. 3 we have numerically evaluated the resulting rf spectra at unitarity for different fields above the Clogston-Chandrasekhar limit. The calculation explains two features which are seen in the experimental data [6], namely, the shift of the rf peak due to pairing fluctuations in the normal state and the decreasing linewidth with increasing population imbalance. The onset of the rf spectrum coincides with the pair binding energy $\Omega_+ \approx 0.6\mu_{\uparrow}$ for $h > h_c$, which is independent of the imbalance. In the presence of a finite $|1\rangle - |3\rangle$ interaction, the detailed spectrum $I(\omega)$ cannot be calculated analytically. Its first moment, however, is again determined by the sum rule Eq. (5). Evaluating the interaction energy $\langle H'_{12} \rangle$ using the variational wave function of Chevy [16], it turns out that the resulting average rf shift for an almost completely polarized gas is equal to $\bar{\omega} = -0.34\hbar k_{F\uparrow}/m a_{13}$. Because of the sharpness of the peak in this limit, the average shift in the strongly imbalanced gas coincides with the experimentally observed peak position. For the parameters in [13], we obtain an average rf shift $\bar{\omega} = 2\pi \times 17$ kHz at the trap center for strong imbalance, close to the observed value in the balanced case. Our theory thus accounts for the observation by Schunck *et al.* [6], where an average over the trap is involved, that there is hardly any difference in the rf shift between the balanced and strongly imbalanced gas.

In conclusion, we have given a theory of rf spectra in ultracold Fermi gases which includes interactions between all three states involved. In the balanced unitary gas, the average rf shift is proportional to $-s v_F/a_{13}$, where s is a universal constant characterizing the fermion momentum distribution at large wave vectors. In the imbalanced case, the rf spectrum exhibits a sharp peak arising from the binding energy of a $\uparrow\downarrow$ -pair which is finite even in the nonsuperfluid state. Including a finite value of a_{13}, the resulting average shift is close to the peak shift in the balanced case.

We gratefully acknowledge very helpful discussions with W. Rantner, Yong-il Shin, and M. Zwierlein. This work was supported by the DFG Forschergruppe "Strong Correlations in multiflavor ultracold Quantum Gases".

Note added in proof.—Equivalent results for the rf shift of balanced gases have been obtained independently by Baym *et al.* [19]. In fact, our value for the prefactor in $\bar{\omega} = -0.46 v_F/a_{13}$ agrees well with the value obtained in this reference, using a different method.

[1] P. Lee, N. Nagaosa, and X. G. Wen, Rev. Mod. Phys. **78**, 17 (2006).
[2] See, e.g., I. Bloch, J. Dalibard, and W. Zwerger, arXiv:0704.3011.
[3] C. Chin *et al.*, Science **305**, 1128 (2004).
[4] J. Kinnunen, M. Rodriguez, and P. Torma, Science **305**, 1131 (2004).
[5] Y. He, Q. Chen, and K. Levin, Phys. Rev. A **72**, 011602 (2005).
[6] C. H. Schunck *et al.*, Science **316**, 867 (2007).
[7] S. Gupta *et al.*, Science **300**, 1723 (2003).
[8] Z. Yu and G. Baym, Phys. Rev. A **73**, 063601 (2006).
[9] M. W. Zwierlein *et al.*, Phys. Rev. Lett. **91**, 250404 (2003).
[10] S. Tan, arXiv:condmat/0505200.
[11] C. Chin and P. S. Julienne, Phys. Rev. A **71**, 012713 (2005).
[12] R. Haussmann *et al.*, Phys. Rev. A **75**, 023610 (2007). Note that the dependence $n_{\mathbf{k}} \rightarrow C/k^4$ and the corresponding value of $s \approx 0.1$ at T_c has been determined earlier in R. Haussmann, Phys. Rev. B **49**, 12 975 (1994).
[13] Y. Shin *et al.*, Phys. Rev. Lett. **99**, 090403 (2007).
[14] The values for a_{13} have been taken from M. Bartenstein *et al.*, Phys. Rev. Lett. **94**, 103201 (2005).
[15] C. Lobo *et al.*, Phys. Rev. Lett. **97**, 200403 (2006).
[16] F. Chevy, Phys. Rev. A **74**, 063628 (2006).
[17] R. Combescot *et al.*, Phys. Rev. Lett. **98**, 180402 (2007).
[18] I. L. Aleiner and B. L. Altshuler, Phys. Rev. Lett. **79**, 4242 (1997).
[19] G. Baym *et al.*, arxiv:0707.0859.

PHYSICAL REVIEW A **80**, 053605 (2009)

Polaron-to-molecule transition in a strongly imbalanced Fermi gas

M. Punk,[1] P. T. Dumitrescu,[2] and W. Zwerger[1]
[1]*Physik Department, Technische Universität München, James-Franck-Strasse, D-85748 Garching, Germany*
[2]*Jesus College, University of Cambridge, Cambridge CB5 8BL, United Kingdom*
(Received 10 August 2009; published 6 November 2009)

A single down-spin fermion with an attractive zero-range interaction with a Fermi sea of up-spin fermions forms a polaronic quasiparticle. The associated quasiparticle weight vanishes beyond a critical strength of the attractive interaction, where a many-body bound state is formed. From a variational wave function in the molecular limit, we determine the critical value for the polaron-to-molecule transition. The value agrees well with the diagrammatic Monte Carlo results of Prokof'ev and Svistunov and is consistent with recent rf-spectroscopy measurements of the quasiparticle weight by Schirotzek *et al.* [Phys. Rev. Lett. **102**, 230402 (2009)]. In addition, we calculate the contact coefficient of the strongly imbalanced gas, using the adiabatic theorem of Tan and discuss the implications of the polaron-to-molecule transition for the phase diagram of the attractive Fermi gas at finite imbalance.

DOI: 10.1103/PhysRevA.80.053605 PACS number(s): 03.75.Ss, 03.75.Hh

I. INTRODUCTION

The physics of single particles immersed in an environment is ubiquitous in physics. It appears, for example, in the large polaron problem where a single electron is dressed by its interaction with phonons [1] or in models for dissipation and decoherence in quantum mechanics [2,3]. In recent years, new directions for exploring quantum many-body problems have been opened through ultracold atoms [4]. In particular, for degenerate Fermi gases, the interaction strength can be tuned over a wide range using Feshbach resonances. This allows us to study impurity problems in a fermionic environment. A specific example is a gas of fermionic ^{6}Li, where the two lowest hyperfine states are populated in a highly imbalanced situation. For this system, recent experiments have shown that the minority atoms ("down spins") apparently form a liquid of quasiparticles [5]. Due to the strong attractive interaction to the up-spin Fermi sea, the associated quasiparticle weight—as determined from a sharp peak in the rf spectrum—is found to vanish beyond a critical interaction strength. This transition may be interpreted as the one, in which a single $\downarrow$ fermion immersed in sea of $\uparrow$ fermions can no longer propagate as a quasiparticle but forms a many-body bound state with the Fermi sea. The existence of such a transition has been predicted by Prokof'ev and Svistunov [6,7]. Using a diagrammatic Monte Carlo method, they have shown that, for strong attractive interactions, a molecular state is energetically favored compared to the one in which the single down-spin forms a polaronic quasiparticle in the up-spin Fermi sea. In the present work, we analyze this problem by a simple variational wave function. It provides an analytically tractable model for the physics on the molecular side, thus complementing the variational description put forward by Chevy [8] for the polaronic quasiparticle. Our wave function gives a ground-state energy that matches perfectly the results of the diagrammatic Monte Carlo method. Moreover, it describes correctly the three-body physics of repulsive atom-dimer interactions in the deep molecular limit and has zero residue for the down-spin Green's function. The variational wave function is also used to determine the saturation field h_s beyond which a two-component Fermi gas is fully polarized and the behavior of the so-called contact coefficient introduced by Tan [9] in the limit of strong imbalance.

II. FERMI POLARON AND ITS QUASIPARTICLE WEIGHT

A simple variational wave function for the $(N+1)$-particle problem of a single down-spin fermion immersed in a sea of spin-up fermions has been introduced by Chevy [8]. It is based on an expansion up to single particle-hole excitations around the unperturbed Fermi sea

$$|\psi_0\rangle = \left(\phi_0 d_{\mathbf{0}}^\dagger + \sum_{\mathbf{k},\mathbf{q}}{}' \phi_{\mathbf{kq}} d_{\mathbf{q}-\mathbf{k}}^\dagger u_{\mathbf{k}}^\dagger u_{\mathbf{q}}\right)|\mathrm{FS}_\uparrow^N\rangle. \tag{2.1}$$

Here and in the following sums on $\mathbf{k}$ and $\mathbf{q}$ with a prime are restricted to $k > k_F$ and $q < k_F$, respectively. Moreover, $|\mathrm{FS}_\uparrow^N\rangle$ is the N-particle Fermi sea and the creation operators of up and down fermions with momentum $\mathbf{k}$ are denoted by $u_{\mathbf{k}}^\dagger$ and $d_{\mathbf{k}}^\dagger$. Despite the restriction to single particle-hole excitations, which is difficult to justify for the relevant case of zero-range interactions that can create particle-hole pairs at arbitrary momentum, Monte Carlo calculations show that the ansatz (2.1) gives a ground-state energy that is very accurate, in particular at unitarity, where the scattering length a is infinite [6,7]. The reason why the leading term in an expansion in the number of particle-hole excitations gives very good results for the ground-state energy can be traced back to the decoupling of higher-order terms for vanishing hole momenta $\mathbf{q}=0$ [10], i.e., contributions with more than one particle-hole excitation interfere destructively.

The wave function (2.1) describes the added down-spin as a quasiparticle dressed by its interaction with the up-spin Fermi sea. The virtual cloud of particle-hole excitations leads to a quasiparticle energy

$$E(\mathbf{p}) = A\varepsilon_F + \frac{\mathbf{p}^2}{2m^\star} + \cdots \tag{2.2}$$

at low momenta $|\mathbf{p}| \ll k_F$ that contains a "binding energy" $A\varepsilon_F < 0$ of a single down-spin to the Fermi sea and an effective mass $m^\star$ [11]. Here, the Fermi energy is defined by $\varepsilon_F = k_F^2/(2m)$ (we use $\hbar = 1$ throughout the paper) with a Fermi momentum k_F that is related to the up-spin density by the standard relation $n_\uparrow = k_F^3/(6\pi^2)$ for a single-component Fermi gas. Since we are interested in the limit of vanishing down-spin density $n_\downarrow \to 0$, these are the relevant energy and momentum scales. The dimensionless coefficient A and the effective mass $m^\star$ have been determined from variational Monte Carlo calculations at the unitarity point [11] and from a T-matrix approximation at arbitrary values of the dimensionless interaction strength $v = 1/(k_F a)$ [12]. Very recently they have also been measured experimentally, giving $A \approx -0.64(7)$ [5] and $m^\star/m = 1.17(10)$ [13] at unitarity, in rather good agreement with the theoretical predictions.

From a many-body point of view, the criterion that a single added down-spin is indeed a proper quasiparticle can be expressed by defining the quasiparticle residue $Z_\downarrow$ from the long-time limit

$$Z_\downarrow = \lim_{t\to\infty} |G_\downarrow(\mathbf{p} = 0, t)| \neq 0 \tag{2.3}$$

of the down-spin Green's function at zero momentum. Within the variational wave function (2.1) this residue is simply given by the probability $Z_\downarrow = |\phi_0|^2$ that an added down-spin at momentum $\mathbf{p} = 0$ is not mixed with plane waves at nonzero momenta $\mathbf{q} - \mathbf{k} \neq 0$ through particle-hole excitations. The fact that the coefficient $|\phi_0|^2$ of the Chevy wave function coincides with the quasiparticle weight can be derived formally by noting that the ansatz (2.1) is equivalent to a non-self-consistent T-matrix approach for the down-spin Green's function, which sums the particle-particle ladder for the vertex part $\Gamma(\mathbf{k}, \omega)$ [12]. It is then straightforward to see that $|\phi_0|^2 = |1 - \partial_\omega \Sigma|_{\omega=0}|^{-1}$ coincides with the standard definition of the quasiparticle weight via the energy derivative of the down-spin self-energy $\Sigma(\mathbf{p}, \omega)$ at zero frequency and momentum. The numerical value of $Z_\downarrow$ at unitarity $v = 0$ is $Z_\downarrow(v = 0) \simeq 0.78$ within the Chevy ansatz. This is much larger than the experimentally observed value $Z_\downarrow = 0.39(9)$, which is likely to be a lower bound, however [5]. Smaller values $Z_\downarrow(v = 0) = 0.47$ of the quasiparticle weight at unitarity are found from a $1/N$ expansion of the attractive fermion problem at strong imbalance, which is equivalent to a non-self-consistent T-matrix approximation with the bare chemical potential [14].

In Fig. 1 we show the quasiparticle residue $Z_\downarrow$ for the minority fermion as a function of $v = 1/(k_F a)$ within the ansatz (2.1) in comparison with the recent experimental results [5]. Apparently, the expansion up to single particle-hole excitations considerably overestimates the quasiparticle residue even though it gives reliable results for the ground-state energy. A much more basic shortcoming of the ansatz (2.1), however, appears if one considers the Bose-Einstein condensate (BEC) limit $v \gg 1$. Indeed, the ansatz predicts a finite value of $Z_\downarrow$ at arbitrary interaction strengths, even in the deep molecular limit. In this limit, however, an added down-spin will form a bound state with one of the up-spin fermions and can no longer propagate as a coherent quasiparticle. One thus expects that $Z_\downarrow$ vanishes identically beyond a critical strength $v_M > 0$ of the interaction, consistent with the experimental findings [5]. It is important to note that the formation of the bound state is a genuine many-body effect at any finite density of the up-spin Fermi sea. Indeed, the binding is of a two-body nature only in the trivial limit $v \gg 1$ (that is, effectively, for $k_F \to 0$), where the bound state is formed with a single up-spin fermion. By contrast, just beyond the critical value v_M, the down-spin is effectively compensated by forming a singlet with many up-spin fermions, somewhat similar to the physics of a localized Kondo spin interacting antiferromagnetically with a sea of conduction electrons at temperatures much below the Kondo temperature [15]. Note, however, that in the Kondo problem the impurity spin is not fixed and the transition from an uncompensated spin to an effective singlet state appears as a continuous crossover from high to low temperatures. In the present problem, instead, there is a discontinuous transition in the ground state as a function of the attractive coupling v.

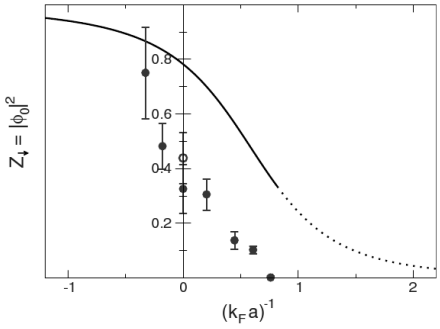

FIG. 1. (Color online) Quasiparticle residue $Z_\downarrow$ of the minority fermion as a function of $(k_F a)^{-1}$, calculated using Chevy's variational ansatz (2.1). In the regime where the ansatz (2.1) breaks down, $Z_\downarrow$ is drawn as a dotted line. The red dots correspond to the experimentally measured quasiparticle residue from the MIT group [5] at a minority concentration of 5%.

An indication that the variational wave function (2.1) is not applicable for strong attractive interactions is provided by considering the Thouless criterion for a superfluid instability in which up and down spins are paired in an s-wave superfluid [16]. Evaluating the relevant vertex function within the T-matrix approximation for arbitrary values of the down-spin chemical potential $\mu_\downarrow$, it is found that the Thouless criterion $\Gamma^{-1}(\mathbf{k} = 0, \omega = 0) = 0$ leads to a critical value for $\mu_\downarrow$ that is below the value $\mu_\downarrow = E(\mathbf{p} = 0)$ obtained from the ground-state energy of the variational state (2.1) provided that $v \geq 1.27$. A second argument that indicates the breakdown of the ansatz (2.1) in the regime $v \gg 1$ is the behavior of the ground-state energy. Indeed, in a systematic expansion in powers of the scattering length $a \to 0^+$ the ground-state energy of a single added down-spin relative to the free up-spin Fermi sea is expected to be of the form

$$E \overset{a\to 0^+}{=} E_b - \varepsilon_F + g_{ad} n_\uparrow + O(a^2). \tag{2.4}$$

Its leading contribution is just the molecular binding energy $E_b = -1/(ma^2) < 0$. The contribution ε_F of order a^0 accounts for the removal of one $\uparrow$ fermion from the Fermi sea that is required for the formation of the molecule. The last term, of order a, is the mean-field repulsion between the molecule and the Fermi sea. Its interaction strength $g_{ad} = 3\pi a_{ad}/m$ is related to the exact atom-dimer scattering length $a_{ad} = 1.18a$ that has first been calculated in connection with neutron-deuteron scattering [17] (for a recent derivation in the cold gas context, see Petrov *et al.* [18]). It turns out, however, that the variational ansatz (2.1) leads to $E \overset{a\to 0^+}{=} E_b - \varepsilon_F/2 + O(a)$, which is too high by $\varepsilon_F/2$ compared to the exact asymptotics (2.4). The reason for this discrepancy can be seen easily from the structure of Chevy's wave function. On the BEC side, the dominant contribution comes from the $q = 0$ terms, i.e.,

$$\sum_{\mathbf{k}}{}' \phi_{\mathbf{k},0} d^\dagger_{-\mathbf{k}} u^\dagger_{\mathbf{k}} u^\dagger_{\mathbf{0}} |\mathrm{FS}^N_\uparrow\rangle \tag{2.5}$$

describing the molecule formation of up and down spins with opposite momenta. This contribution is not optimal, however, since it creates a hole in the center of the $\uparrow$-Fermi sphere. Energetically, it would be favorable to replace $u_{\mathbf{0}}|\mathrm{FS}^N_\uparrow\rangle$ with a $(N-1)$-particle Fermi sea $|\mathrm{FS}^{N-1}_\uparrow\rangle$, leading to a ground-state energy that is lower by ε_F. Within the ansatz (2.1), this would require terms with an arbitrary number of particle-hole excitations in order to reshuffle the Fermi sea in such a way that the hole vanishes.

III. VARIATIONAL ANSATZ IN THE MOLECULAR REGIME

In order to describe the physics of bound-state formation in the regime $v \gg 1$, we propose a variational ansatz for the $(N+1)$-body problem that complements the ansatz (2.1) describing a Fermi polaron with a finite quasiparticle residue. Our ansatz gives the exact behavior (2.4) of the ground-state energy in the BEC limit up to linear order in a. The associated variational wave function

$$|\psi_0\rangle = \left(\sum_{\mathbf{k}}{}' \xi_{\mathbf{k}} d^\dagger_{-\mathbf{k}} u^\dagger_{\mathbf{k}} + \sum_{\mathbf{k}',\mathbf{k},\mathbf{q}}{}' \xi_{\mathbf{k}'\mathbf{k}\mathbf{q}} d^\dagger_{\mathbf{q}-\mathbf{k}-\mathbf{k}'} u^\dagger_{\mathbf{k}'} u^\dagger_{\mathbf{k}} u_{\mathbf{q}} \right) |\mathrm{FS}^{N-1}_\uparrow\rangle \tag{3.1}$$

is a natural generalization of the Chevy ansatz and is constructed by adding a $(\uparrow,\downarrow)$ pair to a $(N-1)$-particle Fermi sea of $\uparrow$ fermions, together with the leading term in an expansion in particle-hole excitations. Again, sums on $\mathbf{k}$, $\mathbf{k}'$, and $\mathbf{q}$ are restricted to $k, k' > k_F$ and $\mathbf{q} < k_F$, respectively. The first term accounts for the formation of the molecule in the presence of the $\uparrow$-Fermi sea and gives the correct next-to-leading-order ground-state energy in the BEC limit, avoiding the problem of creating a hole in the $\uparrow$-Fermi sea. The single particle-hole excitation in the second term describes the leading-order contribution to the interaction of the dimer with the Fermi sea apart from Pauli-blocking effects that are already accounted for in the first term. An important feature brought about by the inclusion of the second term in Eq. (3.1) is that it amounts to an exact treatment of the three-particle problem. Indeed, as is shown in detail in the Appendix, the set of coupled equations (3.6)–(3.9) that determine the coefficients of the variational many-body wave function reduce, in the three-particle limit, precisely to the integral equation for the exact solution of the three-body problem by Skorniakov and Ter-Martirosian [17]. As a result, the exact atom-dimer scattering length $a_{ad} = 1.18a$ appears in the asymptotic behavior of the ground-state energy (2.4), giving rise to the correct next-to-next-to-leading-order behavior of the ground-state energy in the BEC limit.

Obviously, the ansatz (3.1) is not capable of describing the whole range of scattering lengths correctly. In particular, it does not capture the weak-coupling limit $a \to 0^-$. Indeed, the $\downarrow$ fermion in the first term is always added at momenta $k > k_F$, leading to a ground-state energy that is too high by ε_F in the weak-coupling limit. Our ansatz (3.1) is therefore complementary to the Chevy wave function (2.1), which correctly describes the situation at weak coupling up to and slightly beyond the unitarity limit.

From a physical point of view, the two variational wave functions (2.1) and (3.1) characterize very different ground states. Chevy's ansatz describes a Fermi polaron with a finite quasiparticle residue, which allows us to build a normal Fermi liquid at a finite concentration of the down-spin fermions, provided that interactions between the quasiparticles have no attractive channels (see Sec. IV below). By contrast, the wave function (3.1) describes a bosonic molecule interacting with a Fermi sea. At a finite concentration $n_\downarrow \neq 0$, the resulting ground state is expected to be a superfluid, coexisting with unpaired up-spin fermions. The critical coupling v_M, where the ground-state energies of the two variational wave functions intersect, is thus expected to separate a normal fluid from a superfluid ground state of the attractive Fermi gas in the limit of very strong imbalance.

The variational ansatz (3.1) is based on a single channel model that describes the attractive interactions between both spin states. For computational purposes, however, it turns out to be easier to start from the more general two-channel model, which is defined by the Hamiltonian

$$H = \sum_{\mathbf{p}} \left(\frac{\varepsilon_{\mathbf{p}}}{2} + \nu_0 \right) b^\dagger_{\mathbf{p}} b_{\mathbf{p}} + \sum_{\mathbf{p},\sigma} \varepsilon_{\mathbf{p}} c^\dagger_{\mathbf{p},\sigma} c_{\mathbf{p},\sigma} + \frac{g_0}{\sqrt{V}} \sum_{\mathbf{p}',\mathbf{p}} \left(b^\dagger_{\mathbf{p}} c_{\mathbf{p}-\mathbf{p}',\uparrow} c_{\mathbf{p}',\downarrow} + \mathrm{H.c.} \right). \tag{3.2}$$

Here, $b^\dagger_{\mathbf{p}}$ denotes the bosonic creation operator of a molecule with momentum $\mathbf{p}$ and $c^\dagger_{\mathbf{p},\sigma}$ are the fermionic creation operators for the two species $\sigma = \uparrow, \downarrow$. The free particle dispersion is denoted by $\varepsilon_{\mathbf{p}} = p^2/(2m)$ and the factor of 1/2 in the first term accounts for the factor of 2 in the molecule to single fermion mass ratio. The bare values of the detuning ν_0 and the Feshbach coupling strength g_0 can be related to the physical s-wave scattering length a and the interaction range r_0 via [19]

$$\frac{\nu_0}{g_0^2} = -\frac{m}{4\pi a} + \frac{1}{V}\sum_{\mathbf{p}} \frac{1}{2\varepsilon_{\mathbf{p}}}, \tag{3.3}$$

$$r_0 = -\frac{8\pi}{g_0^2 m^2}. \tag{3.4}$$

The two-channel Hamiltonian (3.2) is equivalent to a single-channel model in the interesting limit of zero-range interactions $r_0 \to 0$ (i.e., for broad Feshbach resonances), as can be seen easily by integrating out the bosonic degrees of freedom.

The corresponding variational ansatz to Eq. (3.1) in the two-channel model has two additional terms ($\sim \eta_0, \eta_{\mathbf{kq}}$) where the closed-channel state is occupied

$$|\psi_0\rangle = \left(\eta_0 b_{\mathbf{0}}^\dagger + \sum_{\mathbf{k}}{}' \xi_{\mathbf{k}} d_{-\mathbf{k}}^\dagger u_{\mathbf{k}}^\dagger + \sum_{\mathbf{k},\mathbf{q}}{}' \eta_{\mathbf{kq}} b_{\mathbf{q}-\mathbf{k}}^\dagger u_{\mathbf{k}}^\dagger u_{\mathbf{q}} + \sum_{\mathbf{k}',\mathbf{k},\mathbf{q}}{}' \xi_{\mathbf{k}'\mathbf{kq}} d_{\mathbf{q}-\mathbf{k}-\mathbf{k}'}^\dagger u_{\mathbf{k}'}^\dagger u_{\mathbf{k}}^\dagger u_{\mathbf{q}} \right) |\mathrm{FS}_\uparrow^{N-1}\rangle. \tag{3.5}$$

Calculating the expectation value $\langle\psi_0|\hat{H}-E|\psi_0\rangle$, taking the derivatives with respect to the infinite set of variational parameters η_0, $\xi_{\mathbf{k}}$, $\eta_{\mathbf{kq}}$, $\xi_{\mathbf{k}'\mathbf{kq}}$, and setting them equal to zero leads to the following set of coupled equations:

$$(E + \varepsilon_F - \nu_0)\eta_0 = -\frac{g_0}{\sqrt{V}}\sum_{\mathbf{k}}{}' \xi_{\mathbf{k}}, \tag{3.6}$$

$$(E + \varepsilon_F - 2\varepsilon_{\mathbf{k}})\xi_{\mathbf{k}} = -\frac{g_0}{\sqrt{V}}\eta_0 + \frac{g_0}{\sqrt{V}}\sum_{\mathbf{q}}{}' \eta_{\mathbf{kq}}, \tag{3.7}$$

$$\left(E + \varepsilon_F - \nu_0 - \frac{\varepsilon_{\mathbf{q}-\mathbf{k}}}{2} - \varepsilon_{\mathbf{k}} + \varepsilon_{\mathbf{q}}\right)\eta_{\mathbf{kq}} = \frac{g_0}{\sqrt{V}}\xi_{\mathbf{k}} - \frac{2g_0}{\sqrt{V}}\sum_{\mathbf{k}'}{}' \xi_{\mathbf{k}'\mathbf{kq}}, \tag{3.8}$$

$$(E + \varepsilon_F - \varepsilon_{\mathbf{q}-\mathbf{k}-\mathbf{k}'} - \varepsilon_{\mathbf{k}'} - \varepsilon_{\mathbf{k}} + \varepsilon_{\mathbf{q}})\xi_{\mathbf{k}'\mathbf{kq}} = -\frac{g_0}{2\sqrt{V}}(\eta_{\mathbf{kq}} - \eta_{\mathbf{k}'\mathbf{q}}). \tag{3.9}$$

Note that the ground-state energy E is measured with respect to the N-particle Fermi sea, which explains the occurrence of the ε_F terms in the above equations. Moreover, using the N-particle Fermi sea, as the reference scale, the ground-state energy E is equivalent to the chemical potential $\mu_\downarrow \equiv E$ of the single down-spin.

A. No particle-hole excitation

Neglecting for a moment the contribution of particle-hole excitations in Eq. (3.5), i.e., setting $\eta_{\mathbf{kq}} = \xi_{\mathbf{k}'\mathbf{kq}} = 0$, the ground-state energy is determined by Eqs. (3.6) and (3.7) alone. Performing the integrations and taking the zero-range limit $r_0 \to 0$, they reduce to a simple transcendental equation

$$\frac{\pi}{2k_F a} = 1 + \sqrt{-\frac{E+\varepsilon_F}{2\varepsilon_F}}\arctan\left(\sqrt{-\frac{E+\varepsilon_F}{2\varepsilon_F}}\right). \tag{3.10}$$

In the BEC limit $a \to 0^+$, Eq. (3.10) gives rise to a ground-state energy of the form (2.4). The associated atom-dimer scattering length, however, is given by its value $a_{ad}^{Born} = (8/3)a$ in the Born approximation. More generally, it turns out that Eq. (3.10) is exactly equivalent to the Thouless criterion $\Gamma^{-1}(\mathbf{k}=0,\ \omega=0)=0$ if the vertex function is calculated within a non-self-consistent T-matrix approach where only the particle-particle ladder is summed, as discussed in Sec. II. The resulting ground-state energy is below that of the Fermi polaron if $v \geq 1.27$.

B. Full variational treatment

In the general case $\eta_{\mathbf{kq}} \neq 0$, $\xi_{\mathbf{k}'\mathbf{kq}} \neq 0$, Eqs. (3.6)–(3.9) can be reduced to a single homogeneous Fredholm equation of the second kind for the variational parameters $\eta_{\mathbf{kq}}$ in the thermodynamic limit (again, the zero-range limit has been taken already)

$$\frac{1}{V^2}\sum_{\mathbf{k}',\mathbf{q}'}{}' K(E;\mathbf{k},\mathbf{q};\mathbf{k}',\mathbf{q}')\eta_{\mathbf{k}'\mathbf{q}'} = 0. \tag{3.11}$$

The associated Kernel $K(E;\mathbf{k},\mathbf{q};\mathbf{k}',\mathbf{q}')$ is given by

$$K = \frac{V\delta_{\mathbf{k},\mathbf{k}'}}{E_{\mathbf{k}}} - \frac{1}{\gamma E_{\mathbf{k}} E_{\mathbf{k}'}} - \frac{V\delta_{\mathbf{q},\mathbf{q}'}}{E_{\mathbf{k}'\mathbf{kq}}} - \alpha_{\mathbf{kq}} V^2 \delta_{\mathbf{k},\mathbf{k}'}\delta_{\mathbf{q},\mathbf{q}'} \tag{3.12}$$

with

$$E_{\mathbf{k}} \doteq E + \varepsilon_F - 2\varepsilon_{\mathbf{k}}, \tag{3.13}$$

$$E_{\mathbf{k}'\mathbf{kq}} \doteq E + \varepsilon_F - \varepsilon_{\mathbf{q}-\mathbf{k}-\mathbf{k}'} - \varepsilon_{\mathbf{k}} - \varepsilon_{\mathbf{k}'} + \varepsilon_{\mathbf{q}}, \tag{3.14}$$

$$\alpha_{\mathbf{kq}} \doteq -\frac{\nu_0}{g_0^2} - \frac{1}{V}\sum_{\mathbf{k}'}{}' \frac{1}{E_{\mathbf{k}'\mathbf{kq}}}, \tag{3.15}$$

$$\gamma \doteq \frac{\nu_0}{g_0^2} + \frac{1}{V}\sum_{\mathbf{k}}{}' \frac{1}{E_{\mathbf{k}}}. \tag{3.16}$$

Due to the isotropy of the system, the variational parameters $\eta_{\mathbf{kq}} \equiv \eta(k, q, \cos\theta_{\mathbf{kq}})$ depend only on the magnitudes of the two momenta $\mathbf{k}$ and $\mathbf{q}$ and the angle between them. This allows Eq. (3.11) to be reduced to a three-dimensional integral equation.

The ground-state energy E is now simply obtained by the condition that the Fredholm determinant of the kernel K vanishes. We evaluate the Fredholm determinant numerically by discretizing the integral equation using a Gauss-Legendre quadrature and calculating the determinant of the corresponding linear equation system. The order of the quadrature for the k, q, and $\cos\theta_{\mathbf{kq}}$ integral were chosen as 11, 11, and 4, leading to an error of $\sim 10^{-4}$ of the ground-state energy at the unitarity point $a \to \infty$, where the convergence is slowest.

The ground-state energy as function of $(k_F a)^{-1}$ is shown in Fig. 2. Apparently, our ansatz (3.1) leads to a ground-state

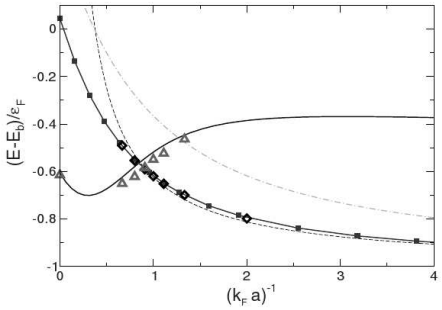

FIG. 2. (Color online) Ground-state energy $E-E_b$ [binding energy $E_b=-1/(ma^2)$ subtracted] in units of the Fermi energy ε_F as a function of $(k_Fa)^{-1}$. Blue solid line: Chevy's ansatz (2.1); red line with full squares: ansatz (3.1); black dashed line: BEC asymptotics (2.4); orange dashed-dotted line: Thouless criterion (3.10). The open black diamonds and green triangles correspond to the QMC results for the molecule and the polaron energies from Prokof'ev and Svistunov [6].

energy that is below that of Chevy's ansatz for interaction strengths larger than $(k_Fa)_M^{-1}=0.84$. This value is in good agreement with the diagrammatic Monte Carlo results by Prokof'ev and Svistunov [6,7], who obtained $(k_Fa)_M^{-1}=0.90$. In fact, the small discrepancy is entirely due to the fact that we intersect our molecular ground-state energy with that obtained using the Chevy wave function, which is not precise near v_M. The Monte Carlo results in turn give better values for the polaron energy, shifting the intersection slightly toward the BEC regime, as can be seen in Fig. 2. Yet, as far as the molecular ground-state energy is concerned, our results agree perfectly with the Monte Carlo data, down to the smallest coupling $v\simeq 0.6$ where they have been calculated.

It is interesting to note that the approximation $\mathbf{q}=0$ in the wave function (3.5) (i.e., pinning the hole wave vector at zero momentum) leads to a ground-state energy that differs from the calculation with the full wave function by at most 3% in the regime $(k_Fa)^{-1}>0.84$, where the ansatz is valid. The situation thus appears similar to that in the polaron case, where Combescot and Giraud [10] showed that an expansion in hole wave vectors works very well for Chevy's ansatz at unitarity.

C. Quasiparticle residue

We now show that the quasiparticle residue $Z_\downarrow$ of the $\downarrow$ fermion, which can be thought of as a kind of order parameter of the transition from the polaron to the molecular state, vanishes identically in the thermodynamic limit for the variational wave function (3.5) that gives a lower ground-state energy on the molecular side of the critical coupling v_M. Since the variational ground-state wave function does not allow us to calculate the full down-spin Green's function, definition (2.3) of the quasiparticle residue is not applicable. Instead, we use the standard connection between $Z_\downarrow$ and the jump in the momentum distribution at the Fermi momentum $k_{F\downarrow}$, and the latter is zero in the limit of a single down-spin. The momentum distribution of the $\downarrow$ fermion within the variational ansatz (3.5) is given by

$$n_{\mathbf{p}}^{\downarrow}=|\xi_{\mathbf{p}}|^2+2\sum_{\mathbf{k}'\mathbf{k}\mathbf{q}}{}'|\xi_{\mathbf{k}'\mathbf{k}\mathbf{q}}|^2\delta_{\mathbf{p},\mathbf{q}-\mathbf{k}'-\mathbf{k}} \tag{3.17}$$

and is normalized via

$$1=\sum_{\mathbf{p}}n_{\mathbf{p}}^{\downarrow}=\sum_{\mathbf{k}}{}'|\xi_{\mathbf{k}}|^2+2\sum_{\mathbf{k}'\mathbf{k}\mathbf{q}}{}'|\xi_{\mathbf{k}'\mathbf{k}\mathbf{q}}|^2. \tag{3.18}$$

The normalization condition requires the coefficients to scale with the system volume as $\xi_{\mathbf{k}}\sim 1/\sqrt{V}$ and $\xi_{\mathbf{k}'\mathbf{k}\mathbf{q}}\sim 1/V^{3/2}$. Since an upper bound to the quasiparticle residue $Z_\downarrow$ is given by the momentum distribution at $\mathbf{p}=0$ and $\xi_{\mathbf{p}}\equiv 0$ for $p<k_F$, we find that

$$Z_\downarrow\le n_{\mathbf{p}=0}^{\downarrow}=2\sum_{\mathbf{k}'\mathbf{k}\mathbf{q}}{}'|\xi_{\mathbf{k}'\mathbf{k}\mathbf{q}}|^2\delta_{\mathbf{q},\mathbf{k}'+\mathbf{k}}\sim\frac{1}{V}. \tag{3.19}$$

As a result, the quasiparticle residue $Z_\downarrow$ of the molecular wave function scales inversely with the volume of the system and thus vanishes in the thermodynamic limit. This is in contrast to Chevy's wave function, where $Z_\downarrow=|\phi_0|^2$ is always finite. The two wave functions (2.1) and (3.1) therefore indeed describe qualitatively different ground states. In particular, no sharp peak is expected in the minority rf spectrum at coupling strengths $v>v_M$, consistent with the experimental observation [5].

In the $\mathbf{q}=0$ approximation, which captures the essential properties of the variational ansatz (3.1), the quasiparticle residue $Z_\downarrow$ in fact vanishes identically. Indeed,

$$Z_\downarrow\le 2\sum_{\mathbf{k}}{}'|\xi_{-\mathbf{k}\mathbf{k}0}|^2=0 \tag{3.20}$$

since, as can be seen from Eq. (3.9), the coefficients $\xi_{-\mathbf{k}\mathbf{k}0}\propto\eta_{\mathbf{k}0}-\eta_{-\mathbf{k}0}=0$ vanish because $\eta_{\mathbf{k}0}$ only depends on the length of $\mathbf{k}$.

IV. CONTACT COEFFICIENT AND PHASE DIAGRAM

The analysis of the polaron-to-molecule transition in the previous section leaves two important questions open: what is the nature of the transition and what are its implications for the phase diagram of the strongly imbalanced gas? Now for the case of a single down-spin in an up-spin Fermi sea, the transition from a polaronic to a molecular state is a first-order transition, where the quasiparticle residue $Z_\downarrow$ exhibits a discontinuous jump from a finite value to zero at the critical coupling $v_M\simeq 0.9$. This is a result of the fact that the energies of the two ground states, which have different quantum numbers, cross with a finite slope at v_M (see Fig. 2). It is important to note that this crossing is not an artifact of extending the different variational states beyond their domain of validity. Indeed, as shown by Prokof'ev and Svistunov [6,7], both the polaronic and the molecular states exist as stable excitations for $v>v_M$ or $v<v_M$, respectively, because the phase space for decay vanishes linearly with the magnitude of the energy difference. Both states are thus reachable as metastable configurations coming from the weak coupling

or the molecular side, as expected for a first-order transition.

A different perspective on the first-order nature of the polaron-to-molecule transition is provided by considering the so-called contact coefficient C. As shown by Tan [9], the momentum distribution of Fermi gases with zero-range interactions generically decays with a power law $n_\sigma(k) \to C/k^4$ for large momenta. The associated coefficient C is identical for both spin components $\sigma = \uparrow, \downarrow$ [20] and is a measure of the probability that two fermions with opposite spins are close to each other [21]. Using the adiabatic theorem derived by Tan [22], the contact density can be determined from the derivative

$$\frac{\partial u}{\partial(1/a)} = -\frac{\hbar^2}{4\pi m} C \tag{4.1}$$

of the ground-state energy density $u = E/V$ with respect to the inverse scattering length. Now the definition of the down-spin chemical potential $\mu_\downarrow$ implies that the energy density u of the strongly imbalanced Fermi gas $n_\downarrow \ll n_\uparrow$ to linear order in the minority density $n_\downarrow$ is of the form

$$u = \frac{3}{5}\varepsilon_{F\uparrow} n_\uparrow + \mu_\downarrow n_\downarrow + \cdots, \tag{4.2}$$

where the first term is simply the energy of a noninteracting gas of spin-up fermions. The dimensionless contact coefficient s defined by $C = s k_F k_{F\downarrow}^3$ for a strongly imbalanced Fermi gas can thus be obtained from the derivative

$$s = \frac{1}{3\pi} \frac{\partial(-\mu_\downarrow/\varepsilon_F)}{\partial v} \tag{4.3}$$

of the negative down-spin chemical potential in units of the Fermi energy with respect to the coupling constant v. Since $\mu_\downarrow$ is precisely the energy E associated with adding a single down-spin, our result for the ground-state energy of the $(N+1)$-particle problem immediately gives the contact density of an almost fully polarized attractive Fermi gas (note that this applies even on the molecular side $v > v_M$, where the single added down-spin is not a propagating quasiparticle). The associated dimensionless constant s is shown in Fig. 3. It increases monotonically from weak coupling to unitarity and up to the critical coupling v_M. At this point, there is a discontinuous jump upward that reflects the transition to a molecular state. Note that the proportionality $C \sim k_{F\downarrow}^3 \sim n_\downarrow$ of the contact to the down-spin density makes C vanish in the limit of full polarization. This is expected, because the fully polarized gas at zero temperature is an ideal Fermi gas, with no tails in the momentum distribution. Apart from the jump at v_M, the behavior of the dimensionless contact coefficient s is rather close to that obtained for the contact coefficient $C = s\tilde{k}_F^4$ of the balanced superfluid along the BCS-BEC crossover [23] [note that the Fermi momentum $\tilde{k}_F$ of the balanced gas is related to that of the up-spin component used here by $k_F^3 = \tilde{k}_F^3(1+\sigma)$, where $\sigma = (n_\uparrow - n_\downarrow)/(n_\uparrow + n_\downarrow)$ is the degree of polarization at a fixed total number of particles]. Indeed, in weak coupling one obtains $s_{wc} = (2/3\pi v)^2$ from the mean-field attraction of the polaron to the up-spin Fermi sea, while $s \simeq 0.08$ at unitarity and $s_{BEC} = 4v/3\pi$ in the molecular limit, very similar to the behavior that is found for s in the balanced superfluid [23].

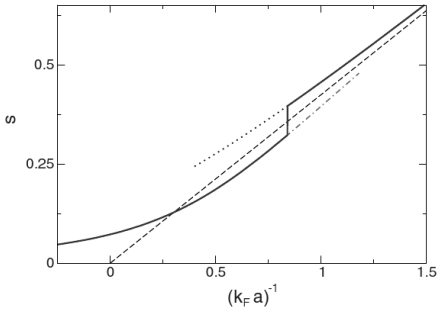

FIG. 3. (Color online) Dimensionless contact coefficient s as a function of $(k_F a)^{-1}$, calculated from the two variational wave functions (2.1) and (3.1). Within this approach s is discontinuous at the critical coupling v_M. The black dashed line marks the asymptotics in the molecular limit, where $s = 4v/3\pi$ is fixed by the two-particle bound-state wave function in momentum space.

The solution of the $(N+1)$-body problem for arbitrary coupling strengths v has also implications for the phase diagram of the imbalanced Fermi gas in the regime of near complete polarization. For a discussion of this issue, it is convenient to introduce an effective magnetic field h that couples to the two different spin states $\sigma = \uparrow, \downarrow$ in the standard form

$$\hat{H}' = -h(\hat{N}_\uparrow - \hat{N}_\downarrow) \tag{4.4}$$

of a "Zeeman" field that favors a finite population imbalance $\sigma = (n_\uparrow - n_\downarrow)/(n_\uparrow + n_\downarrow) > 0$. At a fixed total density n, the ground-state energy u per volume is then a function of n and h. It determines the chemical potentials of the majority and minority species from $\mu_{\uparrow,\downarrow} = \mu \pm h$, where $\mu = \partial u(n,h)/\partial n$ is the average chemical potential. In addition, it also fixes the imbalance from $n_\uparrow - n_\downarrow = -\partial u(n,h)/\partial h$. The choice of an ensemble with fixed values of n and h is convenient for a discussion of the ground-state phase diagram of the attractive Fermi gas at arbitrary coupling v, both in the homogeneous case and in the presence of a harmonic trap [24]. Indeed, there are two critical fields $h_c(v)$ and $h_s(v)$ that separate two simple limiting phases from a regime, in which nontrivial ground states are expected: the lower critical field h_c is defined by $\sigma(h) \equiv 0$ for $h < h_c$ and determines the boundary of the balanced superfluid phase (denoted by SF_0 in Fig. 4, following the notation used by Pilati and Giorgini [25]). The upper critical (or "saturation") field h_s, in turn, is defined by the condition of complete polarization $\sigma(h) \equiv 1$ for $h > h_s$. Since a single-component Fermi system has vanishing interactions in the ultracold limit, this regime is just an ideal Fermi gas, i.e., it is a normal fully polarized state. The qualitative structure of the zero-temperature phase diagram as a function of the interaction parameter $v = 1/(k_F a)$ and the effective magnetic field h in units of the bare Fermi energy ε_F of the fully polarized gas is shown in Fig. 4.

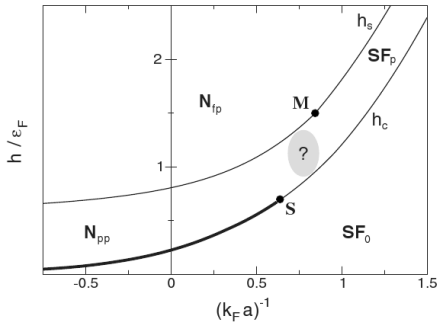

FIG. 4. Qualitative phase diagram of the imbalanced Fermi gas as a function of the inverse coupling strength $(k_F a)^{-1}$ and the effective magnetic field h/ε_F. The thick line indicates a first-order phase transition and the different phases are labeled as in [25], i.e., N_{fp}: fully polarized normal phase; N_{pp}: partially polarized normal phase; SF_0: balanced superfluid; SF_{p}: polarized superfluid. The points M and S are discussed in the text. The precise structure of the phase diagram in the nontrivial regime $h_c < h < h_s$ is likely to contain unconventional superfluid phases in addition to the N_{pp} and SF_{p} phases, which are not shown in our figure.

In this diagram, the upper line $h_s(v)$ is completely fixed by our calculation above of the energy $\mu_\downarrow$ associated with adding a single down-spin to an up-spin Fermi sea. Indeed, since $\mu_\uparrow \equiv \varepsilon_F$ along this line, we have $h_s = (\varepsilon_F - \mu_\downarrow)/2$. In terms of the constant $A(v)$ introduced in Eq. (2.2), this leads to $h_s/\varepsilon_F = (1-A)/2$, giving $h_s = 0.81\varepsilon_F$ at unitarity from the precise numerical value of the polaron energy [7]. On the molecular side, Eq. (2.4) gives

$$\frac{h_s}{\varepsilon_F} = v^2 + 1 - \frac{a_{ad}/a}{2\pi v} + \cdots, \tag{4.5}$$

which is very accurate even at $v = v_M$. The point M along this line separates a regime where a single down-spin is a well-defined fermionic quasiparticle from the one, in which it is bound to the up-spin Fermi sea. The first-order nature of the transition shows up as a discontinuity of the slope in $h_s(v)$ at M which is, however, hardly visible in Fig. 4. For a finite density of down spins, the point M appears as an end point of a line that separates a phase with a finite Fermi surface volume $\Omega_\downarrow \neq 0$ to its left from one with $\Omega_\downarrow = 0$ [26]. Using the generalized Luttinger theorem derived by Sachdev and Yang [27], the expected polarized superfluid (SF_p) phase on the molecular side has a condensate of "dimers" plus an up-spin Fermi sea, whose volume $\Omega_\uparrow = (2\pi)^3(n_\uparrow - n_\downarrow)$ is set by the imbalance. This is consistent with the naive picture that the density of unpaired up spins is simply $n_\uparrow - n_\downarrow$ even though the dimers in the vicinity of the transition are far from local $(\uparrow,\downarrow)$ pairs. In principle, this simple picture of the SF_p phase as a BEC coexisting with a sharp single Fermi surface of unpaired up spins is unstable with respect to p-wave pairing due to the induced interactions between the unpaired fermions through the superfluid [28]. In practice, the nontrivial superfluid phase of the unpaired up spins is exponentially suppressed for strong imbalance. Moreover, quantitative results for the p-wave instability can be derived only in second order in $1/v \ll 1$, where the resulting energy scales are exponentially small compared with ε_F. In practice, therefore, the phase with p-wave pairing among the unpaired up spins seems hardly accessible experimentally.

A nontrivial issue that has been neglected in the discussion so far is the question whether a gas of polarons or bound molecules is indeed stable at low but finite densities $n_\downarrow$. On the weak-coupling side, there is again an induced attractive interaction in the p-wave channel among both the up spins and the down spins, mediated by the other species. The ground state is thus expected to be a two-component p-wave superfluid and not a normal Fermi-liquid state [28]. Similar to the situation in the BEC limit, however, the energy scale for this instability is exponentially small in the regime where the calculation can be controlled. More importantly, as has been shown recently by Nishida [29], the effective interaction between two heavy down-spin fermions immersed in an up-spin Fermi sea is attractive in the p-wave channel only for weak coupling. Approaching unitarity, the p-wave interaction becomes repulsive. Assuming that this result carries over to the relevant case of equal masses of the up- and down-spin fermions, a finite density gas of down spins will indeed form a normal Fermi liquid at unitarity, as was implicitly assumed in the calculations of the equation of state and density profiles of the unitary gas beyond the critical imbalance $\sigma_c \simeq 0.4$, where the balanced superfluid is no longer stable [11,30]. On the molecular side, the phase immediately below the saturation field line $h_s(v)$ is expected to be a superfluid of $(\uparrow,\downarrow)$ pairs at a very low density $n_\downarrow \to 0$ immersed in an up-spin Fermi sea. The fact that the atom-dimer repulsion $a_{ad} = 1.18a$ is much larger than the dimer-dimer repulsion $a_{dd} = 0.6a$ [18], however, indicates that a low density gas of molecules tends to phase separate from the up-spin Fermi gas. This phase separation has indeed been found from an extended BCS description of the BCS-BEC crossover in an imbalanced gas [31–34]. It has recently been seen also in the variational Monte Carlo calculations by Pilati and Giorgini [25]. Their results indicate that a section between $v_N \simeq 0.73$ and a triple point at $v_T \simeq 1.7$ along the h_s line is actually a first-order line, where the polarized superfluid disappears with a finite jump in density as the effective field h increases through h_s. As shown above, the point M lies in the interval between v_N and v_T and thus the polaron-to-molecule transition would not be accessible at any finite minority density, at least not in an equilibrium situation. Clearly, our variational calculation for the single down-spin problem cannot address the question of phase separation. An unexpected feature of the h_s line in the presence of phase separation is the fact that the transition across h_s is predicted to be continuous up to v_N, first order between v_N and v_T, and continuous again for $v > v_T$. The rather large value $v_T \simeq 1.7$ up to which phase separation is predicted also appears surprising. Indeed, in this regime a mean-field theory describing a Fermi gas coexisting with a BEC of molecules gives for the energy per volume as a functional of the density difference $\delta n = n_\uparrow - n_\downarrow$ and the dimensionless field $\tilde{h} = h/\varepsilon_F$ the simple form

$$\frac{u(n,\delta n,h)}{\varepsilon_F} = \frac{3}{5}\left(\frac{\delta n}{n}\right)^{2/3}\delta n - v^2(n-\delta n) + \frac{\tilde{a}_{ad}}{2\pi v}\frac{(n-\delta n)\delta n}{n} + \frac{\tilde{a}_{dd}}{12\pi v}\frac{(n-\delta n)^2}{n} - \tilde{h}\delta n. \quad (4.6)$$

Here, $\tilde{a}_{ad}=a_{ad}/a$ and $\tilde{a}_{dd}=a_{dd}/a$ are the atom-dimer and the dimer-dimer scattering lengths measured in units of the atom-atom scattering length and $v=(k_F a)^{-1}$. The true ground-state energy density $u(n,h)$ as a function of the total density n and the effective magnetic field h is determined by the minimum of the Landau energy (4.6) with respect to the density imbalance

$$\frac{\partial(u/\varepsilon_F)}{\partial\delta n} = \left(\frac{\delta n}{n}\right)^{2/3} + v^2 + \frac{\tilde{a}_{ad}}{2\pi v}\left(1-2\frac{\delta n}{n}\right) + \frac{\tilde{a}_{dd}}{6\pi v}\left(\frac{\delta n}{n}-1\right) - \tilde{h} \overset{!}{=} 0. \quad (4.7)$$

This equation determines the imbalance $\sigma=\delta n/n$ as a function of the field h and, indeed, it correctly describes the exact asymptotic results for both the saturation field h_s and the lower critical field h_c in the limit $v \gg 1$ [see Eqs. (4.5) and (4.9)]. In this simple model, phase separation between a polarized superfluid phase and a fully polarized Fermi gas appears for coupling constants $v < v_{c,PS}$, below which the energy density (4.7) has a second minimum at full polarization $\sigma \equiv 1$. This occurs at

$$v_{c,PS} = \frac{3}{2\pi}\left(\tilde{a}_{ad} - \frac{\tilde{a}_{dd}}{6}\right). \quad (4.8)$$

With the exact values $\tilde{a}_{ad}=1.18$ and $\tilde{a}_{dd}=0.6$ one obtains $v_{c,PS}=0.516$, where the simple expansion (4.6), however, is no longer valid. From the calculation above, the triple point v_T beyond which phase separation appears in an almost fully polarized gas lies at a much smaller value of the coupling strengths than found previously [25,34]. At finite temperatures, phase separation is suppressed by the presence of a mixing entropy, which may explain that it is not observed in the experiments, where $T \approx 0.15 T_F$.

Concerning the lower critical field $h_c(v)$, its weak-coupling limit is determined by the well-known Chandrashekar-Clogston result $h_c=\Delta/\sqrt{2}$, beyond which the balanced BCS pairstate is unstable [35,36]. In the molecular limit $v \gg 1$, the critical field

$$\frac{h_c}{\varepsilon_F} = v^2 + \frac{1}{2\pi v a}\left(a_{ad} - \frac{a_{dd}}{6}\right) + \cdots \quad (4.9)$$

follows essentially the two-particle binding energy with corrections due to the atom-dimer and dimer-dimer scattering lengths a_{ad} and a_{dd}, respectively. At unitarity, $h_c=0.26\varepsilon_F$ is a universal constant times the bare up-spin Fermi energy ϵ_F [11]. As a result, there is a wide range $h_s/h_c=3.12$ between the balanced superfluid and the fully polarized gas, much larger than that found in an $N=\infty$ theory of the imbalanced attractive Fermi gas, where $h_s/h_c=1.24$ [37]. For $h > h_c$ the balanced superfluid is destroyed by the onset of a finite polarization $\sigma \neq 0$, which leads to a mismatch of the Fermi energies. An effective-field theory due to Son and Stephanov [38] indicates that the phase beyond the balanced superfluid exhibits a spatially varying superfluid order of the Fulde-Ferrell-Larkin-Ovchinnikov (FFLO) type as also found at weak coupling. The transition is first order with a jump both in polarization σ an total density, a situation that is also found in the case of a direct transition between a balanced superfluid and a partially polarized normal phase [11,30]. In an ensemble with a given density that is used here, the h_c line would then split into two distinct lines h_{c1} and h_{c2}, as noted by Sheehy and Radzihovsky [32]. In our diagram in Fig. 4, h_c denotes the boundary of the balanced superfluid at given density, which is well defined without specifying the state that is reached at nonzero polarization. The first-order nature of the transition is found only up to a splitting point S, beyond which the fermionic excitations have their minimum at $\mathbf{p}=0$. When this is the case, additional up-spin fermions can be added by filling up a Fermi surface whose volume $\Omega_\uparrow \sim \sigma \sim (h-h_c)^{3/2}$ increases continuously from zero. The transition from the balanced superfluid to a polarized superfluid with unpaired excess fermions is therefore continuous and preserves superfluidity. The precise location of the splitting point S has been determined recently from a calculation of the fermionic excitation spectrum along the BCS-BEC crossover of the balanced gas [23]. It is located at $v_S \simeq 0.63$ and $h_c(v_S)=\Delta \simeq 0.6\varepsilon_F$ at considerably larger coupling strengths than predicted by mean-field theory where the splitting point coincides with the zero crossing of the chemical potential (note the factor-of-$2^{1/3}$ difference with the result in Ref. [23], which is due to the fact that the up-spin Fermi wave vector and not that of the balanced case appears in our present coupling constant v). This is in agreement with the calculation of the splitting point within an $\epsilon=4-d$ expansion by Nishida and Son [39] but is larger than the value $v_S \simeq 0.5$ found for the splitting point in the Monte Carlo calculations of Pilati and Giorgini [25]. Note that the possibility of extracting the critical coupling v_S of the splitting point from a calculation of the balanced gas relies on the fact that the ground-state energy is independent of the field h in the whole regime $h \leq h_c$ because the polarization $\sigma=-n\partial u(n,h)/\partial h$ vanishes. The nature of the phase diagram near the splitting point has been discussed by Son and Stephanov [38] using an effective-field theory. In particular, the phase immediately beyond h_c is expected to be of the FFLO type, with a spatially oscillating superfluid order parameter that appears also in weak coupling beyond the Chandrasekhar-Clogston limit [40]. It is an open question of how this nontrivial superfluid evolves into a normal phase in which the two spin components each form a Fermi liquid. In fact it is this latter phase, which describes the experimentally observed density profiles [41] at unitary extremely well [11,30]. It is also an open issue of how to separate in detail the regime between the lower critical field and the saturation field into a regime where an imbalanced Fermi liquid or a polarized superfluid phase appears as ground states. In the phase diagram of Pilati and Giorgini, the first-order line that bounds the balanced superfluid up to the splitting point S extends as a first-order line up to h_s at the coupling v_N and then continues along h_s up to the tricritical point v_T.

V. CONCLUSIONS

From a variational wave function that describes the $(N+1)$-particle problem of a single down-spin interacting strongly with an up-spin Fermi sea, we have discussed the physics of the strongly imbalanced Fermi gas. In particular, we have focused our attention on the quasiparticle residue and the contact coefficient C. The latter exhibits a discontinuous jump at the polaron-to-molecule transition, which might be detected by measurements of the closed-channel fraction similar to the analysis of the experiments by Partridge *et al.* [42] due to Werner *et al.* [43]. A motivation for this work were the recent experiments of Schirotzek *et al.* [5], who observed a transition from a Fermi-liquid phase of polaronic quasiparticles near unitarity to a phase in which the quasiparticle residue vanishes. As shown above, this transition is expected to be a discontinuous one in the single down-spin limit. Apparently, however, $Z_\downarrow$ vanishes in a continuous manner in the experiment (see Fig. 1). Apart from the uncertainty in extracting $Z_\downarrow$ from the sharp structure in the minority rf spectrum, this discrepancy is probably due to the fact that the Chevy wave function (2.1) strongly overestimates the quasiparticle residue $Z_\downarrow$ near the polaron-to-molecule transition. A reliable quantitative calculation of the rf spectra for both finite concentrations and at finite temperatures is, unfortunately, not available. The existence of a stable finite density gas of polarons in the regime up to $v \simeq 0.9$ however indicates that the interaction between them is repulsive, so that they indeed form a Landau Fermi liquid below the critical coupling v_M. As discussed in Sec. IV, the detailed structure of how this phase connects to the nontrivial superfluid phases expected near the splitting point S and on the BEC side is a major and still open problem.

Note added. The variational wave function (3.1) for the $(N+1)$-particle problem in the molecular regime has been found independently by Mora and Chevy [44]. For the calculation of the ground-state energy they have assumed a vanishing hole wave vector $\mathbf{q}=0$, which reduces the resulting integral equation to a one-dimensional problem.

ACKNOWLEDGMENTS

We acknowledge many useful discussions with T. Enss, A. Recati, and M. Zwierlein. Moreover, we would like to thank A. Schirotzek, N. Prokof'ev, and B. Svistunov for providing their experimental, respectively, their numerical results for comparison. W.Z. is grateful to W. Ketterle and M. Zwierlein for their hospitality at the MIT-Harvard Center for Ultracold Atoms during a sabbatical, where this work was started. Furthermore, we are grateful to R. Combescot for pointing out their closely related work [45].

APPENDIX: THREE-PARTICLE LIMIT

In the following we briefly show how the exact solution of the three-fermion problem can be obtained from the integral equation (3.11) for the full variational wave function (3.5). If the $(N-1)$-particle Fermi sea is reduced to a single $\uparrow$ fermion, only the $\mathbf{q}=0$ terms remain in the variational wave function (3.5). Thus, starting from the integral equation (3.11) in the thermodynamic limit, taking the limit $k_F \to 0$ and setting $\mathbf{q}=0$, one arrives at the simplified equation

$$\alpha_{\mathbf{k}0}\eta_{\mathbf{k}0} = -\int \frac{d^3k'}{(2\pi)^3}\frac{\eta_{\mathbf{k}'0}}{E_{\mathbf{k}'\mathbf{k}0}}. \tag{A1}$$

Inserting the coefficients $\alpha_{\mathbf{k}0}$ and $E_{\mathbf{k}'\mathbf{k}0}$ from Eqs. (3.14) and (3.15) explicitly, the integral equation (A1) takes the form

$$\left(\frac{1}{a} - \sqrt{\frac{3k^2}{4} - mE}\right)\eta_{\mathbf{k}} = \int \frac{d^3k'}{(2\pi)^3}\frac{4\pi\eta_{\mathbf{k}'}}{k^2 + k'^2 + \mathbf{k}\cdot\mathbf{k}' - mE}. \tag{A2}$$

Note that $\eta_{\mathbf{k}} \equiv \eta_{\mathbf{k}0}$ corresponds to the Fourier transform of the relative wave function between the $(\uparrow,\downarrow)$ molecule and the additional $\uparrow$ fermion. The integral equation (A2) is exactly the same as the one obtained by Skorniakov and Ter-Martirosian [17] for the three-fermion problem. In particular it is equivalent to Eq. (29) in [17], which corresponds to three-nucleon scattering with total isospin $T=1/2$ and total spin $S=3/2$ (note that the spin part only contributes an unimportant prefactor to the wave function in this case).

[1] See, e.g., R. P. Feynman, *Statistical Mechanics* (W. A. Benjamin, Reading, MA, 1972).
[2] A. O. Caldeira and A. J. Leggett, Phys. Rev. Lett. **46**, 211 (1981).
[3] A. J. Leggett, S. Chakravarty, A. T. Dorsey, M. P. A. Fisher, A. Garg, and W. Zwerger, Rev. Mod. Phys. **59**, 1 (1987).
[4] I. Bloch, J. Dalibard, and W. Zwerger, Rev. Mod. Phys. **80**, 885 (2008).
[5] A. Schirotzek, C. H. Wu, A. Sommer, and M. W. Zwierlein, Phys. Rev. Lett. **102**, 230402 (2009).
[6] N. Prokof'ev and B. Svistunov, Phys. Rev. B **77**, 020408(R) (2008).
[7] N. V. Prokof'ev and B. V. Svistunov, Phys. Rev. B **77**, 125101 (2008).
[8] F. Chevy, Phys. Rev. A **74**, 063628 (2006).
[9] S. Tan, Ann. Phys. (N.Y) **323**, 2952 (2008).
[10] R. Combescot and S. Giraud, Phys. Rev. Lett. **101**, 050404 (2008).
[11] C. Lobo, A. Recati, S. Giorgini, and S. Stringari, Phys. Rev. Lett. **97**, 200403 (2006).
[12] R. Combescot, A. Recati, C. Lobo, and F. Chevy, Phys. Rev. Lett. **98**, 180402 (2007).
[13] S. Nascimbene, N. Navon, K. Jiang, L. Tarruel, M. Teichmann, J. McKeever, F. Chevy, and C. Salomon, e-print arXiv:0907.3032.
[14] M. Veillette, E. G. Moon, A. Lamacraft, L. Radzihovsky, S. Sachdev, and D. E. Sheehy, Phys. Rev. A **78**, 033614 (2008).
[15] K. G. Wilson, Rev. Mod. Phys. **47**, 773 (1975).

[16] D. J. Thouless, Ann. Phys. (N.Y.) **10**, 553 (1960).
[17] G. V. Skorniakov and K. A. Ter-Martirosian, Zh. Eksp. Teor. Fiz. **31**, 775 (1956) [Sov. Phys. JETP **4**, 648 (1957)].
[18] D. S. Petrov, C. Salomon, and G. V. Shlyapnikov, Phys. Rev. A **71**, 012708 (2005).
[19] G. M. Bruun and C. J. Pethick, Phys. Rev. Lett. **92**, 140404 (2004).
[20] The fact that C is identical for both spin components σ implies, for instance, that the minority and majority rf spectra are identical at high frequencies, as observed experimentally [5]. Indeed, as shown recently by W. Schneider, V. Shenoy, and M. Randeria, e-print arXiv:0903.3006, the rf spectra normalized to the total particle number decay like $C/\omega^{3/2}$ at high frequencies.
[21] E. Braaten and L. Platter, Phys. Rev. Lett. **100**, 205301 (2008).
[22] S. Tan, Ann. Phys. (N.Y.) **323**, 2971 (2008).
[23] R. Haussmann, M. Punk, and W. Zwerger, e-print arXiv:0904.1333.
[24] Within a local-density approximation, the different phases that appear in a trap with a spatially dependent coupling constant $v(\mathbf{x})$ due to the decrease in the local Fermi wave vector $k_F(\mathbf{x})$ from the center of the trap to its edge simply follow from a parabolic (vertical at unitarity) line in Fig. 4, $h/\varepsilon_F(\mathbf{x}) = (2h/|E_b|)v^2(\mathbf{x})$, where $|E_b| = 1/(ma^2)$ for both positive and negative scattering lengths a. Its curvature $2h/|E_b|$ is fixed by the global imbalance, while the initial point $v(\mathbf{x}=0)$ is determined by the local Fermi wave vector at the trap center $\mathbf{x}=0$. Note that in a trap different phases are spatially separated for both continuous and first-order transition lines. By contrast, genuine phase separation is associated with a first-order transition and appears only in the homogeneous system.
[25] S. Pilati and S. Giorgini, Phys. Rev. Lett. **100**, 030401 (2008).
[26] Note the down-spin Fermi surface volume $\Omega_\downarrow$ vanishes also along the h_s line to the left of M. This continuous transition, however, becomes a smooth crossover at any finite temperature. By contrast, the transition between normal and superfluid states that are both partially polarized also remains at finite temperature.
[27] S. Sachdev and K. Yang, Phys. Rev. B **73**, 174504 (2006).
[28] A. Bulgac, M. McNeil Forbes, and A. Schwenk, Phys. Rev. Lett. **97**, 020402 (2006).
[29] Y. Nishida, Phys. Rev. A **79**, 013629 (2009).
[30] S. Giorgini, L. P. Pitaevskii, and S. Stringari, Rev. Mod. Phys. **80**, 1215 (2008).
[31] P. F. Bedaque, H. Caldas, and G. Rupak, Phys. Rev. Lett. **91**, 247002 (2003).
[32] D. E. Sheehy and L. Radzihovsky, Phys. Rev. Lett. **96**, 060401 (2006).
[33] C.-H. Pao, S.-T. Wu, and S.-K. Yip, Phys. Rev. B **73**, 132506 (2006); **74**, 189901(E) (2006).
[34] M. M. Parish, F. M. Marchetti, A. Lamacraft, and B. D. Simons, Nat. Phys. **3**, 124 (2007).
[35] B. S. Chandrasekhar, Appl. Phys. Lett. **1**, 7 (1962).
[36] A. M. Clogston, Phys. Rev. Lett. **9**, 266 (1962).
[37] P. Nikolić and S. Sachdev, Phys. Rev. A **75**, 033608 (2007).
[38] D. T. Son and M. A. Stephanov, Phys. Rev. A **74**, 013614 (2006).
[39] Y. Nishida and D. T. Son, Phys. Rev. A **75**, 063617 (2007).
[40] The Sarma phase predicted in Ref. [38] near the splitting point beyond the FFLO regime maybe a metastable phase due to interactions between the quasiparticles (D. T. Son, private communication). The existence of an FFLO phase at unitarity and for small polarizations σ is supported by recent density-functional calculations; see A. Bulgac and M. McNeil Forbes, Phys. Rev. Lett. **101**, 215301 (2008).
[41] Y. Shin, C. H. Schunck, A. Schirotzek, and W. Ketterle, Nature (London) **451**, 689 (2008).
[42] G. B. Partridge, K. E. Strecker, R. I. Kamar, M. W. Jack, and R. G. Hulet, Phys. Rev. Lett. **95**, 020404 (2005).
[43] F. Werner, L. Tarruell, and Y. Castin, Eur. Phys. J. B **68**, 401 (2009).
[44] C. Mora and F. Chevy, Phys. Rev. A **80**, 033607 (2009).
[45] R. Combescot, S. Giraud, and X. Leyronas, e-print arXiv:0907.3197.

PHYSICAL REVIEW A **80**, 063612 (2009)

Spectral functions and rf response of ultracold fermionic atoms

R. Haussmann,[1] M. Punk,[2] and W. Zwerger[2]
[1]*Fachbereich Physik, Universität Konstanz, D-78457 Konstanz, Germany*
[2]*Physikdepartment, Technische Universität München, D-85748 Garching, Germany*
(Received 8 April 2009; published 4 December 2009)

We present a calculation of the spectral functions and the associated rf response of ultracold fermionic atoms near a Feshbach resonance. The single-particle spectra are peaked at energies that can be modeled by a modified BCS dispersion. However, even at very low temperatures their width is comparable to their energy except for a small region around the dispersion minimum. The structure of the excitation spectrum of the unitary gas at infinite scattering length agrees with recent momentum-resolved rf spectra near the critical temperature. A detailed comparison is made with momentum integrated, locally resolved rf spectra of the unitary gas at arbitrary temperatures and shows very good agreement between theory and experiment. The pair size defined from the width of these spectra is found to coincide with that obtained from the leading gradient corrections to the effective-field theory of the superfluid.

DOI: 10.1103/PhysRevA.80.063612 PACS number(s): 03.75.Ss, 03.75.Hh, 74.20.Fg

I. INTRODUCTION

The existence of well-defined noninteracting quasiparticles above a possibly strongly correlated ground state is a central paradigm of many-body physics. In interacting Fermi systems, this concept applies both in a Fermi liquid and in a BCS-like superfluid state, whose elementary excitations have an infinite lifetime at the Fermi surface. More generally, the nature of quasiparticle excitations may be used to characterize many-body ground states both with and without long-range order [1]. Typically, it is only near a quantum phase transition between ground states with different types of order where a quasiparticle description fails and is replaced by a continuum of gapless excitations [2]. In our present work, we discuss ultracold fermionic atoms with a tunable attractive interaction. The ground state is a neutral s-wave superfluid at arbitrary coupling. Thus, it has gapless bosonic quasiparticles of the Bogoliubov-Anderson type with a linear spectrum $\omega = c_s q$. Its fermionic excitations have a finite gap. Within a BCS description, the associated Bogoliubov quasiparticles are exact eigenstates of the interacting system at arbitrary momenta. As will be shown below, this central feature of the BCS picture of fermionic superfluids fails for the strong coupling situation that is relevant in the cold gases context, where the excitation energy is no longer exponentially small compared with the Fermi energy. In this regime, the fermionic particle excitations acquire a significant lifetime broadening even at zero temperature, except near the dispersion minimum (or maximum for holes), where there is no available phase space for decay. The lifetime broadening arises both from the residual interaction between quasiparticles and their coupling to the collective sound mode. Moreover, the particle-hole symmetry characteristic for the Bogoliubov quasiparticles of the BCS theory is violated in the strong coupling regime. With increasing temperatures, the particlelike and holelike branches merge into a single broad excitation branch with a free-particle-like dispersion shifted by the binding energy.

Fermions with a tunable attractive interaction and the associated BCS-BEC crossover have been studied experimentally using ultracold Fermi gases near a Feshbach resonance [3–5]. The fact that the balanced system with an equal number of particles in the two different hyperfine states ("spins") that undergo pairing is superfluid at sufficiently low temperatures has been inferred from the observation of a finite condensate fraction on the BCS side [6] and from the collective mode frequencies in a trap that agree with superfluid hydrodynamics [7,8]. It was demonstrated quite directly by the observation of a vortex lattice in the rotating gas, which evolves continuously from the Bose-Einstein condensate (BEC) to the BCS side of the transition [9]. To study the excitation spectrum, in particular the evolution of the expected gap for fermionic excitations due to pairing, rf spectroscopy was performed by Chin *et al.* [10]. The interpretation of these measurements [11] in terms of an effective "pairing gap," however, is made difficult by the existence of strong final state interactions and the fact that the signal is an average over the whole cloud, with a spatially dependent excitation gap. For a homogeneous system, the average rf shift is in fact dominated by large mean-field effects and final state interactions [12–15] and is hardly changed, even if superfluidity is suppressed by a rather strong imbalance [16]. The problems associated with final state interactions and the inhomogeneity of the cloud have been overcome only recently by the possibility to perform spatially resolved rf measurements [17], combined with a suitable choice of the hyperfine states which undergo pairing and the final state of the rf transition [18]. Moreover, it has also become possible to measure rf spectra in a momentum-resolved way [19]. This opens the possibility to infer the full spectral functions as suggested theoretically by Dao *et al.* [20].

Our aim in the following is to present a calculation of the spectral functions and the associated rf response of strongly interacting fermions which covers the whole regime of temperatures both above and below the superfluid transition and also arbitrary coupling constants. The theory is based on a conserving, so-called Φ-derivable approach to the many-body problem due to Luttinger and Ward, in which the exact one-particle Green's functions serve as an infinite set of variational parameters. This approach has been used previously to describe the thermodynamic properties of the uni-

form [21] and the trapped gas [22]. The Luttinger-Ward formulation of the many-body problem relies on expressing the thermodynamic potential $\Omega[G]$ in terms of the exact Green's function G. The condition that the functional $\Omega[G]$ is stationary with respect to small variations in the Green's functions then leads to a set of integral equations for the matrix Green's function G which have to be solved in a self-consistent manner. Since the Green's functions contain information about the full dynamical behavior via the imaginary time dependence of the Matsubara formalism, the Luttinger-Ward approach not only provides results for the equilibrium thermodynamic quantities but also determines the full spectral functions upon analytic continuation from Matsubara to real frequencies. This is done explicitly in our present work using the maximum-entropy technique.

The paper is organized as follows: in Sec. II we introduce the Luttinger-Ward formalism and discuss the calculation of the momentum and frequency-dependent spectral functions. The relation between the spectral functions and the experimentally measured rf spectra is outlined in general and discussed in the BCS and BEC limit, where analytical results are available. We also discuss the behavior of the rf spectra at high frequencies and the associated contact coefficient introduced by Tan [23] and by Braaten and Platter [24]. In Sec. III, we show that a pair size can be defined via the momentum dependence of the superfluid response in analogy to the nonlocal penetration depth in superconductors. Using an effective-field theory due to Son and Wingate [25], we find that the resulting pair size of the unitary gas coincides with that inferred experimentally from the width of the rf spectrum [18]. The numerical results and the physical interpretation of spectral functions and rf spectra obtained within the Luttinger-Ward approach are discussed in Sec. IV, both in the normal and superfluid phase. These results are compared quantitatively with measured data. A summary and discussion are given in Sec. V. There are two appendixes, one on the maximum-entropy method and one on a perturbative calculation of the quasiparticle lifetime due to interactions with the collective mode.

II. LUTTINGER-WARD THEORY, SPECTRAL FUNCTIONS, AND RF RESPONSE

Our calculation of the spectral functions for a dilute system of ultracold fermionic atoms is based on a Luttinger-Ward approach to the BCS-BEC crossover that has been presented in detail previously [21,26]. As a starting point, we use the standard single-channel Hamiltonian that contains the essential physics of the BCS-BEC crossover in a dilute gas of ultracold fermionic atoms with a short-range (s-wave) interaction [4]

$$\hat{H} = \int d^3r \sum_\sigma \frac{\hbar^2}{2m} [\nabla \psi_\sigma^+(\mathbf{r})][\nabla \psi_\sigma(\mathbf{r})] + \frac{g_0}{2} \int d^3r \sum_\sigma \psi_\sigma^+(\mathbf{r}) \psi_{-\sigma}^+(\mathbf{r}) \psi_{-\sigma}(\mathbf{r}) \psi_\sigma(\mathbf{r}). \quad (2.1)$$

Here $\psi_\sigma(\mathbf{r})$ and $\psi_\sigma^+(\mathbf{r})$ are the usual fermion field operators. The formal spin index σ labels two different hyperfine states which interact via a zero-range delta potential $g_0\delta(\mathbf{r})$. Since a delta function in three dimensions leads to no scattering at all, the bare coupling strength

$$g_0(\Lambda) = \frac{g}{1 - 2a\Lambda/\pi} \quad (2.2)$$

needs to be expressed in terms of renormalized scattering amplitude $g = 4\pi\hbar^2 a/m$ that is proportional to the s-wave scattering length a and an ultraviolet momentum cutoff Λ that is taken to infinity at fixed g. The limiting process $g_0(\Lambda \to \infty) \to -0$ accounts for the replacement of the bare delta potential by a pseudopotential with the proper scattering length. The description of a Feshbach resonance by a single-channel Hamiltonian of the form given in Eq. (2.1) is valid for the experimentally relevant case of broad Feshbach resonances, where the effective range r^* of the resonant interaction is much smaller than the Fermi wavelength λ_F [4].

We consider a homogeneous situation described by a grand canonical distribution at fixed temperature and chemical potential. The grand partition function

$$Z = \mathrm{Tr}\{\exp(-\beta[\hat{H} - \mu\hat{N}])\} \quad (2.3)$$

then determines the grand potential

$$\Omega = \Omega(T, \mu) = -\beta^{-1} \ln Z. \quad (2.4)$$

For a quantitative discussion of the results, it is more convenient to switch to a canonical description at a given density n by a Legendre transformation to the free energy $F = \Omega + \mu N$. Within our zero-range interaction model, the Fermi system at total density $n = k_F^3/3\pi^2$ is then completely characterized by two parameters: the dimensionless temperature $\theta = k_B T/\varepsilon_F$ and the dimensionless inverse interaction strength $v = 1/k_F a$. In the special case of an infinite scattering length (the so-called unitarity limit), the parameter v drops out. The resulting spectral functions $A(\mathbf{k}, \varepsilon)$ are then universal functions of θ and the dimensionless momentum and energy scales k/k_F and $\varepsilon/\varepsilon_F$ that are set by the density of the gas.

A. Luttinger-Ward formalism

In thermal equilibrium at temperature T the properties of an interacting fermion system which exhibits a superfluid transition are described by two Matsubara Green's functions, the normal Green's function (T denotes the standard time ordering)

$$\langle \mathrm{T}[\psi_\sigma(\mathbf{r}, \tau) \psi_{\sigma'}^+(\mathbf{r}', \tau')] \rangle = \delta_{\sigma\sigma'} \mathcal{G}(\mathbf{r} - \mathbf{r}', \tau - \tau') \quad (2.5)$$

and the anomalous Green's function

$$\langle \mathrm{T}[\psi_\sigma(\mathbf{r}, \tau) \psi_{\sigma'}(\mathbf{r}', \tau')] \rangle = \varepsilon_{\sigma\sigma'} \mathcal{F}(\mathbf{r} - \mathbf{r}', \tau - \tau'), \quad (2.6)$$

where the antisymmetric Levi-Civita tensor $\varepsilon_{\sigma\sigma'}$ represents the spin structure of s-wave pairing. In the translation invariant and stationary case studied here, it is convenient to switch to a Fourier representation of the Matsubara Green's functions. The normal and anomalous functions (2.5) and (2.6) can then be combined into a matrix Green's function

$$G_{\alpha\alpha'}(\mathbf{k},\omega_n)=\begin{pmatrix}\mathcal{G}(\mathbf{k},\omega_n) & \mathcal{F}(\mathbf{k},\omega_n)\\ \mathcal{F}(\mathbf{k},\omega_n)^* & -\mathcal{G}(\mathbf{k},\omega_n)^*\end{pmatrix}, \tag{2.7}$$

with momentum variable $\mathbf{k}$ and fermionic Matsubara frequencies $\omega_n=2\pi(n+1/2)/\beta\hbar$ with $n\in\mathbb{Z}$. The nondiagonal elements represent the order parameter of the superfluid transition. Using matrix Green's function (2.7), it is possible to generalize the Luttinger-Ward formalism [27] to superfluid systems [21,26]. In particular, the grand thermodynamic potential (2.4) can be expressed as a unique functional of Green's function (2.7) in the form

$$\Omega[G]=\beta^{-1}\left(-\frac{1}{2}\mathrm{Tr}\{-\ln G+[G_0^{-1}G-1]\}-\Phi[G]\right). \tag{2.8}$$

The interaction between the fermions is described by the functional $\Phi[G]$, which can be expressed in terms of a perturbation series of irreducible Feynman diagrams. The full matrix Green's function G is then determined uniquely by the condition that the grand potential functional (2.8) is stationary with respect to variations in G, i.e.,

$$\delta\Omega[G]/\delta G=0. \tag{2.9}$$

It is important to note that the thermodynamic potential $\Omega[G]$ is a functional of the exact Green's function G. The formalism of Luttinger and Ward thus leads via Eq. (2.9) to a self-consistent theory for the matrix Green's function.

Since the exact form of $\Phi[G]$ is unknown, we employ a ladder approximation [21,26,28]. In the weak-coupling limit, this is exactly equivalent to the standard BCS description of fermionic superfluids. In the BEC limit, where the fermions form a Bose gas of strongly bound pairs, the ladder approximation correctly accounts for the formation of pairs (i.e., the two-particle problem). The residual interaction between the pairs, however, is described only in an approximate manner. Indeed, it turns out [21,28] that in the BEC limit the ladder approximation for the functional $\Phi[G]$ gives rise to a theory for a dilute Bose gas with repulsive interactions that are described by a dimer-dimer scattering length $a_{dd}=2a$. This is a qualitatively correct description of the BEC limit of the crossover problem; however, from an exact solution of the four-particle problem in this limit the true dimer-dimer scattering length should be $a_{dd}=0.6a$ [29].

The ladder approximation leads to the following closed set of equations for the matrix of single-particle Green's functions (2.7) [21,26,28]:

$$G^{-1}_{\alpha\alpha'}(\mathbf{k},\omega_n)=G^{-1}_{0,\alpha\alpha'}(\mathbf{k},\omega_n)-\Sigma_{\alpha\alpha'}(\mathbf{k},\omega_n), \tag{2.10}$$

$$\Sigma_{\alpha\alpha'}(\mathbf{k},\omega_n)=\Sigma_{1,\alpha\alpha'}+\int\frac{d^3K}{(2\pi)^3}\frac{1}{\beta}\sum_{\Omega_n}\Gamma_{\alpha\alpha'}(\mathbf{K},\Omega_n)\times G_{\alpha'\alpha}(\mathbf{k}+\mathbf{K},\omega_n+\Omega_n), \tag{2.11}$$

$$\Gamma^{-1}_{\alpha\alpha'}(\mathbf{K},\Omega_n)=\frac{\delta_{\alpha\alpha'}}{g}+\int\frac{d^3k}{(2\pi)^3}\left[\frac{1}{\beta}\sum_{\omega_n}G_{\alpha\alpha'}(\mathbf{k},\omega_n)\times G_{\alpha\alpha'}(\mathbf{K}-\mathbf{k},\Omega_n-\omega_n)-\frac{m}{\hbar^2\mathbf{k}^2}\delta_{\alpha\alpha'}\right]. \tag{2.12}$$

Here,

$$G^{-1}_{0,\alpha\alpha'}(\mathbf{k},\omega_n)=\begin{pmatrix}[-i\omega_n+\varepsilon_{\mathbf{k}}-\mu] & 0\\ 0 & -[i\omega_n+\varepsilon_{\mathbf{k}}-\mu]\end{pmatrix} \tag{2.13}$$

is the inverse free Green's function where $\varepsilon_{\mathbf{k}}=\hbar^2k^2/2m$. Furthermore,

$$\Sigma_1=\begin{pmatrix}0 & \Delta\\ \Delta^* & 0\end{pmatrix} \tag{2.14}$$

is a $\mathbf{k}$- and ω_n-independent matrix, whose off-diagonal elements represent the order parameter of the superfluid transition. By definition, Δ is related to the anomalous Green's function $\mathcal{F}(\mathbf{k},\tau)$ by the renormalized gap equation

$$\Delta=g\int\frac{d^3k}{(2\pi)^3}\left[\mathcal{F}(\mathbf{k},\tau=0)+\Delta\frac{m}{\hbar^2\mathbf{k}^2}\right]. \tag{2.15}$$

The vertex function $\Gamma_{\alpha\alpha'}(\mathbf{K},\Omega_n)$ defined in Eq. (2.12) may be identified with the T matrix for the scattering of two particles in a many-body Fermi system. Since $G_{\alpha\alpha'}(\mathbf{k},\omega_n)$ is the exact one-particle Green's function, the vertex function is that of a self-consistent T-matrix approximation. The Luttinger-Ward approach in ladder approximation is thus equivalent to a self-consistent T-matrix approximation. The specific structure of the GG term in Eq. (2.12) with respect to the Nambu indices α and α' implies that the particle-particle ladder is considered here, which properly describes the formation of Fermion pairs in normal and superfluid Fermi systems.

As a result of the Goldstone theorem, a neutral superfluid Fermi system must exhibit a gapless Bogoliubov-Anderson mode. Formally, this is guaranteed by a Ward identity, which can be derived from the Luttinger-Ward formalism for any gauge invariant functional $\Phi[G]$. This functional defines an associated inverse vertex function which in short-hand notation is given by

$$\Gamma^{-1}=\Gamma_1^{-1}+\chi, \tag{2.16}$$

where $\Gamma_1=-\delta^2\Phi[G]/\delta G^2$ is the irreducible vertex and $\chi=-GG$ is the pair propagator. The existence of a Bogoliubov-Anderson mode is then guaranteed by the property that $\mathbf{\Gamma}^{-1}$ has an eigenvalue $\lambda(\mathbf{K},\Omega_n)$ which has to vanish for $\mathbf{K}=\mathbf{0}$ and $\Omega_n=0$ [26]. This Ward identity is equivalent, in the present case, to the well known Thouless criterion [30]. Unfortunately, the inverse vertex (2.12) obtained from our self-consistent ladder approximation does not agree with the exact inverse vertex function as defined by Eq. (2.16). As shown in our previous publication [21], however, the requirement of a gapless Bogoliubov-Anderson mode can be imposed on Eq. (2.12) as an additional constraint by choos-

ing a modified coupling constant in the renormalized gap Eq. (2.15). This modified approach is still compatible with the Luttinger-Ward formalism so that our method is both conserving and gapless. In the following numerical calculations we always employ this modified approach which is described in detail in Ref. [21].

In a homogeneous gas, the normal to superfluid transition is a continuous phase transition of the 3D XY type along the complete BCS to BEC crossover. By contrast, our approach [21] gives rise to a weak first-order superfluid transition because the superfluid phase of the Luttinger-Ward theory does not smoothly connect with the normal-fluid phase at a single critical temperature $\theta_c = k_B T_c / \varepsilon_F$. Fortunately, this problem is confined to a rather narrow regime of temperatures. In particular, at unitarity, the upper and lower values for θ_c are 0.1604 and 0.1506, which is within the present numerical uncertainties in the determination of the critical temperature of the unitary gas [31,32]. For our discussion of spectral functions in the present work, which does not focus on the critical behavior near T_c, the problem with the weak first-order nature of the transition is therefore not relevant.

Keeping these caveats in mind, the ladder approximation for the Luttinger-Ward functional provides quantitatively reliable results for the thermodynamic properties of the BCS-BEC crossover problem [21,22]. This applies, in particular, for the most interesting regime near unitarity, where weak-coupling approximations fail. As an example, the value of the critical temperature $T_c/T_F = 0.16$ right at unitarity agrees with recent quantum Monte Carlo (QMC) results $T_c/T_F = 0.152(7)$ for this problem within the error bars [31,32]. It is also consistent with recent calculations of the onset temperature of a finite condensate density [33]. Moreover, there is also quite good agreement with field-theoretic results for ground-state properties, which are characterized by a single universal constant, the so-called Bertsch parameter $\xi(0)$ defined, e.g., by $\mu(T=0) = \xi(0)\varepsilon_F$ at unitarity [4]. In fact, the value $\xi(0) = 0.36$ obtained within the Luttinger-Ward approach [21] agrees perfectly with the result $\xi(0) = 0.367(9)$ from an $\epsilon = 4 - d$ expansion up to three loops [34] and—in particular—with the more recent value $\xi = 0.36 \pm 0.002$ obtained by Nishida [35]. Variational Monte Carlo calculations [36,37] or a Gaussian fluctuation expansion around the BCS mean-field results [38,39], in turn, give somewhat higher values $\xi(0) = 0.42(1)$ or $\xi(0) = 0.40$, respectively.

B. Spectral functions

The Matsubara Green's function $\mathcal{G}(\mathbf{k}, \omega_n)$ can be expressed in terms of a spectral function $A(\mathbf{k}, \varepsilon)$ by using the Lehmann spectral representation [40]

$$\mathcal{G}(\mathbf{k}, \omega_n) = \int d\varepsilon \frac{A(\mathbf{k}, \varepsilon)}{-i\hbar\omega_n + \varepsilon - \mu}. \tag{2.17}$$

The spectral function associated with the normal, single-particle Green's function $\mathcal{G}(\mathbf{k}, \omega_n)$ is positive $A(\mathbf{k}, \varepsilon) \geq 0$ and normalized according to

$$\int d\varepsilon \, A(\mathbf{k}, \varepsilon) = 1. \tag{2.18}$$

It can be decomposed into two contributions

$$A(\mathbf{k}, \varepsilon) = A_+(\mathbf{k}, \varepsilon) + A_-(\mathbf{k}, \varepsilon), \tag{2.19}$$

which describe the particle and hole excitation part of the complete excitation spectrum. The individual contributions

$$A_+(\mathbf{k}, \varepsilon) = Z^{-1} \sum_{mn} e^{-\beta(E_m - \mu N_m)} |\langle m|\psi_\sigma(\mathbf{0})|n\rangle|^2 (2\pi)^3 \times \delta(\mathbf{k} - [\mathbf{P}_n - \mathbf{P}_m]/\hbar)\, \delta(\varepsilon - [E_n - E_m]) \tag{2.20}$$

and

$$A_-(\mathbf{k}, \varepsilon) = Z^{-1} \sum_{mn} e^{-\beta(E_n - \mu N_n)} |\langle m|\psi_\sigma(\mathbf{0})|n\rangle|^2 (2\pi)^3 \times \delta(\mathbf{k} - [\mathbf{P}_n - \mathbf{P}_m]/\hbar)\, \delta(\varepsilon - [E_n - E_m]) \tag{2.21}$$

can be expressed in terms of matrix elements of single fermion field operators $\psi_\sigma(\mathbf{0})$ at the origin between the exact eigenstates $|n\rangle$ of the many-body system. Here $\mathbf{P}_n$, E_n, and N_n are the corresponding eigenvalues of momentum, energy, and particle number, respectively. In thermal equilibrium, the partial spectral functions are related by the detailed balance condition

$$A_-(\mathbf{k}, \varepsilon) = e^{-\beta(\varepsilon - \mu)} A_+(\mathbf{k}, \varepsilon). \tag{2.22}$$

At zero temperature, therefore, the hole part $A_-(\mathbf{k}, \varepsilon)$ of the spectral function vanishes for $\varepsilon > \mu$ and vice versa the particle part $A_+(\mathbf{k}, \varepsilon)$ vanishes for $\varepsilon < \mu$. The total spectral weight in the hole part

$$\int d\varepsilon \, A_-(\mathbf{k}, \varepsilon) = n_\sigma(\mathbf{k}) \tag{2.23}$$

at arbitrary temperatures is equal to the fermion occupation number $n_\sigma(\mathbf{k}) = -\mathcal{G}(\mathbf{k}, \tau = -0)$ for a single spin orientation σ (in the balanced gas discussed here, both components $\sigma = \pm 1$ have the same occupation, of course).

Within the BCS description of fermionic superfluids, the spectral function consists of two infinitely sharp peaks [40]

$$A(\mathbf{k}, \varepsilon) = u_\mathbf{k}^2 \delta(\varepsilon - E_\mathbf{k}^{(+)}) + v_\mathbf{k}^2 \delta(\varepsilon - E_\mathbf{k}^{(-)}), \tag{2.24}$$

which represent the particle and hole part of the spectral function. The associated energies

$$E_\mathbf{k}^{(\pm)} = \mu \pm \sqrt{(\varepsilon_\mathbf{k} - \mu)^2 + \Delta^2} \tag{2.25}$$

describe the standard dispersion of the Bogoliubov quasiparticles. They exhibit a finite gap, whose minimum value Δ is taken at a finite momentum $k_\mu = \sqrt{2m\mu}/\hbar$ (note that $\mu \to \varepsilon_F > 0$ in the BCS limit). Within the standard BCS theory, these excitations have infinite lifetime at arbitrary momenta $\mathbf{k}$ and there is no broadening or incoherent background. Going beyond the exactly solvable BCS Hamiltonian, however, gives rise to a finite lifetime of the fermionic excitations and thus will broaden the two delta peaks in Eq. (2.24) even at zero

temperature. It is our aim in the following to calculate these effects quantitatively for the simple model Hamiltonian Eq. (2.1) in the whole range of coupling strengths and temperatures.

Equation (2.17) has the form of a Cauchy integral in the theory of complex functions. It is therefore convenient to define a complex Green's function $G(\mathbf{k},z)$ depending on a complex frequency z, which is analytic in the upper and lower complex half planes $\mathrm{Im}(z)\gtrless 0$, respectively. This complex Green's function is related the Matsubara Green's function and to the spectral function by

$$\mathcal{G}(\mathbf{k},\omega_n) = G(\mathbf{k},z=\mu/\hbar + i\omega_n), \tag{2.26}$$

$$A(\mathbf{k},\varepsilon) = +\pi^{-1}\,\mathrm{Im}[G(\mathbf{k},z=\varepsilon/\hbar + i0)], \tag{2.27}$$

respectively. Thus, in a first step we obtain the complex Green's function $G(\mathbf{k},z)$ as an analytic continuation from the Matsubara Green's function $\mathcal{G}(\mathbf{k},\omega_n)$. In a second step, we insert the complex frequency $z=\varepsilon/\hbar \pm i0$ and obtain the spectral function $A(\mathbf{k},\varepsilon)$ from Eq. (2.27). The fact that $\mathcal{G}(\mathbf{k},\omega_n)$ uniquely determines the spectral function has been proven by Baym and Mermin [41].

In practice the analytic continuation for calculating the spectral function $A(\mathbf{k},\varepsilon)$ is done by using the maximum-entropy method [42] which is described in detail in Appendix A. We have checked the accuracy of our results *a posteriori* by inserting the calculated spectral functions in Eq. (2.17). The given "initial" data $\mathcal{G}(\mathbf{k},\omega_n)$ are then found to be reproduced with a relative accuracy that is typically in the 10^{-5} range.

C. rf response

In radio-frequency experiments, the external rf field transfers atoms from one of the two occupied spin states (as initial state) into an empty final state. In the following, we assume that the final state, which is denoted by an index f, has a negligible interaction with the initial one. It can thus be described by the free-fermion spectral function

$$A_f(\mathbf{k},\varepsilon) = \delta(\varepsilon - [E_f + \varepsilon_{\mathbf{k}}]), \tag{2.28}$$

where E_f is the excitation energy of the final state, which has a free particle dispersion $\varepsilon_{\mathbf{k}}=\hbar^2\mathbf{k}^2/2m$. Within linear response, the rate of transitions out of the initial state induced by the rf field with frequency ω and wave vector $\mathbf{q}$ is given by a convolution

$$I(\mathbf{q},\omega) = \hbar\int \frac{d^3k}{(2\pi)^3}\int d\varepsilon[A_{f,+}(\mathbf{k}+\mathbf{q},\varepsilon+\hbar\omega)A_-(\mathbf{k},\varepsilon) - A_{f,-}(\mathbf{k}+\mathbf{q},\varepsilon+\hbar\omega)A_+(\mathbf{k},\varepsilon)] \tag{2.29}$$

of the spectral functions A and A_f of the initial and final states. Here, an unknown prefactor that depends on the interaction parameters for the coupling to the rf field has been set equal to $\hbar$, which provides a convenient normalization for the total weight integrated over all frequencies [see Eq. (2.36) below]. This overall constant drops out in normalized spectra by dividing out the zeroth moment $\int d\omega I(\mathbf{q},\omega)$ or has—in any case—to be adjusted to the measured signal in comparison with experimental data. Since the wave vector $\mathbf{q}$ of the rf field is much smaller than those of the atoms, it is an excellent approximation to set $\mathbf{q}=\mathbf{0}$. In the absence of a probe that selects atoms according to their momenta $\mathbf{k}$, the spectrum $I(\mathbf{q}=\mathbf{0},\omega)=I(\omega)$ is thus only a function of the rf frequency ω. In addition, for the standard situation with an empty final state f, the partial spectral functions are $A_{f,+}(\mathbf{k},\varepsilon)=A_f(\mathbf{k},\varepsilon)$ and $A_{f,-}(\mathbf{k},\varepsilon)=0$. Using Eq. (2.28), the resulting rf spectrum

$$I(\omega) = \hbar\int \frac{d^3k}{(2\pi)^3}A_-(\mathbf{k},\varepsilon_{\mathbf{k}}-\hbar\omega) \tag{2.30}$$

is an integral over the hole part $A_-(\mathbf{k},\varepsilon)$ of the single-particle spectral function in the initial strongly correlated state. For convenience we have taken $E_f=0$, which redefines the position of zero frequency $\omega=0$ in the rf spectrum.

Within a BCS description, the spectral function is given by Eq. (2.24). Its hole excitation part has a delta peak at $E^{(-)}_{\mathbf{k}}$ whose weight is equal to the occupation number $n_\sigma(\mathbf{k})=v^2_{\mathbf{k}}$. This reflects the simple fact that a hole with momentum $\mathbf{k}$ can only be created if a fermion is present with this momentum. The resulting rf spectrum in our normalization is

$$I_{BCS}(\omega) = \frac{m^{3/2}}{2^{1/2}\pi^2\hbar^2}\left[\frac{\hbar\omega}{2}+\mu-\frac{\Delta^2}{2\hbar\omega}\right]^{1/2}\frac{\Delta^2}{2(\hbar\omega)^2}. \tag{2.31}$$

It exhibits a sharp onset at $\hbar\omega_{min}=\sqrt{\Delta^2+\mu^2}-\mu$. As will be shown below, such a sharp onset is not found from our numerical results for the spectral function even in the weak-coupling limit $v\ll -1$. The origin of this discrepancy may be traced back to the fact that the dominant contributions to the rf spectrum near ω_{min} arise from the spectral function $A_-(\mathbf{k},\varepsilon)$ in the limit $\mathbf{k}\to\mathbf{0}$, i.e., far from the Fermi surface at k_F. Now, deep in the Fermi sea, the true spectral function is not described properly by an extended BCS description, which has sharp quasiparticles at *arbitrary* momenta. In fact, the simple form (2.24) of the single fermion spectral function holds only if the interaction part of the full Hamiltonian Eq. (2.1) is approximated by the exactly soluble reduced BCS Hamiltonian [43]. Its interaction term

$$\hat{H}'_{BCS} = \frac{g_0}{2V}\sum_\sigma\sum_{\mathbf{k},\mathbf{k}'} c^+_{\mathbf{k},\sigma}c^+_{-\mathbf{k},-\sigma}c_{-\mathbf{k}',-\sigma}c_{\mathbf{k}',\sigma} \tag{2.32}$$

involves only pairs with vanishing total momentum $\mathbf{Q}=\mathbf{0}$. This approximation excludes density fluctuations and therefore does not account for the collective Bogoliubov-Anderson mode [4]. Moreover, its fermionic quasiparticles are exact eigenstates of the reduced BCS Hamiltonian at arbitrary momenta. The difference

$$\hat{H}_{\mathrm{res}} = \frac{g_0}{2V}\sum_\sigma\sum_{\mathbf{k},\mathbf{k}',\mathbf{Q}\neq\mathbf{0}} c^+_{\mathbf{k}+\mathbf{Q},\sigma}c^+_{-\mathbf{k},-\sigma}c_{-\mathbf{k}',-\sigma}c_{\mathbf{k}'+\mathbf{Q},\sigma} \tag{2.33}$$

between the full Hamiltonian Eq. (2.1) and that of the reduced BCS model therefore gives rise to residual interactions between the quasiparticles and their coupling to the collec-

tive Bogoliubov-Anderson mode. This will be discussed in more detail in Appendix B. As will be shown quantitatively in Sec. IV, the residual interactions result in an appreciable broadening $\gamma(\mathbf{k})$ of the spectral functions. In particular, the hole part becomes increasingly broad as $\mathbf{k}\to\mathbf{0}$ [see Fig. 2(a) for a coupling strength $v=-1$]. A BCS-type rf spectrum (2.31) requires that $\gamma(\mathbf{k}=\mathbf{0})\ll\hbar\omega_{min}\approx\Delta^2/2\varepsilon_F$ in weak coupling. This condition is never fulfilled in practice, because the gap $\Delta\sim\exp(\pi v/2)$ vanishes exponentially in the BCS limit $v\ll-1$, while $\gamma(\mathbf{k}=\mathbf{0})$ can be shown to be of order $(k_Fa)^2$ as $k_F|a|\ll1$ due to the decay via intermediate states involving three quasiparticles [see Eq. (B8) in Appendix B]. As a result, the onset and peak shift of the rf spectrum in weak coupling are dominated by the Hartree contributions and do not reflect the appearance of a pairing gap.

In the limit $v\gg+1$ of a molecular BEC, the fermions form a superfluid of strongly bound dimers. In this regime, the gap parameter Δ becomes negligible compared with the magnitude of the chemical potential and hole excitation energy (2.25) approaches $E_{\mathbf{k}}^{(-)}\to2\mu-\varepsilon_{\mathbf{k}}$. Since the extended BCS description of the crossover becomes exact again in the molecular limit, where it reduces to an ideal Bose gas of dimers, one can use Eq. (2.24) for the associated spectral function of fermionic excitations, which gives

$$A_-(\mathbf{k},\varepsilon)=v_{\mathbf{k}}^2\delta(\varepsilon+\varepsilon_{\mathbf{k}}-2\mu) \tag{2.34}$$

in the BEC limit. The weight $v_{\mathbf{k}}^2=4\pi na^3(1+\mathbf{k}^2a^2)^{-2}$ now coincides with the square of the bound state wave function in momentum space. The resulting rf spectrum

$$I_{BEC}(\omega)=\frac{n}{\pi a\sqrt{m}}\frac{(\hbar\omega+2\mu)^{1/2}}{\omega^2} \tag{2.35}$$

is a special case of that derived by Chin and Julienne [44] in the molecular limit for bound-free transitions in the absence of final state interactions. It has an onset $\hbar\omega_{min,BEC}=-2\mu\to\varepsilon_b$ that is determined by the molecular binding energy $\varepsilon_b=\hbar^2/ma^2$ as expected. This energy also sets the scale for the half width of the rf spectrum, which is $E_w=\gamma\varepsilon_b$ with a numerical factor $\gamma=1.89$.

D. rf spectra at high frequencies and contact density

Our definition of the rf spectrum in Eq. (2.30) and normalization (2.23) of the hole part of the spectral function imply that the total weight integrated over all frequencies

$$\int d\omega\, I(\omega)=n_\sigma=n/2 \tag{2.36}$$

is determined by the density n_σ of atoms from which the transfer to the empty final state f occurs. This normalization fixes the overall prefactor and determines the normalized form of the rf spectra in which the zeroth moment is divided out. An analysis of the spectra in terms of their nontrivial higher moments, however, does not seem to work. Indeed, it follows from Eqs. (2.31) and (2.35) that the rf spectra at high frequencies fall off like $\omega^{-3/2}$ both in the BCS and the BEC limit. Thus, already the first moment of the spectrum diverges. The issue of the behavior at high frequencies has been investigated recently by Schneider *et al.* [45]. They have shown that the exact expression (2.30) quite generally implies an $\omega^{-3/2}$ power-law decay

$$I(\omega\to\infty)=\frac{C}{4\pi^2}\left(\frac{\hbar}{m}\right)^{1/2}\omega^{-3/2}. \tag{2.37}$$

Here, the coefficient C is defined by the behavior $n_\sigma(k)\to C/k^4$ of the momentum distribution at large momenta. It was introduced by Tan [23] as a parameter that characterizes quite generally fermionic systems with zero-range interactions. As shown by Braaten and Platter [24], this coefficient is a measure of the probability that two fermions with opposite spin are close together and is thus called a contact density or simply the contact. In the balanced superfluid, it has actually been determined from a measurement of the closed channel fraction by Partridge *et al.* [46], as analyzed in detail by Werner *et al.* [47]. In the BEC limit, the well known expression for $n_\sigma(k)$ in terms of the square of the bound state wave function yields $C_{BEC}=4\pi n/a$, consistent with the explicit form (2.35) of the spectrum in the BEC limit.

There are two important points in this context, which we discuss in the following. First of all, the asymptotic $\omega^{-3/2}$ power-law decay of the exact rf spectrum is valid only in the ideal case of zero-range interactions and identically vanishing final state effects. Indeed, an explicit calculation of the rf spectrum in the molecular limit by Chin and Julienne [44] shows that in the presence of a nonzero scattering length $a_f\neq0$ between the hyperfine state that is not affected by the rf pulse and the final state of the rf transition, the spectrum decays like $\omega^{-5/2}$ at large frequencies. The short-range part of the interaction, which is responsible for the slow decay of the spectrum, is therefore cancelled out by the interaction between the final state and the state that remains after the rf transition. This result remains valid quite generally along the whole BCS-BEC crossover as discussed by Zhang and Leggett [48,49]. In particular, this behavior guarantees that the rf spectrum has a finite first moment. As shown in Refs. [12,13], it allows to define an average "clock shift"

$$\hbar\bar{\omega}=s\frac{4\varepsilon_F^2}{n_\sigma}\left(\frac{1}{g}-\frac{1}{g_f}\right) \tag{2.38}$$

that is again determined by the contact coefficient $C=sk_F^4$ and the renormalized interaction constants $g=4\pi\hbar^2a/m$ and $g_f=4\pi\hbar^2a_f/m$. In particular, there is a perfect "atomic peak" $I(\omega)\sim\delta(\omega)$ and no clock shift at all if $a=a_f$. The existence of higher moments of the rf spectrum relies on accounting for the nonzero range $r_0\neq0$ of the interaction. Since this is expected to affect the spectrum only at frequencies of order $\hbar/mr_0^2$, this regime, however, will hardly be accessible experimentally.

As a second point, we consider the behavior of the contact coefficient C in the weak-coupling limit. Standard BCS theory for the momentum distribution at large k predicts that the corresponding dimensionless factor $s=C/k_F^4$ is exponentially small, $s_{BCS}=(\Delta/2\varepsilon_F)^2$. This is in agreement with the high frequency asymptotics of the ideal BCS spectrum (2.31) without final state interactions according to the result in Eq. (2.37).

It turns out, however, that the exponentially small value of the contact coefficient in the BCS limit is an artifact of working with a reduced BCS Hamiltonian, which only takes into account pairing part (2.32) of the interaction. By contrast, the full Hamiltonian gives an additional contribution that is associated with noncondensed close pairs. For weak coupling, this is much larger than that of the condensed pairs described by the BCS theory. More precisely, it turns out that the coefficient

$$s = [\Delta^2 - \Gamma_{11}(\mathbf{r}=\mathbf{0}, \tau=-0)]/(4\varepsilon_F^2) \tag{2.39}$$

in front of the $n_\sigma(k) = s(k_F/k)^4$ behavior of the momentum distribution at large k contains a nontrivial contribution associated with the upper diagonal element Γ_{11} of the vertex function defined in Eq. (2.12) in the limit of vanishing spatial and temporal separation. In the molecular limit, the contribution from this term is negligible. The asymptotic result $\Delta_{BEC} = 2\varepsilon_F\sqrt{4v/3\pi}$ for the gap parameter then gives rise to a linearly increasing dimensionless contact parameter $s_{BEC} = 4v/3\pi$ consistent with the naive result discussed above. On the contrary, in the weak-coupling limit, the contribution from noncondensed close pairs is dominant compared with the exponentially small BCS contribution from condensed pairs. In the limit $v \ll -1$ the leading behavior is given by

$$-\Gamma_{11}(\mathbf{0}, -0) = \left(\frac{4\varepsilon_F}{3\pi v}\right)^2. \tag{2.40}$$

The resulting dimensionless contact coefficient $s_{wc} = (2/3\pi v)^2$ in weak coupling is therefore much larger than the exponentially small BCS contribution. It is remarkable that the leading term in the weak-coupling contact density of the superfluid with $a<0$ is identical to the one that is obtained in a *repulsive* dilute normal Fermi liquid with $a>0$, which has first been calculated by Belyakov [50]. This shows that the dominant contribution to the contact density is independent of the sign of the interaction consistent with the "adiabatic theorem"

$$\frac{\partial u}{\partial(1/a)} = -\frac{\hbar^2}{4\pi m} C(a) \tag{2.41}$$

that relates the derivative of the energy per volume u with respect to the inverse scattering length to the contact coefficient C [24,51]. In fact, the simple mean-field interaction energy linear in a, which is the leading correction to the ground-state energy of the ideal Fermi gas, shows that $C(a) \sim a^2$ is independent of the sign of interactions to lowest order. The BCS pairing effects, that appear in the case of a negative scattering length, only give a subdominant, exponentially small reduction in the energy that is reflected in a corresponding tiny enhancement of the contact density. The full dependence of $s(v)$ along the BCS to BEC crossover for the balanced gas at zero temperature is shown in Fig. 1. The particular value $s(0) = 0.098$ at unitarity has in fact been determined before in the context of the average clock shift (2.38) [12] and is close to our present value $s(0) = 0.102$ that follows from Eq. (2.39). Since the contact density is a short-range correlation property, it is not very sensitive to temperature; see [52].

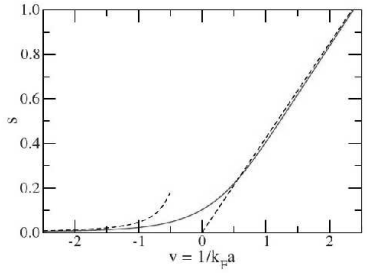

FIG. 1. (Color online) The dimensionless contact coefficient s is shown as a function of the dimensionless coupling strength $v = 1/k_F a$. The red solid line represents our numerical result obtained from Eq. (2.39). The left and right black dashed lines represent the asymptotic formulas s_{wc} and s_{BEC} given in the text, respectively.

An important consequence of the failure of naive BCS theory to account for the correct value of the contact density C in weak coupling is the fact that the weight of the rf spectrum at high frequencies that is determined by Eq. (2.37) in the absence of final state interactions or by the average clock shift (2.38) is strongly underestimated by using the idealized form (2.24) of the spectral functions that follow from a naive BCS theory. It is an interesting open problem to determine analytically the explicit form of the spectral functions in the weak-coupling limit which is consistent with the correct high frequency asymptotics (2.37) with the proper value for the contact density.

III. EFFECTIVE-FIELD THEORY AND PAIR SIZE

For a molecular BEC that consists of tightly bound dimers, the notion of a pair size is well defined. In the relevant case of a zero-range two-particle interaction with positive scattering length a, it is determined by the rms extension $\xi_m = a/\sqrt{2}$ of the two-body bound state. Since $k_F a \ll 1$ in the BEC limit, the size of the pairs in this regime is much smaller than the average interparticle spacing $(3\pi^2)^{1/3}/k_F \approx 3.1/k_F$ of the fermionic gas in the absence of an attractive interaction. Motivated by the fact that rf spectroscopy in this limit effectively reduces to a two-body molecular spectrum, a spectroscopic pair size ξ_w has been determined from the half width of the measured rf spectrum $I(\omega)$ by the relation $\xi_w^2 = \gamma \times \hbar^2/2mE_w$ [18]. By its definition, this pair size coincides with the molecular size $\xi_m = a/\sqrt{2}$ in the appropriate limit. Extending this definition to arbitrary coupling strengths, one obtains a ground-state pair size $\xi_w = 0.86\hbar v_F/\Delta_0$ in the opposite BCS limit, which correctly describes the exponentially large size of Cooper pairs characteristic for weak-coupling BCS superconductors [53]. It is thus plausible to use this spectroscopic definition of the pair size for the complete range of couplings, in particular also near the unitarity limit [18]. The measured rf spectrum at the lowest temperature, that has been reached experimentally, is then found to give an effective pair size $\xi_w \simeq 2.6/k_F$ at unitarity [18]. This is somewhat smaller than the average inter-

particle spacing indicating that the unitary gas has pairs that no longer overlap. The numerical value for the pair size is in fact close to that obtained from calculating the width of the pair wave function in a variational ansatz for the ground state of the BCS-BEC crossover [54].

An obvious question in this context is whether there are independent measures of the pair size which do not rely on the spectroscopic definition that is motivated by the extrapolation from the molecular limit or on the related variational approximation for the ground state in terms of a product of two-body wave functions. In the following, we will show that a many-body definition of the pair size can be obtained from the q-dependent superfluid response function following the basic concept of a nonlocal penetration depth in superconductors [53]. This response can be calculated from an effective-field theory of the superfluid state including the next-to-leading order corrections to the standard quantum hydrodynamic Lagrangian. Remarkably, the value of the pair size at unitarity that follows from the q-dependent superfluid response is close to that inferred spectroscopically from the half width of the rf spectrum.

The basic idea that allows to define a characteristic length ξ_p of a fermionic superfluid without reference to an approximate BCS or molecular description of the many-body ground state is related to the well known calculation of the q-dependent penetration depth $\lambda(q)$ in charged superconductors. The latter is defined by the nonlocal generalization $\mathbf{j}(q)=-\mathbf{A}(q)/4\pi\lambda^2(q)$ of the London equation relating the current density induced by a transverse vector potential in linear response [53]. The square of the inverse effective penetration depth determines the superfluid density $n_s(q)$, which obeys $n_s(q=0)=n$ in any Galilei invariant superfluid. For finite momentum q the superfluid response is reduced by a correction that has to vanish like q^2 in an isotropic system. The correction defines a characteristic length ξ_p according to

$$n_s(q) = n\left(1 - \frac{\pi^2}{30} q^2 \xi_p^2 + \cdots\right) \tag{3.1}$$

in the limit of small wave vectors q. Here, the prefactor in the q^2 correction has been chosen in such a way that the characteristic length ξ_p coincides with the Pippard length $\xi_P=\hbar v_F/\pi\Delta_0$ in the weak-coupling limit.

In order to determine the value of ξ_p at unitarity, one needs the leading order corrections in an expansion in small gradients to the universal quantum hydrodynamic Lagrangian density

$$\mathcal{L}_0 = \frac{\hbar^2 n}{2m}\left[\frac{1}{c_s^2}\dot{\varphi}^2 - (\nabla\varphi)^2\right] \tag{3.2}$$

of a translation invariant, neutral superfluid with (Bogoliubov-Anderson) sound velocity c_s. For the unitary Fermi gas, where $c_s^2=2\mu/3m$ exactly, these corrections have been discussed in detail by Son and Wingate [25]. Restricting ourselves to the harmonic description of the Goldstone mode described by Eq. (3.2) to leading order, the next-to-leading terms in the effective-field theory are of the form [25]

$$\mathcal{L}' = \hbar\left[c_1\sqrt{\frac{m}{\mu}}(\nabla\dot{\varphi})^2 + c_2\sqrt{\frac{\mu}{m}}(\nabla^2\varphi)^2\right]. \tag{3.3}$$

The associated dimensionless coefficients $c_{1,2}$ can only be determined from a microscopic theory. Their physical meaning becomes evident from the fact that c_2 determines the reduction of the superfluid response for finite wave vectors q as described in Eq. (3.1). In terms of the pair size ξ_p defined there, one finds

$$\frac{\pi^2}{30}\xi_p^2 = 9c_2\frac{\sqrt{m\mu}}{\hbar n}, \tag{3.4}$$

which also makes clear that c_2 has to be positive. In contrast to c_2, the coefficient c_1 has no direct physical interpretation. From the plane-wave solution of the linear equations of motion for the phase fluctuations that follow from the total Lagrangian density $\mathcal{L}_0+\mathcal{L}'$ it is easy to see, however, that this coefficient appears in the next-to-leading corrections in the dispersion $\omega(q)=c_s q(1-aq^2/k_F^2+\cdots)$ of the Bogoliubov-Anderson mode with a dimensionless coefficient [25]

$$a = \pi^2\sqrt{2\xi(0)}\left(\frac{3}{2}c_2 + c_1\right). \tag{3.5}$$

Here $\xi(0)\approx 0.36$ is the Bertsch parameter, which relates the sound and bare Fermi velocities by $c_s^2=\xi(0)v_F^2/3$. Similar to the Bertsch parameter, which appears in the leading order Lagrangian (3.2), the coefficients $c_{1,2}$ can be calculated in an expansion around the upper critical dimension four of the unitary Fermi gas as suggested originally by Nussinov and Nussinov [55] and started by Nishida and Son [56]. A one-loop calculation of the coefficients $c_{1,2}$ has recently been performed by Rupak and Schäfer [57]. The resulting value of c_1 at $\epsilon=4-d=1$ turns out to be $c_1\approx -0.02$. Unfortunately, for c_2, the one-loop calculation is not sufficient, because a finite value of c_2 only appears at order ϵ^2 [57]. This is easy to understand from connection (3.4) between c_2 and the pair size, which is expected to vanish linearly in $\epsilon=4-d$. Indeed in four dimensions, a two-particle bound state in a zero-range potential only appears at infinitely strong attraction [55]. The unitary gas in $d=4$ therefore has a vanishing dimer size and is effectively an ideal Bose gas similar to the situation in the BEC limit in $d=3$ [58]. In order to fix the value of c_2 for the unitary gas in three dimensions, we use connection (3.5) between the next-to-leading order coefficients of the effective-field theory and the q^3 corrections to the dispersion $\omega(q)$ of the Bogoliubov-Anderson mode. This dispersion has been calculated within a Gaussian fluctuation approximation for arbitrary coupling strengths v [39] and exhibits a negative curvature with $a\approx 0.06$ right at unitarity [59]. Combined with the value of c_1 from the ϵ expansion, this leads to the estimate $c_2\approx 0.02$ for the unitary gas in three dimensions. As a result, the pair size that follows from Eq. (3.4) turns out to be $\xi_p\approx 2.62/k_F$. It is remarkable that this value essentially coincides with that inferred from the spectroscopic definition in Ref. [18] or the width of the pair wave function in Ref. [54]. It should be noted, though, that apart from the uncertainties in the precise values of $c_{1,2}$, there is a certain amount of arbitrariness in defining a "pair size," both from the rf

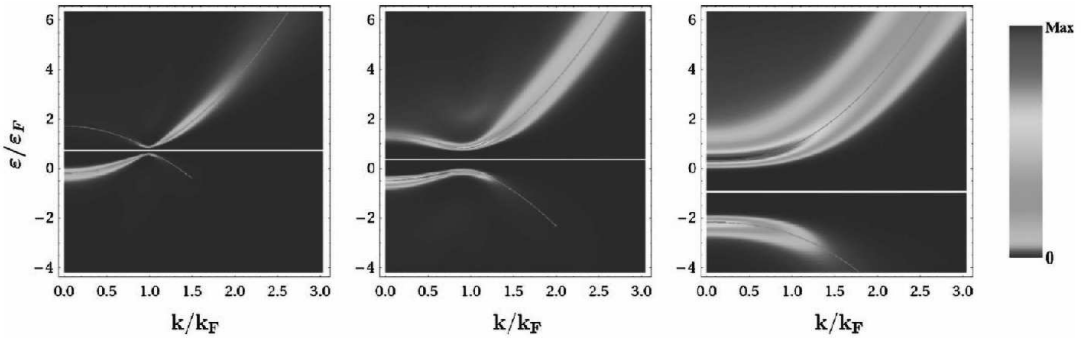

FIG. 2. (Color) Density plots of the spectral function $A(k,\varepsilon)$ at temperature $T=0.01T_F$ for the interaction strengths $v=1/(k_Fa)=-1,0,+1$ from left to right. The white horizontal lines indicate the chemical potential μ. The gray lines are fits to the maxima of $A(\mathbf{k},\varepsilon)$ using Eq. (4.1).

spectrum or from the q-dependent superfluid response via Eq. (3.4). This is related to the precise choice of the prefactor both in the spectroscopic definition and in Eq. (3.4), where the Pippard length has been used as a reference scale. The naive conclusion that the unitary gas has nonoverlapping pairs in its ground state should therefore be viewed with a great deal of caution.

The fact that the coefficients $c_{1,2}$ of the next-to-leading order Lagrangian (3.3) have a comparable magnitude at unitarity has a further interesting consequence. Indeed, these coefficients determine the magnitude of the Weizsäcker inhomogeneity correction [60,61]

$$\varepsilon_W(x) = b\frac{\hbar^2}{2m}\frac{[\nabla n(x)]^2}{n(x)} \tag{3.6}$$

to the ground-state energy density of the unitary Fermi gas [57]. The associated dimensionless coefficient b is related to the q^2 corrections of the density response [25]

$$\chi(q) = \chi(0)\left[1 - b\left(\frac{\hbar q}{mc_s}\right)^2 + \cdots\right]. \tag{3.7}$$

For the unitary Fermi gas, the coefficient b is again determined by the next-to-leading order Lagrangian (3.4) via [57]

$$b = \frac{32\pi^2}{3}[\sqrt{2\xi(0)}]^3\left(\frac{9}{2}c_2 - c_1\right). \tag{3.8}$$

Using our estimates for $c_{1,2}$, this leads to $b\approx 0.22$, a value that is almost one order of magnitude larger than the result $b^{(0)}=1/36=0.028$ which is obtained for an ideal Fermi gas. The unitary gas is therefore remarkable in the sense that its kinetic energy density $\varepsilon_{kin}(x)\sim\xi(0)n^{5/3}(x)$ is *reduced* by the Bertsch parameter $\xi(0)\approx 0.36$ compared with the noninteracting gas, yet the coefficient b of the Weizsäcker inhomogeneity correction is strongly *enhanced* [57].

IV. NUMERICAL RESULTS

In the following, we present numerical results for the spectral function $A(\mathbf{k},\varepsilon)$ and the rf spectrum $I(\omega)$ which can be compared with experimental data. The numerical calculations are performed in two steps. First, the Matsubara Green's function $\mathcal{G}(\mathbf{k},\omega_n)$ is calculated by solving the self-consistent Eqs. (2.10)–(2.15). In a second step the spectral function $A(\mathbf{k},\varepsilon)$ is calculated from Eq. (2.17) by analytical continuation as described in Sec. II B. For this purpose we employ a maximum-entropy method that is described in Appendix A. Eventually, the rf spectrum $I(\omega)$ is calculated by evaluating momentum integral (2.30) numerically.

A. Spectral functions

Our numerical results for the spectral functions $A(\mathbf{k},\varepsilon)$ in the experimentally relevant range of interaction strengths $v=-1$, 0, and $+1$ are shown in Fig. 2. The associated temperature is $T=0.01T_F$, i.e., deep in the superfluid regime in all three cases. Evidently, both at $v=-1$ and at unitarity $v=0$, a BCS-like quasiparticle structure appears with an excitation gap whose minimum is at a finite value of the momentum. On the BEC side, at $v=+1$, the backbending in the dispersion curve has apparently disappeared. This is consistent with the expected existence of a critical value $v_s>0$, beyond which the fermionic excitations have their minimum at $\mathbf{k}=0$. From our numerical data on the momentum dependence of the fermionic excitation spectrum, the associated critical coupling constant is $v_s=0.8$. This is about a factor of 2 larger than the mean-field prediction, which is determined by the zero crossing of the chemical potential. The fact that v_s occurs in the regime where the chemical potential is already negative has been noted before in an $\varepsilon=4-d$ expansion by Nishida and Son [62]. Extrapolating their one-loop result to $\varepsilon=1$ gives $\mu_s\simeq -0.5\varepsilon_F$ at the critical coupling v_s in rather good agreement with our result $\mu_s=-0.54\varepsilon_F$. In population imbalanced gases the change in the curvature of the fermionic excitation spectrum at v_s determines the critical coupling of the splitting point S at which the continuous transition from a balanced to an imbalanced superfluid on the BEC side splits into two first-order transitions [63].

Empirically, the form of the quasiparticle dispersion relations may be extracted from the peak position of the spectral

TABLE I. Effective mass m^* and Hartree shift U of the quasiparticle dispersion relations at $T=0.01T_F$ obtained by fitting Eq. (4.1) to the peak maxima of the spectral functions in Fig. 2.

			Particle		Hole	
v	μ/ε_F	Δ/ε_F	m^*/m	U/ε_F	m^*/m	U/ε_F
−1	0.73	0.14	1.05	−0.26	1.12	−0.17
0	0.36	0.46	1.00	−0.50	1.19	−0.35
+1	−0.93	1.10	1.02	−0.42	1.28	−0.37

function. It turns out that these peaks fit reasonably well to a modified dispersion

$$\tilde{E}_{\mathbf{k}}^{(-)} = \mu + \sqrt{\left(\frac{m}{m^*}\varepsilon_{\mathbf{k}} + U - \mu\right)^2 + \Delta^2} \tag{4.1}$$

of Bogoliubov quasiparticles, in which the effective mass m^* and an additional Hartree shift U are used as fit parameters. The associated values for m^* and U that follow from the spectral functions shown in Fig. 2 are summarized in Table I. It is interesting to note that both the masses and the Hartree shifts are different for particle and hole excitations. The particle-hole symmetry of the standard BCS description of the quasiparticle dispersion is therefore broken at these large coupling strengths. A second feature of interest is that the hole dispersion relation $E_{\mathbf{k}}^{(-)}$ starts to deviate from BCS form (4.1) only for momenta $k \gtrsim 1.5k_F$, when the spectral weight of the hole peak is smaller than 0.5%.

Using QMC methods, the particle dispersion relation at unitarity and $T=0$ has been calculated previously by Carlson and Reddy [64]. Our values for the Hartree shift U and the effective mass m^* of the particle dispersion relation agree reasonably well with the QMC values. Experimentally, the Hartree shift U was extracted recently from rf measurements by Schirotzek *et al.* [65]. In this work, the measured peak positions of the rf spectra were fitted with the peak position obtained from BCS formula (2.31) including an additional Hartree shift: $\omega_{\text{peak}}^{BCS}=4[\sqrt{(\mu-U)^2+15\Delta^2/16}-\mu+U/4]/3$. If we apply this method to our calculated rf spectra, we obtain different values for U than those listed in Table I. In particular, this method gives $U=-0.28,-0.52,-0.22$ for $v=-1,0,+1$ at $T=0.01T_F$ and does not take the effective mass into account (we note that the rf spectrum is only sensitive to the hole excitation part of the spectral function). This discrepancy is probably due to the fact that the assumption of having sharp quasiparticles is not reliable in this regime.

It is evident from the quantitative form of the spectral functions that the parametrization of the fermionic excitations by a modified dispersion (4.1) is not an adequate description of the excitation spectrum because of the rather strong broadening of the quasiparticle peaks even at very low temperatures. The physical origin of this broadening is the residual interaction between the quasiparticles that follows from the Hamiltonian in Eq. (2.33). As shown in Appendix B, this interaction leads to a finite width of the spectral functions even at $T=0$, except near the minimum of the dispersion curve for the particle excitations and close to the maximum of the dispersion for the hole excitations. Here, the quasiparticle lifetime broadening has to vanish because there are no available final states into which it may decay. Focusing on the interaction of the quasiparticles with the collective Bogoliubov-Anderson mode, which is the dominant mechanism for decay near the minimum (maximum) of the particle (hole) dispersion curve, it is straightforward to see that there is actually a finite interval in momentum space where the spectral width vanishes identically. This width is determined by the kinematic constraint that that the quasiparticle decay by emission of phonons is possible only if the group velocity $\partial E_{\mathbf{k}}/\partial \mathbf{k}$ of the fermionic excitations becomes larger than the sound velocity c_s. In fact a similar situation appears for a hole in a Néel-ordered antiferromagnet, whose spectral function is sharp as long as its group velocity is below the spin-wave velocity of antiferromagnetic magnons [66]. The fact that our numerically calculated spectral functions $A(\mathbf{k},\varepsilon)$ exhibit a finite broadening at the lowest temperature $T=0.01T_F$ even near the dispersion minimum is probably related both to the numerical procedure of evaluating $A(\mathbf{k},\varepsilon)$ using the Maxent technique which can never give rise to perfectly sharp peaks, but also to the self-consistent structure of our Luttinger-Ward formulation. Indeed, in a diagrammatic language, the latter implies summation of diagrams with identical intermediate states for fermions, which—in an exact theory—are excluded by the Pauli principle. Unfortunately, to our knowledge, there exist no analytical results on the broadening of the Bogoliubov quasiparticles beyond the perturbative treatment outlined in Appendix B. Experimentally, this question may in principle be resolved by studying momentum-resolved rf spectra that have recently been obtained by Stewart *et al.* [19]. Unfortunately, at present, experimental data on spectral functions are available only near the critical temperature of the superfluid transition, where the finite lifetime arises due to the scattering with thermally excited quasiparticles.

To discuss the situation at finite temperature, we plot the spectral function $A(\mathbf{k},\varepsilon)$ at unitarity for different temperatures above and below T_c in Figs. 3 and 4. It is interesting to observe how the two BCS-like quasiparticle peaks evolve with increasing temperature and finally merge into a single excitation structure with a quadratic dispersion at temperatures around T_c. Note, however, that the spectral peak in the normal phase is shifted to negative energies compared to the free fermion dispersion relation $\varepsilon_{\mathbf{k}}=\hbar^2\mathbf{k}^2/2m$. This Hartree shift is responsible for the observation of shifts in experimentally measured rf spectra above T_c, which will be discussed in detail below. The observation of such a shift in the rf spectra in the normal state is therefore not necessarily a signature of pseudogap effects.

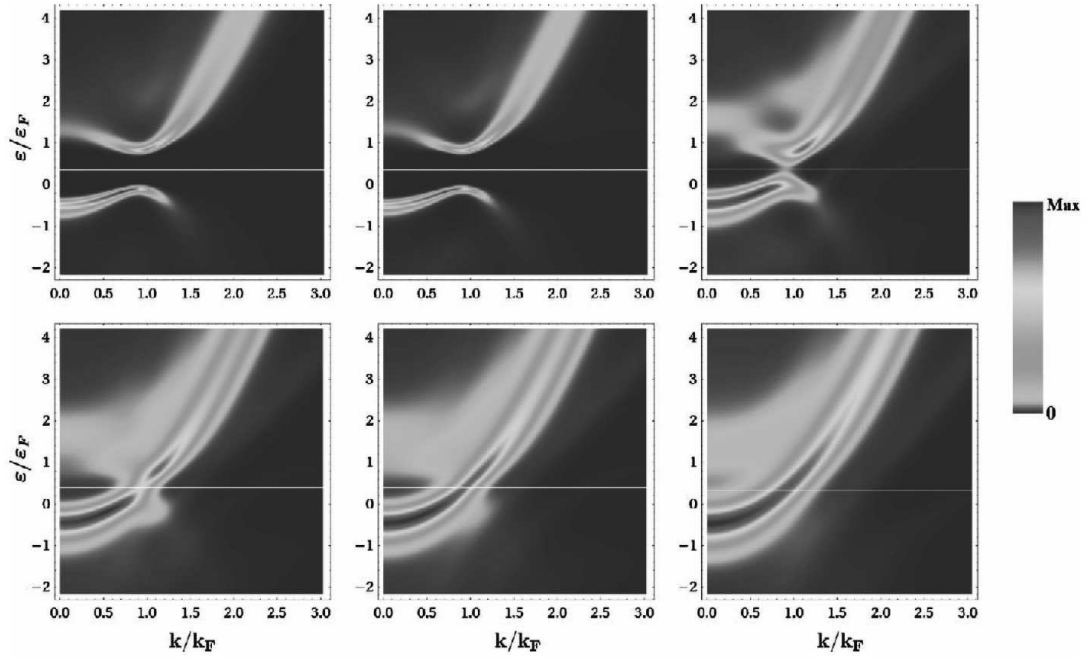

FIG. 3. (Color) Density plots of the spectral function $A(\mathbf{k},\varepsilon)$ at unitarity $[v=1/(k_F a)=0]$ for different temperatures. From top left to bottom right: $T/T_F=0.01$, 0.06, 0.14, $0.160(T_c)$, 0.18, and 0.30. The white horizontal lines mark the chemical potential μ. At temperatures smaller than the superfluid transition temperature T_c two quasiparticle structures with a BCS-like dispersion can be seen. The width of the spectral peaks is of the same order as the quasiparticle energy. With increasing temperature the two branches gradually merge into a single quasiparticle structure with a quadratic dispersion above T_c. Note, however, that the quadratic dispersion is shifted to negative frequencies compared to the bare fermion dispersion relation. This Hartree shift is of the order of $U=-0.46\varepsilon_F$ and is essentially responsible for the shifted rf spectra in the normal phase in Fig. 6.

Finite temperature QMC calculations of the spectral function at unitarity by Bulgac *et al.* [67] indicate the presence of a gapped particle excitation spectrum of form (4.1) also above the critical temperature, which is not found in our approach. More generally, it is evident from the spectral functions of the unitary gas above T_c which are shown in Fig. 3 that a simple pseudogap ansatz for the spectral function [69] is not consistent with our results. As can be seen from the lower three graphs in Fig. 3, our approach leads to a single, broad, ungapped excitation peak with a quadratic dispersion at temperatures $T>T_c$ instead of two excitation branches with a gapped BCS-like dispersion as expected from the pseudogap approach. In particular we do not observe a strong suppression of spectral weight near the chemical potential.

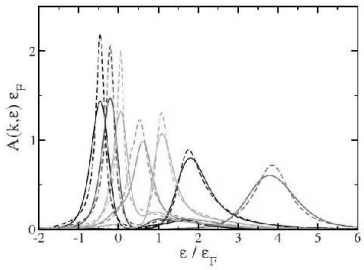

FIG. 4. (Color online) The spectral function $A(\mathbf{k},\varepsilon)$ as a function of ε for selected fixed values k at unitarity $v=1/(k_F a)=0$ and at criticality $T/T_F=0.160(T_c)$. The selected values of the wave number k are represented by the colors of the lines corresponding to the peaks from left to right: $k/k_F=0.00$ (black), 0.52 (red), 0.77 (orange), 1.00 (green), 1.26 (cyan), 1.51 (blue), and 2.02 (magenta). The different methods for calculating the spectral function are distinguished by the line styles: maximum-entropy method (solid lines) and Padé approximation (dashed lines).

Apart from the dominant peaks discussed above our spectral functions show some additional structures that have much smaller weight, however. Specifically, at unitarity and temperatures above T_c a small second peak is visible for $k \lesssim k_F$ in Fig. 3. At $T=0.3T_F$ this residual peak contains $\sim 17\%$ of the spectral weight. The situation is similar on the BEC side of the Feshbach resonance at $v=1$, where above T_c a second peak at negative energies is present for $k \lesssim k_F$, with a spectral weight of $\sim 22\%$.

Recent experiments by Stewart *et al.* [19] have succeeded to perform rf spectroscopy in a momentum-resolved manner from which one directly obtains the hole spectral function $A_-(\mathbf{k},\varepsilon)$ as a function of both momentum and energy. A

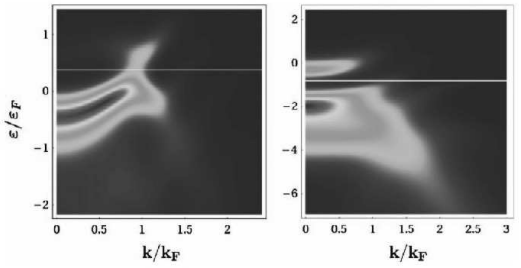

FIG. 5. (Color) Density plot of the hole part of the spectral function $A_-(\mathbf{k},\varepsilon)$ at unitarity $v=1/(k_F a)=0$ and $T/T_F=0.150$ slightly below T_c (left) and in the BEC regime at $v=1/(k_F a)=+1$ and $T/T_F=0.207$ at the superfluid transition temperature (right). The white horizontal line marks the chemical potential μ. The color scheme is the same as in Figs. 2 and 3.

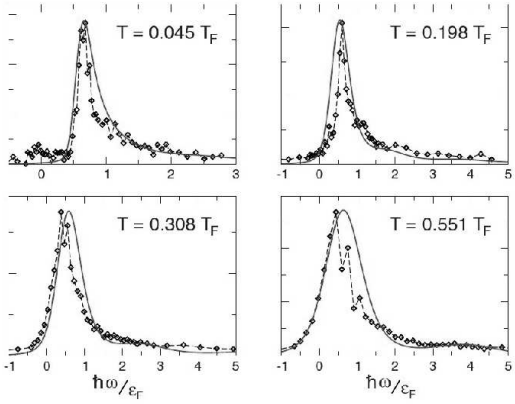

FIG. 6. (Color online) Comparison of the calculated rf spectra at unitarity with the experimental data of Schirotzek *et al.* [65] from MIT at different temperatures T. Our numerical result is shown by the red solid line. The experimental data are represented by open diamonds connected by straight thin dashed lines. Apart from adjusting the peak heights, no fitting parameters have been used.

quantitative comparison with our calculated spectral functions is difficult, however, since the measured spectral functions involve an average over the inhomogeneous density profile of the trapped atoms. Nevertheless, as shown in Fig. 5, the qualitative structure of our hole spectral function of the uniform system near the critical temperature is similar to that observed experimentally. To separate the intrinsic from an inhomogeneous broadening in a trap requires combining momentum and local resolution, which is currently investigated in the group at JILA. Experiments of this kind would allow to distinguish between different models for the spectral functions, in particular for the "pseudogap" phase immediately above T_c. The existence of preformed pairs in this regime is often described by sharp spectral functions of form (2.24) with a nonvanishing gap parameter Δ_{pg}. As shown recently by Chen *et al.* [70] and Dao *et al.* [71], this assumption is also consistent with present experimental data due to the inhomogeneous averaging associated with the position-dependent gap parameter in a trap.

B. rf response

In Fig. 6 we show the calculated rf spectra together with the locally resolved experimental data of Schirotzek *et al.* [65] from MIT. The measured rf data shown in Fig. 6 have been corrected for the small mean-field final state interaction energy, which allows for a direct comparison with our calculated spectra. For a detailed comparison we must take the finite experimental resolution into account, however. Schirotzek *et al.* use an approximately rectangular rf pulse with a length of $T=200$ μs in order to transfer atoms to the empty hyperfine state. Thus, the Fourier spectrum of the radio-frequency source has a finite width and the calculated spectra obtained using Eq. (2.30) need to be convolved with $\mathrm{sinc}^2(\omega T/2)$, i.e.,

$$I_{\mathrm{exp}}(\omega)=\int d\omega' I(\omega-\omega')\mathrm{sinc}^2(\omega' T/2). \qquad (4.2)$$

The finite experimental resolution thus leads to a slight broadening and a small shift to higher frequencies of the calculated rf spectra. At unitarity and $T=0.01T_F$, the broadening is $\sim 0.07\varepsilon_F$ and the shift $\sim 0.01\varepsilon_F$.

As can be seen in Fig. 6, the rf spectra in the homogeneous system show a single peak that is shifted compared to the bare transition frequency, which is set to $\omega=0$ for convenience. Apart from slightly overestimating the width of the spectral lines, our numerically obtained spectra agree very well with the experimental data. Note that no fitting parameters have been used apart from adjusting the absolute height.

In the first rf measurements by Chin *et al.* [10] a secondary peak at the bare transition frequency has been observed and attributed to the presence of unpaired atoms. In these experiments, however, the measurement of the spectra involved an average over the inhomogeneous density profile of the trapped atoms. Since more recent locally resolved rf measurements [17] did not show signs of an atomic peak, it is likely that these peaks either originate from the low density regions at the edge of the atomic cloud or are an effect of the strong final state interactions.

It is important to notice that there are essentially two contributions to the rf peak shift. The first one is due to pairing correlations, which are particularly important in the superfluid phase and give the dominant contribution to the peak shift on the BEC side of the crossover, where the fermions are paired in two-body bound states. The second contribution comes from Hartree-type correlations. The Hartree contribution dominates the peak shift in the normal phase, where pairing correlations are small. Furthermore, it also dominates in the BCS regime, since the gap is exponentially small whereas the Hartree contribution scales linearly with $k_F a$. Together with the discussion of the residual interaction between the quasiparticles in Sec. II C this implies that BCS formula (2.31) for the rf spectrum in weak coupling is completely misleading.

V. DISCUSSION

The results presented above on the spectral functions and the associated rf spectra of ultracold fermionic gases near a Feshbach resonance have two major aspects. First of all, they provide a quantitative description of recent experiments on the excitation spectra of the near unitary gas. The theory covers the complete range of temperatures from the superfluid near zero temperature to the anomalous normal state above T_c which is characterized by strong pairing fluctuations. From a theoretical point of view, our results are of relevance as a simple example, where the standard quasiparticle description of BCS theory is strongly modified. As a result of interactions between quasiparticles and their coupling to the collective Bogoliubov-Anderson phonon, the spectral functions acquire a finite broadening even at zero temperature except for a small range of momenta around the dispersion minimum (maximum) of the particle (hole) excitations. Effectively, the fermionic excitations along the BCS-BEC crossover are not a Fermi gas as in BCS theory but are described by a Fermi-liquid picture. The spectral functions therefore have vanishing width at zero temperature at a sharply defined surface in momentum space, where the excitation energy has its minimum [68]. Within a perturbative calculation around the BCS limit, this has been shown explicitly in Appendix B. More generally, it is expected to be valid for arbitrary coupling because the phase space for quasiparticle decay vanishes near the dispersion minimum. We are not aware, however, of a general proof of this statement for the simple model (2.1) of attractively interacting fermions studied here.

As discussed in Sec. II C, the finite lifetime of the fermionic excitations at small momenta is particularly important for the onset of the rf spectra shown in Fig. 6. In the BCS picture, where the spectral function has vanishing width at arbitrary momentum $\mathbf{k}$, the rf spectra would exhibit a sharp onset. As argued above, however, the fermionic excitations near $\mathbf{k}=0$ have a finite width even at $T=0$ up to the critical coupling v_s because they are far away from the maximum of the hole dispersion. As a result, the rf spectra have no sharp onset in agreement with the experimental observation. A further important aspect of our results is that the naive description of the BCS-BEC crossover problem by an extended BCS ansatz [4], that appears to work qualitatively at least for the ground state, is completely inadequate as far as dynamical correlations are concerned. In particular, the simple form of the spectral function in Eq. (2.24) that follows from a naive BCS theory is never valid because the pure pairing Hamiltonian on which it is based misses both the broadening, e.g., due to collective excitations, and the large contribution to the contact coefficient due to noncondensed close pairs. A rather surprising conclusion of our work is that the next-to-leading terms in the effective-field theory for the Bogoliubov-Anderson mode allow us to give a many-body definition of the pair size which agrees quite well with the result found experimentally from the half width of the rf spectrum.

There are of course a number of open problems which should be addressed in future work. In particular, it would be interesting to understand to which extent the normal phase above T_c can be understood in terms of a pseudogap model, which has been applied with reasonable success to understand angle-resolved photoemission spectroscopy experiments in the context of high T_c cuprates [69]. As far as pseudogap effects are concerned, our spectral functions close to T_c show a different behavior than previous non-self-consistent calculations [72–74] and more recent QMC calculations [67], which exhibit a pseudogap. Quite generally it is known that non-self-consistent calculations favor pseudogap behavior, whereas self-consistent calculations suppress pseudogap effects (cf. [75] and references therein). We emphasize, however, that in the context of ultracold gases, the available momentum and energy resolution in experiments at present is not good enough to map out the spectral function in sufficient detail. Apart from the rather good agreement between the observed rf spectra and our results for the underlying spectral function, the confidence that our self-consistent Luttinger-Ward approach to the BCS-BEC crossover gives quantitatively reliable results is supported by the very precise description it provides for thermodynamic properties (see the discussion at the end of Sec. II A) much better than non-self-consistent approaches. It is an open problem to determine spectral functions, e.g., from QMC data, at the level of accuracy that has now been achieved for equilibrium properties.

ACKNOWLEDGMENTS

W.Z. is grateful for the hospitality as a visitor at the MIT-Harvard Center for Ultracold Atoms during the academic year 2007/2008, where this work was started. We acknowledge many useful discussions with W. Ketterle, A. Schirotzek, Yong-Il Shin, and M. Zwierlein. In particular, we are grateful to Schirotzek *et al.* for making their data available for a comparison with theory. We are also grateful to S. Biermann from the Ecole Polytechnique in Paris for checking some of our numerical results using her Padé code and to T. Enss, A. Georges, A. J. Leggett, M. Randeria, and P. Schuck for discussions. Part of this work was supported by the Deutsche Forschungsgemeinschaft within the Forschergruppe 801 "Strong correlations in multiflavor ultracold quantum gases."

APPENDIX A: MAXIMUM-ENTROPY METHOD

In order to solve Eq. (2.17) explicitly for $A(\mathbf{k},\varepsilon)$ the integral is discretized. We chose equally spaced energies ε in the inner interval $-10\varepsilon_F<\varepsilon<+10\varepsilon_F$ and logarithmically spaced energies in the outer regions $-10^6\varepsilon_F<\varepsilon<-10\varepsilon_F$ and $+10\varepsilon_F<\varepsilon<+10^6\varepsilon_F$. We evaluate the integral by using the trapezoid formula. On the right-hand side of Eq. (2.17) the Matsubara Green's function $\mathcal{G}(\mathbf{k},\omega_n)$ is given for selected Matsubara frequencies $\omega_n^{(l)}$ on a logarithmic scale, which are ordered according to $0<\omega_n^{(1)}<\omega_n^{(2)}<\cdots<\omega_n^{(l_{\max})}\sim 10^6\varepsilon_F$. In this way, Eq. (2.17) is transformed into a set of linear equations which can be solved by standard numerical methods.

Unfortunately, the linear equations are nearly singular even if the number of discrete energies ε (number of un-

known variables) is smaller than $l_{\max}$ (number of equations). Many eigenvalues of the linear matrix are very close to zero, so that small numerical errors in the Matsubara Green's function $\mathcal{G}(\mathbf{k},\omega_n)$ are enhanced exponentially. As a result, the spectral function $A(\mathbf{k},\varepsilon)$ cannot be calculated by this simple method.

In order to improve and stabilize the method we need some prior information. We assume that a smooth backgroundlike prior spectral function $A_0(\varepsilon)$ is given. We define the *entropy*

$$S(\mathbf{k}) = \int d\varepsilon \{A(\mathbf{k},\varepsilon) - A_0(\varepsilon) - A(\mathbf{k},\varepsilon)\ln[A(\mathbf{k},\varepsilon)/A_0(\varepsilon)]\}, \tag{A1}$$

where the integral is evaluated numerically by the trapezoid formula for the above defined discrete energies ε. The spectral function $A(\mathbf{k},\varepsilon)$ is obtained by maximizing the entropy (A1) for given wave vectors $\mathbf{k}$ where Eq. (2.17) is used as a constraint. This procedure is known as the maximum-entropy method and can be derived by Bayes inference [76]. It has been applied successfully for calculating the spectral function $A(\mathbf{k},\varepsilon)$ from the Matsubara Green's function $\mathcal{G}(\mathbf{k},\omega_n)$ in Monte Carlo simulations [42].

In order to implement the constraints we define the chi square

$$[\chi(\mathbf{k})]^2 = \frac{1}{l_{\max}} \sum_{l=1}^{l_{\max}} |d(\mathbf{k},\omega_n^{(l)})|^2/\sigma^2, \tag{A2}$$

where

$$d(\mathbf{k},\omega_n) = -i\hbar\omega_n \left[\mathcal{G}(\mathbf{k},\omega_n) - \int d\varepsilon \frac{A(\mathbf{k},\varepsilon)}{-i\hbar\omega_n + \varepsilon - \mu} \right] \tag{A3}$$

is a dimensionless difference and σ is a dimensionless standard deviation. Minimizing $[\chi(\mathbf{k})]^2$ we recover the constraint equations (2.17).

By solving the self-consistent equations of Sec. II we calculate the Matsubara Green's function $\mathcal{G}(\mathbf{k},\omega_n)$ with a relative accuracy of about 10^{-5}. For this reason, we expect $|d(\mathbf{k},\omega_n)| \sim 10^{-5}$ and chose the fixed value $\sigma = 10^{-5}$ for the standard deviation. As a result we observe $\chi(\mathbf{k}) \sim 1$ in our numerical calculations where variations occur by a factor of 10 for different wave vectors $\mathbf{k}$.

Using Bayes inference [76] it can be shown that

$$Q(\mathbf{k}) = \alpha S(\mathbf{k}) - \frac{1}{2}[\chi(\mathbf{k})]^2 \tag{A4}$$

is the functional which must be maximized by variation in the spectral function $A(\mathbf{k},\varepsilon)$ for every fixed wave vector $\mathbf{k}$. The related necessary condition is

$$\frac{\delta Q(\mathbf{k})}{\delta A(\mathbf{k},\varepsilon)} = 0, \tag{A5}$$

which implies the equations to be solved numerically for $A(\mathbf{k},\varepsilon)$. In Eq. (A4) α is a Lagrange parameter which balances the weight between entropy (A1) and constraints (A2). For $\alpha = 0$ we recover constraint equations (2.17). On the other hand, in the limit $\alpha \to \infty$ we obtain the prior spectral function $A(\mathbf{k},\varepsilon) = A_0(\varepsilon)$. Thus, α is a parameter which must be adjusted to an intermediate value in order to obtain an optimum result for the spectral function $A(\mathbf{k},\varepsilon)$. For low values α the constraints are overweighted. A more accurate result is obtained for $A(\mathbf{k},\varepsilon)$; however, instabilities may occur. On the other hand, for higher values α the entropy is overweighted. A more stable result is obtained which, however, may be less accurate.

We have defined entropy (A1) and chi square (A2) as dimensionless quantities which are of order unity. For this reason, we expect that α must be of order unity, too. Actually, we find that $\alpha = 1$ is an optimum choice in most areas of the phase diagram except for low temperatures. For this reason, we use $\alpha = 1$ in most cases. However, for low temperatures $T \lesssim 0.5T_c$ the spectral function $A(\mathbf{k},\varepsilon)$ is very close to zero in the gap region. Since the numerical algorithm considers the logarithm $\ln[A(\mathbf{k},\varepsilon)]$ an instability occurs. Hence, in this latter case for low temperatures we choose $\alpha = 100$ in the crossover and BEC regime, and $\alpha = 1000$ in the BCS regime.

For the success of the method an appropriate choice for the prior spectrum $A_0(\varepsilon)$ is very important. First of all the prior spectrum $A_0(\varepsilon)$ should be a smooth function of the energy ε which models a broad background spectrum. The special form of entropy (A1) does *not* require $A_0(\varepsilon)$ to be normalized. Constraint equations (2.17) will determine the spectral function $A(\mathbf{k},\varepsilon)$ for small and intermediate energies in the inner interval $-10\varepsilon_F \lesssim \varepsilon \lesssim +10\varepsilon_F$. However, the constraints will provide less information in the tail regions $\varepsilon \ll -10\varepsilon_F$ and $\varepsilon \gg +10\varepsilon_F$. For this reason our method is considerably improved if the prior spectrum $A_0(\varepsilon)$ already shows the correct wings for $\varepsilon \to +\infty$.

Investigating the Matsubara Green's function for large Matsubara frequencies $\omega_n \to +\infty$ we obtain the asymptotic formula

$$\mathcal{G}(\mathbf{k},\omega_n) \approx (-i\hbar\omega_n)^{-1} + a_{\mathbf{k}}(-i\hbar\omega_n)^{-2} + \pi b(-i\hbar\omega_n)^{-5/2}, \tag{A6}$$

where $a_{\mathbf{k}} = -(\varepsilon_{\mathbf{k}} - \mu)$ and $b = (2/3\pi^2)(2\varepsilon_F)^{3/2}$. The analytic continuation by substitution $i\hbar\omega_n \to \hbar z - \mu$ yields the asymptotic complex Green's function

$$G(\mathbf{k},z) \approx (-\hbar z)^{-1} - \varepsilon_{\mathbf{k}}(-\hbar z)^{-2} + \pi b(-\hbar z)^{-5/2} \tag{A7}$$

for $|z| \to \infty$. Eventually from Eq. (2.27) we obtain the asymptotic spectral function $A(\mathbf{k},\varepsilon) \approx b\theta(\varepsilon)\varepsilon^{-5/2}$ for $\varepsilon \to +\infty$. Thus, the weight of the asymptotic power law of the spectral function is described by the constant factor b which is real, positive, and independent of $\mathbf{k}$.

A prior spectrum which meets all these requirements and which shows the correct wings is given by

$$A_0(\varepsilon) = b\frac{[\varepsilon^2 + \gamma^2]^{1/2} + \varepsilon}{2[\varepsilon^2 + \gamma^2]^{7/4}}. \tag{A8}$$

The denominator represents a modified Lorentz spectrum with a nontrivial exponent. In order to have a smooth func-

tion, we choose a large spectral width $\gamma=20\varepsilon_F$. The specific form of the numerator and the exponent of the denominator guarantee the correct wings for $\varepsilon\to+\infty$ in leading order. It turns out that the prior spectrum $A_0(\varepsilon)$ can be chosen independent of $\mathbf{k}$.

In our implementation of the method we solve Eq. (A5) numerically by using Bryan's algorithm [77]. The rectangular matrix of the discretized constraint equations (2.17) is decomposed by using a singular-value decomposition. Eventually we observe that only a small fraction of about 15–20 eigenvalues provide essential contributions for the spectral function $A(\mathbf{k},\varepsilon)$.

The maximum-entropy method must be applied for each value of the wave vector $\mathbf{k}$ in order to obtain the complete spectral function $A(\mathbf{k},\varepsilon)$. We find that the parameters of the method σ, α, γ, and b can be chosen independent of $\mathbf{k}$. We observe that entropy (A1) together with the prior spectrum (A8) guarantees a positive spectral function $A(\mathbf{k},\varepsilon)>0$. Finally, in our numerical calculations we observe that the dimensionless difference (A3) has the same order $\sim 10^{-5}$ over the whole range of Matsubara frequencies ω_n and for all $\mathbf{k}$ which is essential for the quality of our implementation of the maximum-entropy method.

APPENDIX B: LIFETIME OF FERMIONIC EXCITATIONS AT ZERO TEMPERATURE

In this appendix we outline an analytical calculation of the lifetime of fermionic excitations at zero temperature, which is perturbative in deviations from the exactly soluble reduced BCS Hamiltonian (2.32). For arguments that indicate a breakdown of well-defined fermionic excitations in the opposite BEC limit see [78].

Quite generally a quasiparticle description of the BCS-BEC crossover problem requires that the low lying excitations above the exact ground state with energy E_0 can be described by a noninteracting gas of quasiparticles,

$$H = E_0 + \sum_q \omega_{\mathbf{q}} b_{\mathbf{q}}^\dagger b_{\mathbf{q}} + \sum_{\mathbf{k},\sigma} \tilde{E}_{\mathbf{k}} \alpha_{\mathbf{k}\sigma}^\dagger \alpha_{\mathbf{k}\sigma}. \tag{B1}$$

The first term accounts for the Bogoliubov-Anderson phonons with linear dispersion $\omega_{\mathbf{q}}=c_s q$ for momenta $\mathbf{q}$ that are small compared to the inverse healing length. The second term describes the fermionic excitations which have a gapped spectrum $\tilde{E}_{\mathbf{k}}$. The crucial requirement that the lifetime of the quasiparticles by far exceeds their energy is trivially fulfilled for the bosonic excitations. In the weak-coupling BCS regime their lifetime is actually infinite up to an energy 2Δ, which is necessary for a decay into two fermionic quasiparticles. On the BEC side they can decay through nonlinear corrections to the quantum hydrodynamic Lagrangian (3.2). Provided that the curvature parameter a introduced in Sec. III is negative, this leads to a width $\sim q^5$ by Beliaev damping, which is negligible in the $\mathbf{q}\to 0$ limit.

Regarding the fermionic quasiparticles, their lifetime turns out to be infinite near the dispersion minimum despite the fact that their excitation energy becomes of the order of the Fermi energy in the experimentally relevant regime near a Feshbach resonance. At unitarity, for instance, the zero-temperature gap is $\Delta=0.46\varepsilon_F$ [21] in very good agreement with recent quantum Monte Carlo results [79]. The fermionic spectral function should therefore exhibit a sharp peak near the dispersion minimum at zero temperature. Indeed, the relevant process that limits the lifetime close to the dispersion minimum is the emission of a Bogoliubov-Anderson phonon with momentum $\mathbf{q}$. Due to energy and momentum conservation, this process must obey the kinematic constraint

$$E_{\mathbf{k}} = E_{\mathbf{k}-\mathbf{q}} + c_s|\mathbf{q}|, \tag{B2}$$

where $\mathbf{k}$ is the initial momentum of the fermionic excitation with dispersion $E_{\mathbf{k}}=\mu+\sqrt{(\varepsilon_{\mathbf{k}}-\mu)^2+\Delta^2}$ and c_s is the sound velocity. Equation (B2) implies that the emission of a phonon is impossible as long as the group velocity of the fermionic excitations is smaller than the sound velocity $|\partial E_{\mathbf{k}}/\partial\mathbf{k}|<c_s$. This condition is always true for a small interval of momenta around the dispersion minimum implying that the lifetime of a fermionic excitation is infinite in this region.

In the following we show briefly how the kinematic constraint (B2) arises, if the residual interaction (2.33) between BCS quasiparticles is taken into account perturbatively. Our starting point is a reformulation of BCS-BEC crossover Hamiltonian (2.1) in terms of BCS quasiparticle operators. The reduced BCS Hamiltonian (2.32) can be diagonalized exactly [43,80] and takes the form

$$H_{BCS} = E_0^{BCS} + \sum_{\mathbf{k},\sigma} E_{\mathbf{k}} \alpha_{\mathbf{k}\sigma}^\dagger \alpha_{\mathbf{k}\sigma}. \tag{B3}$$

It has the form of the more general quasiparticle Hamiltonian (B1), but is actually valid at arbitrary momenta and energies. However, it misses completely the Bogoliubov-Anderson phonons. The quasiparticle operators $\alpha_{\mathbf{k}\sigma}$ are related to the fermionic operators $c_{\mathbf{k}\sigma}$ via the usual Bogoliubov transformation

$$c_{\mathbf{k}\uparrow} = u_{\mathbf{k}} \alpha_{\mathbf{k}\uparrow} + v_{\mathbf{k}} \alpha_{-\mathbf{k}\downarrow}^\dagger, \tag{B4}$$

$$c_{-\mathbf{k}\downarrow} = -v_{\mathbf{k}} \alpha_{\mathbf{k}\uparrow}^\dagger + u_{\mathbf{k}} \alpha_{-\mathbf{k}\downarrow}, \tag{B5}$$

with the coefficients $u_k^2=[1+(\varepsilon_{\mathbf{k}}-\mu)/(E_{\mathbf{k}}-\mu)]/2$ and $v_k^2=[1-(\varepsilon_{\mathbf{k}}-\mu)/(E_{\mathbf{k}}-\mu)]/2$. The ground state is determined by the condition $\alpha_{\mathbf{k}\sigma}|GS\rangle=0$. Before proceeding, we mention that the lifetime of the fermionic excitations is directly related to the lifetime of the BCS quasiparticles, since the fermionic Green's function $G(\mathbf{k},\omega)$ can be expressed in terms of the BCS quasiparticle Green's function $\mathcal{G}(\mathbf{k},\omega)$ as

$$G_\sigma(\mathbf{k},\omega) = u_k^2 \mathcal{G}_\sigma(\mathbf{k},\omega) - v_k^2 \mathcal{G}_{-\sigma}(-\mathbf{k},-\omega) \tag{B6}$$

using the Bogoliubov transformation defined in Eqs. (B4) and (B5). Note that the second term in Eq. (B6) leads to the fermionic hole excitation spectrum with dispersion $E_{\mathbf{k}}^{(-)}$ [see Eq. (2.25)], even though the excitation energies of the BCS quasiparticles are strictly positive. The residual interaction (2.33) describes the interaction between BCS quasiparticles and their coupling to the collective Bogoliubov-Anderson mode. Explicitly, Eq. (2.33) gives rise to three different types of quasiparticle interactions $\hat{H}_{\text{res}}=\hat{H}_{40}+\hat{H}_{31}+\hat{H}_{22}$ that have been discussed previously, e.g., in nuclear physics [81],

$$\hat{H}_{40} = \frac{g_0}{V} \sum_{\mathbf{k},\mathbf{k}',\mathbf{Q}\neq 0} v_{\mathbf{k}+\mathbf{Q}} v_{\mathbf{k}} u_{\mathbf{k}'} u_{\mathbf{k}'+\mathbf{Q}} \alpha_{\mathbf{k}\uparrow} \alpha_{-\mathbf{k}-\mathbf{Q}\downarrow} \alpha_{-\mathbf{k}'\downarrow} \alpha_{\mathbf{k}'+\mathbf{Q}\uparrow} + \text{H.c.}, \tag{B7}$$

$$\hat{H}_{31} = \frac{g_0}{V} \sum_{\mathbf{k},\mathbf{k}',\mathbf{Q}\neq 0,\sigma} (v_{\mathbf{k}'} v_{\mathbf{k}'+\mathbf{Q}} v_{\mathbf{k}} u_{\mathbf{k}-\mathbf{Q}} - u_{\mathbf{k}'} u_{\mathbf{k}'+\mathbf{Q}} u_{\mathbf{k}} v_{\mathbf{k}-\mathbf{Q}}) \alpha^{\dagger}_{\mathbf{k}\sigma} \alpha_{\mathbf{k}-\mathbf{Q}\sigma} \alpha_{-\mathbf{k}'\downarrow} \alpha_{\mathbf{k}'+\mathbf{Q}\uparrow} + \text{H.c.}, \tag{B8}$$

$$\begin{aligned}\hat{H}_{22} = \frac{g_0}{V} \sum_{\mathbf{k},\mathbf{k}',\mathbf{Q}\neq 0} [&(u_{\mathbf{Q}-\mathbf{k}} u_{\mathbf{k}} u_{\mathbf{k}'} u_{\mathbf{Q}-\mathbf{k}'} \\ &+ v_{\mathbf{Q}-\mathbf{k}} v_{\mathbf{k}} v_{\mathbf{k}'} v_{\mathbf{Q}-\mathbf{k}'}) \alpha^{\dagger}_{\mathbf{Q}-\mathbf{k}\uparrow} \alpha^{\dagger}_{\mathbf{k}\downarrow} \alpha_{\mathbf{k}'\downarrow} \alpha_{\mathbf{Q}-\mathbf{k}'\uparrow} \\ &+ (u_{\mathbf{k}} u_{\mathbf{k}'-\mathbf{Q}} v_{\mathbf{k}'} v_{\mathbf{k}-\mathbf{Q}} \\ &+ v_{\mathbf{k}} v_{\mathbf{k}'-\mathbf{Q}} u_{\mathbf{k}'} u_{\mathbf{k}-\mathbf{Q}}) \alpha^{\dagger}_{\mathbf{k}\uparrow} \alpha^{\dagger}_{-\mathbf{k}'\downarrow} \alpha_{\mathbf{Q}-\mathbf{k}'\downarrow} \alpha_{\mathbf{k}-\mathbf{Q}\uparrow} \\ &+ u_{\mathbf{k}+\mathbf{Q}} u_{\mathbf{k}'+\mathbf{Q}} v_{\mathbf{k}} v_{\mathbf{k}'} \alpha^{\dagger}_{\mathbf{k}+\mathbf{Q}\uparrow} \alpha^{\dagger}_{\mathbf{k}'\downarrow} \alpha_{\mathbf{k}'+\mathbf{Q}\uparrow} \alpha_{\mathbf{k}\uparrow} \\ &+ v_{\mathbf{k}+\mathbf{Q}} v_{\mathbf{k}'+\mathbf{Q}} u_{\mathbf{k}} u_{\mathbf{k}'} \alpha^{\dagger}_{\mathbf{k}+\mathbf{Q}\downarrow} \alpha^{\dagger}_{\mathbf{k}'\downarrow} \alpha_{\mathbf{k}'+\mathbf{Q}\downarrow} \alpha_{\mathbf{k}\downarrow}]\end{aligned} \tag{B9}$$

corresponding to four-wave annihilation, quasiparticle decay, and quasiparticle scattering. The only processes that limit the lifetime of a quasiparticle excitation at zero temperature are the decay into three (or more) quasiparticles and the emission of a Bogoliubov-Anderson phonon or a combination thereof. The decay into three quasiparticles via H_{31} has a threshold energy of 3Δ and is forbidden in a rather broad range around the dispersion minimum. As discussed above, the emission of a Bogoliubov-Anderson phonon has a much less restrictive kinematic constraint and thus is the relevant lifetime-limiting process close to the dispersion minimum. In order to estimate this contribution, we need to know how the BCS quasiparticles couple to the collective Bogoliubov-Anderson mode. It is important to notice that the phonons in Hamiltonian (B1) are not independent excitations but are actually bound states of two BCS quasiparticles. Indeed, as shown already by Galitskii [82], the vertex function $\Gamma(\mathbf{q},\omega)$ for the scattering of an up- and a down-BCS quasiparticle with total energy ω and total momentum $\mathbf{q}$ has a pole at $\omega^2 = c_s^2 q^2$ corresponding to the Bogoliubov-Anderson phonon mode. Within a diagrammatic formulation, the leading order self-energy contribution to the BCS quasiparticle Green's function $\mathcal{G}$ corresponding to the emission of a Bogoliubov-Anderson phonon is thus given by the diagram shown in Fig. 7. Explicitly, this gives rise to an imaginary part of the retarded self-energy given by

$$\begin{aligned}\text{Im}\,\Sigma^R_{\sigma}(\mathbf{k},\omega) = \int \frac{d^3q d^3k' d^3k''}{(2\pi)^9} V^{(1,3)}_{\mathbf{k},\mathbf{q},\mathbf{k}'} V^{(3,1)}_{\mathbf{k},\mathbf{q},\mathbf{k}''} Z_{\text{BA}}(q) \\ \times \delta(\omega - E_{\mathbf{k}-\mathbf{q}} - c_s|\mathbf{q}|) \\ \times \text{Re}\,\mathcal{G}_{-\sigma}(\mathbf{k}', \omega - E_{\mathbf{k}-\mathbf{q}} - E_{\mathbf{q}-\mathbf{k}'}) \\ \times \text{Re}\,\mathcal{G}_{-\sigma}(\mathbf{k}'', \omega - E_{\mathbf{k}-\mathbf{q}} - E_{\mathbf{q}-\mathbf{k}''}) + \cdots,\end{aligned} \tag{B10}$$

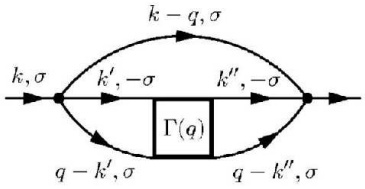

FIG. 7. Dominant contribution to the BCS-quasiparticle self-energy at zero temperature.

where $Z_{\text{BA}}(q)$ denotes the quasiparticle weight of the Bogoliubov-Anderson mode and $V^{(1,3)}$ is the bare vertex related to H_{31}. The dots indicate two more terms coming from the imaginary parts of the two BCS quasiparticle Green's functions in Eq. (B10). However, these terms are not important close to the minimum of the dispersion curve, since they give rise to a kinematic constraint related to the decay into three quasiparticles which has a threshold energy of 3Δ.

Assuming that the real part of the self-energy is small, we evaluate the self-energy at $\omega = E_{\mathbf{k}}$ and extract from Eq. (B10) the kinematic constraint (B2). Thus, in the weak-coupling limit, the spectral function exhibits sharp peaks in an exponentially small interval

$$\frac{|k-k_F|}{k_F} < \frac{c_s}{2v_F} \frac{\Delta}{\epsilon_F} \tag{B11}$$

around the minimum of the dispersion relation. Extrapolated to unitarity, the range where no broadening of the spectral function is expected is $|k-k_\mu| \lesssim 0.1 k_F$. In the BEC regime, where the chemical potential is negative and the minimum of the dispersion relation is at $\mathbf{k}=0$, Eq. (B2) indicates that the spectral function is sharp for momenta $k < mc_s$.

Interestingly, kinematic constraint (B2) that leads to an infinite lifetime of the fermionic excitations around the dispersion minimum is implicitly also present in our Luttinger-Ward theory. Indeed, if Eq. (2.11) is reformulated in terms of mean-field Green's functions, the second term corresponds exactly to the self-energy contribution coming from the virtual emission of a Bogoliubov-Anderson phonon due to the phonon pole of the vertex function Γ. Again, this process causes constraint (B2). Nevertheless, our numerics show a finite lifetime at the dispersion minimum. Apart from the fact that a sharp feature in the spectral function can hardly be resolved numerically, we attribute the finite lifetime to the self-consistent solution of the equations, since the replacement of bare with dressed Green's functions gives rise to diagrams that explicitly violate the Pauli principle.

[1] X. G. Wen, *Quantum Field Theory of Many-Body Systems* (Oxford University Press, New York, 2004).
[2] S. Sachdev, *Quantum Phase Transitions* (Cambridge University Press, Cambridge, England, 1999).
[3] W. Ketterle and M. W. Zwierlein, in *Proceedings of the International School of Physics "Enrico Fermi," Course CLXIV, Varenna, 2006*, edited by M. Inguscio, W. Ketterle, and C. Salomon (IOS Press, Amsterdam, 2008).
[4] I. Bloch, J. Dalibard, and W. Zwerger, Rev. Mod. Phys. **80**, 885 (2008).
[5] S. Giorgini, L. P. Pitaevskii, and S. Stringari, Rev. Mod. Phys. **80**, 1215 (2008).
[6] C. A. Regal, M. Greiner, and D. S. Jin, Phys. Rev. Lett. **92**, 040403 (2004).
[7] M. Bartenstein, A. Altmeyer, S. Riedl, S. Jochim, C. Chin, J. H. Denschlag, and R. Grimm, Phys. Rev. Lett. **92**, 203201 (2004).
[8] J. Kinast, S. L. Hemmer, M. E. Gehm, A. Turlapov, and J. E. Thomas, Phys. Rev. Lett. **92**, 150402 (2004).
[9] M. W. Zwierlein, J. R. Abo-Shaeer, A. Schirotzek, C. H. Schunck, and W. Ketterle, Nature (London) **435**, 1047 (2005).
[10] C. Chin, M. Bartenstein, A. Altmeyer, S. Riedl, S. Jochim, J. Hecker Denschlag, and R. Grimm, Science **305**, 1128 (2004).
[11] J. Kinnunen, M. Rodriguez, and P. Törmä, Science **305**, 1131 (2004).
[12] M. Punk and W. Zwerger, Phys. Rev. Lett. **99**, 170404 (2007).
[13] G. Baym, C. J. Pethick, Z. Yu, and M. W. Zwierlein, Phys. Rev. Lett. **99**, 190407 (2007).
[14] A. Perali, P. Pieri, and G. C. Strinati, Phys. Rev. Lett. **100**, 010402 (2008).
[15] S. Basu and E. J. Mueller, Phys. Rev. Lett. **101**, 060405 (2008).
[16] C. H. Schunck, Y. Shin, A. Schirotzek, M. W. Zwierlein, and W. Ketterle, Science **316**, 867 (2007).
[17] Y. Shin, C. H. Schunck, A. Schirotzek, and W. Ketterle, Phys. Rev. Lett. **99**, 090403 (2007).
[18] Y. Shin, C. H. Schunck, A. Schirotzek, and W. Ketterle, Nature (London) **451**, 689 (2008).
[19] J. T. Stewart, J. P. Gaebler, and D. S. Jin, Nature (London) **454**, 744 (2008).
[20] T. L. Dao, A. Georges, J. Dalibard, C. Salomon, and I. Carusotto, Phys. Rev. Lett. **98**, 240402 (2007).
[21] R. Haussmann, W. Rantner, S. Cerrito, and W. Zwerger, Phys. Rev. A **75**, 023610 (2007).
[22] R. Haussmann and W. Zwerger, Phys. Rev. A **78**, 063602 (2008).
[23] S. Tan, Ann. Phys. **323**, 2971 (2008).
[24] E. Braaten and L. Platter, Phys. Rev. Lett. **100**, 205301 (2008).
[25] D. T. Son and M. Wingate, Ann. Phys. **321**, 197 (2006).
[26] R. Haussmann, *Self-Consistent Quantum-Field Theory and Bosonization for Strongly Correlated Electron Systems*, Lecture Notes in Physics M56 (Springer, Berlin, 1999).
[27] J. M. Luttinger and J. C. Ward, Phys. Rev. **118**, 1417 (1960).
[28] R. Haussmann, Z. Phys. B **91**, 291 (1993).
[29] D. S. Petrov, C. Salomon, and G. V. Shlyapnikov, Phys. Rev. Lett. **93**, 090404 (2004).
[30] D. J. Thouless, Ann. Phys. (N.Y.) **10**, 553 (1960).
[31] E. Burovski, N. Prokof'ev, B. Svistunov, and M. Troyer, Phys. Rev. Lett. **96**, 160402 (2006).
[32] E. Burovski, E. Kozik, N. Prokof'ev, B. Svistunov, and M. Troyer, Phys. Rev. Lett. **101**, 090402 (2008).
[33] A. Bulgac, J. E. Drut, and P. Magierski, Phys. Rev. A **78**, 023625 (2008).
[34] P. Arnold, J. E. Drut, and D. T. Son, Phys. Rev. A **75**, 043605 (2007).
[35] Y. Nishida, Phys. Rev. A **79**, 013627 (2009).
[36] J. Carlson, S.-Y. Chang, V. R. Pandharipande, and K. E. Schmidt, Phys. Rev. Lett. **91**, 050401 (2003); S.-Y. Chang, V. R. Pandharipande, J. Carlson, and K. E. Schmidt, Phys. Rev. A **70**, 043602 (2004).
[37] G. E. Astrakharchik, J. Boronat, J. Casulleras, and S. Giorgini, Phys. Rev. Lett. **93**, 200404 (2004).
[38] H. Hu, X. J. Liu, and P. D. Drummond, Europhys. Lett. **74**, 574 (2006).
[39] R. B. Diener, R. Sensarma, and M. Randeria, Phys. Rev. A **77**, 023626 (2008).
[40] A. W. Fetter and J. D. Walecka, *Quantum Theory of Many-Particle Systems* (McGraw-Hill, New York, 1971).
[41] G. Baym and N. D. Mermin, J. Math. Phys. **2**, 232 (1961).
[42] M. Jarrell and J. E. Gubernatis, Phys. Rep. **269**, 133 (1996).
[43] J. Dukelsky, S. Pittel, and G. Sierra, Rev. Mod. Phys. **76**, 643 (2004).
[44] C. Chin and P. S. Julienne, Phys. Rev. A **71**, 012713 (2005).
[45] W. Schneider, V. B. Shenoy, and M. Randeria, e-print arXiv:0903.3006; note that, in contrast to our discussion of the balanced superfluid, Schneider *et al.* consider the case of an imbalanced *normal* Fermi liquid. The relation (2.37), however, is valid in both cases.
[46] G. B. Partridge, K. E. Strecker, R. I. Kamar, M. W. Jack, and R. G. Hulet, Phys. Rev. Lett. **95**, 020404 (2005).
[47] F. Werner, L. Tarruell, and Y. Castin, Eur. Phys. J. B **68**, 401 (2009).
[48] S. Zhang and A. J. Leggett, Phys. Rev. A **77**, 033614 (2008).
[49] S. Zhang and A. J. Leggett, Phys. Rev. A **79**, 023601 (2009).
[50] A. A. Abrikosov, L. P. Gorkov, and I. E. Dzyaloshinskii, *Methods of Quantum Field Theory in Statistical Physics* (Dover, New York, 1963); see, e.g., Chap. I.5.
[51] S. Tan, Ann. Phys. **323**, 2952 (2008).
[52] Z. Yu, G. M. Bruun, and G. Baym, Phys. Rev. A **80**, 023615 (2009).
[53] M. Tinkham, *Introduction to Superconductivity* (McGraw-Hill, New York, 1996).
[54] J. R. Engelbrecht, M. Randeria, and C. A. R. Sa de Melo, Phys. Rev. B **55**, 15153 (1997).
[55] Z. Nussinov and S. Nussinov, Phys. Rev. A **74**, 053622 (2006).
[56] Y. Nishida and D. T. Son, Phys. Rev. Lett. **97**, 050403 (2006).
[57] G. Rupak and T. Schäfer, Nucl. Phys. A **816**, 52 (2009).
[58] It is easy to see that $c_2=0$ in the BEC limit implying a vanishing pair size. This is a consequence of the relation $n_s(q)=n$ for arbitrary wave vectors q that holds for a weakly interacting BEC described within Bogoliubov theory. The latter is appropriate in the molecular limit of the BCS-BEC crossover with dimer-dimer scattering length $a_{dd}=0.6a$.
[59] R. Sensarma (private communication).
[60] M. Brack and R. K. Bhaduri, *Semiclassical Physics* (Addison-Wesley, Reading, MA, 1997).
[61] Note that the Weizsäcker inhomogeneity correction has precisely the form of the quantum pressure contribution in the Gross-Pitaevskii theory of a Bose superfluid, which describes

the ground state of the BCS-BEC crossover in the molecular limit. Accounting for the factors 2 in the associated Bose mass or density, the corresponding value of b in this limit consistent with Eq. (3.6) is $b=1/16=0.0625$.
[62] Y. Nishida and D. T. Son, Phys. Rev. A **75**, 063617 (2007).
[63] D. T. Son and M. A. Stephanov, Phys. Rev. A **74**, 013614 (2006).
[64] J. Carlson and S. Reddy, Phys. Rev. Lett. **95**, 060401 (2005)
[65] A. Schirotzek, Y. I. Shin, C. H. Schunck, and W. Ketterle, Phys. Rev. Lett. **101**, 140403 (2008).
[66] C. L. Kane, P. A. Lee, and N. Read, Phys. Rev. B **39**, 6880 (1989).
[67] P. Magierski, G. Wlazlowski, A. Bulgac, and J. E. Drut, Phys. Rev. Lett. (in print).
[68] For the case of quasiparticle decay due to single phonon emission, there is actually a shell of finite thickness in momentum space where the width vanishes identically at $T=0$.
[69] M. R. Norman, M. Randeria, H. Ding, and J. C. Campuzano, Phys. Rev. B **57**, R11093 (1998).
[70] Q. Chen and K. Levin, Phys. Rev. Lett. **102**, 190402 (2009).
[71] T.-L. Dao, I. Carusotto, and A. Georges, Phys. Rev. A **80**, 023627 (2009).
[72] Q. Chen, K. Levin, and I. Kosztin, Phys. Rev. B **63**, 184519 (2001).
[73] A. Perali, P. Pieri, G. C. Strinati, and C. Castellani, Phys. Rev. B **66**, 024510 (2002).
[74] P. Pieri, L. Pisani, and G. C. Strinati, Phys. Rev. B **70**, 094508 (2004).
[75] S. Moukouri, S. Allen, F. Lemay, B. Kyung, D. Poulin, Y. M. Vilk, and A.-M. S. Tremblay, Phys. Rev. B **61**, 7887 (2000).
[76] D. Sivia and J. Skilling, *Data Analysis: A Bayesian Tutorial* (Oxford University Press, Oxford, 2006).
[77] R. K. Bryan, Eur. Biophys. J. **18**, 165 (1990).
[78] N. Lerch, L. Bartosch, and P. Kopietz, Phys. Rev. Lett. **100**, 050403 (2008).
[79] J. Carlson and S. Reddy, Phys. Rev. Lett. **100**, 150403 (2008).
[80] B. Mühlschlegel, J. Math. Phys. **3**, 522 (1962).
[81] P. Ring and P. Schuck, *The Nuclear Many-Body Problem* (Springer, Berlin, 2000).
[82] V. M. Galitskii, Sov. Phys. JETP **7**, 698 (1958).

PRL 102, 130603 (2009) PHYSICAL REVIEW LETTERS week ending 3 APRIL 2009

Relaxation of Antiferromagnetic Order in Spin-1/2 Chains Following a Quantum Quench

Peter Barmettler,[1] Matthias Punk,[2] Vladimir Gritsev,[1,3] Eugene Demler,[3] and Ehud Altman[4]

[1]*Department of Physics, University of Fribourg, CH-1700 Fribourg, Switzerland*
[2]*Department of Physics, Technical University Munich, D-85748 Garching, Germany*
[3]*Department of Physics, Harvard University, Cambridge, Massachusetts 02138, USA*
[4]*Department of Condensed Matter Physics, Weizmann Institute of Science, Rehovot, 76100, Israel*

(Received 28 October 2008; revised manuscript received 5 February 2009; published 1 April 2009)

We study the unitary time evolution of antiferromagnetic order in anisotropic Heisenberg chains that are initially prepared in a pure quantum state far from equilibrium. Our analysis indicates that the antiferromagnetic order imprinted in the initial state vanishes exponentially. Depending on the anisotropy parameter, oscillatory or nonoscillatory relaxation dynamics is observed. Furthermore, the corresponding relaxation time exhibits a *minimum* at the critical point, in contrast to the usual notion of critical slowing down, from which a maximum is expected.

DOI: 10.1103/PhysRevLett.102.130603 PACS numbers: 75.10.Pq, 05.70.Ln, 37.10.Jk, 64.70.Tg

Introduction.—Experiments with ultracold atoms offer a highly controlled environment for investigating open questions of quantum magnetism. In particular, coherent spin dynamics in a lattice of double wells has been observed in recent experiments, which have demonstrated remarkable precision in tuning magnetic exchange interactions [1]. The ability to observe quantum dynamics over long time intervals allows one to study strongly correlated states from a new perspective. The idea is to prepare the system in a simple quantum state which, in general, is not an eigenstate of the Hamiltonian and investigate the dynamics that follows. In the two-spin system, studied in Ref. [1], the dynamics is completely tractable and describes simple oscillations between a singlet and a triplet state.

In the present Letter, we investigate how the nature of the dynamics changes in the case of a macroscopic number of spins interacting via nearest neighbor magnetic exchange. Are there new effects, and, in particular, new time scales, dynamically generated by the complex many-body evolution? Our starting point for investigating this question is the spin-$\frac{1}{2}$ anisotropic Heisenberg (or XXZ) model on a one-dimensional lattice

$$H_{XXZ} = J\sum_j \{S_j^x S_{j+1}^x + S_j^y S_{j+1}^y + \Delta S_j^z S_{j+1}^z\}. \quad (1)$$

This model provides a good effective description of two-component Bose or Fermi systems deep in the Mott-insulating phase. The interaction parameters are dynamically tunable [2], realizing ferro- ($J < 0$) or antiferromagnetic ($J > 0$) couplings over large ranges of the anisotropy parameter $\Delta \geq 0$. We take the initial state to be a perfect antiferromagnetic (Néel) state $|\psi_0\rangle = |\uparrow\downarrow\uparrow \ldots \downarrow\uparrow\downarrow\rangle$. Such a state has been achieved with high fidelity by Trotzky *et al.* [1] using decoupled double wells. Note that $|\psi_0\rangle$ is the ground state of the Hamiltonian with $\Delta = \infty$. We study the subsequent time evolution of the staggered magnetic moment $m_s(t) = \frac{1}{N}\sum_j (-1)^j \langle\psi_0|S_j^z(t)|\psi_0\rangle$ under the influence of the Hamiltonian (1) at different values of anisotropy Δ using a numerical matrix-product method [3]. The dynamics is independent of the sign of J, and the results are valid for both ferro- and antiferromagnetic couplings. To substantiate our findings, we consider another, closely related model, given by the XZ Hamiltonian [see Eq. (5)], which allows exact calculation of the dynamics and displays similar behavior.

Theoretical interest in this class of problems, known as quantum quenches [4–8], has been invigorated by advances in experiments with ultracold atoms [9]. In particular, macroscopic order parameter oscillations have been predicted to occur following a quantum quench in a variety of such systems [10–13]. We shall see that such oscillations are also found in the XXZ chain with easy-plane anisotropy ($\Delta < 1$) and that they are essentially the same as the singlet-triplet oscillations observed in the two-spin system [1]. Accordingly, the oscillation frequency is directly related to the magnetic exchange interaction J. More importantly, for nonzero Δ we find a fundamentally new mode of many-body dynamics which always leads to *exponential* decay of the staggered moment regardless of whether the short-time dynamics is oscillatory or not. In contrast with the oscillation frequency, the relaxation time is an emergent scale generated by the highly correlated dynamics and hence cannot be simply related to the microscopic parameters. We find a diverging relaxation time in the two limits $\Delta \to 0$ and $\Delta \to \infty$. Of particular interest is the relaxation time at the isotropic point $\Delta = 1$, which for the ground state properties marks a quantum phase transition from a gapless "Luttinger liquid" phase ($\Delta < 1$) to a gapped, Ising-ordered antiferromagnetic phase ($\Delta > 1$). Interestingly, the relaxation time is *minimal* in the vicinity of the critical point, where its value is simply determined by the magnetic exchange interaction $\tau \sim 1/J$. This accelerated relaxation stands in remarkable contrast to the notion of *critical slowing down*, valid for a small perturbation of the order parameter from equilibrium. In fact, if the prepared initial state is close to the equilibrium state, then the

relaxation time of the order parameter is expected to diverge as the system approaches the critical point [14]. We find an opposite trend in the dynamics of the prepared Néel state. In the long-time limit, our results suggest that local magnetic order vanishes for all values $\Delta < \infty$.

The solution of the quench dynamics in the XXZ chain involves, in principle, all energy scales of the Hamiltonian, and approximative methods become essentially inaccurate in many cases. The mean field approximation, for example, leads to contradictions with our results—an algebraic decay for $\Delta \leq 1$ and a nonvanishing asymptotic value of the staggered moment for $\Delta > 1$ [13]. Renormalization group based approaches [5] are restricted to low-lying modes, which is not sufficient in the present case. The exact numerical results presented in this study go further than the predictions of low-energy theories [5].

Before delving into a more detailed study, it is instructive to consider the so-called XX limit ($\Delta = 0$) of the Heisenberg chain (1), which can be mapped onto the problem of free fermions. In this case, one easily obtains an analytic expression for the time evolution of the staggered magnetization: $m_s(t) = J_0(2Jt)/2$ (Fig. 1). Here J_0 denotes the zeroth-order Bessel function of the first kind. Thus, after a short transient time $t \sim J^{-1}$, the staggered magnetization displays algebraically decaying oscillations originating from the finite bandwidth of the free-fermionic model:

$$m_s(t) \sim \frac{1}{\sqrt{4\pi t}} \cos\left(2Jt - \frac{\pi}{4}\right). \tag{2}$$

In general, we are interested in generic behavior of the relaxation dynamics on large time scales. We adopt a definition of relaxation which does not rely on time-averaged equilibration of the observable but instead requires *exact* convergence to the asymptotic value, as defined in Ref. [15]. From this point of view, the oscillations in the XX limit are characterized by an infinite relaxation time.

XXZ model.—In the general case of $\Delta \neq 0$, the problem is no longer analytically treatable, and we have to resort to numerical techniques. We use the infinite-size time-evolving block decimation (iTEBD) algorithm [3], which implements the ideas of the density matrix renormalization group (DMRG) method [16] for an infinite system. The algorithm uses an optimal matrix-product representation of the infinitely extended chain, keeping only the dominant eigenstates of the density matrix of a semi-infinite subsystem, in combination with a Suzuki-Trotter decomposition of the evolution operator. This method is very efficient for small t; however, the increasing entanglement under time evolution [17] requires one to retain an exponentially growing number of eigenstates. We find that the error of our calculations behaves in a similar way to that of the finite-size DMRG algorithm, and the methodology developed in Ref. [18] can be applied in order to control the accuracy [19]. By carefully estimating the *runaway time* via comparing results with different control parameters [18], the absolute error in the plotted data is kept below 10^{-6}. Using 2000 states and a second-order Suzuki-Trotter decomposition with a time step $\delta \sim 10^{-3}J^{-1}$ for large Δ and up to 7000 states with $\delta \sim 10^{-2}J^{-1}$ for small Δ, an *intermediate* time regime $Jt \lesssim 16$ can be reached, which, in general, far exceeds the short transient time.

An overview of the results is presented in Fig. 1(a). For small anisotropies we find oscillations of the order parameter similar to those in the XX limit but with a decay time decreasing upon approaching the isotropic point $\Delta = 1$. In the easy-axis regime $\Delta > 1$ of the XXZ model, the relaxation slows down again for increasing Δ, and we observe nonoscillatory behavior for $\Delta \gg 1$.

Figure 2 focuses on easy-plane anisotropy $0 < \Delta < 1$. The results for $0 < \Delta \leq 0.4$ are well described, for accessible time scales, by exponentially decaying oscillations

$$m_s(t) \propto e^{-t/\tau} \cos(\omega t + \phi). \tag{3}$$

The oscillation frequency is almost independent of the

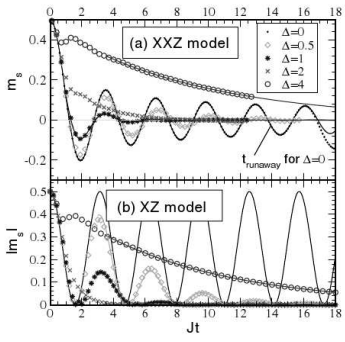

FIG. 1 (color online). Dynamics of the staggered magnetization $m_s(t)$ in (a) the XXZ chain and (b) the XZ chain. Symbols correspond to numerical results, and lines represent analytical results or fits by corresponding laws (see text). For $\Delta = 0$ the typical behavior of the error is illustrated by comparing the numerical iTEBD result with 2400 retained states to the exact curve: The absolute deviation from the exact curve is less than 10^{-6} for $t < t_{\text{runaway}}$. For $\Delta \neq 0$ data beyond t_{runaway} is omitted.

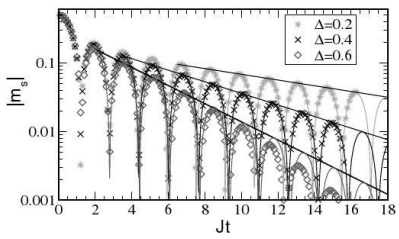

FIG. 2 (color online). Absolute value of the staggered magnetization in the XXZ model. Symbols represent numerical results, solid curves correspond to fits by the exponential law (3), and straight lines point out the exponential decay.

PRL 102, 130603 (2009) PHYSICAL REVIEW LETTERS week ending 3 APRIL 2009

anisotropy, while the relaxation time τ increases with decreasing Δ. Logarithmic divergence of the relaxation time in the limit $\Delta \to 0$ is suggested by the fit shown in Fig. 4(a). The picture is less clear closer to the isotropic point. For the range $0.5 \leq \Delta < 1$, there appears to be an additional time scale after which the oscillations start to decay even faster than exponentially; simultaneously, the period of the oscillations is reduced. Therefore, the relaxation times plotted in Fig. 4(a) are valid only within an intermediate time window, whose width shrinks upon approaching the critical point.

For intermediate easy-axis anisotropies $1 \leq \Delta \leq 3$, the magnetization does not reach a stable regime within the numerically accessible time window [Fig. 3(a)]. The complicated behavior of $m_s(t)$ in this parameter range can be ascribed to the interplay of processes at all energy scales. Nevertheless, the numerical data suggest that the relaxation is fastest close to the isotropic point, in the range between $\Delta = 1$ and $\Delta = 1.6$. A simple generic type of behavior is recovered for large anisotropies $\Delta \gtrsim 3$. The numerical data in Fig. 3(b) indicate exponential relaxation of the staggered magnetization

$$m_s(t) \propto e^{-t/\tau}. \tag{4}$$

The relaxation time scales roughly quadratically with Δ [Fig. 4(a)]. Oscillations do persist on top of the exponential decay, but they fade out quickly.

XZ model.—We now turn to the study of the XZ Hamiltonian

$$H_{XZ} = J\sum_j \{2S_j^x S_{j+1}^x + \Delta S_j^z S_{j+1}^z\}. \tag{5}$$

In this model, a quantum phase transition separates two gapped phases at $\Delta_c = 2$, with antiferromagnetic order in the z direction for $\Delta > \Delta_c$ and in the x direction for $\Delta < \Delta_c$. Unlike the XXZ model, it can be easily diagonalized analytically. In order to study the staggered magnetization of the XZ model, we have to calculate the two-spin correlation function $C(n, t) = (-1)^n \langle \psi_0 | S_0^z(t) S_n^z(t) | \psi_0 \rangle$ in the infinite-range limit, since $m_s^2(t) = \lim_{n\to\infty} C(n, t)$. Using standard techniques (see [4] and references therein), we express this two-spin correlator as a Pfaffian, with coefficients calculated in a similar manner as for the Ising model in a transverse field [12]. Exploiting the light-cone effect [17,20], we are able to evaluate numerically the order parameter dynamics up to times of the order of $Jt \approx 100$. The results are displayed in Fig. 1(b). An analytic expression can be derived for $\Delta = 0$, which is given by $m_s(t) = 0.5\cos^2(Jt)$. For $\Delta < \Delta_c$, exponentially decaying oscillations

$$m_s(t) \propto e^{-t/\tau}[\cos^2(\omega t) - \text{const}] \tag{6}$$

reproduce the numerical results at large times very well. For $\Delta \geq \Delta_c$, the staggered magnetization decays exponentially with no oscillations at large times [Eq. (4)]. In contrast to the XXZ model, the oscillation period in the XZ model diverges at the isotropic point $\Delta = \Delta_c$, and the latter exactly marks the crossover between oscillatory and nonoscillatory behavior of $m_s(t)$. We have extracted the relaxation times from exponential fits to the numerical data, showing a clearly pronounced minimum right at the isotropic point [see Fig. 4(b)]. The relaxation time scales as $\tau \propto \Delta^{-1}$ for $\Delta \leq \Delta_c$ and as $\tau \propto \Delta^2$ for $\Delta \gg \Delta_c$.

Apart from the numerical evaluation of the Pfaffian, we can prove rigorously that in the infinite-time limit the staggered magnetization vanishes for all anisotropies in the range $\Delta_c < \Delta < \infty$. Indeed, since the Pfaffian reduces to a Toeplitz determinant at $t \to \infty$ [12], we can use Szegö's lemma to calculate the large-distance asymptotics of the two-spin correlator in the above-mentioned regime, obtaining, for $n \gg 1$, $\lim_{t\to\infty} C(n, t) \sim \frac{1}{4}[(1 + \sqrt{1 - 4/\Delta^2})/2]^n$, which immediately implies that $m_s(t \to \infty) = 0$.

Discussion.—We have analyzed the dynamics of the staggered magnetization in the XXZ and XZ models following a quantum quench. Our main result is that in both models there is a dynamically generated relaxation rate which is fastest close to the critical point. This point also marks a crossover between oscillatory and nonoscillatory dynamics of the order parameter. The dynamics of the magnetic order parameter turns out to be a good observable for the quantitative extraction of nontrivial time scales. In

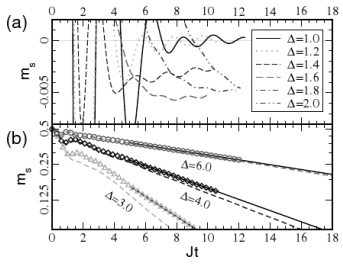

FIG. 3 (color online). (a) Focus on the XXZ chain close to the critical point $\Delta = 1$. (b) Comparison of the XXZ chain (symbols) and the XZ chain (dashed lines) for strong anisotropies; solid lines correspond to an exponential fit. The dynamics of the staggered magnetization of the XXZ and XZ chains converge towards each other in the large-Δ limit.

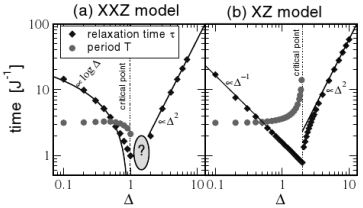

FIG. 4 (color online). Relaxation time τ and oscillation period $T = \frac{2\pi}{\omega}$ as a function of anisotropy in the XXZ and XZ models. Logarithmic or algebraic laws are emphasized by solid lines. In the region close to the critical point of the XXZ model (indicated by the question mark), it becomes impossible to extract a relaxation time from the numerical results.

general, this is not possible from other observables such as correlation functions, which reveal interesting features such as the horizon effect [5] but exhibit only slow relaxation dynamics [8,19]. Furthermore, we have focused on the Néel state as an experimentally relevant initial condition. We point out, however, that our results are generic and hold for all antiferromagnetic initial states with sufficiently small correlation length [19].

The existence of a minimal relaxation time at the critical point is opposite to what one would expect from the phenomenon of critical slowing down of order parameter dynamics near equilibrium. In the XZ model and the easy-axis phase of the XXZ model, where the excitation spectrum is gapped, the effect can be understood using a phase-space argument: The relaxation of the initial state is dominated by scattering events between high-energy excitations introduced into the system through the initial state. As a result of the existence of the gap, the phase space for scattering events is restricted. This leads to an increasing relaxation time as the gap increases, whereas one expects a minimal relaxation time at the critical point, where the gap vanishes. The above argument cannot be applied directly to a quench into the gapless phase in the easy-plane regime of the XXZ model. Rather, the situation seems to be similar to a quantum quench of the Bose-Hubbard model from a Mott insulator to a superfluid phase. In the latter case, oscillations of the superfluid order parameter have been predicted, with a damping rate that diverges at the critical point in one and two dimensions [10].

The absence of a sharp signature of the quantum phase transition in the XXZ chain prepared in a Néel state is in contrast with what one has in the case of the initially prepared ferromagnet with a single kink impurity, studied, for example, in Ref. [18], where the two phases are characterized by clearly distinct transport properties. We note that this initial state is much closer to the ground state of the Hamiltonian and the important energy scales are considerably smaller than in the case of the initial Néel state. The opening of an exponentially small gap at the phase transition is therefore more likely to be relevant.

The time evolution of an initial state which is equivalent to the Néel state has been recently studied by Cramer *et al.* [7] in the context of the one-dimensional Bose-Hubbard (BH) model with on-site repulsion U as the interaction parameter (the equivalence becomes apparent in the fermionic representation of the XXZ Hamiltonian). Although the BH Hamiltonian itself and the XXZ model share some properties in the noninteracting limit, there is one substantial difference: In the BH model at half filling, no equilibrium critical point is crossed by changing the interaction U and the symmetry-broken initial state never becomes the ground state. Unlike the XXZ model, the oscillations of the local observable in the BH model appear to be decaying *algebraically* for all values of interaction U, and no crossover to a nonoscillatory regime has been observed [7]. These differences point out the crucial role of the equilibrium phase transition to the reported behavior of the order parameter dynamics of the XXZ chain.

Experimental results [1] suggest that effects of density fluctuations beyond second-order magnetic exchange may be important for reproducing the dynamics in full detail. This statement is also supported by very recent numerical results [21]. Nevertheless, we expect that our main result, the existence of a minimum in the dynamically generated relaxation time close to the critical point, is insensitive to these details.

We thank D. Baeriswyl, I. Bloch, M. Lukin, M. Menteshashvili, A. M. Rey, S. Trotzky, and W. Zwerger for fruitful discussions. This work was supported by SNF (P. B.), DFG-FOR 801 and the Feinberg Graduate School (M. P.), U.S.–Israel Binational Science Foundation (E. A. and E. D.), and AFOSR, CUA, DARPA, MURI, and NSF DMR-0705472 (V. G. and E. D.).

[1] S. Trotzky *et al.*, Science **319**, 295 (2008).
[2] A. B. Kuklov and B. V. Svistunov, Phys. Rev. Lett. **90**, 100401 (2003); L.-M. Duan, E. Demler, and M. D. Lukin, *ibid.* **91**, 090402 (2003); E. Altman *et al.*, New J. Phys. **5**, 113 (2003).
[3] G. Vidal, Phys. Rev. Lett. **98**, 070201 (2007).
[4] E. Barouch, B. M. McCoy, and M. Dresden, Phys. Rev. A **2**, 1075 (1970).
[5] P. Calabrese and J. Cardy, Phys. Rev. Lett. **96**, 136801 (2006); M. A. Cazalilla, *ibid.* **97**, 156403 (2006).
[6] C. Kollath, A. M. Läuchli, and E. Altman, Phys. Rev. Lett. **98**, 180601 (2007).
[7] M. Cramer *et al.*, Phys. Rev. Lett. **101**, 063001 (2008); A. Flesch *et al.*, Phys. Rev. A **78**, 033608 (2008).
[8] G. D. Chiara *et al.*, J. Stat. Mech. (2006) P03001; S. R. Manmana *et al.*, Phys. Rev. Lett. **98**, 210405 (2007); S. R. Manmana *et al.*, arXiv:0812.0561; P. Barmettler *et al.*, Phys. Rev. A **78**, 012330 (2008).
[9] M. Greiner *et al.*, Nature (London) **419**, 51 (2002); O. Kinoshita, T. Wenger, and D. S. Weiss, *ibid.* **440**, 900 (2006).
[10] E. Altman and A. Auerbach, Phys. Rev. Lett. **89**, 250404 (2002).
[11] A. Polkovnikov, S. Sachdev, and S. M. Girvin, Phys. Rev. A **66**, 053607 (2002); R. A. Barankov, L. S. Levitov, and B. Z. Spivak, Phys. Rev. Lett. **93**, 160401 (2004).
[12] K. Sengupta, S. Powell, and S. Sachdev, Phys. Rev. A **69**, 053616 (2004).
[13] M. B. Hastings and L. S. Levitov, arXiv:0806.4283.
[14] L. Van Hove, Phys. Rev. **95**, 1374 (1954); W. H. Zurek, U. Dorner, and P. Zoller, Phys. Rev. Lett. **95**, 105701 (2005).
[15] M. Cramer *et al.*, Phys. Rev. Lett. **100**, 030602 (2008).
[16] U. Schollwöck, Rev. Mod. Phys. **77**, 259 (2005).
[17] P. Calabrese and J. Cardy, J. Stat. Mech. (2007) P06008.
[18] D. Gobert *et al.*, Phys. Rev. E **71**, 036102 (2005).
[19] P. Barmettler *et al.* (to be published).
[20] E. H. Lieb and D. W. Robinson, Commun. Math. Phys. **28**, 251 (1972).
[21] T. Barthel *et al.*, arXiv:0809.5141.

Bibliography

[1] M.H. Anderson, J.R. Ensher, M.R. Matthews, C.E. Wieman, and E.A. Cornell, Science **269**, 198 (1995).

[2] K.B. Davis, M.O. Mewes, M.R. Andrews, N.J. van Druten, D.S. Durfee, D.M. Kurn, and W. Ketterle, Phys. Rev. Lett. **75**, 3969 (1995).

[3] B. DeMarco and D.S. Jin, Science **285**, 1703 (1999).

[4] I. Bloch, J. Dalibard, and W. Zwerger, Rev. Mod. Phys. **80**, 885 (2008).

[5] S. Giorgini, L.P. Pitaevskii, and S. Stringari, Rev. Mod. Phys., **80**, 1215, (2008).

[6] J. Bardeen, L.N. Cooper, and J.R. Schrieffer, Phys. Rev. **108**, 1175 (1957).

[7] B. Eagles, Phys. Rev. **186**, 456 (1969).

[8] A.J. Leggett, J Phys. C (Paris) **41**, 7 (1980).

[9] K. Huang, *"Statistical Mechanics"*, John Wiley & Sons (1963).

[10] L.D. Landau und E.M. Lifshitz, Vol. III "*Quantenmechanik*".

[11] F. Chevy, Phys. Rev. A **74**, 063628 (2006).

[12] C. Chin, M. Bartenstein, A. Altmeyer, S. Riedl, S. Jochim, J. Hecker Denschlag, and R. Grimm, Science **305**, 1128 (2004).

[13] C.H. Schunck, Y. Shin, A. Schirotzek, M.W. Zwierlein, and W. Ketterle, Science **316**, 867 (2007).

[14] A.M. Clogston, Phys. Rev. Lett. **9**, 266 (1962).

[15] B.S. Chandrasekhar, App. Phys. Lett. **1**, 7 (1962).

[16] J. Kinnunen, M. Rodriguez, and P. Torma, Science **305**, 1131 (2004).

[17] Y. He, Q. Chen, and K. Levin, Phys. Rev. A **72**, 011602 (2005).

[18] L. Radzihovsky and D.E. Sheehy, eprint arXiv:0911.1740 (2009).

[19] D.E. Sheehy and L. Radzihovsky, Phys. Rev. Lett. **96**, 060401 (2006).

[20] D.S. Petrov, C. Salomon, G.V. Shlyapnikov, Phys. Rev. A **71**, 012708 (2005).

[21] S. Pilati and S. Giorgini, Phys. Rev. Lett. **100**, 030401 (2008).

[22] C. Lobo, A. Recati, S. Giorgini, and S. Stringari, Phys. Rev. Lett. **97**, 200403 (2006).

[23] N. V. Prokof'ev, B. V. Svistunov, Phys. Rev. B **77**, 020408(R) (2008).

[24] N. V. Prokof'ev, B. V. Svistunov, Phys. Rev. B **77**, 125101 (2008).

[25] M.M. Parish, F.M. Marchetti, A. Lamacraft, and B.D. Simons, Nature Phys. **3**, 124 (2007).

[26] Y. Shin, C. H. Schunck, A. Schirotzek, and W. Ketterle, Nature **451**, 689 (2008).

[27] D.T. Son and M.A. Stephanov, Phys. Rev. A **74**, 013614 (2006).

[28] R. Haussmann, M. Punk, and W. Zwerger, Phys. Rev. A **80**, 063612 (2009).

[29] S. Sachdev and K. Yang, Phys. Rev. B **73**, 174504 (2006).

[30] A. Bulgac, M. McNeilForbes, and A. Schwenk, Phys. Rev. Lett. **97**, 020402 (2006).

[31] Y. Shin, A. Schirotzek, C.H. Schunk, and W. Ketterle, Phys. Rev. Lett. **101**, 070404 (2008).

[32] P.F. Bedaque, H. Caldas, and G. Rupak, Phys. Rev. Lett. **91**, 247002 (2003).

[33] C.-H. Pao, S.-T. Wu, and S.-K. Yip, Phys. Rev. B **73**, 132506 (2006). Erratum: C.-H. Pao, S.-T. Wu, and S.-K. Yip, Phys. Rev. B **74**, 189901(E) (2006).

[34] G.D. Mahan, *"Many particle physics"*, Plenum Press (1990).

[35] Z. Yu and G. Baym, Phys. Rev. A **73**, 063601 (2006).

[36] Y. Ohashi and A. Griffin, Phys. Rev. A **72**, 013601 (2005).

[37] S. Tan, Ann. Phys. (N.Y.) **323**, 2952 (2008).

[38] S. Tan, Ann. Phys. (N.Y.) **323**, 2971 (2008).

[39] S. Tan, Ann. Phys. (N.Y.) **323**, 2987 (2008).

[40] E. Braaten and L. Platter, Phys. Rev. Lett. **100**, 205301 (2008).

[41] G. Baym, C.J. Pethick, Z. Yu, and M.W. Zwierlein, Phys. Rev. Lett. **99**, 190407 (2007).

[42] M. Punk and W. Zwerger, Phys. Rev. Lett. **99**, 170404 (2007).

[43] G. Ortiz and J. Dukelsky, Phys. Rev. A **72**, 043611 (2005).

[44] C. Chin and P.S. Julienne, Phys. Rev. A **71**, 012713 (2005).

[45] A.A. Abrikosov, L.P. Gorkov, and I.E. Dzyaloshinski, *"Methods of Quantum Field Theory in Statistical Physics"*, Dover Publications (1975).

[46] A.L. Fetter, and J.D. Walecka, *"Quantum Theory of Many-Particle Systems"*, Dover (2003).

[47] Q. Chen, K. Levin, and I. Kosztin, Phys. Rev. B **63**, 184519 (2001).

[48] A. Perali, P. Pieri, G.C. Strinati, and C. Castellani, Phys. Rev. B **66**, 024510 (2002).

[49] D. Rohe and W. Metzner, Phys. Rev. B **63**, 224509 (2001).

[50] R. Combescot, A. Recati, C. Lobo, and F. Chevy, Phys. Rev. Lett. **98**, 180402 (2007).

[51] A. Larkin and A. Varlamov, *"Theory of fluctuations in superconductors"*, International Series of Monographs on Physics 127, Oxford University Press (2005).

[52] D. J. Thouless, Ann. Phys. (N.Y.) **10**, 553 (1960).

[53] M. Veillette, E.G. Moon, A. Lamacraft, L. Radzihovsky, S. Sachdev, and D.E. Sheehy, Phys. Rev. A **78**, 033614 (2008).

[54] I.L. Aleiner and B.L. Altshuler, Phys. Rev. Lett. **79**, 4242 (1997).

[55] M. Babadi, D. Pekker, R. Sensarma, A. Georges, and E. Demler, eprint arXiv:0908.3483.

[56] R. Haussmann ,*"Self-Consistent Quantum-Field Theory and Bosonization for Strongly Correlated Electron Systems"*, Lecture Notes in Physics M56, Springer (1999).

[57] A. Schirotzek, C. H. Wu, A. Sommer, and M.W. Zwierlein, Phys. Rev. Lett. **102**, 230402 (2009).

[58] S. Nascimbene, N. Navon, K.J. Jiang, L. Tarrruel, M. Teichmann, J. McKeever, F. Chevy, and C. Salomon, Phys. Rev. Lett. **103**, 170402 (2009).

[59] W. Schneider, V.B. Shenoy, and M. Randeria, eprint arXiv:0903.3006.

[60] R.P. Feynman, *"Statistical Mechanics"*, Westview Press (1998).

[61] L.N. Cooper, Phys. Rev. **104**, 1189 (1956).

[62] R. Combescot, S. Giraud, Phys. Rev. Lett. **101**, 050404 (2008).

[63] G. V. Skorniakov, and K. A. Ter-Martirosian, Zh. Eksp. Teor. Fiz. **31**, 775 (1956) [Sov. Phys. JETP **4**, 648 (1957)].

[64] A.B. Migdal, Sov. Phys. JETP **5**, 333 (1957).

[65] M. Punk, P.T. Dumitrescu, and W. Zwerger, Phys. Rev. A **80**, 053605 (2009).

[66] G.M. Bruun, and C.J. Pethick, Phys. Rev. Lett. **92**, 140404 (2004).

[67] D.R. Phillips and T.D. Cohen, Phys. Lett. B **390**, 7 (1997).

[68] I.N. Bronstein, K.A. Semendjajew, G. Musiol, and H. Mühlig, *"Taschenbuch der Mathematik"*, Verlag Harri Deutsch (2001).

[69] M. Cramer, C.M. Dawson, J. Eisert, and T.J. Osborne, Phys. Rev. Lett. **100**, 030602 (2008).

[70] T. Barthel and U. Schollwöck, Phys. Rev. Lett. **100**, 100601 (2008).

[71] M. Rigol, V. Dunjko, and M. Olshanii, Nature **452**, 854 (2008).

[72] M. Cramer and J. Eisert, eprint arXiv:0911.2475.

[73] M. Greiner, O. Mandel, T.W. Hänsch, and I. Bloch, Nature **419**, 51 (2002).

[74] S. Trotzky, P. Cheinet, S. Flling, M. Feld, U. Schnorrberger, A.M. Rey, A. Polkovnikov, E.A. Demler, M.D. Lukin, and I. Bloch, Science **319**, 295 (2008).

[75] A. Auerbach, *"Interacting Electrons and Quantum Magnetism"*, Springer (1998).

[76] B. Sutherland, *"Beautiful Models"*, World Scientific Publishing (2004).

[77] P. Jordan and E. Wigner, Z. Phys. **9**, 631 (1928).

[78] M. Cramer, A. Flesch, I.P. McCulloch, U. Schollwöck, and J. Eisert, Phys. Rev. Lett. **101**, 063001 (2008).

[79] M.B. Hastings and L.S. Levitov, eprint arXiv:0806.4283.

[80] U. Schollwöck, Rev. Mod. Phys. **77**, 259 (2005).

[81] P. Barmettler, PhD. Thesis, University of Fribourg, Switzerland (2009).

[82] P. Barmettler, M. Punk, V. Gritsev, E. Demler, and E. Altman, Phys. Rev. Lett. **102**, 130603 (2009).

[83] P. Barmettler, M. Punk, V. Gritsev, E. Demler, and E. Altman, eprint arXiv:0911.1927 (2009).

[84] E. Lieb, T. Schulz, and D. Mattis, Ann. Phys. **16**, 407 (1961).

[85] E. Barouch and B.M. McCoy, Phys. Rev. A **3**, 786 (1971).

[86] K. Sengupta, S. Powell, and S. Sachdev, Phys. Rev. A **69**, 053616 (2004).

[87] G. Szegö, Math. Ann. **76**, 490 (1915).

[88] E.H. Lieb and D.W. Robinson, Commun. Math. Phys. **28**, 251 (1972).

[89] P. Calabrese and J. Cardy, Phys. Rev. Lett. **96**, 136801 (2006) and J. Stat. Mech. P06008 (2007).

[90] H. Widom, Adv. Math. **13**, 284 (1974) and H. Widom, Proc. Am. Math. Soc. **50**, 167 (1975).

[91] T. Giamarchi, *"Quantum physics in one dimension"*, Oxford University Press (2004).

[92] R. Bistritzer, and E. Altman, PNAS 104, 9955 (2004).

[93] A. Polkovnikov, Phys. Rev. A **68**, 033609 (2003).

[94] E.M. Lifshitz und L.P. Pitaevskii, "*Landau, Lifshitz IX, Statistische Physik, Bd. 2*".

[95] B. Mühlschlegel, J. Math. Phys. **3**, 552 (1962).

[96] V.M. Galitskii, Sov. Phys. JETP **7**, 698 (1958).

Danksagung

An dieser Stelle möchte ich mich bei all jenen herzlich bedanken, ohne die ein Zustandekommen dieser Arbeit nicht möglich gewesen wäre. Mein Dank gilt insbesonders

Prof. Zwerger, der mir die Gelegenheit gegeben hat, an brandaktuellen Forschungsthemen zu arbeiten, sowie für die unzähligen interessanten Diskussionen und die andauernde Unterstützung

Ehud Altman und Peter Barmettler für die gute und fruchtbare Zusammenarbeit

allen Mitarbeitern vom Lehrstuhl T34 für die anregenden Diskussionen und die tolle Atmosphäre

meinen Freunden abseits der Physik, die mich immer am Boden der Realität gehalten haben

und nicht zuletzt meiner Familie, der ich alles verdanke, was ich bin

Danke!